

Dissertation

submitted to the
Combined Faculties for the Natural Sciences and for Mathematics
of the Ruperto-Carola University of Heidelberg, Germany
for the degree of
Doctor of Natural Sciences

presented by
Johanna Bischof, M.Res. B.Sc
born in Dresden, Germany

Oral-examination: 15th of June 2016

The Molecular Mechanism of
Surface Contraction Waves in the
Starfish Oocyte

Referees:

Dr. Alexander Aulehla

Prof. Dr. Ulrich Schwarz

ACKNOWLEDGEMENTS

This work would not have been possible without the input and support from a large number of people. I am enormously indebted to them all and extend my sincerest gratitude.

My first big thank you goes to my supervisor, Peter Lenart, for the chance to do my PhD in his lab and the opportunity to work on this exciting project. I want to thank him for his continuous support and the many, many hours of discussion for which he always took the time. It's been a great experience to work with and learn from him.

Next, I would like to thank my university advisor Prof. Ulrich Schwarz for his advice, discussions on the project and the great and fruitful collaboration from which I learned so much.

Equal thanks go to the other members of my thesis committee – Alexander Aulehla and Darren Gilmour. Your advice, support, and insights into the project have been exceptionally important in allowing me to complete my PhD. I could not have imagined having a better thesis advisory committee.

I would furthermore like to thank all the other people who have contributed to this work through collaborations, sharing of experiences and discussions:

Firstly, a big thank you goes to Christoph Brand – working with him has been hugely influential in shaping my project and I learned a lot from him in our long discussions. It was truly an interdisciplinary collaboration of the best kind.

Next, I would like to thank Nicolas Minc for inviting me to his lab and teaching me microfabrication, which was not only very important for the progress of the project but was a great learning experience.

I would also like to thank Kinneret Keren for long discussions, great ideas to push the project forward and infectious enthusiasm.

All this work would not have been possible without Kreso, who takes such good care of the starfish. Thank you for caring about the animals and being up for all the starfish PR shenanigans.

The members of the 'super-secret actin club' – Maria, Francois, Jean-Leon, Herve, Serge, Sourabh, and Julio – provided great insights, discussions and fun with the infamous thought puzzles.

A special thanks goes to Helke Hillebrand, PhD program coordinator, who always encouraged me and who saw when I needed to vent and whose door was always open.

Of course, none of this would have been possible or even vaguely fun without all the members of the Lenart lab! You are all such great people and added so much to my PhD experience.

Kalman – thank you for so much help and advice with all the molecular work, you always knew what to do when I got stuck. Thank you also for the German morning chats, keeping everything shipshape around the lab and moral support.

Joana – thank you for teaching me so much about the starfish, for forging the path and always being happy to share your advice. Thank you also for all the joy you brought to the lab ('are we happy?'), it would have been a very sad (and quiet) four years without you sitting next to me.

Natalia – thank you so much for your support and advice, for being there and always willing to discuss things and share your experiences. I would have been lost without you.

Philippe – thank you for all the great discussions, for bringing physical preciseness from the streets of Paris to biology and being a paragon of scientific thoroughness. And thank you for teaching me about French humour.

Masha – thank you for all your joy and for showing me that there is a bright side to everything and the value of adventure.

I would also like to thank some former members of the lab. Masashi Mori deserves a big thank you for all the starfish knowledge he imparted. Manuela – thank you for all the fun and geekiness. Imre for getting this whole project started and for all the code.

A big thank you goes to the honorary lab members and my 4th-floor companions from the Nedelec lab – Aastha, Sandra, and Iana. Thank you for your support, sharing of all lab things and discussions.

I would also like to thank Joana, Natalia, Aastha and Sandra for their great friendship and support in and out of the lab, for all the coffee breaks, dinners, parties and other adventures. You have been invaluable for making this such a great experience and keeping the madness and 'this-pear' at bay!

So many other people were also instrumental in shaping my daily PhD life. Special shout-out to Simone for fun and conference craziness, Paul for debating fun, Ori for advice and sharing his life experiences, Deepikaa for being a grumpy cat, Thibaut for the always unexpected, and Paola, George Critic (and Cryptic) and Gustavo. It has been a pleasure to get to know all of you.

And last, but most certainly not least, I want to thank my parents, my grandma and my sister, who were always supportive and whose interest in my research and belief in me was a great motivation.

SUMMARY

The cortex is a contractile cross-linked network of actin filaments and myosin motors lining the plasma membrane. It defines the shape of animal cells, and regulated changes in cortex mechanics drive many cellular processes, including cell migration and division. The molecular mechanisms controlling cortical contractility in space and time are therefore essential for cell physiology, but are still not well understood.

During cell division, in cytokinesis, tightly controlled changes to cortical contractility separate the two daughter cells. When very large cells undergo cell divisions, they exhibit highly stereotypical patterns of cortical contractility, termed surface contraction waves (SCWs). These waves occur in cells of a wide variety of species and move across the cells immediately prior to the division. The molecular mechanisms underlying this striking phenomenon are not known.

I set out to investigate SCWs in starfish oocytes, which display a prominent contraction wave during the meiotic division which can be imaged live using fluorescence microscopy. Combined with quantitative image analysis, this allowed me to correlate cell shape changes with the localization of key cortical and cell cycle proteins in untreated oocytes and following biochemical and physical manipulations.

I find that morphologically the contraction wave is a band of flattening that forms at the vegetal pole and moves across the cell to the animal pole. The flattening is driven by increased cortical contractility induced by localisation of myosin II to the cortex. Myosin II recruitment is controlled by RhoA kinase and RhoA, which in turn is activated by release of its inhibition by the cell cycle kinase, cdk1-cyclin B. Importantly, I could show that cdk1-cyclin B activity forms a gradient along the animal-vegetal axis generated by the accumulation of cdk1-cyclin B in the nucleus which is located at the animal pole. Therefore, as cyclin B is degraded, the bottom threshold of cdk1 activity will be reached first opposite of the animal pole, marking the starting point of the contraction wave. The gradient of cdk1-cyclin B activity furthermore controls the progression of the contraction wave across the cell. Additionally, I show that feedback internal to the downstream signalling network contributes to defining the speed of the wave and determines the width of the band of activity.

Overall, this data for the first time establishes the molecular mechanisms underlying SCWs, a phenomenon observed in oocytes of many species. I show that the contraction wave is driven by the highly conserved RhoA-Rok-Myosin II pathway, and is patterned in space and time by an activity gradient of cdk1 as well as feedbacks internal to the signalling pathway. My work thereby reveals how this biochemical signalling network can define a spatially and temporally complex cellular behaviour.

ZUSAMMENFASSUNG

Unterhalb der Zellmembran liegt in allen tierischen Zellen der Zellkortex. Dieser ist ein dicht verknüpftes kontraktiles Netz aus Aktinfilamenten und Myosin- Motorproteinen. Der Kortex definiert die Form aller Zellen. Kontrollierte Veränderungen in der Kortexmechanik steuern viele zelluläre Vorgänge wie Zellmigration und Zellteilung. Auch wenn die molekularen Mechanismen, die die Kontraktilität des Kortexes lokal und temporal kontrollieren, für die Zellphysiologie essentiell sind, wissen wir noch wenig über sie.

Während der Zellteilung führen straff kontrollierte Veränderungen in kortikalen Kontraktilität zur Spaltung der Zelle. Wenn sich sehr große Zellen teilen, zeigen sie in diesem Prozess stereotype Formen kortikaler Kontraktilität, die Oberflächenkontraktionswellen genannt werden. Diese Kontraktionswellen kommen in vielen verschiedenen Spezies vor und laufen kurz vor der Zellteilung über die gesamte Zelloberfläche. Die molekularen Mechanismen, die zu diesen eindrucksvollen Bewegungen führen, waren bisher nicht bekannt.

Ich habe die Oberflächenkontraktionswellen in Seesterneizellen erforscht, da diese eine deutliche Kontraktionswelle während ihrer meiotischen Zellteilung zeigen, die mit Fluoreszenzmikroskopie live gut beobachtet werden kann. In Kombination mit quantitativer Bildanalyse konnte ich die Veränderungen der Zellform mit der Verteilung bedeutender Proteine des Zellkortex und des Zellzyklus jeweils in unbehandelten und biochemisch und physikalisch manipulierten Eizellen in Verbindung bringen.

Ich fand heraus, dass die Kontraktionswelle entsteht, indem sich ein Band des abgeflachten Kortexes am vegetativen Pol der Zelle bildet und sich über die gesamte Zelle zum animalen Pol hin bewegt. Diese Abflachung wird durch die lokal steigende kortikale Kontraktilität ausgelöst, die durch eine Lokalisation von Myosin II Molekülen zum Kortex entsteht. Diese Ansammlung von Myosin II wird von der RhoA Kinase und RhoA gesteuert, welche wiederum selbst aktiviert werden, indem ihre Hemmung durch die wichtige Zellzykluskinase Cdk1-cyclin B aufgehoben wird. Ich konnte zeigen, dass die Aktivität von Cdk1-cyclin B einen Gradienten quer durch die Zelle entlang der animalen-vegetativen Achse bildet. Dieser entsteht durch die Ansammlung von Cdk1-cyclin B im am animalen Pol gelegenen Zellkern. Daher wird, während Cyclin B im Laufe des Zellzyklus abgebaut wird, der untere Grenzwert der Cdk1 Aktivität zuerst gegenüber des animalen Pols erreicht, wo sich der Startpunkt der Kontraktionswelle befindet. Des Weiteren kontrolliert der Gradient der Cdk1-cyclin B Aktivität die Ausbreitung der Welle über die gesamte Zelle hinweg. Außerdem konnte ich zeigen, dass ein Feedback

auf dem Signalweg dazu beiträgt, die Geschwindigkeit mit der sich die Welle ausbreitet und die Breite des Aktivitätsbandes zu definieren.

Die von mir hier vorgestellten Daten beschreiben zum ersten Mal die molekularen Mechanismen die den Oberflächenkontraktionswellen, einem weit verbreiteten Phänomen, welches in den Eizellen vieler Spezies vorkommt, zu Grunde liegen. Ich kann zeigen, dass die Kontraktionswellen von der hoch konservierten Signalkaskade RhoA-Rok-Myosin II kontrolliert werden und dass sie in ihrem räumlichen und zeitlichen Auftreten sowohl durch einen Gradienten von Cdk1 Aktivität als auch durch internes Feedback auf dem Signalweg bestimmt werden. Meine Arbeit zeigt daher, wie ein biochemisches Signalsystem solch ein räumlich und zeitlich komplexes Zellverhalten hervorrufen kann.

TABLE OF CONTENT

Acknowledgements.....	i
Summary	v
Zusammenfassung	vii
Table of Content	xi
List of Figures	xvii
List of Tables	xxi
Abbreviations.....	xxiii
1 Introduction	1
1.1 Cortical contractility.....	3
1.1.1 Cortical contractility controls key cellular functions.....	3
1.1.2 The cortex has a complex molecular architecture.....	3
1.1.2.1 The cortex is an actin meshwork with many associated proteins.....	3
1.1.2.2 Myosin II is the key motor generating cortical contractility.....	6
1.1.3 Cortical contractility is regulated on multiple levels	7
1.1.3.1 Rho GTPases regulate cortical contractility via different pathways.....	7
1.1.3.2 Myosin-driven contractility is regulated via phosphorylation.....	9
1.1.3.3 Microtubules suppress cortical contractility.....	10
1.2 Cytokinesis is a form of highly regulated cortical contractility.....	12
1.2.1 Cytokinesis is spatially regulated by signals originating from the spindle.....	12
1.2.2 Redundancy in the spatial regulation of cytokinesis ensures cytokinesis success	17
1.2.3 The cortex behaves as an excitable medium during cytokinesis.....	18
1.2.4 Cytokinesis is temporally regulated by Cdk1-cyclin B.....	19
1.3 Surface Contraction Waves.....	23
1.3.1 Surface Contraction Waves are division-associated cortical contractility events	23
1.3.2 Surface Contraction Waves are found in many species.....	23
1.3.3 Surface Contraction Waves share a number of common characteristics.....	26

1.3.4	A number of functions have been proposed for Surface Contraction Waves	26
1.3.5	Surface Contraction Waves in the <i>Xenopus</i> embryo are driven by trigger waves.....	27
1.4	Starfish oocytes serve as a model for the study of Surface Contraction Waves	29
1.4.1	Starfish oocytes in meiosis exhibit contraction waves	29
1.4.2	Starfish oocytes are highly specialised cells ideal for molecular imaging studies	30
1.4.3	Meiosis is a specialised form of cell division.....	31
1.4.4	Polar body formation is a specialised form of cytokinesis.....	34
1.4.4.1	Polar body formation is distinct from standard asymmetric divisions	35
1.4.4.2	Multiple mechanisms have been proposed for polar body protrusion	36
2	Aims.....	41
3	Materials and Methods.....	47
3.1	Starfish handling	49
3.1.1	Animals.....	49
3.1.2	Oocyte and sperm collection and maintenance	49
3.2	Cloning and molecular work	50
3.2.1	Cloning and construct preparation	50
3.2.2	Mutagenesis.....	52
3.2.3	RNA preparation	53
3.3	Injection	53
3.4	Imaging.....	55
3.4.1	Confocal fluorescence microscopy	55
3.4.2	Wide-field microscopy	55
3.5	Inhibitor treatments.....	56
3.6	Protein injection.....	59
3.7	Fixation and immunohistochemistry	59
3.8	Physical manipulations.....	61
3.8.1	Surface tension measurements	61
3.8.2	Centrifugation	62

3.8.3	Shape change wells.....	63
3.9	Image analysis and processing.....	65
3.9.1	General image processing.....	65
3.9.2	Curvature measurement.....	65
3.9.3	Flow measurements via STICS.....	67
3.10	Data analysis and plotting.....	68
3.11	Acknowledgments.....	70
4	Results.....	73
4.1	Changes in Cortical Contractility during Meiosis	75
4.1.1	Changes to the cortex from immature to mature oocyte	75
4.1.2	Description of the first surface contraction wave	77
4.2	Molecular Pathway leading to contraction.....	79
4.2.1	Role of myosin II in the contraction wave	79
4.2.1.1	Myosin II is one of the most abundant molecules in the oocyte.....	79
4.2.1.2	Myosin II localises to the flattened cortex.....	79
4.2.1.3	Changing myosin II activity affects strength of contraction wave	81
4.2.2	Myosin II regulation	84
4.2.2.1	Myosin II activity is regulated via the phosphorylation site TS17.18	84
4.2.2.2	Myosin II is phosphorylated by Rok	87
4.2.3	RhoA controls the contraction wave	89
4.2.4	Activation of RhoA	91
4.2.4.1	Contraction wave is independent of microtubules	91
4.2.4.2	Ect2 as a possible RhoA activator	92
4.2.4.3	Alternative GEFs.....	94
4.2.5	The actin cortex serves as a substrate for contraction.....	96
4.2.6	Role of calcium in the contraction wave.....	100
4.2.7	Summary of the molecular pathway controlling contraction.....	102
4.3	How to Form a Wave	103

4.3.1	Initiation of the contraction wave	103
4.3.1.1	The contraction wave starts opposite of the nucleus.....	103
4.3.1.2	A gradient of cell cycle activity is present in the oocyte.....	105
4.3.1.3	The Cdk1 gradient controls the direction of the contraction wave.....	107
4.3.1.4	The Cdk1 gradient controls the starting point of the contraction wave	110
4.3.2	Propagation of the wave.....	111
4.3.2.1	The Cdk1 gradient controls the progression of the contraction wave	111
4.3.2.2	Feedback between contraction strength and wave speed.....	114
4.3.2.3	Feedback to regulate band width	117
4.4	Potential Function of the Contraction Wave	120
4.4.1	Polar Body Formation as a function of contraction wave	120
5	Discussion.....	123
5.1	Contraction Waves as a cortical phenomenon during cytokinesis.....	125
5.2	The spatial dimension of the cell cycle	125
5.3	The cell cycle dependence of the contraction waves in starfish and <i>Xenopus</i>	126
5.4	Linking Cdk1 activity to contractility	129
5.4.1	The contraction wave is independent of microtubules	129
5.4.2	GEFs regulating the contraction wave	130
5.5	Molecular Pathway controlling the contraction wave.....	130
5.5.1	The highly conserved RhoA-Rok-Myosin II signalling axis	130
5.5.2	Feedback in the RhoA-Rok-Myosin II pathway	131
5.6	The oocyte cortex and its dynamics.....	132
5.7	Similarity to other contraction waves.....	133
5.7.1	Other contraction waves in the starfish oocyte.....	133
5.7.2	SCWs in other systems.....	135
5.8	The Contraction wave as a function vs The Function of the contraction wave.....	136
5.8.1	The contraction wave is a result of oocyte adaptation	136
5.8.2	Polar body protrusion is independent of the contraction wave.....	136

5.8.3	Potential function of the contraction wave in development.....	139
6	Conclusion.....	143
7	Bibliography	149

LIST OF FIGURES

Figure 1: Cortical contractility drives diverse cellular functions.....	3
Figure 2: Actin forms a variety of structures in the cell.....	4
Figure 3: Contraction of motors on actin filaments with and without crosslinkers.	5
Figure 4: ERM proteins link the cortex to the membrane.	6
Figure 5: Non-muscle myosin II.....	7
Figure 6: The regulatory cycle of Rho GTPases.....	8
Figure 7: Downstream effectors of the key Rho GTPases family members.	9
Figure 8: Model for oscillations in cells without microtubules.....	11
Figure 9: Formation of a Rappaport furrow.....	13
Figure 10: Function of RhoA in controlling the components of the contractile ring.	14
Figure 11: RhoA signal alone is sufficient to drive contractile ring formation.	15
Figure 12: Ect2 is localised to the contractile furrow via microtubules.	16
Figure 13: Different populations of microtubules in cytokinesis.....	17
Figure 14: RhoA waves at the cortex during C-phase.....	18
Figure 15: Regulation of Cdk1-cyclin B activity.....	20
Figure 16: Phylogenetic tree of SCWs.....	25
Figure 17: The potential function of the SCWs in controlling embryonic polarisation.	27
Figure 18: SCWs in the Xenopus embryo.....	27
Figure 19: Trigger waves of the cell cycle.	29
Figure 20: The SCW in the starfish oocyte.....	29
Figure 21: An immature starfish oocyte with important cellular structures labelled.	31
Figure 22: Meiotic cell cycle in the oocyte.....	32
Figure 23: Meiotic resumption in the starfish oocyte.	33
Figure 24: Mos is the master regulator of meiosis.	34
Figure 25: Geometry of the cell division in symmetric and asymmetric divisions.	36
Figure 26: Polar body protrusion.	38
Figure 27: Copy-and-paste cloning strategy employed to generate constructs.....	51
Figure 28: Mutagenesis strategy.....	52
Figure 29: Chamber setup for injection.	54
Figure 30: Injection of the oocyte.....	54
Figure 31: Surface tension measurements.	62
Figure 32: Set-up for centrifugation of starfish oocytes.....	63

Figure 33: Shape change wells.....	64
Figure 34: Image Analysis pipeline.....	66
Figure 35: Quantifying strength of contraction wave.....	69
Figure 36: Cortical changes during the oocyte maturation.	76
Figure 37: Surface contraction wave.	77
Figure 38: Model of the shape changes of the contraction wave and the cytoplasmic flow.....	78
Figure 39: Myosin II in the contraction wave.	81
Figure 40: Changing myosin II activity.	83
Figure 41: Phosphorylation sites of myosin regulatory light chain (MRLC).....	84
Figure 42: MRLC phosphomutants.....	86
Figure 43: Kinases activating myosin II via phosphorylation.	88
Figure 44: RhoA activity during the contraction wave.....	90
Figure 45: Function of microtubules during the contraction wave.	92
Figure 46: Ect2 in the contraction wave.	93
Figure 47: Alternative GEF candidates for RhoA activation.....	96
Figure 48: Actin localization during the contraction wave.....	97
Figure 49: Actin manipulations during the contraction wave.	99
Figure 50: Role of calcium in the contraction wave.....	101
Figure 51: Molecular pathway regulating myosin II activity in the contraction wave.....	102
Figure 52: Changing AP-VP axis via centrifugation.	104
Figure 53: Cyclin B.....	106
Figure 54: Local Cdk1 inhibitor treatment.	109
Figure 55: Injection of Cdk1-cyclin B protein complex.	111
Figure 56: Effect of shape change on the contraction wave.	113
Figure 57: Correlation of wave speed and contraction strength.....	116
Figure 58: Speed of contraction wave with manipulations of RhoA, Rok and actin.....	117
Figure 59: Regulation of RhoA inactivation.	119
Figure 60: Complete molecular pathway regulation the contraction wave.	119
Figure 61: Polar body formation.....	121
Figure 62: Cell cycle in space and time in starfish oocyte compared to a somatic cell in mitosis.....	126
Figure 63: Comparison of contraction waves in Xenopus and starfish.....	128
Figure 64: Complete molecular pathway regulating the contraction wave.	132
Figure 65: SCW at NEBD in the starfish oocyte.....	134
Figure 66: Curvature change and cytoplasmic flow in the oocyte.....	137

Figure 67: First polar body	138
Figure 68: Cortical differentiation in response to chromatin signal.....	139
Figure 69: Polarisation of developmental determinants.....	139

LIST OF TABLES

Table 1: List of constructs used in the project.	51
Table 2: List of primers used for cloning from cDNA or mutagenesis.	52
Table 3: Used chemicals with function, concentration, solvent and incubation time.	57
Table 4: Microwave protocol for fixation.	60
Table 5: Top 10 proteins in the starfish oocyte as determined by Mass-Spec sorted by counts.	79
Table 6: Results of the shape change experiments	112

ABBREVIATIONS

1-MA	1-methyladenine
AP	Animal pole
CytoD	Cytochalasin D
FSW	Filtered seawater
LatB	Latrunculin B
MI	Meiosis I
MII	Meiosis II
NEBD	Nuclear envelope breakdown
PB	Polar body
SCW	Surface contraction wave
VP	Vegetal pole

1 INTRODUCTION

1.1 CORTICAL CONTRACTILITY

1.1.1 Cortical contractility controls key cellular functions

The cortex is a thin meshwork of actin filaments and many associated proteins which lies directly underneath the cell membrane in all animal cells. The plasticity and contractility of the cortex are key for most cellular processes.

In the steady state the cortex protects cells against outside mechanical disruption (Bray & White 1988) and serves as a counterforce to the internal osmotic pressure (Stewart et al. 2011). In non-animal cells this function is fulfilled by the cell wall. As the cortex determines the cell shape, cortical contractility is key in shaping tissues during development (Figure 1a and b)(Levayer & Lecuit 2012). The ability to the cortex to contract is furthermore important during cell migration, both in normal cells (Cramer 2010) as well as in metastasis of cancer cells (Figure 1d and e)(Sedzinski et al. 2011; Charras & Paluch 2008). Cortical contractility is also the key driving force behind cell division, the process by which a single cell gives rise to two daughter cells (Figure 1c) (Stewart et al. 2011; Kunda et al. 2008).

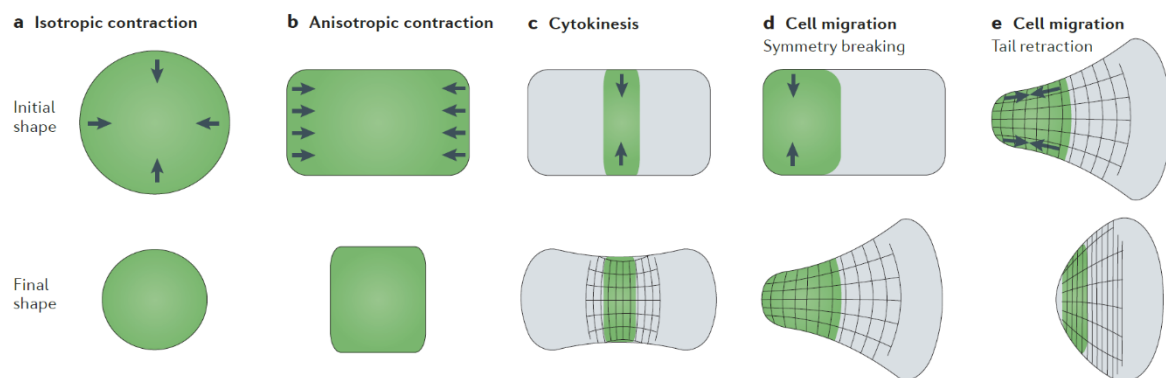


Figure 1: Cortical contractility drives diverse cellular functions. These range from changes in cell shape (a,b), to cytokinesis (c) and cell migration (d,e). The green area shows the parts of the cell cortex that is contracting. Reprinted by permission from Macmillan Publishers Ltd: Nature Reviews (Murrell et al. 2015), copyright 2015.

Even though it is a key feature of cells and their behaviour, a lot of things remain unknown about the cortex and cortical contractility, such as cortical organisation on the filament level or how the cortex's mechanical properties and responses are regulated.

1.1.2 The cortex has a complex molecular architecture

1.1.2.1 The cortex is an actin meshwork with many associated proteins

As the cortex serves such varied and important functions its structure is understandably complex. The key component of the cortex is actin, organised in a highly crosslinked meshwork of filaments. In addition to the actin filaments, the cortex contains a large number of other proteins required for cortical integrity and function. Even though it is a complex assembly of many proteins, the cortex as a

whole is a relatively thin structure with a thickness of around 100 nm (Clark et al. 2013). This thickness seems to be well conserved between different cells, from Dictyostelium (Ogihara et al. 1988) to mammalian cells (Charras et al. 2006; Clark et al. 2013). The whole actin cortex turns over rapidly, in the range of 30 sec (Fritzsche et al. 2013). This allows for stress dissipation and quick responses to the changing environment.

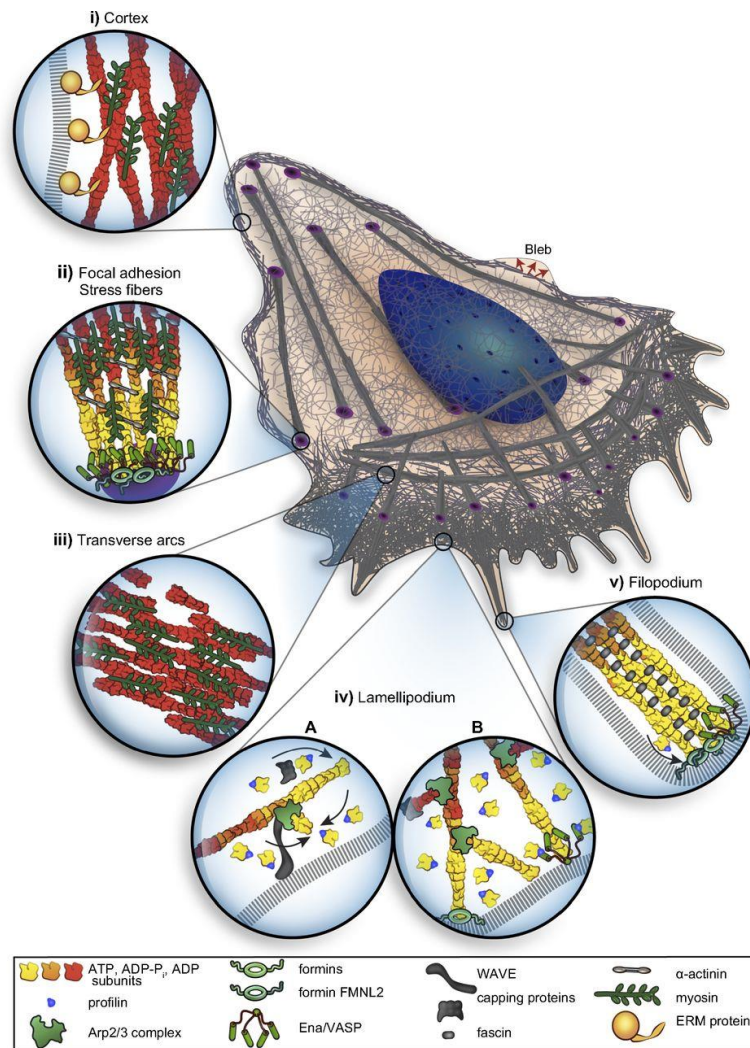


Figure 2: Actin forms a variety of structures in the cell. While all cells have an actin cortex (i), cells under certain conditions also form other complex actin structures, such as lamellipodia (a,b) and filopodia (v). As shown, the actin cortex consists of actin filaments along with myosin and ERM proteins. Figure form (Blanchoin et al. 2014), copyright Physiological Reviews, 2014.

The cortex is one of many actin structures in the cell (Figure 2), in which actin filaments interact with a wide variety of proteins, allowing the cortex to fulfil its various functions. The proteins of the cortex fall into 4 categories: (1) actin nucleators, (2) actin crosslinkers, (3) cortex-membrane crosslinkers, and (4) motor proteins.

(1) The key actin nucleators in the cortex are Arp2/3 and formins, which, at least in human cells, produce roughly half of the actin filaments each (Bovellan et al. 2014). These two actin nucleators give

rise to two different populations of actin filaments. Formins form long, straight actin filaments (Higgs 2005) while Arp2/3 nucleated actin is highly branched (Mullins et al. 1998). These actin nucleators are in turn regulated by a variety of activators. In the cortex Arp2/3, for example, is regulated by the WASP and WAVE protein family (Takenawa & Miki 2001). This allows for the specific regulation of actin polymerisation in the cortex.

(2) The actin filaments in the cortex are highly crosslinked to form a coherent strong network. The actin crosslinkers are a very diverse group, and most actin binding and crosslinking proteins have been shown to localise to the cortex. The key crosslinkers appear to be α -actinin, fimbrin and filamin (Falzone et al. 2012; Stossel et al. 2001). Crosslinkers are key for producing a coherent meshwork, and for allowing force generation between actin filaments. This is achieved by crosslinkers forming points against which forces can be applied, as a non-crosslinked network only undergoes translation of filaments relative to each other (Figure 3) (Schaller et al. 2013).

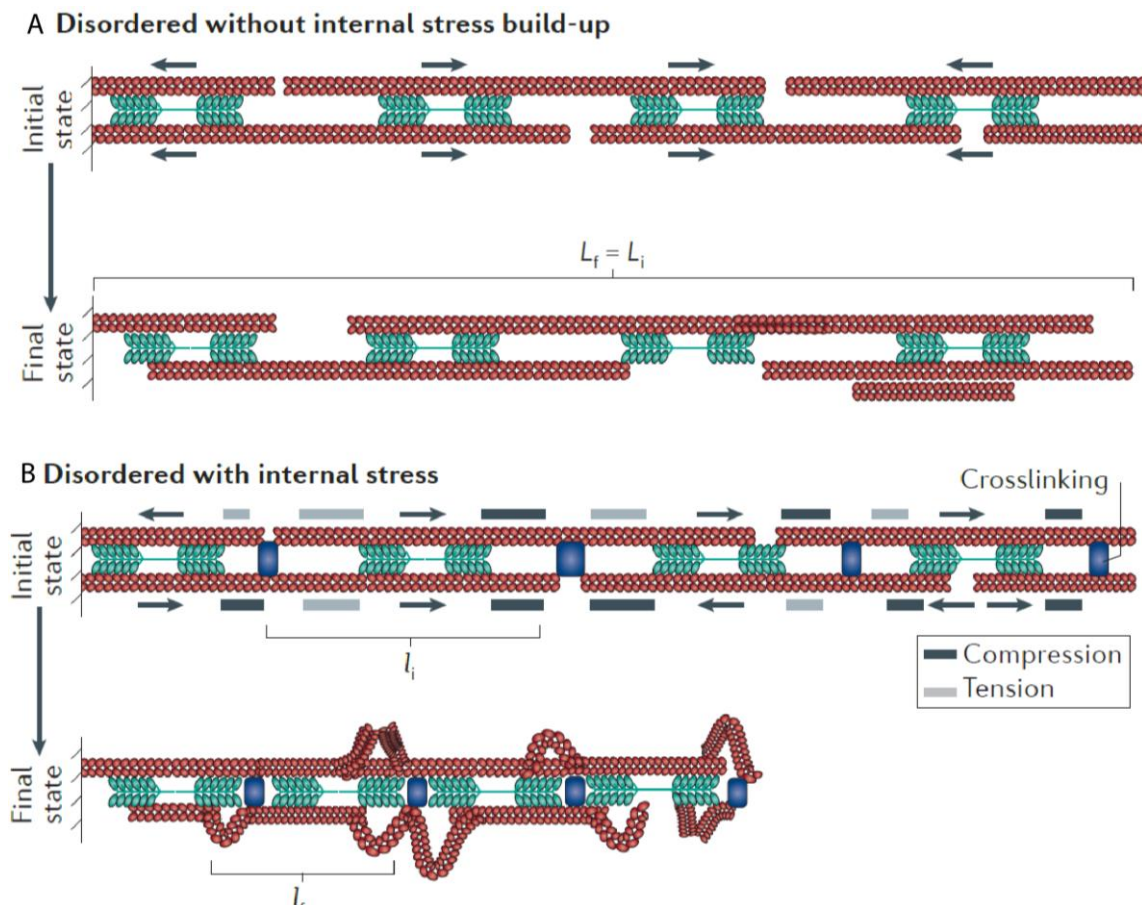


Figure 3: Contraction of motors on actin filaments with and without crosslinkers. A) Motor action on actin filaments without crosslinkers leads to sliding of the filaments against each other. B) When motors work on crosslinked actin filaments internal stress is generated, which can lead to buckling of the actin filaments. Reprinted by permission from Macmillan Publishers Ltd: Nature Reviews (Murrell et al. 2015), copyright 2015.

(3) The cortex is linked to the membrane via a well-conserved protein family called ERMs – Ezrin, Radixin, Moesin (Figure 4) (Fehon et al. 2010). Other anchor-proteins, such as ankyrin B, are also

involved (Charras et al. 2006). The ERMs are multi-domain proteins which can in their active conformation bind to both the plasma membrane and actin filaments and thereby tether the cortex to the membrane. They also play important roles in forming specific membrane domains, by locally increasing the concentration of certain anchored proteins, i.e. during signalling.

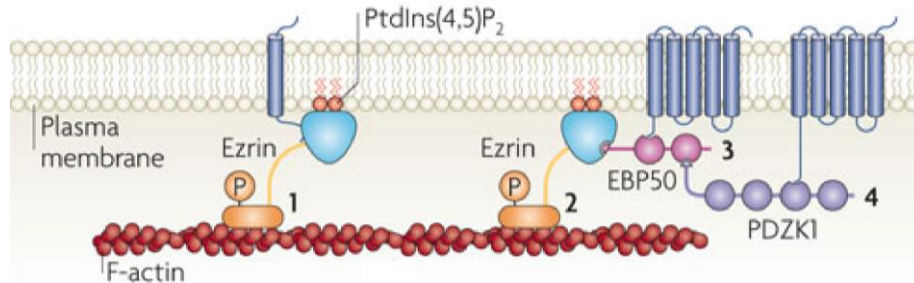


Figure 4: ERM proteins link the cortex to the membrane.

Ezrin, a member of the ERM family of proteins, links actin filaments of the cortex to the membrane via interaction with phosphatidylinositol 4,5-bisphosphate (PtdIns(4,5)P₂). Reprinted by permission from Macmillan Publishers Ltd: Nature Reviews (Fehon et al. 2010), copyright 2010.

(4) To generate cortical tension and contractility, motor proteins which generate force on the actin filaments are required. Even though a variety of motor proteins have been shown to localise to the cortex, such as myosin I, it is clear that the main driver of cortical contractility, as well as cortical tension, is a single protein complex called non-muscle myosin II (Salbreux et al. 2012).

1.1.2.2 Myosin II is the key motor generating cortical contractility

There are 20 known classes of myosins (Krendel & Mooseker 2005), of which myosin II is the most studied and best understood. Non-muscle myosin II, the myosin II isoform found in all cells except striated muscle cells, is a hexamer made up of 2 heavy chains (230 kDa each), 2 essential light chains (17 kDa each) and 2 regulatory light chains (20 kDa each) (Vicente-Manzanares et al. 2009). These six proteins form a structurally highly conserved protein complex, which is characterised by a head, neck, long coiled-coil rod and a short tail (Figure 5a). Myosin binds to its substrate F-actin through the head domain and translocates along the filament.

The movement is achieved through the transfer of chemical energy into mechanical work via a conformational change in the neck region induced by ATP hydrolysis. This moves the myosin head along the actin filament. To achieve efficient contractility, non-muscle myosin II proteins assemble into bipolar filaments through their rod domains (Figure 5b)(Ricketson et al. 2010).

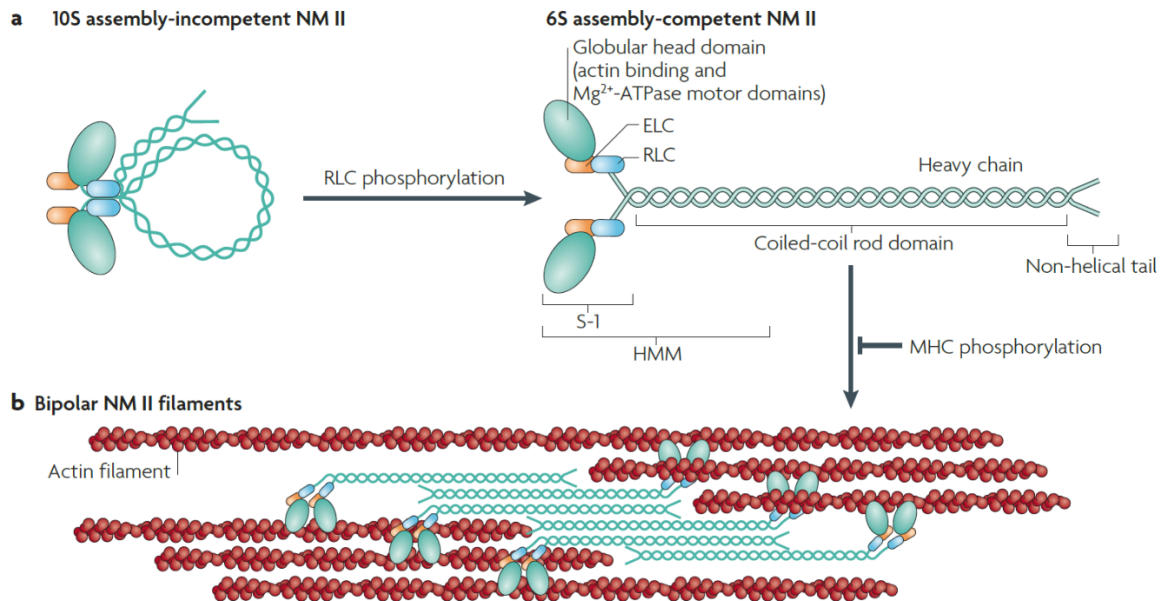


Figure 5: Non-muscle myosin II.

(a) Myosin structure of the individual molecular complex in the active and inactive state, (b) as well as the formation of bipolar filaments and subsequent binding to actin. Reprinted by permission from Macmillan Publishers Ltd: Nature Reviews (Vicente-Manzanares et al. 2009), copyright 2009.

Myosin II driven contraction has mainly been studied in striated muscle cells, where myosin II and the actin filaments on which it contracts are organised in a very ordered manner. We owe a lot of our understanding of the workings of myosin II to this highly organised system. But in most other contexts, such as in the cortex, contractility arises on unorganised actin filaments in a process we understand much less about (Murrell et al. 2015).

1.1.3 Cortical contractility is regulated on multiple levels

1.1.3.1 Rho GTPases regulate cortical contractility via different pathways

The cortical architecture is clearly highly complex with myosin II being one of the main components in addition to the actin filaments. Myosin II in this context drives cortical contractility. This contractility is important for cortical functions and is therefore highly regulated. One of the key regulatory mechanisms is mediated by the Rho family of GTPases.

GTPases are molecular switches, which have an active GTP-bound and an inactive GDP-bound form (Figure 6) (Jaffe & Hall 2005). The GTP-bound active form of these lipid-modified proteins binds to the membrane. This membrane binding is obligatory for the interaction with its downstream effectors while the inactive form of the GTPase is localised in the cytoplasm. While the name suggests that GTPases are able to hydrolyse GTP, on its own this reaction is very slow (Haeusler et al. 2003) and *in vivo* only works with the assistance of a GTPase activating protein (GAPs) (Bernards 2003). GAPs are specific to the individual GTPase and promote the transition from the active to the inactive state (Figure 6). On the activatory side of the cycle, guanine nucleotide exchange factors (GEFs) serve to

activate the GTPases by exchanging GDP for GTP (Schmidt & Hall 2002). An additional layer of control is achieved through the function of guanine nucleotide dissociation inhibitors (GDIs). These proteins bind to the inactive cytoplasmic form and prevent spontaneous activation by inhibiting nucleotide disassociation as well as capping the membrane interacting domain (Figure 6)(Olofsson 1999).

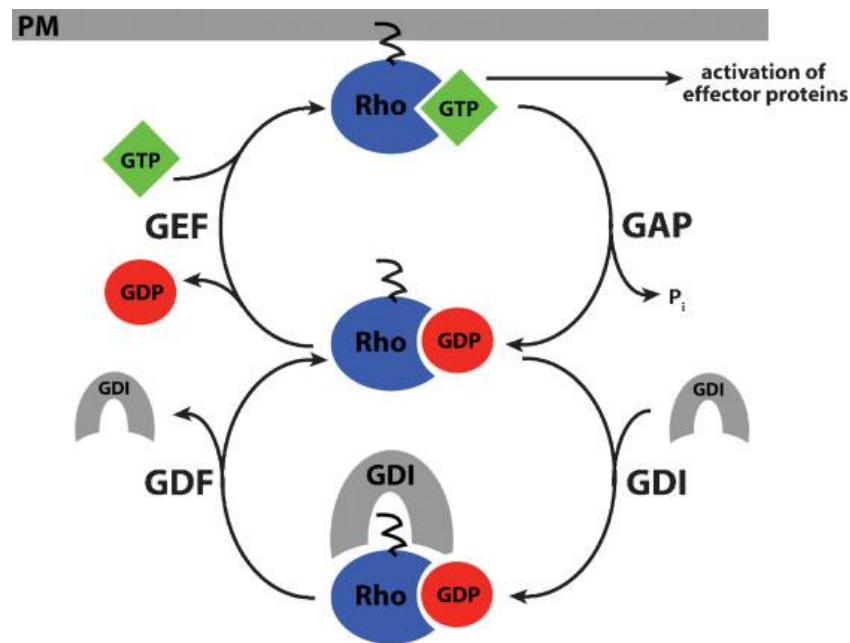
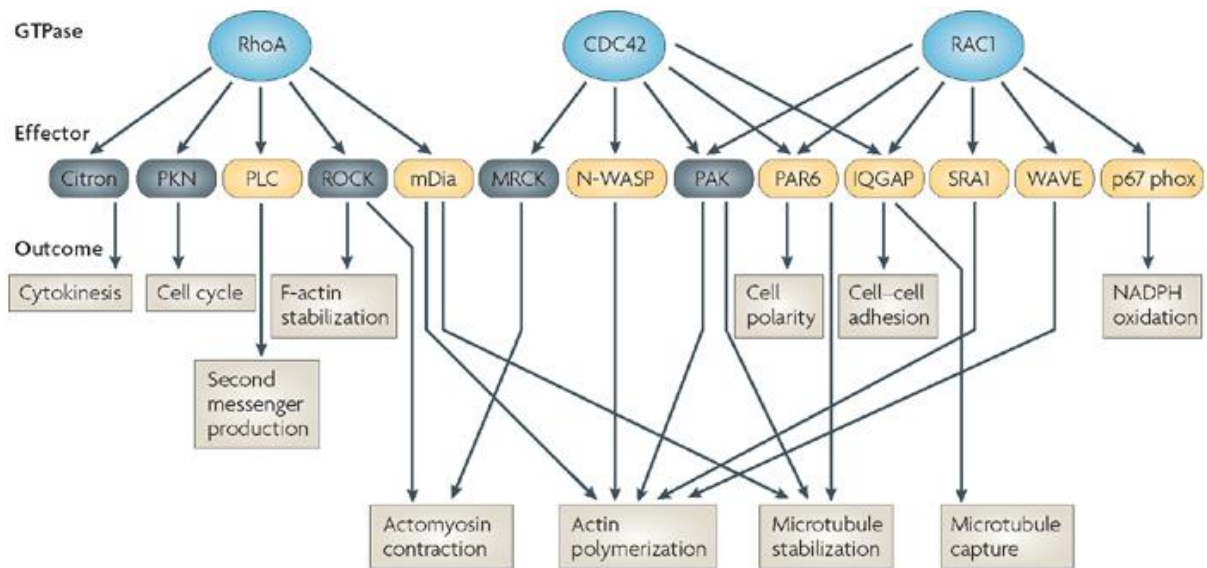


Figure 6: The regulatory cycle of Rho GTPases.

Active GTP-bound Rho is localised to the membrane where it activates its effectors. The active Rho is converted into an inactive GDP-bound Rho by the activity of GAPs while the reverse reaction is driven by GEFs. GDIs maintain Rho in its inactive state while GDFs lift this inhibition. Reprinted with permission from John Wiley and Sons: *BioEssays* (Bement et al. 2006), copyright 2006.

Of the many classes of GTPases, the Rho family is the most important in regulating cortical contractility. It has 22 members in mammals, the most common of which are RhoA, Cdc42 and Rac (Jaffe & Hall 2005; Hall 1998). These 3 proteins alone have many downstream target proteins, affecting varied cellular processes (Figure 7) (Bishop & Hall 2000).



Nature Reviews | Molecular Cell Biology

Figure 7: Downstream effectors of the key Rho GTPases family members.

The three Rho GTPase family members RhoA, Cdc42 and Rac have many downstream effectors which regulate a wide variety of cellular process. Reprinted by permission from Macmillan Publishers Ltd: Nature Reviews (Iden & Collard 2008), copyright 2008.

The Rho GTPases regulate cortical contractility via multiple effectors. One is via a change in the actin polymerisation, either directly by activating actin nucleators like the formin mDia (Otomo et al. 2005), or by activating actin nucleation regulators, such as WASP and WAVE (Takenawa & Miki 2001). These factors, in turn, activate the actin nucleator Arp2/3. At the same time, both RhoA and Cdc42 can activate myosin II contractility via the kinases ROCK or MRCK (Leung et al. 1996), thereby controlling cortical contractility.

1.1.3.2 Myosin-driven contractility is regulated via phosphorylation

Myosin II activity is in the short term regulated by the phosphorylation by such kinases. The target of this phosphorylation is the regulatory light chain (MRLC). The main phosphorylation sites of MRLC are the amino acids Thr18 and Ser19 (Hirata et al. 2009; Ikebe et al. 1986). The phosphorylation of these sites does not result in an increase in actin binding affinity (Sellers et al. 1982), but rather in an increase in the ATPase activity (Somlyo & Somlyo 2003). This increases myosin movement speed and processivity, and it also increases myosin filament assembly (Scholey et al. 1980).

The main kinases phosphorylating this site are myosin light chain kinase (MLCK), citron kinase and Rho kinase (Rok) (Somlyo & Somlyo 2003; Matsumura 2005; Tan et al. 2008). With multiple kinases phosphorylating the same site, the specificity of myosin activation in response to upstream signals is clearly controlled at the kinase level. This means that different kinases are dominant in different cellular contexts.

It is interesting to note that for MLCK the myosin light chain is the only target while both citron kinase and Rok have other phosphorylation targets. Rok can also activate myosin light chain through an interesting round-about way - by inhibiting myosin phosphatase. Myosin phosphatase would otherwise inhibit myosin activity by dephosphorylating MRLC (Matsumura & Hartshorne 2008). This inhibition is lifted by phosphorylation of myosin phosphatase by Rok.

There is also an alternative phosphorylation site in MRLC, targeted by cyclin B related to cell cycle control of myosin activity at Ser1 and Ser2 (Satterwhite et al. 1992). This site is also shared by PKC (Nishikawa et al. 1984). The significance of these phosphorylation sites has been less explored.

From this, it is clear that cortical contractility is regulated on the molecular level by Rho GTPases and specifically myosin II activity is regulated via phosphorylation.

1.1.3.3 Microtubules suppress cortical contractility

In addition to these specific molecular regulations of cortical contractility, interesting evidence exists that cortical contractility in cells is broadly inhibited via microtubules. This was first concluded from observations of periodic contractility induced in spreading fibroblasts whose microtubules were removed via nocodazole treatment (Pletjushkina et al. 2001; Lyass 1988). In these experiments, the authors could show that these periodic contractions were driven by myosin II and were calcium-dependent, and persisted for several hours until the cells attached firmly to their substrate.

A similar phenomenon of periodic contraction based on myosin II activation was observed when cells whose microtubules were removed were prevented from attaching to any surface (Paluch et al. 2005). Interestingly, under these conditions the extent of contractility depended on the cell-cycle stage of the cells, suggesting cell cycle regulation further upstream of the contractility regulation. These periodic contractions could also be observed in cell fragments, indicating that this process can emerge from very simple components. The authors show that the cortical contraction arises from symmetry breaking in the spherical cells or cell fragments which results in the formation of blebs which travel across the cell (Figure 8).

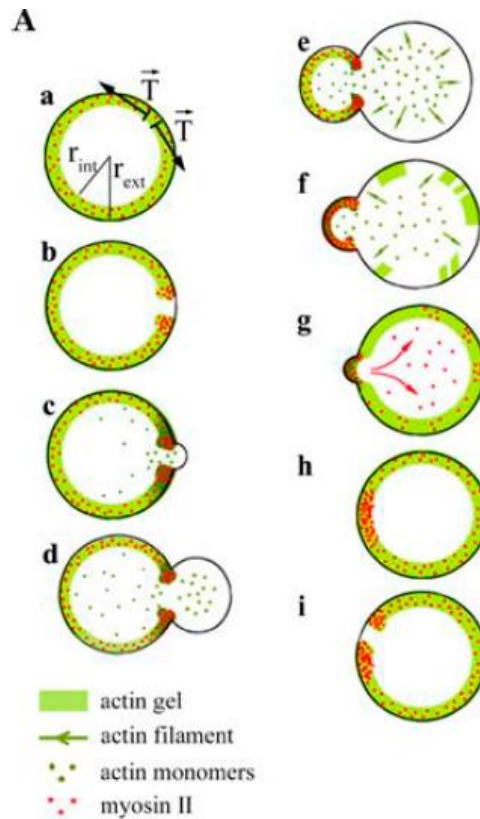


Figure 8: Model for oscillations in cells without microtubules.

A) Small inhomogeneity in the distribution of myosin II in the cortex lead to breakage and bleb formation (b,c). In a self-enhancing process, more myosin accumulates at the break points, increasing the bleb size (d). The contractile myosin moves across the cell and new cortex forms in the bleb (e,f). Myosin in the mainly redistributed across the cell (g,h), until a small inhomogeneity lead to a repeat of the process (i). Reprinted from (Paluch et al. 2006) with permission from Elsevier.

Although these observations have only been made in cultured cells under abnormal conditions, i.e. nocodazole treatment, the data suggests a negative regulation of contractility by microtubules which is consistent with data from cardiomyocytes. In these cells increase in microtubules density leads to a reduction in contractility which occurs in hypertrophied myocardia (Zile et al. 1999; Ishibashi & Tsutsui 1996).

While these datasets seem to converge to illustrate the importance of microtubules in regulating contractility, no data is yet available indicating the specific pathway by which this regulation is achieved.

As the control of cortical contractility is a very varied process, including a large number of disparate signalling pathways, it is easiest to understand this regulation when looking at a specific example of this regulation. In the next section, I will therefore focus on cytokinesis, which is a process driven by strong differentiation of cortical contractility across the cell.

1.2 CYTOKINESIS IS A FORM OF HIGHLY REGULATED CORTICAL CONTRACTILITY

1.2.1 Cytokinesis is spatially regulated by signals originating from the spindle

Cytokinesis is the process by which a single cell is divided into two daughter cells at the end of mitosis. Cytokinesis happens after the chromosomes have been separated and it is a process that involves the whole cell, mainly focussed on and driven by the cell cortex.

During cytokinesis, the cortex differentiates and forms a specialised structure, the contractile ring, in the middle of the cell. The contraction of this ring leads to the formation of the cytokinetic furrow which progressively constricts to separate the cytoplasm of the two cells.

A key part of our mechanistic understanding of the process of cytokinesis was laid by Ray Rappaport, who from 1960 onwards used physical manipulations and simple, low-tech observations of the sand dollar egg to establish the cell cortex' response to the division signal. What became clear from these experiments is that the main factor determining the formation of the cytokinetic furrow is the mitotic apparatus or spindle. In normal cases, the cytokinetic furrow forms directly over the middle of the spindle. Repositioning the spindle led to the formation of a furrow in the new place and disappears in the old (Rappaport 1985). The signal inducing this response responds therefore dynamically to the position of the spindle, due to a positive signal delivered by the microtubules to the cortex (Rappaport 1964).

The most famous of Rappaport's experiment was to investigate which type of microtubule structure is required for the furrow signal (Rappaport 1961). In this experiments, he compressed sand dollar eggs into doughnut shapes (Figure 9A), which led at the first division to the formation of a single horseshoe shaped cells (Figure 9B). This configuration leads to the formation of a binucleated cell, where, in the next division, the asters of the spindle overlapped with no chromosomes between them (Figure 9C). Surprisingly, this overlap was sufficient to induce a furrow and subsequent division (Figure 9D). This type of furrow, caused by the overlap of microtubules with no chromosomes between them, has been termed a Rappaport furrow. They have subsequently also been generated in other systems (Savoian et al. 1999). This indicates that an overlap of antiparallel microtubules is all that is required for furrow formation and chromosomes are not required.

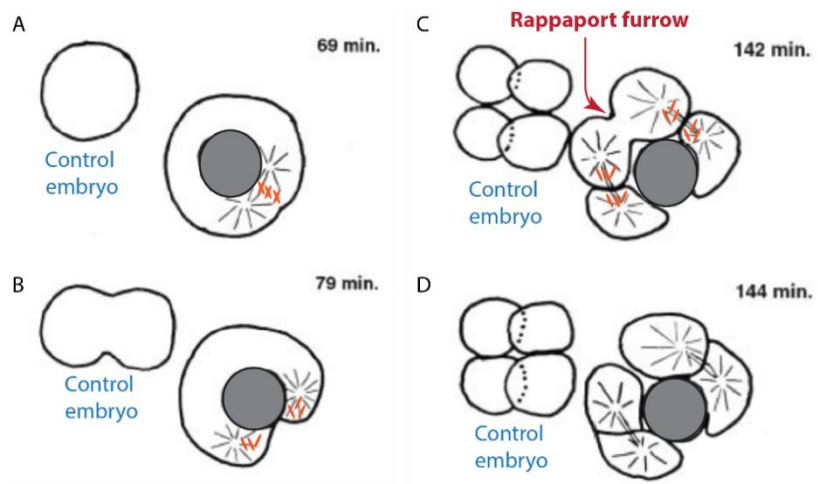


Figure 9: Formation of a Rappaport furrow.

A) An embryo is compressed with a glass bead (grey sphere), pushing the spindle to one side. B) This cell divides only on the side of the sphere where the spindle was located, forming a binucleated cell. C) This cell then in the next round of divisions forms 2 normal furrows as well as a so-called Rappaport furrow. D) This furrow fully constricts to form 4 individual cell, same as in the control embryo. Reprinted with permission from John Wiley and Sons: *Journal of Experimental Zoology* (Rappaport 1961), copyright 1961, with additional labels for clarity.

The molecular understanding of the contractile ring which forms the furrow lagged behind the physical understanding of the process provided by Rappaport for many years. But in recent years the molecular side has caught up and now a fairly complete view of the molecular components of cytokinesis has been established (Green et al. 2012; Eggert et al. 2006).

As the contractile ring is essentially a differentiation of the cortex, it is not surprising that the two key components of the contractile ring are actin (Schroeder 1973) and myosin II (Mabuchi & Okuno 1977). This molecular composition suggests an intuitive mechanism for contractility, with actin acting as a scaffold on which myosin exerts its contraction force to progressively reduce the ring diameter (Murthy & Wadsworth 2005). But intriguingly it appears that myosin, at least under some circumstances, serves in the contractile ring only as a stabiliser or scaffold (Carvalho et al. 2009) and its force generation is not required for contractile ring closure (Beach & Egelhoff 2009). How widespread this function of myosin as a pure scaffold is, remains unclear, as in most circumstances myosin II contractility is in fact required for contractile ring closure (Murthy & Wadsworth 2005).

Assembly and activity of actin and myosin II in the contractile ring are controlled by the GTPase RhoA via two key downstream effectors (Figure 10). Firstly RhoA activates formins, which are actin nucleators producing the straight unbranched actin filaments of the contractile ring (Severson et al. 2002; Otomo et al. 2005; Rose et al. 2005). Secondly, RhoA activates RhoA kinase (Rok) which activates myosin II in the contractile ring, leading to the contraction (Amano et al. 1996; Kimura et al. 1993; Piekny & Mains 2002).

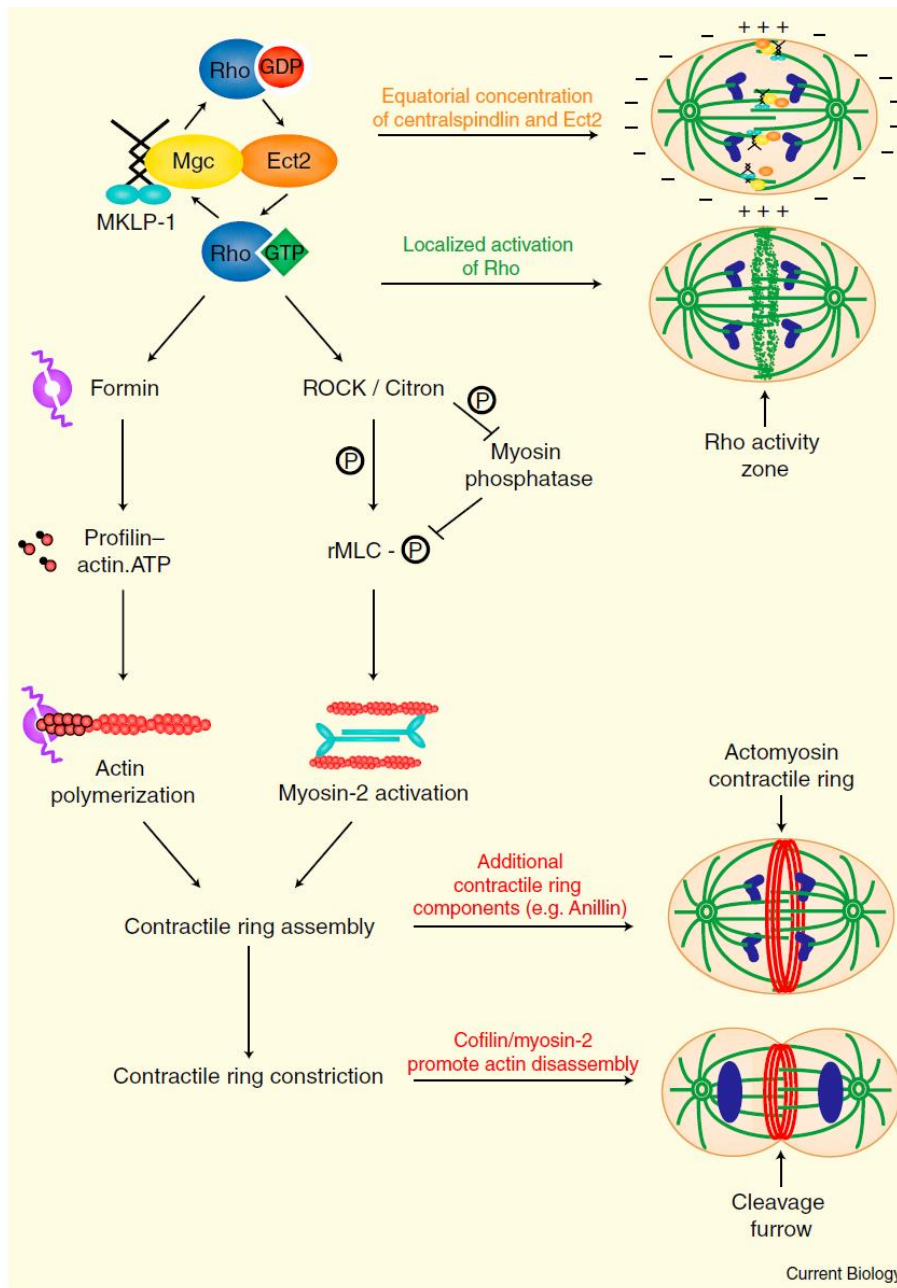


Figure 10: Function of RhoA in controlling the components of the contractile ring. RhoA is localised and activated at the furrow via central spindle and Ect2. RhoA then activates formin to nucleate actin filaments and activates Rok which in turn activates myosin II. The combination of these two processes leads to the formation of the contractile ring and its contraction. Reprinted from (Miller 2011) with permission from Elsevier.

In accordance with the regulation of contractile ring formation by RhoA, recent work by Wagner and Glotzer showed that active RhoA alone is sufficient to induce contractile ring formation, independent of any signal from the spindle (Wagner & Glotzer 2016). They showed this by locally activating RhoA at various membrane sites via an optogenetic construct, leading to accumulation of actin and myosin II at these sites and the so formed contractile rings were functional as seen through partial ingression. This induction of ring formation was surprisingly independent of the cell cycle stage, allowing the

formation of contractile rings even in interphase cells (Figure 11). This shows that the formation of the contractile ring solely requires active RhoA at the cortex.

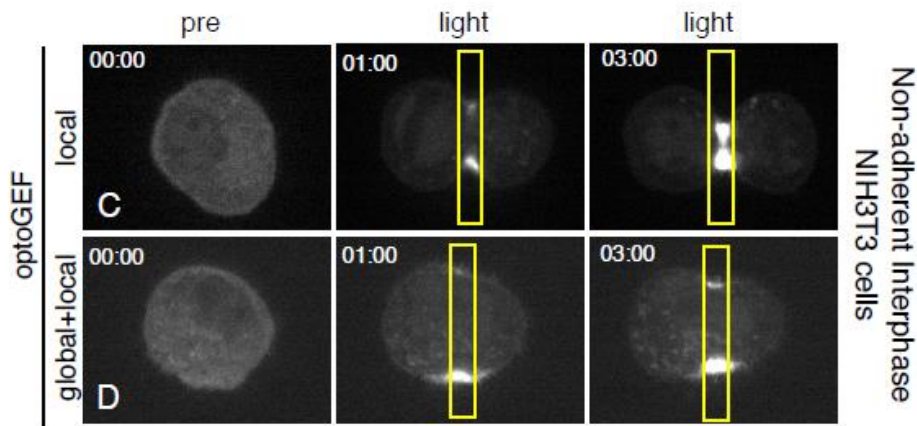


Figure 11: RhoA signal alone is sufficient to drive contractile ring formation. Contractile ring formation in interphase cells was induced by optogenetic activation of RhoA at the cortex. Figure reprinted from (Wagner & Glotzer 2016) under creative commons CC-BY-NC-ND 4.0 international license.

Due to RhoAs function as a master regulator of contractile ring formation, its activation and localisation obviously have to be finely controlled to allow for successful cytokinesis. This control is achieved through RhoA activating factors, termed GEFs.

The main GEF which activates RhoA in the formation of the contractile ring is Ect2 (Yüce et al. 2005), although GEF-H1 is also involved in parallel to Ect2, at least in certain cells (Birkenfeld et al. 2007; Krendel et al. 2002). Ect2 is localised to the prospective contractile furrow overlying the spindle midzone where it activates RhoA (Figure 10). Ect2 is transported to the cortex along microtubules and comes from the central spindle region (Figure 12)(Bement et al. 2005; Bement & von Dassow 2014; Somers & Saint 2003).

At the central spindle region, Ect2 colocalises and is activated by the heterotrimeric centralspindlin complex (Nishimura & Yonemura 2006). This complex is made up of MgcRacGAP and MKLP1 (Mishima et al. 2002; Pavicic-Kaltenbrunner 2007) and localises to the antiparallel microtubule overlap in the spindle midzone and midbody (Lekomtsev et al. 2012). The activation signal is then transmitted from the central spindle region to the cortex through the action of the MKLP1 subunit, which is a kinesin and can travel along the microtubules to the cortex. As this transport is microtubule-based, Ect2 is concentrated in regions with a lot of microtubules touching the cortex, i.e. the region where the microtubules of each aster meet at the cortex (Figure 12) (Lekomtsev et al. 2012; Miller 2011; Su et al. 2014). There it then activates RhoA, which leads to the formation of the contractile ring.

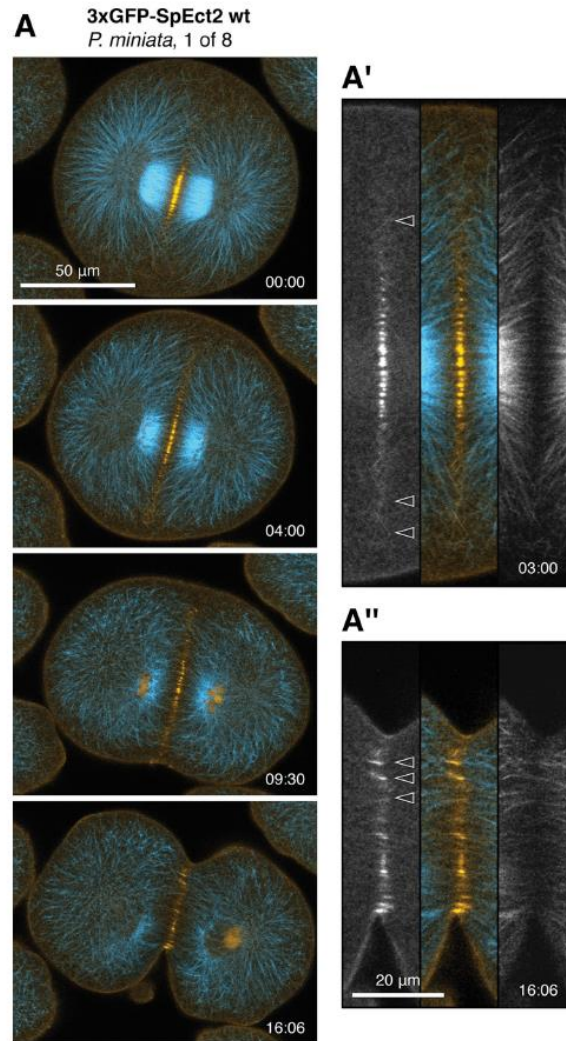


Figure 12: Ect2 is localised to the contractile furrow via microtubules. Sea urchin embryos showing Ect2 (gold) located to the tips of microtubules (blue), leading to its localisation at the furrow. Zooms in A' and A'' show overlaps of Ect2 and microtubules at different stages of furrow ingression. Republished with permission of American Society of Cell Biology, from (Su et al. 2014), permission conveyed through Copyright Clearance Center, Inc.

The GAPs, which in turn inactivate RhoA, are key for driving the flux of RhoA into the inactive form during cytokinesis. This flux through the active (GTP-bound) and inactive (GDP-bound) form is required for the success of cytokinesis (Miller & Bement 2009). There are two RhoA GAPs which have been implicated in cytokinesis – p190RhoGAP and the centralspindlin component MgcRacGAP. p190RhoGAP localises to the cytokinetic furrow and overexpression causes division failure (Su et al. 2009; Mikawa et al. 2008), and its role in cytokinesis in limiting RhoA activity is unambiguous. On the other hand, MgcRacGAP has been much more controversially discussed in the literature. This is partially due to the fact that, as the name suggests, MgcRacGAP functions (at least *in vitro*) specifically as a GAP against the GTPases Rac and Cdc42 and is inefficient as a GAP for RhoA (Touré et al. 1998). At the same time, MgcRacGAP is clearly a necessary component of the centralspindlin complex and artificial localisation to the cortex is sufficient to induce furrowing (D'Avino & Savoian 2006; Jantsch-

Plunger & Gönczy 2000), while knock-out leads to a much broader RhoA zone and cytokinesis failure (Yoshizaki & Ohba 2004; Miller & Bement 2009). While these *in vivo* experiments suggest that MgcRacGAP inactivates RhoA in the required manner, it is possible that this function is indirect, either through Ect2 localisation or through the other GTPase family members.

With this, the molecular toolbox which locally regulates the cortex to form the contractile ring during cytokinesis is fairly well established.

1.2.2 Redundancy in the spatial regulation of cytokinesis ensures cytokinesis success

In addition to the contraction of the contractile ring, it has long been proposed that to allow for cytokinesis, a relaxation of the polar regions of the cell is also necessary (Swann & Mitchison 1958). The original theory suggested that furrowing is achieved or at least allowed by a lessening of the membrane tension at the poles of the cells away from the cytokinetic furrow (Figure 13) (Gudejko et al. 2012).

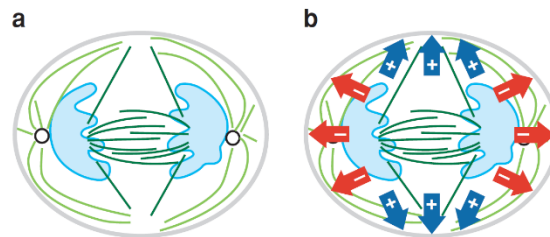


Figure 13: Different populations of microtubules in cytokinesis.

a) Cell in anaphase with chromatin mass in blue and microtubules in green. Astral microtubules (light green) and midzone microtubules (dark green) from two separate populations and contact the cortex at different points. b) Potential polar relaxation signal in red is delivered by astral microtubules, while equatorial stimulation signal in blue is delivered by midzone microtubules. Reprinted from (Eggert et al. 2006), copyright Annual Review of Biochemistry, 2006.

A number of works indicates that microtubule density, the connected differential cortical contractility and the resulting polar relaxation are important for cytokinesis (Glotzer 2004; Foe & von Dassow 2008), even though no molecular mechanism for this has been proposed. This is due to the fact that the molecular work has been focussed on the understanding of the cytokinetic ring and the cortical stimulation that induces furrowing.

These two potentially different signals are most likely born out of two populations of microtubules. The astral microtubules and the central spindle microtubules are these two signalling centres, whose differential importance remains not fully understood. It is very likely that the cortex, once it has been put in its receptive state by the cell cycle incorporates signals from both of these. In normal cells, the cytokinetic furrow may be positioned by a number of parallel signals, and this redundancy is important as the correct localisation of the division furrow is key for forming functional and equal sized daughter cells after division. The cortex seems to respond first to signals from the astral microtubules to initial

furrowing while the signal from the spindle midzone microtubules is required for sustaining the furrow and allowing completion of cytokinesis (Bringmann & Hyman 2005; von Dassow 2009).

To allow the cortex to flexibly react to these varied signals from the spindle, it as a whole has to be adapted to cytokinesis.

1.2.3 The cortex behaves as an excitable medium during cytokinesis

Therefore, the cortex of the whole cell undergoes drastic changes during C-phase, above and beyond those directly related to the formation of the cytokinetic ring. C-phase is the phase of the cell cycle in which cytokinesis takes place, and although it normally overlaps with late anaphase and telophase, it is designated as a separate phase of the cell cycle (Canman et al. 2000). This phase is defined by the cortex being in a division ready state in which it can respond to signals which induce furrowing. And while C-phase is normally a relatively short, it can be extended to last up to 1 hour by preventing completion of cell division using inhibitors (Straight et al. 2003; Martineau et al. 1995).

During this time the altered cortex state gives rise to interesting phenomena. One of these are rapid fluctuations of RhoA activity and actin polymerisation in an activator-inhibitor coupling, inducing fascinating motile patterns (Bement et al. 2015). These RhoA and actin waves are cell-cycle dependent and move across the whole cell cortex in very large cells, such as the *Xenopus* and starfish eggs (Figure 14). This indicated that the cell cortex in C-phase behaves as an excitable medium which shows local amplifications and fast reactivity (Newman 2009; Bement et al. 2015). This is likely beneficial for the cell by allowing quick adaptation to changing environmental circumstances and ensuring cytokinesis success.

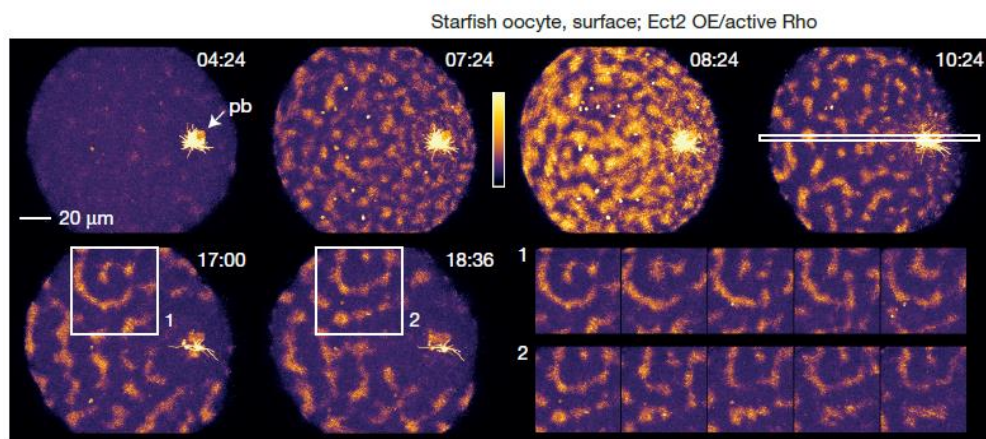


Figure 14: RhoA waves at the cortex during C-phase.

Active RhoA forms spiral patterns in the cortex during the time of C-phase – the temporal development of the patterns and change in signal intensity can be seen at the different time points. These patterns of RhoA activity move across the cell (as seen in the zoom-ins 1 and 2). The patterns are strengthened to these striking levels using Ect2 overexpression. Reprinted by permission from Macmillan Publishers Ltd: *Nature Cell Biology* (Bement et al. 2015), copyright 2015.

1.2.4 Cytokinesis is temporally regulated by Cdk1-cyclin B

Of course, cytokinesis has to be specifically regulated not only in a spatial dimension, with the determination of the position of the contractile ring, but it also has to be regulated in time. The temporal regulation of the cell division process is part of the cell cycle.

After the cell duplicates its DNA in S-phase the actual cell division process happens in M-phase. During this, the cell organises and then divides both its DNA and cytoplasm into two daughter cells.

M-phase consists of a number of well-defined subphases, termed prophase, metaphase, anaphase and telophase. During prophase, the chromosomes condense and cytoplasmic events prepare the cell for the cell cycle, by, among others, separating centrosomes. As prophase progresses into metaphase, the nuclear envelope breaks down, allowing access of the microtubules of the forming spindle to the chromosomes. Once all the chromosomes have assembled into the metaphase plate of the spindle, the cell passes into anaphase where the sister chromatids are separated towards the poles of the spindle. The two groups of chromosomes are enclosed in the forming daughter nuclei during telophase and the cells separate via cytokinesis. Cytokinesis normally overlaps with late anaphase and telophase (Cooper 2000).

The key regulator of M-phase is a protein complex originally termed MPF (mitosis promoting factor) made up of a kinase Cdk1 (cyclin-dependent kinase 1) and a regulatory protein cyclin B (Smith & Ecker 1971; Masui & Markert 1971). Cdk1-cyclin B controls all the changes that go along with mitosis and is, therefore, subject to a complex system of feedback loops to control its activation and inactivation (Lindqvist et al. 2009).

Cdk1 is regulated by phosphorylation and is present at constant levels throughout the cell cycle while cyclin B levels vary periodically. Cyclin B protein levels are controlled transcriptionally (Katula et al. 1997; Fung & Poon 2005) but once cyclin B is produced, it immediately binds to the Cdk1 protein. The complex is then held in an inactive state through two inhibitory phosphorylations at sites T14 and Y15.

The activity state of the Cdk1-cyclin B complex is controlled through the balance between the kinase pair Wee1/Myt1, which inhibits the complex, and the phosphatase Cdc25, which lifts the inhibition (Figure 15)(Morgan 2007). Once Cdk1-cyclin B is activated to a sufficient level, it can, in turn, phosphorylate Wee1/Myt1, leading to their inactivation, resulting in the auto-amplification of Cdk1 activity. The regulators themselves are controlled by a wide variety of inputs, such as the Plk1 and MAPK pathway (Lindqvist et al. 2009). But while the wider regulation is, of course, important for the precise timing of the cell cycle, for our purposes it is sufficient to focus on the inner feedback loop regulating Cdk1-cyclin B activity (Figure 15).

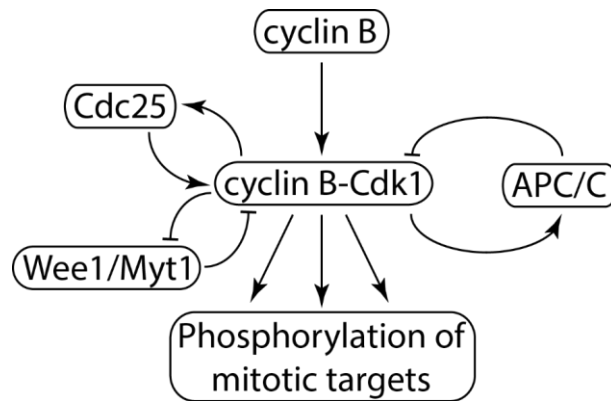


Figure 15: Regulation of Cdk1-cyclin B activity.

The Cdk1-cyclin B activity state is controlled by the balance of activation by Cdc25 and inhibition by Wee1/Myt1. Once activated above a threshold, Cdk1-cyclin B activates its mitotic targets via phosphorylation. At anaphase Cdk1-cyclin B is inactivated by APC/C which is regulated in its activity by Cdk1-cyclin B.

The activation of Cdk1/cyclin B is closely linked to its nuclear import in prophase which is important for the auto-amplification process (Hagting et al. 1999). Once levels of active Cdk1/cyclin B have reached a certain threshold, their many downstream effects become first visible with nuclear envelope breakdown (NEBD) mediated by phosphorylation of NE components (Macaulay et al. 1995; Peter et al. 1991). This is also commonly used as a marker for the start of metaphase.

Cdk1-cyclin B also drives other hallmarks of metaphase – such as cell rounding (Ramanathan et al. 2015), completion of chromosome condensation (Gavet & Pines 2010), spindle assembly (Wu et al. 2013) and ER/Golgi fragmentation (Yeong 2013).

The main cellular process in metaphase though is the formation of the spindle and alignment of the chromosomes at the metaphase plate. Once this process is completed and the spindle checkpoint is satisfied, the cell switches to anaphase. In this switch cyclin B levels again play the key role, although regulated in a different manner than during metaphase entry.

While phosphorylation is a widely used form of activation that is key to cell cycle control, it is by nature a very transient and reversible modification. To commit to the next stage in the cell cycle then, the cell requires a more drastic regulation, in the form of protein degradation. Cyclin B is degraded at anaphase exit by the APC/C (anaphase-promoting complex or cyclosome), which is an E3 ubiquitin ligase, binding ubiquitin chains to its target protein. These proteins are then targeted for destruction by the proteasome. APC/C activity itself is controlled via phosphorylation by Cdk1/cyclin B and by the spindle assembly checkpoint and the APC/C itself has a number of different substrates (Figure 15)(Pines 2006). The key substrates for the synchronicity of the events of anaphase are cyclin B and securin (Clute & Pines 1999; Hagting et al. 2002).

The degradation of securin allows the separation of the chromosomes while the degradation of cyclin B leads to the lifting of the cdk1-cyclin B imposed phosphorylations. The loss of these phosphorylations is responsible for the activation of the molecular cascade leading to cytokinesis and the changes in cortical contractility that go along with it.

1.3 SURFACE CONTRACTION WAVES

1.3.1 Surface Contraction Waves are division-associated cortical contractility events

In 1971, Koki Hara observed a curious phenomenon while studying dividing axolotl embryos, which continues to puzzle us to this day. Hara called what he observed surface contraction waves or SCWs (Hara 1971). These waves are observable as shifts in the pigmentation pattern of the embryo and changes in the cell shape. They precede each cell division in the early embryo and move across the whole cell in a circular pattern. Similar SCWs were observed in the embryos and eggs of a variety of other species, the most famous and well-studied example being in the *Xenopus laevis* embryo (Hara et al. 1980).

It may seem surprising that such an obvious movement of the cell had not been discovered earlier and that so little remains understood of its molecular nature. Especially as the large and abundant eggs of amphibians and echinoderms where SCWs are common, were the workhorses of early cell biology since the 19th century. The explanation lies within the duration of the waves, which last 5 to 10 minutes. This is just slow enough to make the SCWs very hard to notice by observation with the naked eye. Therefore, a true exploration of SCWs only began with the advent of time-lapse imaging or cinematography, as Hara called it in 1971.

1.3.2 Surface Contraction Waves are found in many species

If one looks at the literature, there are very few papers reporting surface contraction waves in eggs or embryos in species other than the ones mentioned above as major findings. But when one carefully reads old papers describing the behaviour of eggs and early embryos in a variety of species, mentions of shape changes, waves of surface stiffening and surface movements keep cropping up. These are indications for the presence of SCWs.

This has allowed me to infer that contraction waves are found in a wide variety of species (Figure 16). Interestingly, these species are spread throughout the animal kingdom. SCWs are for example found in very simple multicellular organisms, in the phyla of ctenophore and cnidaria, that is comb jellies and jellyfish respectively (Houliston et al. 1993).

In deuterostomes, SCWs are found in many species belonging to different phyla. SCWs are found in vertebrate species, many of the class of amphibia, including various species of frogs (Kubota 1967; Hara & Tydeman 1979), newts (Harvey & Fankhauser 1933; Selman & Waddington 1955; Sawai & Yoneda 1974) and axolotls (Hara 1971). A sister subphylum of the vertebrates, in the phylum of chordates, are the tunicates, where SCWs have been reported in a variety of species of sea squirts (Satoh & Deno 1984; Bell 1962; Sardet et al. 1989). The sister phylum of the chordates are the

echinoderms, where contraction waves are found in both sea urchins (Kojima 1962) and starfish (Hamaguchi & Hiramoto 1978).

There is, of course, the large superphylum of protostomes, in which there is very little evidence for SCWs. The two examples I found come from the Lophotrochozoan phylum, in the annelid *Tubifex* (Shimizu 1983), and in the *C. elegans* nematode (Fabritius et al. 2012).

Although evidence can be found for SCWs in these species, SCWs are surely not limited to these species. Given the wide evolutionary spread of SCWs exemplified above, it seems likely that upon investigation such waves could be found in many more species.

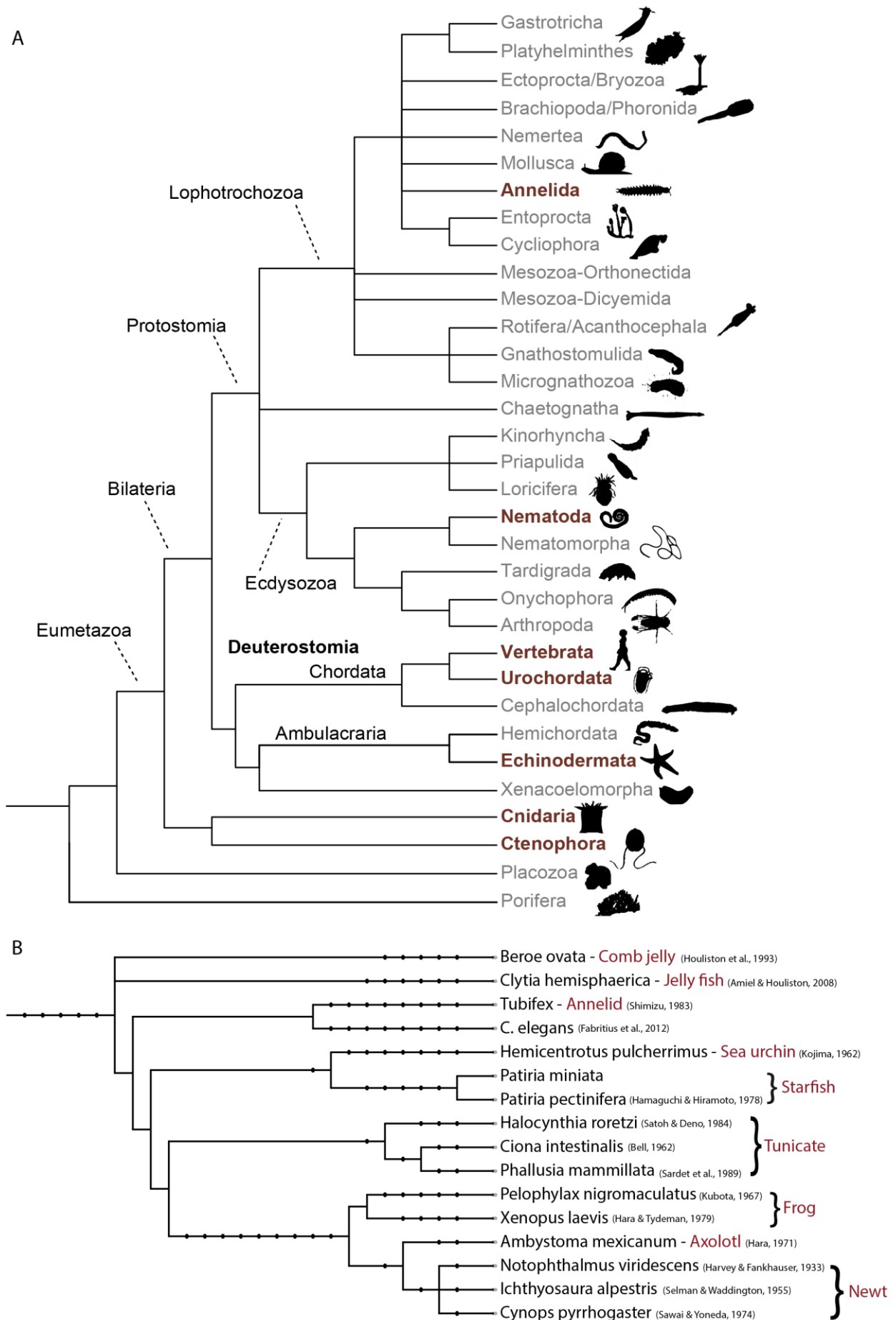


Figure 16: Phylogenetic tree of SCWs.

A) General tree of animal phyla, highlighting those in which SCWs are found. Figure modified from (Telford et al. 2015), reprinted with permission from Elsevier. B) Detailed phylogenetic tree of all species with reported SCWs. Tree generated at <http://phylot.biobyte.de/> (Letunic et al. 2012; Letunic & Bork 2007).

1.3.3 Surface Contraction Waves share a number of common characteristics

There are a few common characteristics that connect the SCWs in all these different species.

(1) They are found exclusively in large cells, namely oocytes and early embryos. All these cells are significantly larger than normal somatic cells. The sizes of cells with reported contraction waves range from the sea urchin with a diameter of 90 μm (Kojima 1962) to newt eggs with a diameter of 2 mm (Selman & Waddington 1955).

(2) Furthermore, SCWs always occur in the context of cell divisions. They have been reported to occur shortly before the cell division during both mitosis in the embryo and meiosis in the oocytes.

(3) As the SCWs are clearly cortical events, it is not surprising that they go along with a rise in surface tension or stiffness (Hara et al. 1980). How this cortical contractility in the SCWs is regulated and what cytoskeletal components are involved remains unclear. Some evidence suggests an involvement of microtubules (Quaas & Wylie 2002; Houliston et al. 1993) while others show an independence from microtubules (Hara et al. 1980) and implicate actomyosin contractility (Pérez-Mongiovi et al. 1998; Prodon et al. 2008; Christensen & Merriam 1982).

These factors make SCWs an interesting system to understand the regulation of cortical contractility by the cell cycle in large cells.

1.3.4 A number of functions have been proposed for Surface Contraction Waves

While SCWs have been described phenomenologically, their function remains unclear in most systems. Potential functions can arise from two characteristics of the waves. The first is the potential generation of force or pressure implied by the contractility and change in cell shape.

This force generation hypothesis has been suggested to assist the cell division process in both meiosis in the starfish (Hamaguchi & Hiramoto 1978) and mitosis (Yoneda & Dan 1972; Sawai 1982), although this has never been conclusively shown in either system.

Secondly, apart from the shape changes the SCWs go along with movements of the cytoplasm (Hamaguchi & Hiramoto 1978), although a causal link between the two processes is not clear. This cytoplasmic flow in the developmental context in which the SCWs occur, led to the hypothesis that SCWs serve to localise some developmental determinants. This has been indicated in the *Xenopus* embryo for the localisation of germplasm (Quaas & Wylie 2002) and for cER-mRNA domains in Ascidians (Figure 17) (Prodon et al. 2008; Prodon et al. 2005). As a specific inhibition of the

contractions has not been described, a proof of a link between the SCWs and the observed localisation defects has not been reported and their developmental consequences remain to be explored.

Mitochondria: DNA

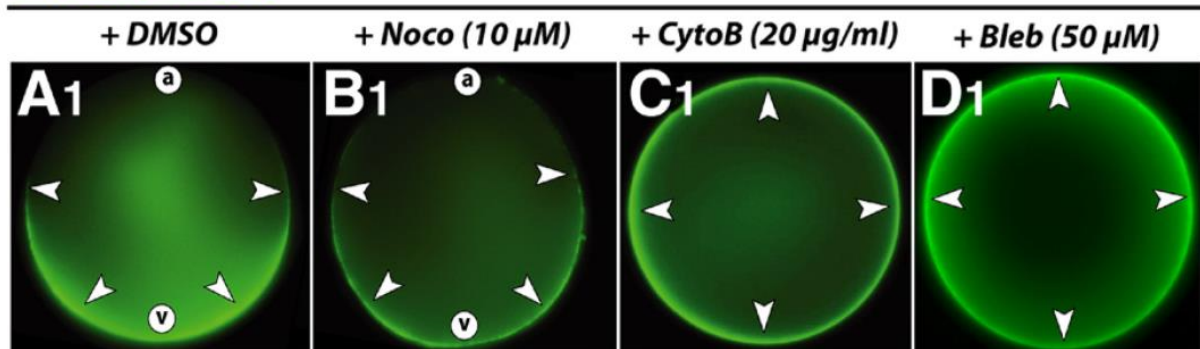


Figure 17: The potential function of the SCWs in controlling embryonic polarisation.

A) Mitochondria (green) are localised in a polarised manner across the ascidian eggs. B) Treatment with microtubule inhibitor Nocodazole did not affect the localisation, while manipulations of both actin (C) and myosin (D) lead to a loss of polarisation, indicating a role of actomyosin contractility in the localisation. Republished from (Prodon et al. 2008), with permission from Elsevier.

1.3.5 Surface Contraction Waves in the *Xenopus* embryo are driven by trigger waves

The best-researched example of SCWs are the ones observed during the early embryonic division of the *Xenopus laevis* embryo. In this system two contraction waves, termed SCWa and SCWb, pass across the cell surface visible through a shift in the pigment pattern (Hara et al. 1980). Both of these waves start at the animal pole of the egg and spreads in a circular pattern across the cell, with a fixed time delay between the two and progress across the cell at a speed of 60 $\mu\text{m}/\text{min}$ (Figure 18) (Hara et al. 1980; Chang & Ferrell 2013).

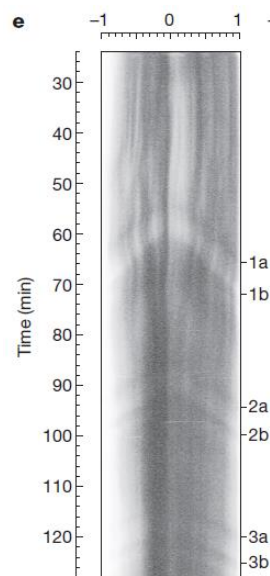


Figure 18: SCWs in the *Xenopus* embryo.

Kymograph of the surface pigmentation pattern of an artificially activated *Xenopus* egg. It shows three pairs of SCWs (1a&1b etc.), going along with 3 rounds of the cell cycle. Reprinted by permission from Macmillan Publishers Ltd: Nature (Chang & Ferrell 2013), copyright 2013.

These SCW reflect switching of the cytoplasm between different cell cycle states going along with each round of cell division (Hara et al. 1980; Pérez-Mongiovi et al. 1998). Specifically, the SCWa correlates with entry into mitosis, while SCWb is associated with mitotic exit (Rankin & Kirschner 1997). This explains why even though both waves were originally termed surface *contraction* waves, the SCWa is, in fact, a wave of relaxation with the cortex softening while the SCWb is a true contraction wave with an increase in surface tension (Yoneda et al. 1982).

While SCWs were first observed right before the first embryonic division, they are independent of fertilisation and even the nuclear content of the egg, as they also occur in artificially activated (i.e. non-fertilised eggs) and de-nucleated eggs (Hara et al. 1980). This underscores the link between the cell cycle and the contraction waves, as the cell cycle oscillation run independently of these factors as well.

The mechanism by which the cell cycle activation is spread across the very large *Xenopus* cell was long a mystery but recent reports have provided a mechanistic explanation (Chang & Ferrell 2013; Ishihara et al. 2014). They showed that the signal transmission in *Xenopus* is driven by a phenomenon called a trigger wave. Diffusion, the classical mechanism for signal spreading, is distinctly too slow in such a large cell to allow efficient synchronisation of the cell cycle processes across the whole cell. The proposed trigger wave or chemical reaction waves can spread the activity across the cytoplasm much faster. This is achieved by local mixing of the cytoplasm by diffusion, which pushes the activity above a certain threshold leading to full activation of one area of cytoplasm. This activity then mixes into the closely neighbouring area, which in turn switches to an activated state. And thus, the activity is transmitted fast across large distances. To allow for such behaviour, the system in which it takes place has to be an excitable medium and locally amplify the active state of the system. The cell cycle regulation of Cdk1-cyclin B activity is exactly such a system. To visualise the trigger wave spreading over large distances Chang and Ferrell placed nuclei in *Xenopus* egg extract that goes through a number of cell cycles and observed the behaviour of the nuclei during these cycles. The nuclei break down at the start of mitosis and reform at its end, and both breakdown and reformation happen in a wave over large distances (Figure 19).

The mechanism by which a trigger wave of cell cycle activity causes the cortical contractile behaviour remains an open question.

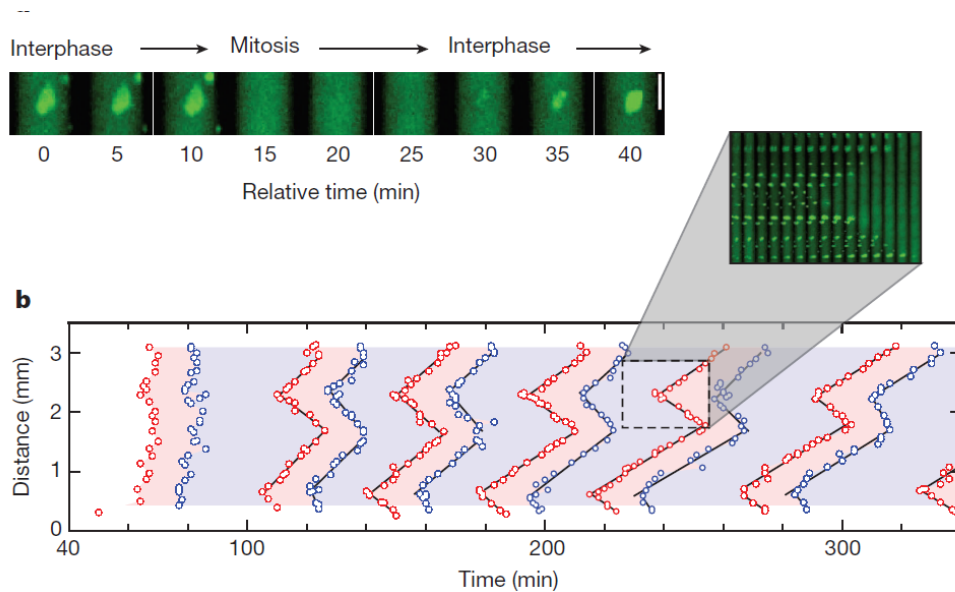


Figure 19: Trigger waves of the cell cycle.

The cell cycle state is measured by the proxy of nuclear envelope breakdown and reformation in cycling *Xenopus* egg extract. b) The signal for nuclear envelope breakdown (red) and reformation (blue) spreads across long distance with constant speed, indicating trigger wave behaviour. Reprinted by permission from Macmillan Publishers Ltd: *Nature* (Chang & Ferrell 2013), copyright 2013.

1.4 STARFISH OOCYTES SERVE AS A MODEL FOR THE STUDY OF SURFACE CONTRACTION WAVES

1.4.1 Starfish oocytes in meiosis exhibit contraction waves

Starfish oocytes are another system which exhibits striking contraction wave alongside their meiotic divisions. These were first described by Hamaguchi and Hiramoto in 1978 in the starfish *Patiria pectinifera* (Hamaguchi & Hiramoto 1978), where both the cell shape changes as well as the concomitant protoplasmic movements were observed (Figure 20). This resulted in the first detailed description of the SCW phenomenon for any organism.

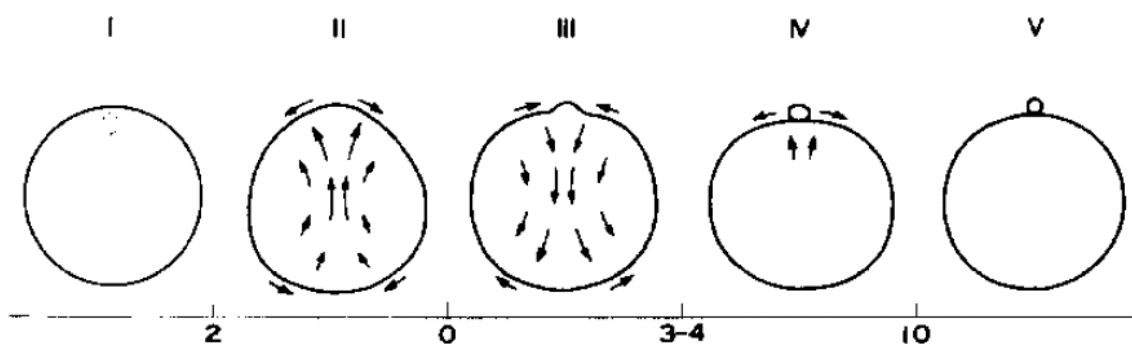


Figure 20: The SCW in the starfish oocyte

An early description of the shape change and cytoplasmic movements occurring during the contraction wave in the starfish oocyte. Reprinted from (Hamaguchi & Hiramoto 1978), with permission from Elsevier.

The contraction waves in the starfish oocyte occur immediately before each of the two meiotic divisions that the oocyte undergoes during the course of maturation. At the same time, the work by Hamaguchi and Hiramoto also proposed a function for the contraction wave, suggesting that they are

functionally linked to polar body formation, the specific form of asymmetric cell division occurring in meiosis. This link was proposed due to the close temporal link between the two events and intuitive appeal but has not been investigated.

1.4.2 Starfish oocytes are highly specialised cells ideal for molecular imaging studies

A number of the characteristics of the starfish oocyte make it ideal to use in investigating SCWs on a molecular level.

The surface contraction wave at the first meiotic division is very pronounced. The system is experimentally easy to handle as meiosis is relatively quick in these cells, lasting only around 90 min in total and it can be induced by the experimenter via the addition of a hormone.

Furthermore, its size and transparency make the oocyte ideal for fluorescence microscopy, which is a key methodology for identifying molecular players. The oocytes are also relatively non-sensitive to light exposure, allowing continuous imaging throughout the whole division process. Given their natural habitat in the open sea, the oocytes are additionally very sturdy which allows a variety of physical manipulations, such as centrifugation (Yoshikawa 1996; Nemoto et al. 1980) and mechanical constriction (Shoji et al. 1978), adding to the toolbox of biochemical manipulations.

The starfish oocytes of the species *Patiria miniata* are the model system used for this study and I will in the following introduce these cells in a bit more detail.

The oocytes are large cells, around 180 μm in diameter, with the nucleus localised at one point of the cortex (Figure 21) (Terasaki et al. 2001). This gives the oocytes an intrinsic polarity and the point where the nucleus is anchored is called the animal pole while the opposite point is called the vegetal pole. The nucleus is held at this position by microtubules nucleated from the centrosomes which are positioned at the animal pole (Miyazaki et al. 2000).

The oocyte reaches its extraordinarily large size due to its large storage of both nutrients and pre-synthesised proteins which are required for the development of the embryo. The nutrients are stored in the form of yolk platelets, roughly 1-2 μm in diameter (Terasaki 2006). The yolk is produced during the growth phase of the oocyte that precedes oocyte maturation (Takahashi & Kanatani 1981).

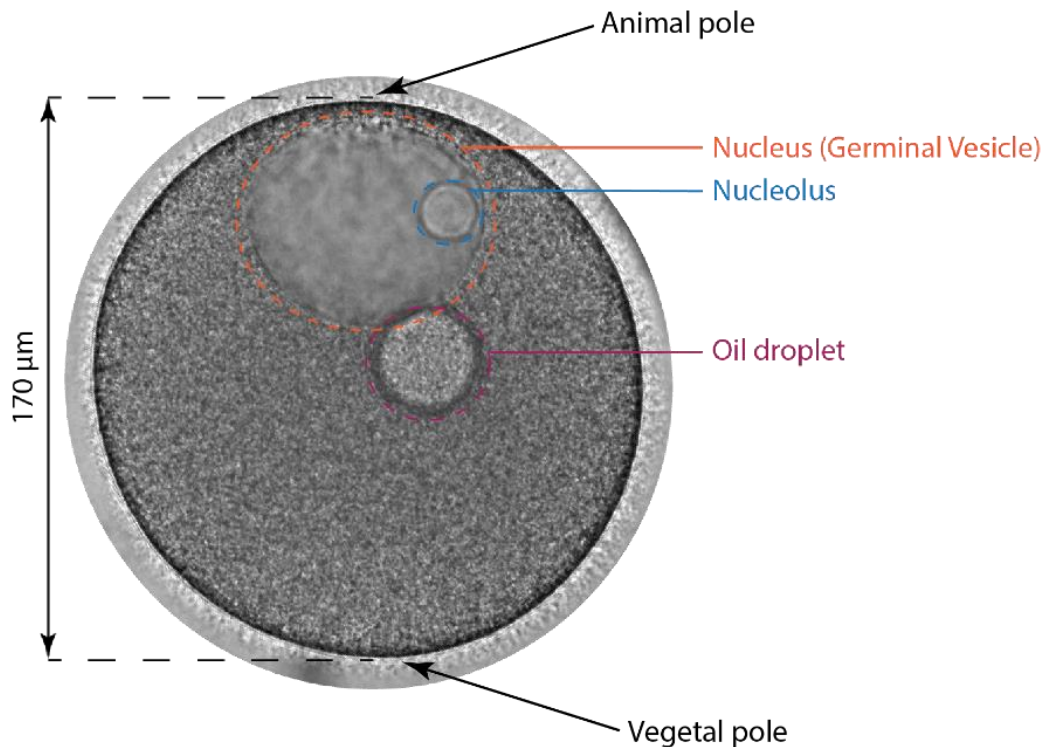


Figure 21: An immature starfish oocyte with important cellular structures labelled.

The oocytes are arrested, tightly packed in the ovaries of the starfish, in prophase of meiosis I and can be easily isolated from there in large numbers. The oocytes begin their maturation upon stimulation by the hormone 1-Methyladenin (Kanatani et al. 1969). In the natural process where maturation is induced in the ovary, the oocytes exhibit the classical metaphase I arrest (Oita et al. 2004; Harada et al. 2003), that oocytes of many other animals share (Yamashita 1998). While in most other animals this arrest is lifted via fertilisation, in starfish it is lifted through spawning of the oocytes into seawater and the resulting pH change (Oita et al. 2004; Harada et al. 2003). When oocytes are artificially induced to undergo meiosis in sea water, there is no metaphase I arrest as the conditions are already fulfilled for the completion of meiosis (Kishimoto 1998).

While starfish oocytes are naturally fertilised around metaphase I of meiosis (Nomura et al. 1991), they can complete the whole division process without fertilisation (Matsuura & Chiba 2004), so meiosis can be studied while disregarding the fertilisation process.

1.4.3 Meiosis is a specialised form of cell division

Meiosis is a very specific type of cell division that occurs only during the generation of the gametes for sexual reproduction. It is a reductive division, which produces both haploid sperm and oocytes. But the division process in these two cases is very different, given that a $4n$ spermatocyte gives rise to four $1n$ sperm while the $4n$ oocyte gives rise to only one $1n$ mature egg. The rest of the genomic content of the oocyte is discarded into the polar bodies (see Figure 22). The main difference between mitosis

and meiosis is the lack of S-phase between meiosis I and meiosis II and extensive recombination with the connected suppression of sister chromatid separation during meiosis I.

I will in the following focus on oocytes and their cell cycle adaptations while disregarding the mechanism of DNA recombination in meiosis and spermatogenesis.

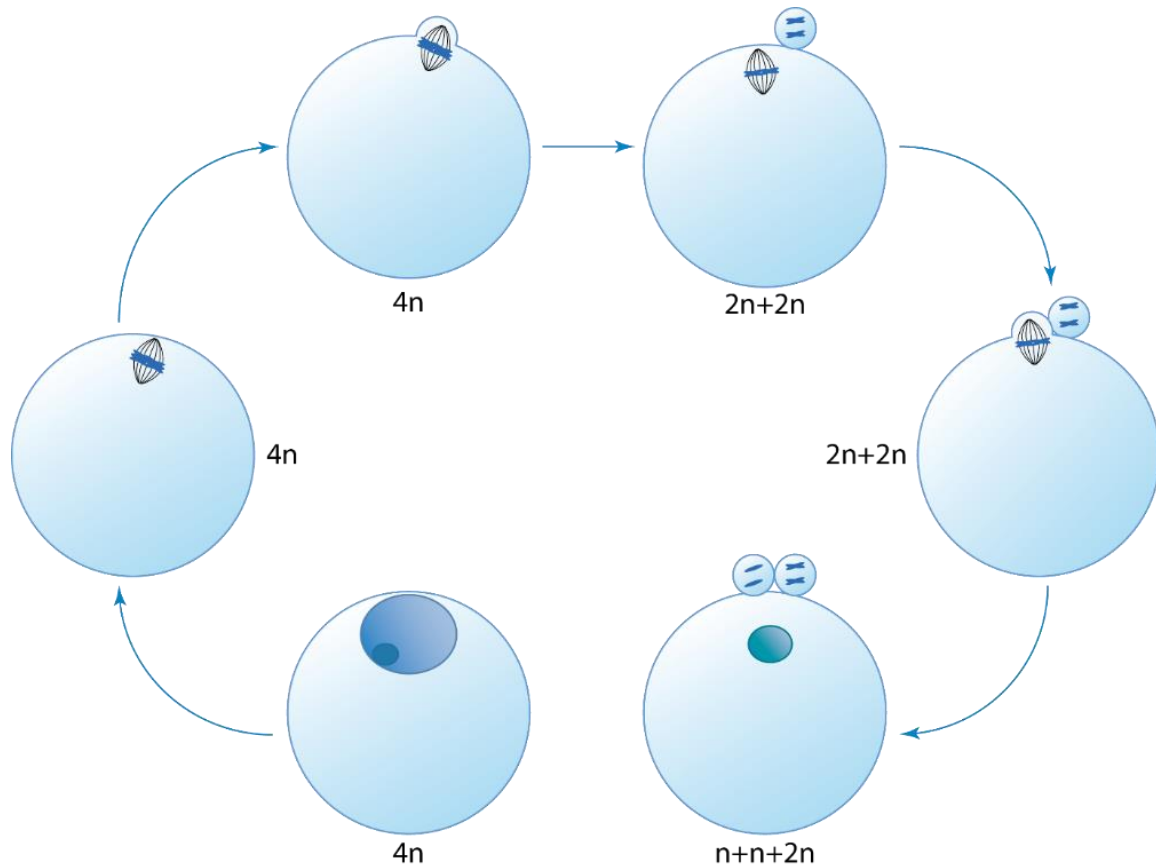


Figure 22: Meiotic cell cycle in the oocyte.

A mature $4n$ oocytes forms a spindle and cell division takes place, giving rise to a $2n$ oocyte and a $2n$ polar body. The oocyte divides again, extruding a $1n$ polar body. This division cycle results in a mature haploid egg. Figure modified from (Borrego Pinto 2015).

Oocytes are commonly arrested for long periods in prophase of meiosis I so the start of the cell division process is named meiotic resumption. Meiotic resumption is in the starfish oocyte very well understood on a molecular level (Figure 23) (Kishimoto 2011). It happens in response to an external hormone signal given by the tissue surrounding the oocytes. In the same manner as in mitosis, entry into meiosis requires activation of Cdk1-cyclin B. This is achieved following hormone stimulation through the Akt/PKB pathway, which inhibits the Cdk1 inhibitor Myt1 and activates the activator Cdc25 (Figure 23) (Okumura et al. 2002).

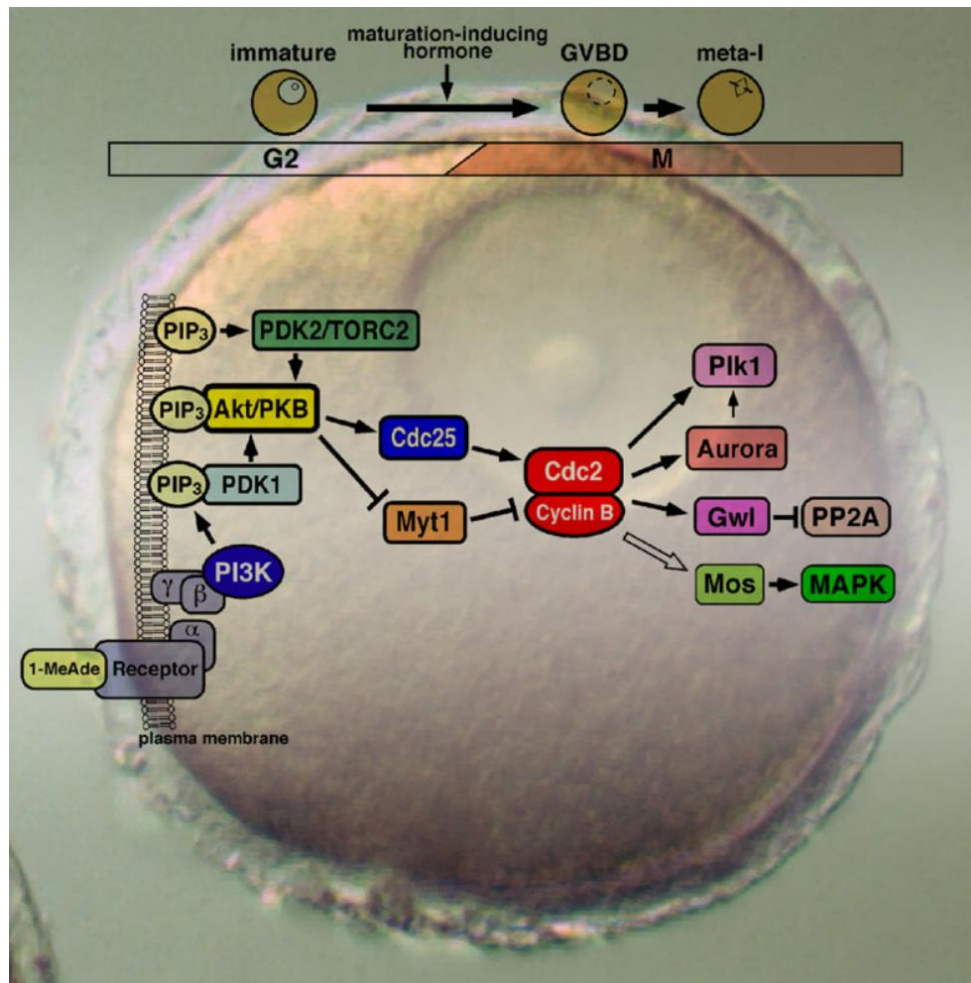


Figure 23: Meiotic resumption in the starfish oocyte.

The 1-Methyladenin hormone signals through a G-protein receptor, leading to the activation of Akt/PKB. This, in turn, leads to the activation of Cdk1-cyclin B (here Cdc2-cyclin B) via inhibition of Myt1 and activation of Cdc25. The activation of Cdk1-cyclin B leads to the start of meiosis and activates downstream targets, including Plk1, Aurora and Mos. Reprinted with permission from John Wiley and Sons: *Molecular Reproduction & Development* (Kishimoto 2011), copyright 2011.

In comparison to meiosis I, meiosis II is a much quicker process which starts immediately after the completion of meiosis I without an intermediated S-phase, but the underlying molecular network is identical. The quick transition between meiosis I and meiosis two is controlled by Mos which prematurely upregulates Cdk1/cyclin B levels after metaphase I to prevent S-phase (Figure 24) (Furuno et al. 1994). In starfish, it was shown that Mos is the master regulator of meiosis and that expression of Mos in mitotic cells induces meiotic-style divisions (Tachibana et al. 2000). Furthermore, overexpression of Mos in oocytes leads to many rounds of meiosis (Figure 24)(Dumollard et al. 2011).

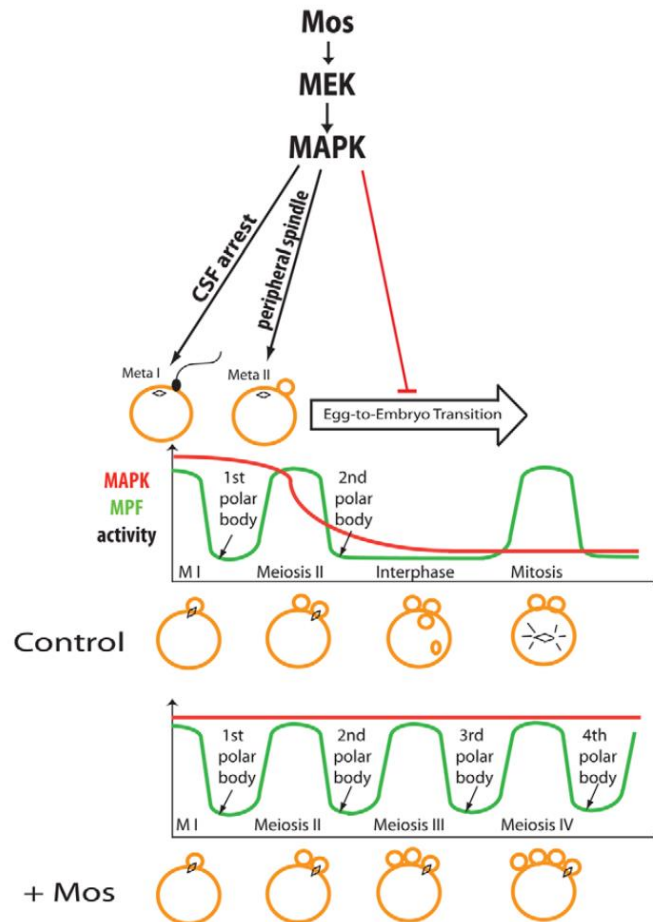


Figure 24: Mos is the master regulator of meiosis.

Mos activity controls meiosis via the MAPK signalling pathway, which induces upregulation of Cdk1-cyclin B activity (here MPF – green) after meiosis I. When Mos is overexpressed (bottom panel) MAPK activity remains high and MPF activity cycles multiple times, resulting in multiple meioses. Reprinted from (Dumollard et al. 2011), with permission from Company of Biologists: Development.

1.4.4 Polar body formation is a specialised form of cytokinesis

Oocyte meiosis goes along with a specialised form of cell division leading to the formation of the polar bodies. It is a hugely asymmetric form of division, even compared to other forms of asymmetric divisions, and has been a focus of research interest since it was first described by Carus in 1824 (Schmerler & Wessel 2011).

This highly asymmetric division is required to allow the oocyte to reduce its genomic content without losing too much of the cytoplasmic content containing precious nutrient. This is achieved by minimising the cytoplasm in one of the daughter cells. The size difference between oocyte and polar body is therefore especially pronounced in animals that undergo *ex utero* development, where the embryo relies solely on its maternal energy stores for early development (Liu 2012).

In animals with *in utero* development, the size difference is not a requirement. This was shown in the mouse system, where an oocyte with half its normal cytoplasmic volume, as would arise after a

symmetric division, can still develop normally (Wakayama & Yanagimachi 1998). At the same time, it has been suggested that the polar body's small size is important to prevent the formation of an additional competing zygote as would result from fertilisation of a larger polar body (Otsuki et al. 2011). This process has been known to happen in humans and result in unviable twins (Bieber et al. 1981). It has also been suggested that asymmetry can assist in ensuring proper chromosome division and preventing aneuploidy (Cortes et al. 2015).

The polar bodies that form during meiosis are usually not destined for much after their formation and in most organisms quickly apoptose. Although in some special cases, they have additional functions during development. They play an important role in parthenogenesis in insect species (Strand & Grbic 1996), and form important nourishing and protective tissues in scale insects (Normark 2004; Ross et al. 2010) and parasitic wasps (Strand & Grbic 1996). On the other hand, modern screening technology often employs polar bodies for diagnosis in IVF treatments (Verlinsky & Rechitsky 1999).

1.4.4.1 *Polar body formation is distinct from standard asymmetric divisions*

Although polar body formation is commonly classified as a form of asymmetric cell divisions, I would argue that this categorisation is in fact neither strictly correct nor helpful for our understanding of either process.

Standard asymmetric divisions are rare compared to symmetric divisions but play crucial roles during development (Betschinger & Knoblich 2004). The asymmetry in these cases is a size inequality but, more importantly, an inequality of their cytoplasmic content and developmental potential. The classical systems in which asymmetric cell divisions are studied are the *Drosophila* neuroblasts and the first embryonic division of the *C. elegans* embryo (Betschinger & Knoblich 2004). Surprisingly in these systems the spindle originally forms in the centre of the cell and only at the end of anaphase the posterior spindle pole is pulled off-centre (Albertson 1984; McCarthy Campbell et al. 2009). Alternatively, the asymmetric placement of the spindle can be achieved by forces generated by asymmetric cortical contractility which pushes the cell around the spindle (Ou et al. 2010). In *Drosophila* neuroblasts, the mechanism for driving asymmetry appears to be unequal microtubules elongation (Kaltschmidt et al. 2000; Yu 2003).

In comparison to these standard asymmetric divisions, polar body formation is of course not less asymmetric – rather the opposite. In standard asymmetric divisions the daughter cells have only slightly different volumes, in *C. elegans* embryos, for example, a ratio of roughly 1/3 to 2/3 between the daughter cells is observed. In polar body formation, on the other hand, the daughter cells can be orders of magnitude different in volume. For example in the *Xenopus* oocyte, the polar body is roughly 10 µm in diameter while the oocyte is 1 mm in size. In standard asymmetric divisions, the asymmetry

is much more on a functional level than on the size level, with the distribution of determinants being key.

There is also a big mechanistic difference between the actual division processes in the two cases (Figure 25). In the normal asymmetric division, the spindle is positioned in the middle of the cell and is only at a late stage shifted slightly to one side. In the case of the polar body formation, the spindle is either formed already off-centre (in starfish, *Xenopus* etc.) (Lenart et al. 2005) or is transported there early in the division process (in mouse) (Chaigne et al. 2013).

Furthermore, in standard asymmetric divisions, the contractile ring is still formed above the middle of the spindle without the cell undergoing any shape changes prior to constriction. In polar body formation, on the other hand, the cells first form the polar body by protruding a bulge into which the spindle subsequently moves, before the contractile ring forms above the spindle midzone at the base of the protrusion (Figure 25).

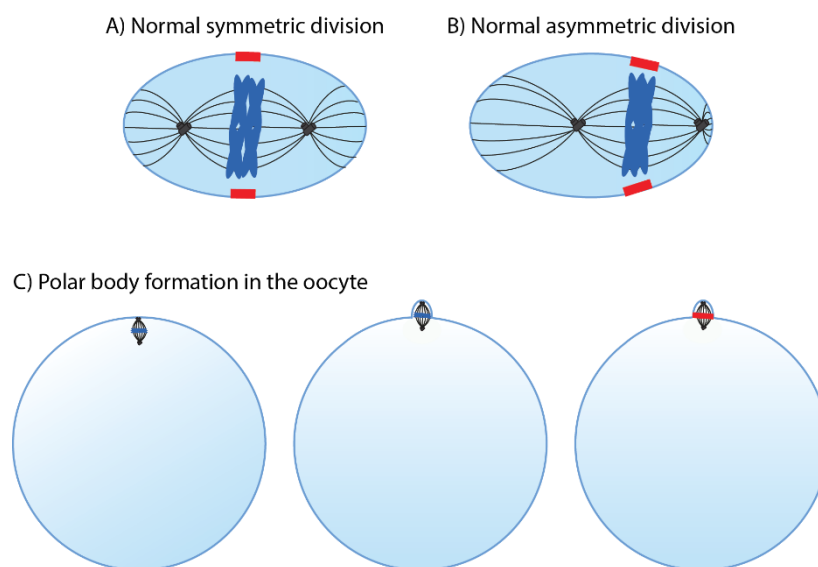


Figure 25: Geometry of the cell division in symmetric and asymmetric divisions. A) In a symmetric cell division the contractile ring (red) forms in the middle of the cell above the spindle midzone. B) In the standard asymmetric division the spindle is positioned slightly off-centre and the contractile ring forms above the spindle midzone. C) In polar body formation, the spindle is located strongly off-centre and the cell protrudes the polar body before cytokinesis can take place. Cell sizes not to scale.

1.4.4.2 Multiple mechanisms have been proposed for polar body protrusion

Polar body formation is, therefore, a 2-step process, consisting of the formation of the protrusion and the cutting off of that protrusion.

All data present is consistent with the hypothesis that the actual contractile ring in polar body is very similar, if not identical, to that formed in symmetric cell division (Maddox et al. 2012; Liu 2012). Therefore, the main mechanistic question concerns the formation of the protrusion.

The by far most widespread hypothesis concerning the mechanism of protrusion formation is the pressure model, which has a large intuitive appeal. It dates back almost all the way in polar body research, with the oldest proposal of this mechanism made by Conklin in his 1902 investigation of egg maturation in the sea snail *Crepidula* (Conklin 1902). He proposed that the polar body is pushed out by cytoplasmic pressure or flow at the site where the cortex is weakest.

This idea has remained popular to this day (Sato et al. 2013) and in the case of the starfish oocyte has been mechanistically linked to the surface contraction waves. When Hiramoto and Hamaguchi described the SCWs in starfish oocytes as preceding the polar body formation, they suggested that the waves built up the force necessary to push out the polar body (Hamaguchi & Hiramoto 1978).

This pressure model was strongly argued against by a series of detailed experiments performed by Ray and Barbara Rappaport in the starfish oocyte (Rappaport & Rappaport 1985). They came to the conclusion that rather than the polar body forming at the weakest site of the cortex in a global pressure mechanism, the protrusion formed in a very local mechanism at a strong cortex site. This local stimulation hypothesis was based on a large number of physical perturbations of the oocyte. They showed that moving the spindle to a new cortical site lead to the formation of the polar body at the new site, showing that there was no predetermined weak site of the cortex. Furthermore neither flattening of the oocyte, osmotic swelling nor sucking on the forming polar body lead to increases in polar body size as would have been expected by the pressure hypothesis. And a release of potential pressure by injuring the oocyte close to the polar body did not block protrusion formation.

Which of these two models – global pressure with local weakness or local stimulation – correctly described the mechanism behind polar body protrusion has remained unresolved to this day.

The molecular mechanism that drives protrusion formation too remains a little-explored area, but recent work has strongly implicated the GTPase Cdc42 in this process, at least in *Xenopus* oocytes. Cdc42 is closely related to RhoA, which is the key GTPase in cytokinesis. Cdc42 is thought to bring about polar body protrusion by the activation of the Arp2/3 complex which nucleates branched actin (Ma et al. 2006). When Cdc42 is inhibited, the protrusion no longer forms and while the contractile ring still forms normally at the cortex, it contracts over nothing and polar body formation fails (Leblanc et al. 2011). So Cdc42 and RhoA in polar body formation form two concentric zones of activity around each other, leading to the assembly of different actin structures which result in protrusion and cytokinesis respectively (Figure 26) (Zhang et al. 2008).

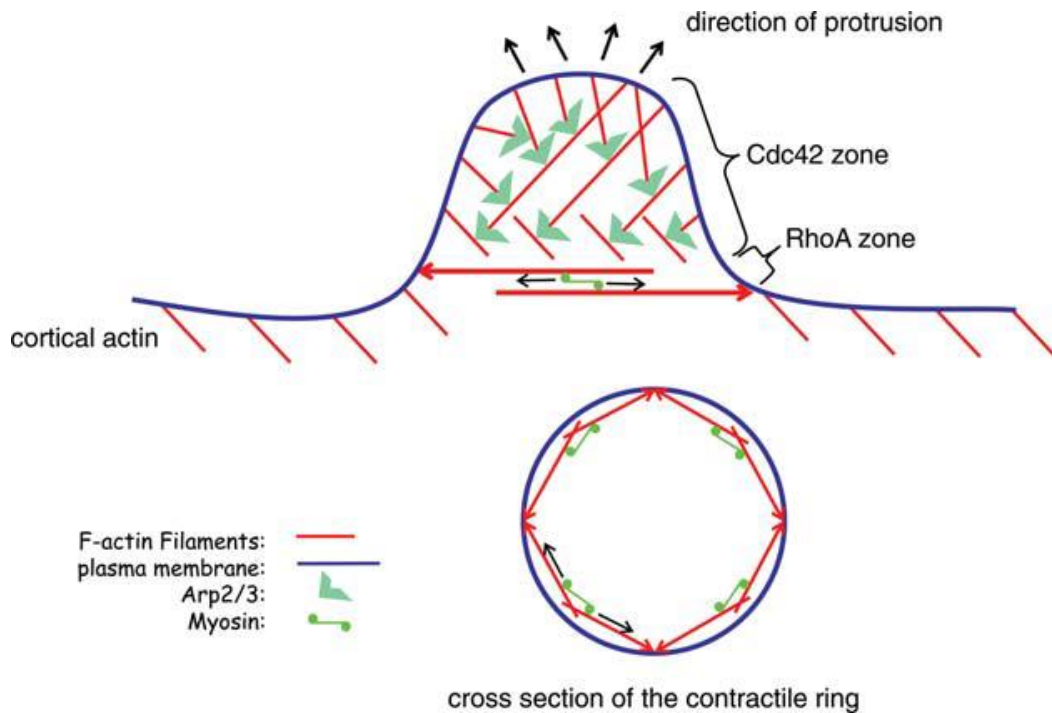


Figure 26: Polar body protrusion.

Protrusion formation is driven by Cdc42, activating Arp2/3-driven actin polymerisation, in the *Xenopus* oocyte. RhoA activity results in the formation of the contractile ring and activation of myosin II. Reprinted from (Leblanc et al. 2011) by permission of Oxford University Press.

Evidence from a number of other systems also indicates an actin-rich protrusion overlying the future polar body, strengthening this hypothesis (Pielak et al. 2004; Dorn et al. 2010; Deng et al. 2007). This suggests that the cortex is not likely to be weaker at the site of polar body formation, but it is interesting to speculate that the cortex in this area might be less contractile. If actin here is indeed nucleated by Arp2/3, it is highly branched and highly dynamic, and thereby potentially a less efficient substrate for myosin II contractility, compared to the straight formin-nucleated actin of the contractile ring. This could give rise to potential mechanical differentiation of this small cortex regions leading to polar body protrusion.

2 AIMS

Cell division is key for all life and it is a complex process in which spatially and temporally tightly coordinated changes to the actomyosin contractility of the cortex physically separate the two daughter cells. The regulation of the behaviour of the cortex during division is important for successful divisions as the cortex undergoes a series of complex changes to accommodate the changing cell shape and produce the required force. Apart from cytokinesis, the regulation of cortical contractility is a general feature of many cellular processes, including cell migration and shape changes.

To explore the regulation of cortical contractility during cell division, I specifically studied a phenomenon termed surface contraction waves. These waves are striking changes in cortical contractility, which occur in very large cells, in close correlation with the cell division process. Surface contraction waves have been observed in diverse animal phyla, from one the most basic metazoan life forms of cnidarian to vertebrates, but their underlying mechanism is not known. They offer a chance to study the regulation of cortical contractility in general and the link between the cell cycle and contractility in particular.

The general aim of my PhD project was to reveal the molecular regulatory pathways underlying surface contraction waves and understand how these signalling networks can spatially and temporally pattern this complex cellular behaviour.

The model system I used to study the surface contraction waves were starfish oocytes, which exhibit dramatic contraction waves that can be imaged at high spatial and temporal resolution in the transparent oocytes. Indeed, surface contraction waves were first described in the starfish oocyte almost 40 years ago (Hamaguchi & Hiramoto 1978), and with the molecular tool and imaging technology now available they provide an exceptional opportunity to analyse this fundamental yet poorly understood phenomenon.

Specifically, I focused on the following two main questions:

1) What are the molecular mechanisms of contraction and its regulation underlying surface contraction waves?

Although surface contraction waves have been described in several species, no molecular details had previously been identified. But of course, a detailed knowledge of the molecules that drive contractility and the upstream regulatory pathway is required for a broader understanding of the process. Therefore, as a necessary first step, I set out to characterise the molecular regulatory pathway driving the contraction wave. I took a candidate approach and used the literature to identify proteins involved in cortical contractility in other physiological contexts and tested their role in the regulation of the contraction wave. To this end, I used live-cell imaging of the starfish homologs of these

regulatory and contractile proteins to follow their localization to the contraction wave, and, where available, I used small molecule inhibitors against some of the candidate proteins.

Additionally, the size of the cell and the dynamic motion of the contraction across the cell allowed me to explore the regulatory pathway that drives contractility from a different perspective compared to that commonly used in the literature and elucidates feedback mechanisms within the regulatory pathway.

2) What is the link between the cell cycle processes and the contraction wave?

Data from previous studies indicates a link between cell cycle progression and the contraction wave (Rankin & Kirschner 1997; Chang & Ferrell 2013; Hara et al. 1980). However, how these two processes are coupled in space and time and at the molecular level was not known. As a first step to answering this question, I visualised the spatial and temporal pattern of key cell cycle components in relation to the contraction wave. Additionally, I locally manipulated the activity of cell cycle kinases, and used other chemical and physical manipulations to observe the effects on the direction and speed of the contraction wave, to understand how the dynamic nature of the contraction wave arises from cell cycle regulation.

In summary, I present here a comprehensive model for the molecular mechanism controlling surface contraction waves in space and time. My data provides an explanation for the widespread phenomenon of surface contraction waves in oocytes, and at the same time reveals novel internal feedback mechanisms within the conserved molecular network regulating cortical contractility.

3 MATERIALS AND METHODS

3.1 STARFISH HANDLING

3.1.1 Animals

All the work presented herein was performed using the oocytes of the bat star *Patiria miniata*. These animals originate from the North American coastline of the Pacific Ocean. We receive shipments of *Patiria miniata* from Southern California Sea Urchin Co. (Corona del Mar, CA), Marinus Scientific LLC (Newport Beach, CA) and Monterey Abalone Company (Monterey, CA) who collect the animals directly from the ocean. In the lab, the animals are maintained in seawater tanks at 15 °C, salinity of 4 ‰, pH 7.8. The animals are fed with shrimp every 2-3 days.

3.1.2 Oocyte and sperm collection and maintenance

To collect the oocytes from the starfish a small hole is made laterally on the dorsal side of an arm of the animal using a surgical biopsy puncher (Miltex). Through this hole, a segment of the ovary can be extracted. The ovary is placed in calcium-free seawater with 50 mM L-Phenylalanine (Sigma) (pH 8) for 15 – 20 min. The treatment with calcium-free seawater leads to the shedding of the follicle cells, which surround the oocyte, while the L-Phenylalanine acts as a hormone homolog, blocking spontaneous maturation which can occur during collection. The ovary is subsequently transferred into filtered sea water (FSW) containing 100 µM Acetylcholine (Sigma-Aldrich). This leads to the contraction of the ovary and the subsequent extrusion of the oocytes into the sea water. The thus retrieved oocytes are transferred into pure FSW and maintained at 14 °C in plastic petri dishes.

The oocytes were always used within at most 3 days after collection.

Oocyte maturation was induced by adding the hormone 1-Methyladenin (1-MA) to the FSW at a concentration of 10 µM.

Sperm is collected from the animal by similarly making a small hole and extracting some testis tissue using forceps and placing the tissue in an Eppendorf tube which is kept on ice or at 4 °C. The tissue is kept as dry as possible to avoid premature activation of the sperm. Before fertilisation, sperm is activated by mixing a small piece of testis with FSW at 1:8000. Sperm quality is visually assessed and sperm is added to mature oocytes at low concentration to avoid polyspermy.

Ca-free seawater

437	mM	NaCl
9	mM	KCl
22.9	mM	MgCl ₂ x 6 H ₂ O
25.5	mM	MgSO ₄ x 6 H ₂ O
2.1	mM	NaHCO ₃

3.2 CLONING AND MOLECULAR WORK

3.2.1 Cloning and construct preparation

To generate the constructs use for the experiments described here I used the following general strategy. Firstly, I identified the amino acid sequence of the human protein of interest from the NCBI database, which I then used to perform a BLAST search in the starfish transcriptome database (<http://starblast.embl.de/>). This transcriptome was generated by the EMBL Sequencing facility using *Patiria miniata* oocytes. If the proteins could not be directly found in the starfish transcriptome I used the sea urchin genome as an intermediate step (<http://Echinobase.org>)(Cameron et al. 2009) to find the homolog there and using the sea urchin sequence probe the starfish transcriptome again. Using the thus obtained sequence I either designed primers for PCR amplification in the 5' and 3' UTR of the respective gene or designed a construct for synthesis by Genewiz (GENEWIZ, South Plainfield).

Using the primers I set up PCR reactions to amplify the protein sequence using cDNA as template. The cDNA was generated from all the mRNAs of mature eggs and embryos, isolated using the Invitrogen Dynabead® Oligo(dT)₂₅ kit and reverse transcribed using the Invitrogen GeneRacer® kit. After PCR clean-up using the Qiagen kit (PCR purification #28104), I ligated the resulting DNA fragment into the pJet1.2 vector system using the corresponding kit (ThermoScientific #K1232). For a list of primers used in this project see Table 2.

The so clones constructs as well as those synthesised were tagged using genetically encoded fluorescent proteins linked either N- or C-terminally to the protein sequence (see Table 1). The tags used were either EGFP or mCherry, either as single proteins or in triplicate. To achieve the tagging a conventional “copy-and-paste” approach was employed, wherein both the receiving vector as well as the construct and the fluorescent proteins were cut using restriction enzymes and then ligated together (see Figure 27). The restriction enzymes used were purchased from either NEB or ThermoScientific. The ligation was performed using the T4 ligase (NEB #M0202).

The vector system into which the sequences were inserted is the pGEMHE vector, with an Ampicillin resistance and a T7 promoter for the RNA production. The constructs were validated using sequencing by GATC (GATC Biotech AG, Constance) and amplified using either Mini- or Midi-preps (Qiagen kit #27106).

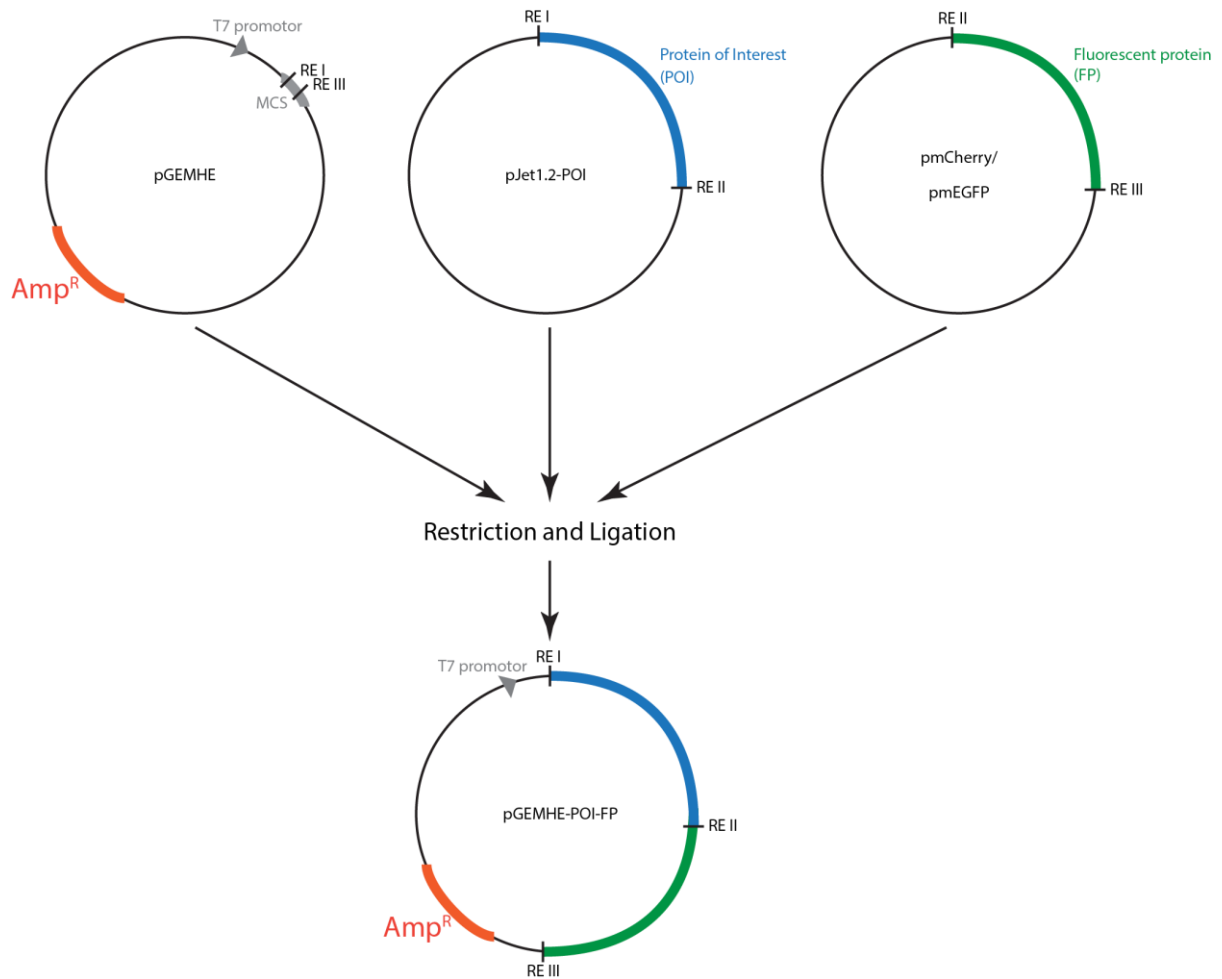


Figure 27: Copy-and-paste cloning strategy employed to generate constructs.

The receiving vector pGEMHE with a T7 promoter was cut with two restriction enzymes (RE I and RE III) while the pJet1.2 vector containing the sequence of the protein of interest (POI) was cut with RE I and RE II. The fluorescent protein sequence was cut from its donor vector using RE II and RE III. All 3 fragments were ligated to generate the pGEMHE-POI-FP construct containing the protein of interest fused to the fluorescent tag.

Table 1: List of constructs used in the project.

Protein name	Vector	C-/N-terminal tag	Fluorescent protein	Species of origin	Generated by
Utrophin	pGEMHE	N	EGFP3, mCherry3		Originally (Burkel et al. 2007), subcloned by Lenart lab
Lifect	pGEMHE	N	EGFP	<i>Mus musculus</i>	Originally (Riedl et al. 2008), subcloned by Lenart lab
EB3	pGEMHE	N	EGFP3, mCherry3		Originally (Stepanova et al. 2003), subcloned by Lenart lab
MRLC	pGEMHE	N	EGFP, mCherry	<i>Patiria miniata</i>	Originally by Masashi Mori, Subcloned by me
Myo-II HC	pGEMHE	C	EGFP, mCherry	<i>Patiria miniata</i>	Originally by Sarah Thome and Kalman Somogyi, subcloned by me
rGBD	pCS2	C	EGFP	<i>Mus musculus</i>	(Benink & Bement 2005)
Ect2	pCS2	C	EGFP, mCherry	<i>Xenopus laevis</i>	(Bement et al. 2015)

Cyclin B	pGEMHE	N	EGFP3, mCherry3	<i>Patiria miniata</i>	Johanna Bischof
MBS/ MYPT1	pGEMHE	N	EGFP	<i>Patiria miniata</i>	Johanna Bischof
MyoGEF	pGEMHE	C	EGFP	<i>Patiria miniata</i>	Johanna Bischof
GEF-H1	pGEMHE	C	EGFP	<i>Patiria miniata</i>	Johanna Bischof

Table 2: List of primers used for cloning from cDNA or mutagenesis.

Name	Sequence	Length
cycB-f4	CCATGGCAGTACAAGCATTGCTAT	24
cyclinB-r3	TCGAGATTTTATCGAAGAAGAAGCTTG	26
MLC-S1.2A_fwd	ATCACAATGGCTGCTAGAAAGACG	24
MLC-S1.2A_rev	CGTCTTTCTAGCAGCCATTGTGAT	24
MLC-S1.2E_fwd	ATCACAATGGAAGAAAGAAAGACG	24
MLC-S1.2E_rev	CGTCTTTCTTTCTTCCATTGTGAT	24
MRLC-TS17.18AA(2)_fwd	GCTCAGCGTGCGGCTGCTAACGTGTTTGCG	30
MRLC-TS17.18AA(2)_rev	CGCAAACACGTTAGCAGCCGCACGCTGAGC	30
MRLC-TS17.18EE_rev	AAACACGTTTTCTTCCGCACGCTG	24
MRLC-TS17.18EE_fwd	CAGCGTGCGGAAGAAAACGTGTTT	24
MYPT1_I_fwd	GCACTGCATCATGGGTAGGTGA	22
MYPT1_II_rev2	ACACTACAGGACGCTAAGCGAG	22

3.2.2 Mutagenesis

I generated mutations of both MRLC (see results) as well as cyclin B on the basis of the existing constructs using the Clontech In-Fusion® HD Cloning Plus Mutagenesis kit. This was done by producing a primer (see Table 2) covering the intended mutation site facing outwards to generate via PCR an open vector containing at each end the desired mutation. These linear vectors were re-circularised using the In-Fusion HD Enzyme (Clontech), generating a full vector containing the mutation (see Figure 28). The mutations were validated by sequencing.

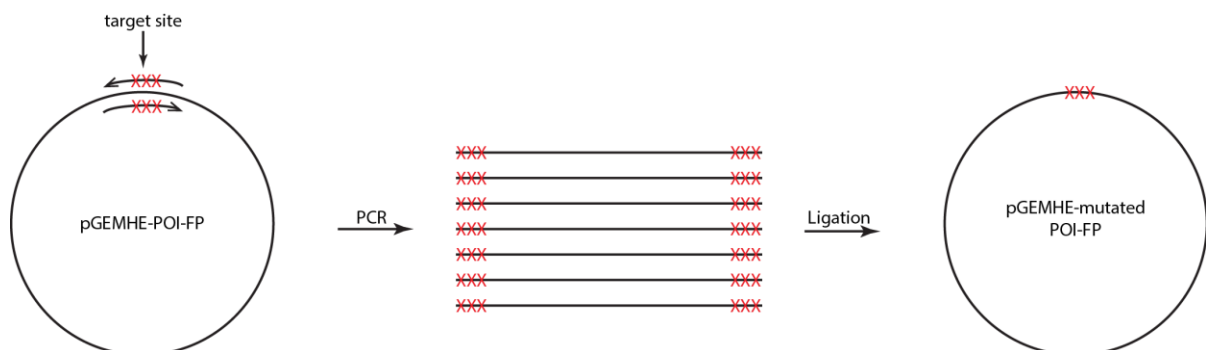


Figure 28: Mutagenesis strategy.

Mutagenesis was performed by introducing the mutation via PCR with primers containing the mutation and ligation of the resulting PCR copies of the vector containing overlap sufficient for ligation. This was done using the Clontech In-Fusion Mutagenesis kit.

3.2.3 RNA preparation

To visualise the localisation of the proteins in the oocyte I injected RNA of the respective constructs into the oocyte. The RNA was produced *in vitro* from the above constructs using CellScript AmpliCap-Max™ T7 High Yield Message Maker Kit for the pGEMHE constructs and AmpliCap™ SP6 High Yield Message Maker Kit for the pCS2 constructs and the A-Plus™ Poly(A) Polymerase Tailing Kit for both. Briefly, the constructs are first linearized, *in vitro* transcription and subsequent addition of a polyA-tail.

Linearization is performed by digestion with a set of restriction enzymes, always a combination of SgrAI, Ascl, and AflIII, depending on the specific construct sequence. The linearized DNA was purified using a phenol/chloroform extraction and subsequently dissolved in RNase-free water to a concentration of around 1 µg/µl. The linearization success, as well as DNA quality, was tested by running a sample on a gel.

This linear DNA construct served as a starting point for the *in vitro* transcriptions and polyA-tailing using the CellScript kits. The instructions in the kits were followed with no modifications. The final RNA was purified via an isopropanol extraction, diluted in RNase-free water to a final concentration of 5 µg/µl and the quality checked on a gel.

3.3 INJECTION

The microinjection system was pioneered in its current form and application to starfish oocytes by Mark Terasaki and Rindy Jaffe and is described in detail at <http://mterasaki.us/panda/injection/>. It was originally applied to the starfish by (Hiramoto 1962) and is based on the idea of allowing picolitre precise injections using a syringe system. The high precision of the injected volumes is achieved by using microneedles containing small amounts of mercury, which allows the conversion of millilitre changes in syringe volume to picolitre changes in the tip of the needle.

The starfish oocytes are sensitive to contaminations of the glass coverslips, which therefore have to be specifically washed before use. To wash coverslips, they (Menzel Gläser #1) are heated and incubated in a detergent-water solution before overnight incubation in 1 M HCl. The coverslips were then washed stringently in ddH₂O and kept in Ethanol until being dried before use.

To allow for injection and subsequent imaging, the starfish oocytes are kept in a specially designed U-shaped injection chamber (Figure 29B), in which the oocytes are positioned on a shelf-like structure atop a coverslip to hold in the correct position for injection (Figure 29A). The shelf is constructed using specifically washed coverslips, a combination of single-sided and double-sided tape and a small piece of glass (Figure 29A). A standard coverslip, as well as the shelf coverslip, are attached to the injection

chambers using silicon grease (GE Bayer Silicones) which seals the sides of the chamber. It is then filled with FSW and the oocytes can be incubated in this chamber with regular washes for a number of days.

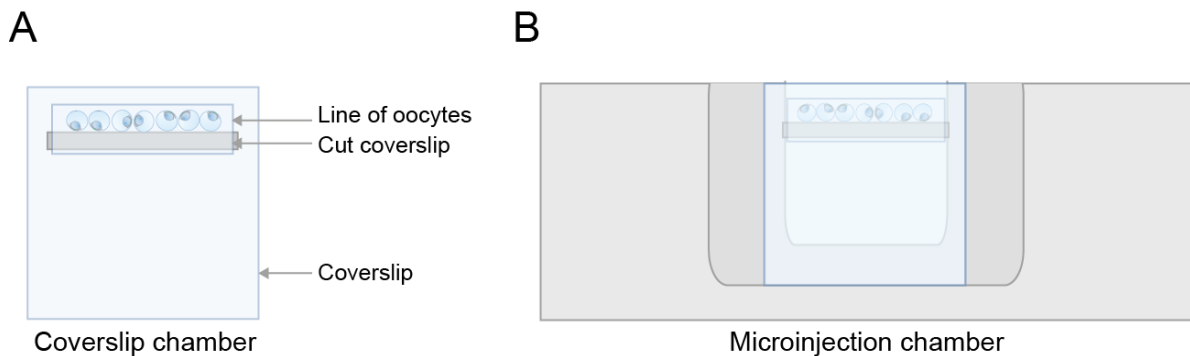


Figure 29: Chamber setup for injection.

A) Shelf coverslip holding the oocytes in position for injection. B) Complete microinjection chamber with oocytes in position. Figure from (Borrego Pinto 2015)

To inject the oocytes, the following procedure is used:

The solution that is to be injected is loaded into a loading capillary (Drummond) between portions of dimethylpolysiloxane silicone oil (20 cts viscosity, Sigma). The oocytes can be injected with a wide variety of liquids – e.g. RNA, proteins, drugs, marker molecules. The loading capillary is placed in the holding ridges of the injection chamber.

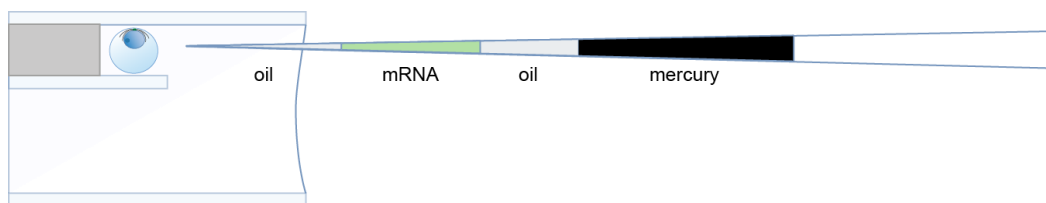


Figure 30: Injection of the oocyte.

The needle is filled with oil, mRNA and another layer of oil, as well as mercury and at the open end connected to the injection system. It is then positioned next to the oocyte which is to be injected (not to scale), held on the injection shelf. From (Borrego Pinto 2015).

The microneedles are fabricated by pulling a capillary (Drummond) on the needle puller (Narishige PN-3 Glass Microelectrode Horizontal Needle Pipette Puller settings Heater 9, Magnet 8, Main Magnet 8). The needle is filled from the back with a small volume of mercury (Sigma). The needle is then placed into the syringe injection system CellTram Oil manual injector, which is attached to a wide-field Nikon Eclipse Ti. The syringe system is filled with mineral oil (Sigma). The tip of the needle is broken via gentle tapping against the loading capillary and the mercury is pushed to the very tip of the needle and the needle is then filled with a buffer of oil from the loading capillary before sucking in the desired amount of liquid from the loading capillary. The needle filling is capped with a small amount of silicon oil to prevent mixing of RNA and sea water during the passage of the needle through the chamber (Figure 30). The needle is then gently pushed into the oocyte and the liquid extruded together with a small

droplet of oil before the needle is removed. The procedure is then repeated for all the oocytes in the chamber which have the correct orientation towards the cover slip, amenable for imaging.

In the case of RNA injection, the cells are incubated overnight at 14 °C to allow for translation of the RNA, while for other injections imaging can proceed immediately.

To calibrate the injected volume, I measured the diameter of oil droplets of units of injection volume (determined by scale in the microscope eyepiece) extruded into the water and calculated the conversion between arbitrary units of injection volume (IU) and volume as $V[pl] = 3.033 * IU$.

3.4 IMAGING

3.4.1 Confocal fluorescence microscopy

The vast majority of the imaging for this project was performed on a Leica SP5 confocal microscope using the Leica LAS software, with a SuperZ Galvo stage, a 1.1 NA HC PL APO 40x water immersion objective (Leica), and two Hybrid detectors (Leica HyD).

The oocytes were imaged directly in the injection chambers by placing these upside-down on the microscope stage in which case the oocytes rest directly on the cover slip above the objective. The standard imaging settings I used were 400-700 Hz scan speed, zoom 1.5-1.7, line average 2-3x, bidirectional scan on a single z-slice over time (xyt mode) on multiple positions. I selected oocytes for imaging which had a specific orientation with the AP-VP axis orthogonal to the objective and selected a single z-plane as close as possible to the AP-VP equator. This meant imaging relatively deep into the oocyte, which necessitated high fluorescence levels of my markers and the use of relative high laser power. I always attempted to minimise the used laser power to avoid photo-damage while achieving good signal levels. To allow for parallel imaging of a number of oocytes in a single chamber I selected a time resolution of 10 sec. Occasionally 15 sec frame intervals were also used. This time resolution allowed on average 5 to 7 oocytes to be imaged in parallel.

In the case of acquiring z-stacks, I limited the number of z-slices to 5 per oocyte to minimise exposure and chose a z-spacing between 1.5 and 2 μm .

3.4.2 Wide-field microscopy

Some experiments were performed on the Zeiss Celloobserver at the EMBL Advance Light Microscopy Facility as this is a wide-field system, allowing for the observation of a larger number of cells simultaneously with very high time resolution. This system also contains a SuperZ Galvo stage and a high-power LED light source (Colibri LED illumination system), a CCD camera and a Zeiss 10x/ 0.30 Ph1 air objective. Cells were imaged with 100 ms exposure and a time interval of at most 10 sec.

3.5 INHIBITOR TREATMENTS

A list of all the chemicals used in this project can be found below with their specific solvents, concentrations, and delivery methods. All chemical stocks were kept at -20 °C in small aliquots and defrosted immediately prior to use. The chemical inhibitors which were applied to the cells were dissolved in FSW which was exchanged for the water covering the cells and incubated for the given times prior to hormone addition. Inhibitors which were injected were loaded into a loading capillary and injected as described above. Inhibitors were injected around 10 min after NEBD, roughly 20 min before the contraction wave as the direct delivery makes long incubation times unnecessary. Controls were performed using the respective solvent as the only treatment.

For the local inhibitor treatments, cells were imaged in an adapted set-up to allow application of the drug on the microscope. To do this, the shelf coverslips containing the injected oocytes were sealed to the bottom of μ -Dish (Ibidi) which had their plastic bottom removed. The local inhibitor treatments were performed by adding the inhibitor directly on the open front of the shelf containing the oocytes using a small pipet.

Table 3: Used chemicals with function, concentration, solvent and incubation time.

Name	Supplier	Function	Stock conc.	Final conc.	Solvent	Delivery method	Incubation time/time to action	Other comments
Actinase E	Sigma-Aldrich	Removal of jelly coat	10 mg/ml	Dilution 1:100	Water	Added to medium	30 min	Wash 3x with FSW after incubation
EGTA	Sigma-Aldrich	Chelate Ca ²⁺ ions	0.2 M	5 mM – 100 mM	Water	Added to medium	20 min	Added in Ca-free SW
Roscovitine	Merck Millipore	Cdk1 inhibitor	50 mM	n/a	DMSO	Local treatment	5 min	Added 2 µl of stock locally
Flavopiridol	Santa Cruz	Cdk1 inhibitor	10 mM	n/a	DMSO	Local treatment	5 min	Added 2 µl of stock locally
RO-3306	Santa Cruz	Cdk1 inhibitor	10 mM	n/a	DMSO	Local treatment	5 min	Added 2 µl of stock locally
Cytochalasin D	Sigma	Actin depolym. via filament capping	10 mM	20 µM	DMSO	Added to medium	40 min	
Latrunculin B	Cayman Chemical	Actin depolym. via monomer sequestering	50 mM	5 µM	DMSO	Added to medium	5 min	
Nocodazole	Sigma	MT depolymerisation	20 mM	3.3 µM	DMSO	Added to medium	5 min	
ML-7	Enzo	MLCK inhibitor	20 mM	100 µM	DMSO	Added to medium	40 min	
Peptide 18	Tocris	MLCK inhibitor	1 mg/ml	30 µM in medium 286 pg injected	Water	Added or injected	20 min	
Y27632	Enzo	Rok inhibitor	100 mM	3 mM – 12 mM	Water	injected	20 min	Effect from 3 mM , full inhibition >7 mM
Phalloidin	Invitrogen	F-actin stabilising drug	10 mg/ml	250 pg	MeOH	Inject	5 min	10 mg redissolved in 1 µl PBS before injection

C3 transferase	Enzo	RhoA inhibitor	1 µg/µl	35.5 pg – 143 pg	Water	Inject	20 min	
Blebbistatin	Abcam	Myosin II inhibitor	100 mM	300 µM	DMSO	Added to medium	1 h	At this concentration aggregates form in FSW
Para-Nitroblebbistatin	Drugmotif	Myosin II inhibitor	50 mM	300 µM	DMSO	Added to medium	1 h	
10kDa-Dextran tagged with Alexa647	Invitrogen	Passive fluorescently labelled marker	20 mg/ml	2 ng	Water	injected	n/a	30 units were injected
Ampicillin	Sigma	Antibiotic	100 mg/ml	1:1000	Water	n/a	n/a	Added to LB for bacteria culture
Kanamycin	Sigma	Antibiotic	50 mg/ml	1:1000	Water	n/a	n/a	Added to LB for bacteria culture
500kDa-Dextran tagged with Cy5	Invitrogen	Passive fluorescently labelled marker	20 mg/ml	2 ng	Water	injected	n/a	Mixed 1:1 with Cdk1
Paraformaldehyde	EMS	Fixative	16 %	1 %	Fix buffer	n/a	n/a	
Glutaraldehyde		Fixative	25 %	0.1 %	Fix buffer	n/a	n/a	

3.6 PROTEIN INJECTION

The method to purify active Cdk1/cyclin B complex from starfish oocytes was pioneered by the Kishimoto lab (Okumura 1996). I was kindly gifted some of the active protein by Eiichi Okumura, so did not perform the purification myself. In short it is done by generating high-speed extracts of maturing starfish oocytes, before incubating on a p13^{suc1}-Sepharose column before elution by buffer A (80 mM Na-β-glycerophosphate, 20 mM EGTA, 15 mM MgCl₂, 1 mM DTT, 10 % sucrose, 01 % Nonidet P-40). The procedure is described in detail in (Okumura 1996).

I prepared aliquots of the active protein and froze in liquid nitrogen and kept the aliquots at -80 °C. To inject the protein was defrosted and loaded in a loading capillary and used immediately to maintain functionality. The capillary was kept on ice between the injections and refrozen in liquid nitrogen between experiments. As the protein is unlabelled, I co-injected it with large fluorescently-labelled Dextran to mark the site of injection.

I also injected other fluorescently labelled proteins as an alternative to expression from mRNA. The proteins I used were H1 from calf thymus (Merck), Alexa647 labelled and tubulin from pig brain labelled with Cy3. The labelled tubulin was prepared by Kasia Tarnawska (Nedelec group, EMBL). These proteins were injected immediately prior to live imaging.

When required for normalisation, I injected the oocytes with 10 kDa Dextran tagged with Alexa647, which serves as a passive marker to normalise optical effect brought on by imaging. This normalisation was performed for the quantifications of cyclin B and CalciumGreen.

3.7 FIXATION AND IMMUNOHISTOCHEMISTRY

To test for the presence of a gradient of Cdk1 activity in the oocytes, I fixed starfish oocytes and tested different antibodies on them. The antibodies tested were two versions of a rabbit antibody against starfish cyclin B – one generated by the Kishimoto lab and one generated by the Chiba lab – and an antibody against the active form of Cdk1, specifically the Tyr 15 phosphorylation site (Cell Signalling Phospho-cdc2 (Tyr15) Antibody #9111). This antibody has been reported to respond to a wide range of species from *S. cerevisiae* to *Xenopus* and human (Cell Signalling). I also fixed oocytes expressing injected cyclin B-EGFP RNA and staining using a GFP antibody (Rabbit anti-GFP #598 MBL Life Science).

I tested both fixation protocols using aldehyde fixes as well as cold Methanol fixes. For the aldehyde fix I used a variation of the recipe developed by George von Dassow for echinoderm oocytes and embryos (Strickland et al. 2004), where a mixture of formaldehyde and glutaraldehyde in a specialised buffer (100 mM HEPES, 50 mM EGTA, 10 mM MgSO₄, 0.5 % Triton, 1 % formaldehyde, 0.1 %

glutaraldehyde) is used to fix the oocytes for 1 h at room temperature. For the methanol fix I followed the protocol outlined in (Terasaki et al. 2003), where oocytes are incubated in -80 °C cold methanol for 1 h for fixation before rewarming to room temperature and washing in PBS.

To perform both the fixation as well as the subsequent antibody staining I used both standard protocols with long incubation times at room temperature - primary AB overnight at 4 °C and secondary AB for 2 h, as well as 3x 5 min washes in PBS-T – as well as the specialised PELCO Biowave Pro microwave (Ted Pella, Inc.) which allows a much quicker procedure by increasing chemical penetration without heating the samples (see Table 4).

Table 4: Microwave protocol for fixation.

Originally developed by Joana Pinto and Natalia Wesolowska.

Step#	Description	User Prompt (on/off)	Time (Hr:min:sec)	Power (Watts)	Temp (°C)	Load Cooler (off/auto/on)	Vacuum/ Bubbler/ Pump	SteadyTemp pump (on/off)	SteadyTemp temp (°C)
Protocol #7.1 IMMUNO FLUORESCENT - Joana Pinto oocytes									
1	Fixation on	Off	0: 2: 0	150	50	Off	vacuum cycle	On	23
2	Fixation off	Off	0: 2: 0	0	50	Off	vacuum cycle	On	23
3	Fixation on	Off	0: 2: 0	150	50	Off	vacuum cycle	On	23
4	Rinse	On	0: 0: 40	150	50	Off	off	On	23
5	Rinse	On	0: 0: 40	150	50	Off	off	On	23
6	Permeabilise ON	On	0: 2: 0	150	50	Off	vacuum cycle	On	23
7	Permeabilise OFF	Off	0: 2: 0	0	50	Off	vacuum cycle	On	23
8	Permeabilise ON	Off	0: 2: 0	150	50	Off	vacuum cycle	On	23
9	Permeabilise OFF	Off	0: 2: 0	0	50	Off	vacuum cycle	On	23
10	Permeabilise ON	Off	0: 2: 0	150	50	Off	vacuum cycle	On	23
11	Permeabilise OFF	Off	0: 2: 0	0	50	Off	vacuum cycle	On	23
12	Permeabilise ON	Off	0: 2: 0	150	50	Off	vacuum cycle	On	23
13	Permeabilise OFF	Off	0: 2: 0	0	50	Off	vacuum cycle	On	23
14	Permeabilise ON	Off	0: 2: 0	150	50	Off	vacuum cycle	On	23
15	Primary AB ON	On	0: 2: 0	150	50	Off	vacuum cycle	On	23
16	Primary AB OFF	Off	0: 2: 0	0	50	Off	vacuum cycle	On	23
17	Primary AB ON	Off	0: 2: 0	150	50	Off	vacuum cycle	On	23
18	Primary AB OFF	Off	0: 2: 0	0	50	Off	vacuum cycle	On	23
19	Primary AB ON	Off	0: 2: 0	150	50	Off	vacuum cycle	On	23
20	Primary AB OFF	Off	0: 2: 0	0	50	Off	vacuum cycle	On	23
21	Primary AB ON	Off	0: 2: 0	150	50	Off	vacuum cycle	On	23
22	Rinse	On	0: 0: 40	150	50	Off	off	On	23
23	Rinse	On	0: 0: 40	150	50	Off	off	On	23
24	2 Antibody ON	On	0: 2: 0	150	50	Off	vacuum cycle	On	23
25	2 Antibody OFF	Off	0: 2: 0	0	50	Off	vacuum cycle	On	23
26	2 Antibody ON	Off	0: 2: 0	150	50	Off	vacuum cycle	On	23
27	Rinse	On	0: 0: 40	150	50	Off	off	On	23
28	Rinse	On	0: 0: 40	150	50	Off	off	On	23

All oocytes were stained using either an antibody against nuclear pore protein complexes (MAb414 from Biologend) or against tubulin (DM1A Sigma-Aldrich) and Draq5 (Biostatus) in addition to the antibody being tested, to ensure that the staining itself was successful. The secondary antibodies used were goat-anti-mouse IgG Alexa488 and goat-anti-rabbit IgG Alexa 546 from Invitrogen. Once the staining was complete oocytes were placed in a drop of ProLong® Gold Antifade (Life Technologies) between an objective slide with a spacer of double sided tape and a coverslip and imaged on the confocal as described above.

3.8 PHYSICAL MANIPULATIONS

3.8.1 Surface tension measurements

The technique to use pipet suction to measure surface tension has been well-established and has historically been applied to measure these in a number of marine animals including starfish. I performed surface tension measurements with the help of Jean-Leon Maitre from the Hiiragi lab at EMBL, using the set-up he established and which has previously been described for use in mouse embryos (Maître et al. 2015). Briefly, I forged the micropipettes for the measurements from capillaries (World Precision Instruments TW100-3) in a needle puller (Flaming Brown Sutter Instrument) and then cut them so that an opening of a diameter of $\approx 30 \mu\text{m}$ for measurements on mature oocytes and $\approx 70 \mu\text{m}$ for measurements in immature oocytes was generated. The needles were then bent to an angle of roughly 45° .

The thus produced micropipette was mounted in a Narishige micromanipulator connected to a liquid reservoir. The pressure in the system is controlled by a microfluidic pump which has a pressure resolution of 7 Pa, using the Labview software (National Instruments) (Maître et al. 2012).

The jelly coat of the oocyte was removed previous to the measurements using Actinase E treatment for 30 min and subsequent washes. The cells were first measured either in the immature state as well as in the mature state after meiosis was completed. Secondly, two oocytes were measured during meiosis at roughly 5 min time intervals.

To perform the actual measurements, the pipette is placed next to oocyte and the pressure is slowly increased until the protrusion into the pipette forms a half-sphere, i.e. it has the same radius as the pipette opening (Figure 31). In the immature oocyte, care was taken to measure not at the animal pole but laterally in the oocyte. The surface tension T_c was calculated from the size of the cell (R_c), the size of the bulge (R_p) and the required negative pressure (ΔP) using the following formula based on Young-Laplace's law.

$$\Delta P = 2T_c \left(\frac{1}{R_p} - \frac{1}{R_c} \right)$$

$$T_c = \frac{\Delta P}{2 \left(\frac{1}{R_p} - \frac{1}{R_c} \right)}$$

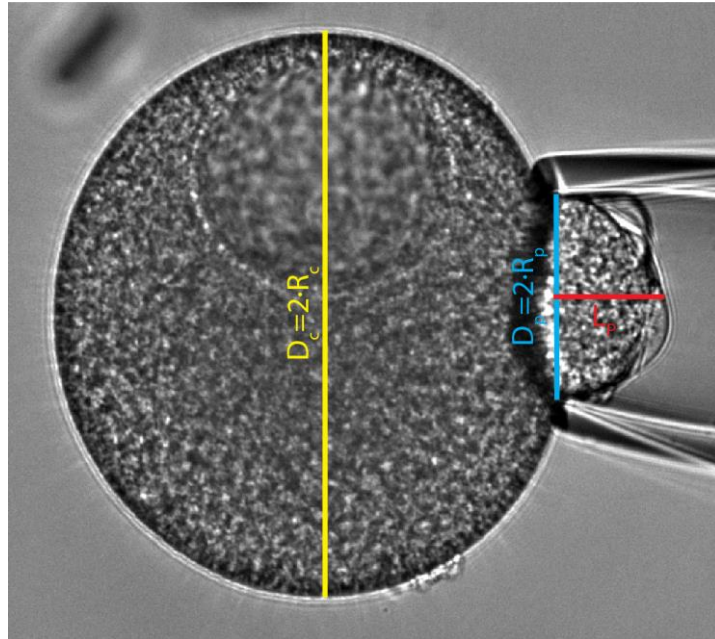


Figure 31: Surface tension measurements.

Picture of an immature oocyte on which the measurement is being performed with a hemisphere sucked into the pipette and showing the relevant measurements for calculating the tension.

3.8.2 Centrifugation

In the starfish oocyte, the nucleus can be moved from its original position at the animal pole to another site of the cortex by centrifugation (Miyazaki et al. 2000). To perform centrifugation oocytes are placed in the shelf chambers used for injection and these chambers are positioned in 50 ml Falcon tubes using custom-designed holders (Figure 32). The tubes are filled with FSW and centrifuged at 420 g (2400 rpm Heraeus Multifuge) for 45 min at 4 °C.

To determine the effect of the centrifugation I measured the relative angles between the axis of contraction and the old and new animal-vegetal axis respectively. I determined the old animal-vegetal axis using a marker for the centrosomes, EB3 or POC1, which sit at the animal pole and are not moved by centrifugation. While the new animal-vegetal axis is set by the point at which the nucleus connects to the cortex. The angle between the contraction wave and the two animal-vegetal axes was measured using the ImageJ Angle tool.

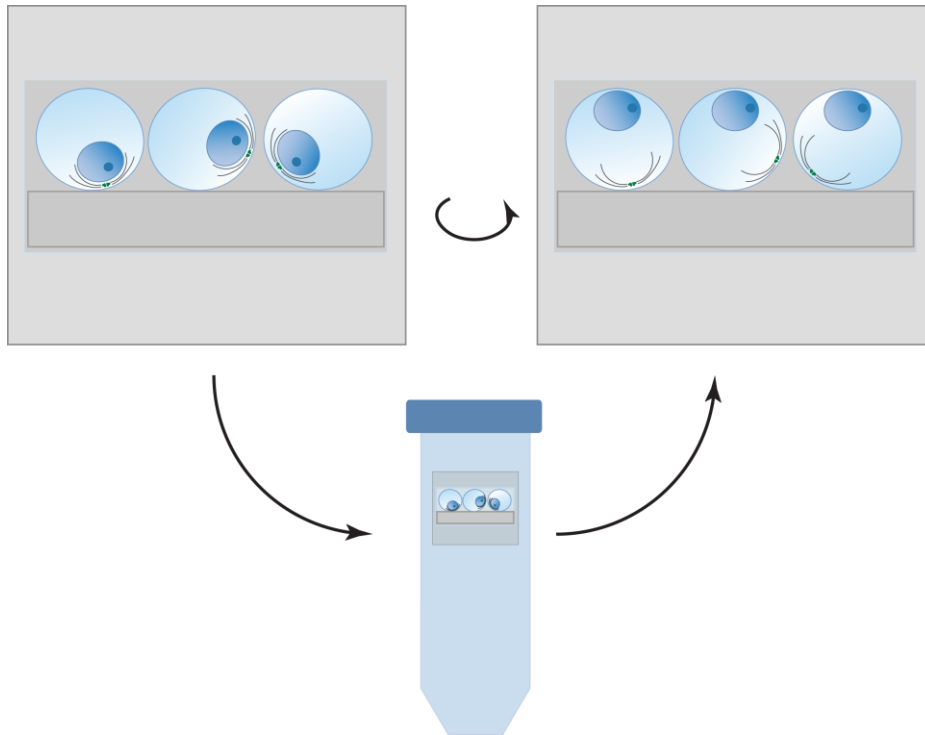


Figure 32: Set-up for centrifugation of starfish oocytes. Oocytes are placed on the coverslip shelves in random orientation and centrifuged in 50 ml Falcon tubes, resulting in all nuclei facing the top after centrifugation. Figure adapted from (Borrego Pinto 2015).

3.8.3 Shape change wells

To modify the geometry of the oocytes I used microfabricated chambers, which were originally developed by Nicolas Minc for application in sea urchin embryos (Minc et al. 2011). He helped me in the design and fabrication of the chambers which was performed by me in his lab at Institute Monod, Paris.

To generate the chambers, I first designed the mask with a variety of shapes (Figure 33). To ensure that the cells move into the shapes, the shapes are designed for a height of 140 μm and the surface area of the desired shapes calculated accordingly. The mask was designed using the free Software QCAD and printed by Selba S.A.

The chambers are produced using a photolithographic process. In this the wavers which form the substrate were first stringently cleaned using Acetone, Isopropanol, and ddH₂O, and subsequently dehydrated by baking. The wavers were then pre-coated using the MicroChem OmniCoat. As the desired film thickness was at the highest limit possible with the used resin, the wavers were spin-coated with SP8-50 at 750 rpm. Next, the wavers with the resin on them are soft baked to evaporate the solvent for 20 min at 65 °C and for 60 min at 98 °C. The mask with the designed shapes was placed on top of the thus prepared wavers and exposed to UV light for 22 sec, and then baked again to crosslink the just irradiated portions of the waver for 1 min at 65 °C and 12 min at 98°C. The wavers

were then placed in the SU-8 Developer for 18 min or until the run-off after isopropanol wash was clear. The finished chips were washed thoroughly with isopropanol and then cured at 130 °C, before slowly cooling down over 30 min to avoid cracking.

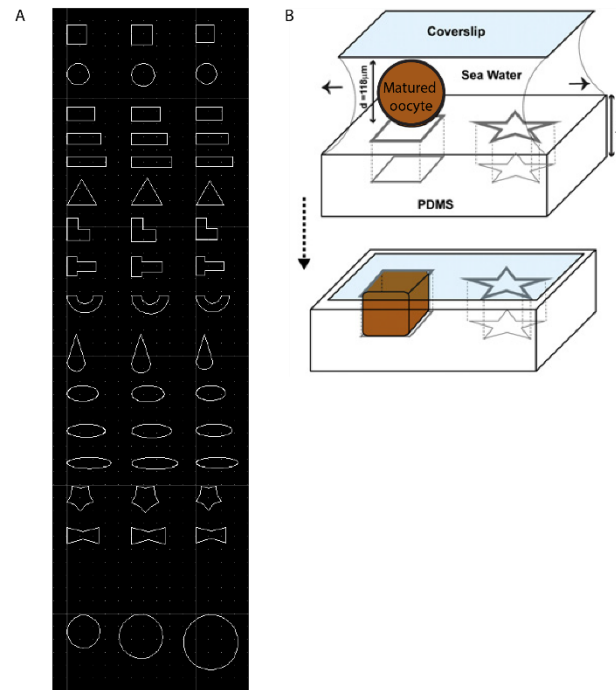


Figure 33: Shape change wells.

A) Mask design of the chosen shapes including control shapes in the last row. The final chip includes many repetitions of these blocks. B) Mechanism of introducing the cell into the shapes, republished from (Minc et al. 2011), with permission by Elsevier.

The PDMS chips were cast by pouring a mixture of PDMS and curing agent (10:1, Sigma) onto the positive and baking for at least 4 h at 65 °C. The hardened PDMS was then carefully cut with a scalpel and peeled away from the master. Immediately before each experiment, the PDMS chip was cleaned sequentially in acetone, isopropanol, and ddH₂O. It was then attached to an objective slide with feet via double-sided tape and surface-activated by plasma cleaning (Zepto Plasma Cleaner from Diener). A drop of FSW was placed in the middle of the chip immediately after plasma treatment.

As the immature oocytes are too stiff to enter into the shapes, I matured the cells in a dish before placing them onto the prepared and activated chip 40 min after hormone addition. At this stage, the cells are in the middle of metaphase and 10-15 minutes remain until the start of the contraction wave. A coverslip was then gently lowered onto the chip and the cells were pushed into the shapes by sucking out some of the water between chip and coverslip.

The chip was then inverted and imaged on the confocal microscope as described above. After treatment, the chip was cleaned to remove the oocytes left in the moulds. The chips were reused multiple times.

3.9 IMAGE ANALYSIS AND PROCESSING

3.9.1 General image processing

I used ImageJ/Fiji for general viewing and processing of the imaging data (Schneider et al. 2012; Schindelin et al. 2012). For the images presented here, I adjusted the brightness and contrast settings to allow the important aspects to be seen as well as reversing the LUT for better visualisation in print. For multi-channel images, I overlaid the channels using the Image->Colour->Channel Tools and adjusting the relative intensities of each channel. In the cases of z-stacks, I applied the Image->Stacks->Z Project with maximum intensity projection.

3.9.2 Curvature measurement

To quantify the contraction wave I used an algorithm originally written for this specific problem by Imre Majer as an undergrad student in the Lenart lab. I used his code as the basis for my work with only a few modifications to improve functionality and usability.

This analysis uses Matlab (MathWorks® Inc.) and Miji – a java package allowing interchange of image data between Matlab and ImageJ (Sage et al. 2012).

The goal of the analysis is to automatically segment each image in a time series, calculate the curvature of the thus segmented cortex and for fluorescent images measure the fluorescence intensity along the cortex during the contraction process. To do this the workflow shown in Figure 34 was used. This analysis pipeline is designed to work with both brightfield and fluorescence images with varied fluorescence distributions.

Firstly I want to allow ImageJ to automatically pick a rough outline of the cell. To do this I run a Laplacian filter and an averaging filter on the images which causes a sharpening of the edges and a reduction of any potential gaps in the signal respectively. Then a threshold is picked manually and the resulting mask (with any holes filled if necessary) is used as the starting point for the proper segmentation. This first mask already matched the rough shape of the cell but is not sufficient for detailed analysis. To perform a detailed segmentation a sparse-field Level Set algorithm is used with a lambda value of 2, which determines the sensitivity of the segmentation to small signal changes. The mask serves as a starting point for the algorithm which moves iteratively inwards. For the first image the algorithm running with 300,000 iterations, normally gives a good segmentation result, but this value can be adjusted based on the particular image quality. After the first image of the time series is segmented the user is consulted to check the quality of segmentation and potentially change the segmentation parameters. The following images in the time series are then automatically segmented using Level Set with the outline of the previous image serving as a starting point.

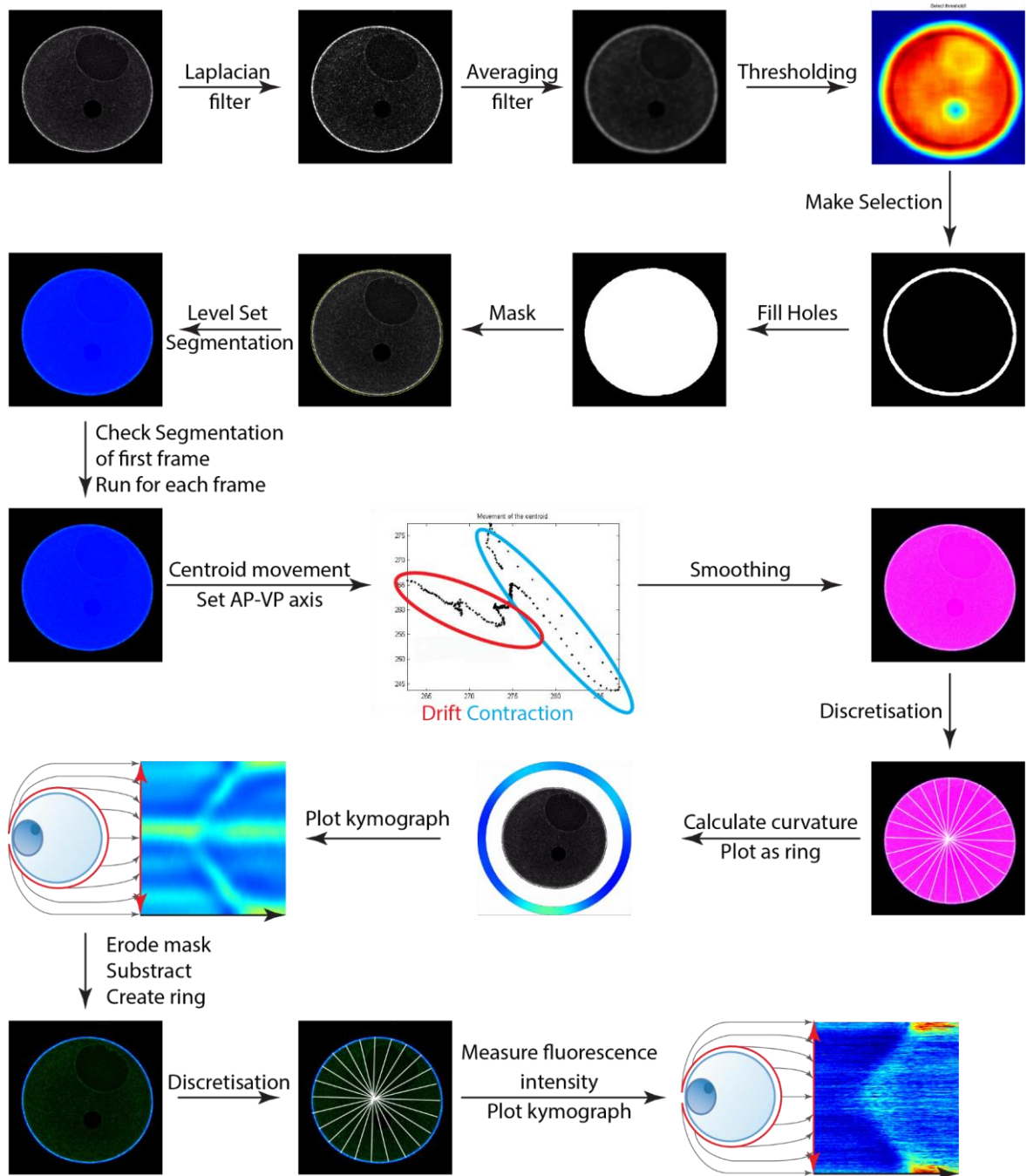


Figure 34: Image Analysis pipeline.

This details the individual steps for a single example image as well as the different output types of the calculated data.

Once the whole time series has been segmented, the curvature of the cortex is to be calculated. Before this can be done, the segmented outline needs to be smoothed as the Level Set algorithm gives a pixel-fine outline and in this local curvature changes give high background noise level compared to the cell-level curvature changes in which I am interested. To perform this smoothing the segmented outline is transposed into polar coordinates and smoothed by fitting a piecewise polynomial. The standard

settings I used for the smoothing were a 5th order polynomial with the cortex segmented into 200 points.

Furthermore, the axis of the cell is determined at this step, by detecting the movement of the centroid of the segmented object and plotting this point over time. The movement of the centroid has commonly two components – firstly the drift of the system which only leads to small displacements, and secondly the contraction wave which leads to a big shift in the centroid position between time points. The user can fit a line through the points representing the contraction wave and thereby set the animal-vegetal pole axis. When the contraction is not present, the axis is set based on the orientation of the oocyte in the images.

The curvature that is calculated is specifically the radius of the first principal curvature in a small segment of the cortex (200 segments along the contour) and is calculated using finite differences by minimising the Chan-Vese energy function (Chan & Vese 2001; Lankton & Tannenbaum 2008). As the oocyte can have a non-circular starting shape due to compression by neighbouring oocytes the surface curvature relative to the first image is also calculated.

The resulting curvature per point along cortex values can be plotted in two ways. Firstly the values can be plotted as a ring around an image of the oocytes for each time point generating a new time series which dynamically shows the changes in cortical curvature. Secondly, the values can be plotted in a static form as a kymograph, where the curvature values are plotted for each point along the cortex as a line for each time point. The kymographs are the main representation of the curvature used here as they allow the observation of time behaviour in a single plot. The curvature values are encoded using the jet LUT and to allow easy comparison between plots, all are scale to show values between 100 and 500 μm .

To measure the fluorescence intensity along the cortex the segmented mask for each image is used as a starting point. This mask is then eroded a number of pixels set by the user to contain part or the whole cortex area, and a subtraction of the two masks gives a ring overlying the cortex. This ring is segmented into small areas similar to those used for the curvature measurements and the fluorescence intensity in each of these areas is measured. The values are only plotted in the kymograph form as described above.

3.9.3 Flow measurements via STICS

To measure the flow of the cytoplasm during the contraction wave a version of spatiotemporal image correlation spectroscopy (STICS) was implemented in the Matlab code. STICS was originally developed by (Hebert et al. 2005) and relies on measuring the correlation of image intensities across selected

spatial and temporal windows. This technology allows us to measure both the directionality and velocity of the cytoplasmic flow. In the starfish oocytes, we can measure the flow on both brightfield images as well as fluorescent images as the yolk platelets in the cytoplasm form a high-contrast (black compared to grey values for cytoplasm both in bright-field as well as in fluorescence microscopy) substrate whose movement STICS can measure. The STICS measurements were performed by calculating the cross-correlation in an interrogation window with a size of 16 px without overlap in space and 6 frames with a time resolution of 50 ms in time. To avoid false result at the boundary the edges were avoided by picking a suitable offset and filled by extrapolation from the internal data. All these analyses were done on a single 2D plane which was chosen to optically bisect the oocyte at the equator along the animal-vegetal axis.

3.10 DATA ANALYSIS AND PLOTTING

To compare the measured curvature values between different oocytes and especially between treatments is key to allow quantification of the observed changes but it is not trivial. The interesting aspect is not so much the maximum or minimum curvature value reached during the contraction process. Nor is the average curvature value very informative as the contractile cortex is only a small part of the whole cortex and averaging obscures the true effect.

After testing a wide variety of methods to condense this complex multidimensional data set of curvature values during contraction into a single reliable and relevant number, I chose to quantify the contraction strength using the variance of the radius of curvature values during the contraction wave. To do this I summed all cortex area segments having specific curvature values. As the oocyte has a certain intrinsic curvature, I quantified the curvature during the contraction wave and during metaphase when the curvature is not changing and subtract the background value (Figure 35A). The dataset with different strengths have different variance as more areas of the cortex have either a high or low radii of curvature (Figure 35B). These measurements were performed in Matlab or in Excel.

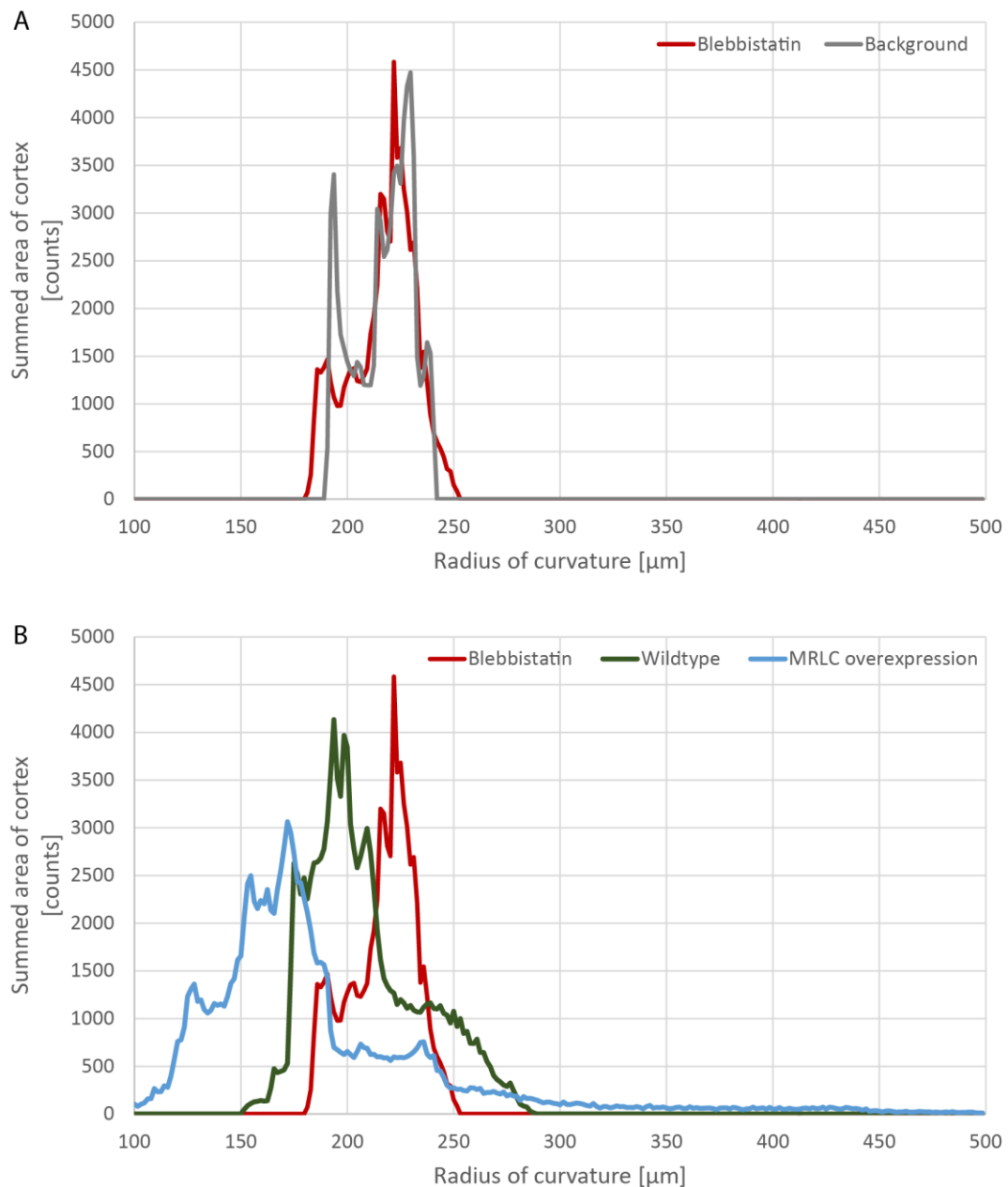


Figure 35: Quantifying strength of contraction wave.

A) The oocytes have an intrinsic curvature which is subtracted from the measured curvature values, here for an oocyte treated with Blebbistatin which shows very low contraction, i.e. no large difference compared to the background. B) Surface curvature measurements for different treatments with different strengths, showing different spreads of values, which are measured in the variance.

The duration of the contraction wave was determined either in the image series or additionally also in the kymographs, depending on data quality, and the speed was calculated based on the duration and distance along the oocyte cortex.

All data was plotted in the software R using the ggplot2 package (R Core Team 2016; Wickham 2009). In the boxplots used, the top and bottom lines of the box mark the 25th and 75th percentile of the data, while the line in the middle marks the median. The whiskers mark the highest and lowest data points still within 1.5 interquartile range.

3.11 ACKNOWLEDGMENTS

I had a tremendous amount of help and support while completing this work. Without the generosity of a lot of people, both with regards to their time as well as reagents, this would not have been possible. I would like to thank them all very sincerely. Their specific contributions are listed below and mentioned throughout the text at the appropriate occasions.

Imre Majer wrote the image analysis scripts in Matlab which formed the basis of the analysis for my project and did a number of preliminary experiments when he was an undergrad student in the Lenart lab.

Nicolas Minc (Institute Jacques Monod) was of enormous help with the design and production of the shape change wells and I would like to thank him for hosting me in his lab and teaching me the photolithography process and fruitful discussion.

Jean-Leon Maitre from the Hiragi group at EMBL helped me with the surface tension measurements and allowed me the use of the measurement system he developed. I would also like to thank him for his willingness to have recurring great discussions about contraction waves.

Sarah Thome cloned the starfish homolog of myosin II when she was an undergrad in the lab, which was of great help for my project.

Bill Bement (University of Wisconsin-Madison) and George von Dassow (University of Oregon) generously provided me with the constructs for detection of active RhoA (rGBD) and Ect2.

Professor Chiba (Ochanomizu University) generously send me an aliquot of the antibody against starfish cyclin B his lab generated.

Professor Kishimoto (Tokyo Institute of Technology) also generously provided me with an aliquot of the antibody against starfish cyclin B his lab generated.

Eiichi Okumura (Tokyo Institute of Technology) contributed an aliquot of the active Cdk1 protein purified from starfish oocytes.

Kasia Tarnawska (Nedelec group, EMBL) provided me with the fluorescently labelled tubulin.

I would also like to thank Joana Pinto, my PhD predecessor in the lab, who figured out many of the details of the general starfish handling and experiments and was always happy to share her knowledge and her awesome Illustrator skills and model.

Kalman Somogyi, our lab technician, I would like to thank for his help with general lab work, cloning, and his advice.

Natalia Wesolowska and Masha Burdyniuk were both great help with improving fixation protocols, use of the specialised microwave and helping me with the antibodies.

I would also like to thank the staff of the advanced light microscopy facility (ALMF) at EMBL for maintaining the microscope systems and their support, especially Yury Belyaev and Christian 'Tischl' Tischler, as well as the staff of the workshop at EMBL.

4 RESULTS

4.1 CHANGES IN CORTICAL CONTRACTILITY DURING MEIOSIS

4.1.1 Changes to the cortex from immature to mature oocyte

During the process of maturation, the immature oocyte is transformed into a fertilisable egg via meiosis. This division process goes along with changes in the cortical contractility, which manifest in the contraction waves passing across the cell. The first marker for changes to the cortex is the change in surface tension observed during meiosis. Measurements of surface tension have a long tradition in the study of eggs and embryos and have previously been performed on the starfish oocytes, using both pipet suction (Sawai & Yoneda 1974; Yoneda et al. 1982) and plate compression (Hiramoto 1976; Ikeda et al. 1976). Therefore, I first set out to confirm the published results in the particular starfish species I used, *Patiria miniata*.

The measured surface tension in the immature oocytes is very large (Figure 36A) with values averaging around 10 000 pN/ μm , which is identical after conversion to the value of 1 dyne/cm measured in 1976 by Ikeda and colleagues for a related species (Ikeda et al. 1976). After meiosis is completed, the cells are an order of magnitude softer (Figure 36A), indicating the drastic change in the cortex.

To determine the specific time point at which this drastic change in the surface tension takes place, I also measured the surface tension over the course of the whole division process (Figure 36B). From this, it becomes clear that the change in the surface tension occurs alongside nuclear envelope breakdown (NEBD) around 20 min after hormone addition, which signals the beginning of metaphase (Figure 36B). The surface tension that the oocyte reaches at metaphase is around 1000 pN/ μm . This value is very similar to the surface tension measured both in other oocytes in metaphase (e.g. mouse (Larson et al. 2010)), as well as in mitotic cells in metaphase (Fischer-Friedrich et al. 2014). Interestingly though, while the target value for metaphase is very similar between these different systems, oocytes and mitotic cells reach it from two different directions: oocytes reduce their surface tension (Larson et al. 2010; Chaigne et al. 2013), while cells in mitosis increase their surface tension to reach the metaphase surface tension (Stewart et al. 2011).

In the starfish oocyte, the surface tension stays relatively constant throughout metaphase and then sharply peaks at the transition into anaphase around 70 min after hormone addition. This is the point at which the surface contraction wave passes across the cell (Figure 36B). The surface tension levels then drop again as the cell enters into metaphase II, before spiking again at anaphase II as the second contraction wave crosses the cell. This repetitive behaviour is consistent with our knowledge of meiosis, in which two cell cycles immediately follow each other.

These changes in the surface tension affect the cell shape and these shape changes can be quantified by measuring the radius of the surface curvature. When these curvature values across the whole maturation process are plotted in a kymograph certain characteristics become apparent (Figure 36C). Both the softening at NEBD as well as the spikes in surface tension at anaphase I and anaphase II go along with waves of shape changes moving across the cell, although the extent of these differs.

The observation that the shape change travels across the cell tells us that the changes to the surface tension do not happen everywhere at once but move progressively across the cell, which was not detected in the surface tension measurements in Figure 36B as they were performed only at one point of the cortex. Simultaneously it becomes clear that the waves are not equal, as the wave of softening at NEBD starts at the animal pole (AP) of the cell, where the nucleus is, and moves towards the vegetal pole (VP), while the two contraction waves at anaphase move in the opposite direction (Figure 36C). Of these two surface contraction waves (SCWs), the first one is much more pronounced and was the focus of the investigation described in the following.

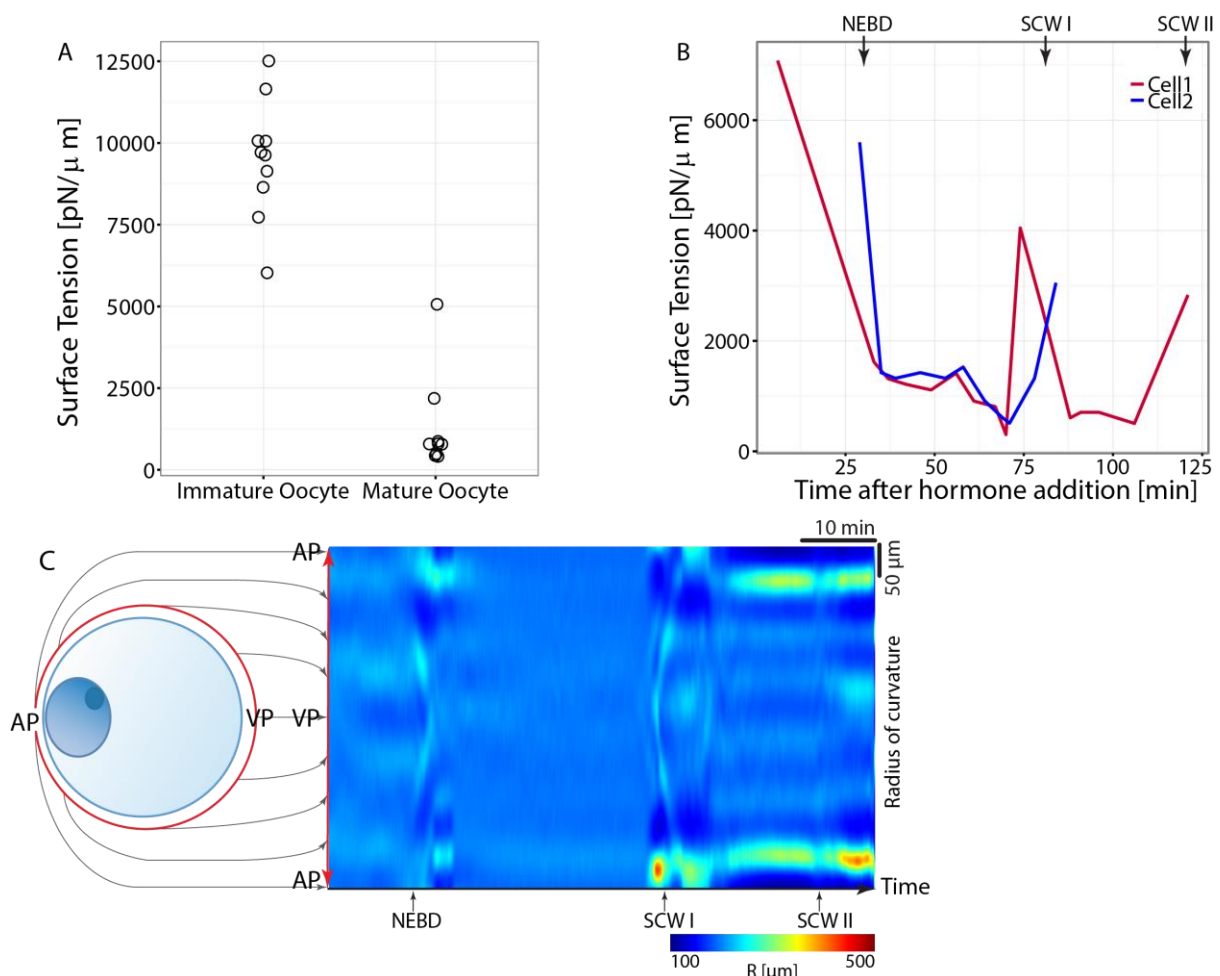


Figure 36: Cortical changes during the oocyte maturation.

A) Surface tension in the immature and mature oocyte shows a significant difference ($p < 0.0005$). B) Surface tension over the time course of meiosis for two example cells, showing the softening at NEBD and the spikes in tension at the two contraction waves. C) The radius of surface curvature of the oocyte plotted as kymograph showing the changes in curvature at NEBD, SCW I and SCW II.

4.1.2 Description of the first surface contraction wave

If we look in more detail at the first surface contraction wave occurring at anaphase of meiosis I, the quantification shows that the contraction wave is, in fact, a band of flattening. This starts at the vegetal pole (VP) and moves across the oocyte towards the animal pole (AP) (Figure 37A and C). It arrives at the animal pole at the time of polar body formation, as visible in Figure 37A.

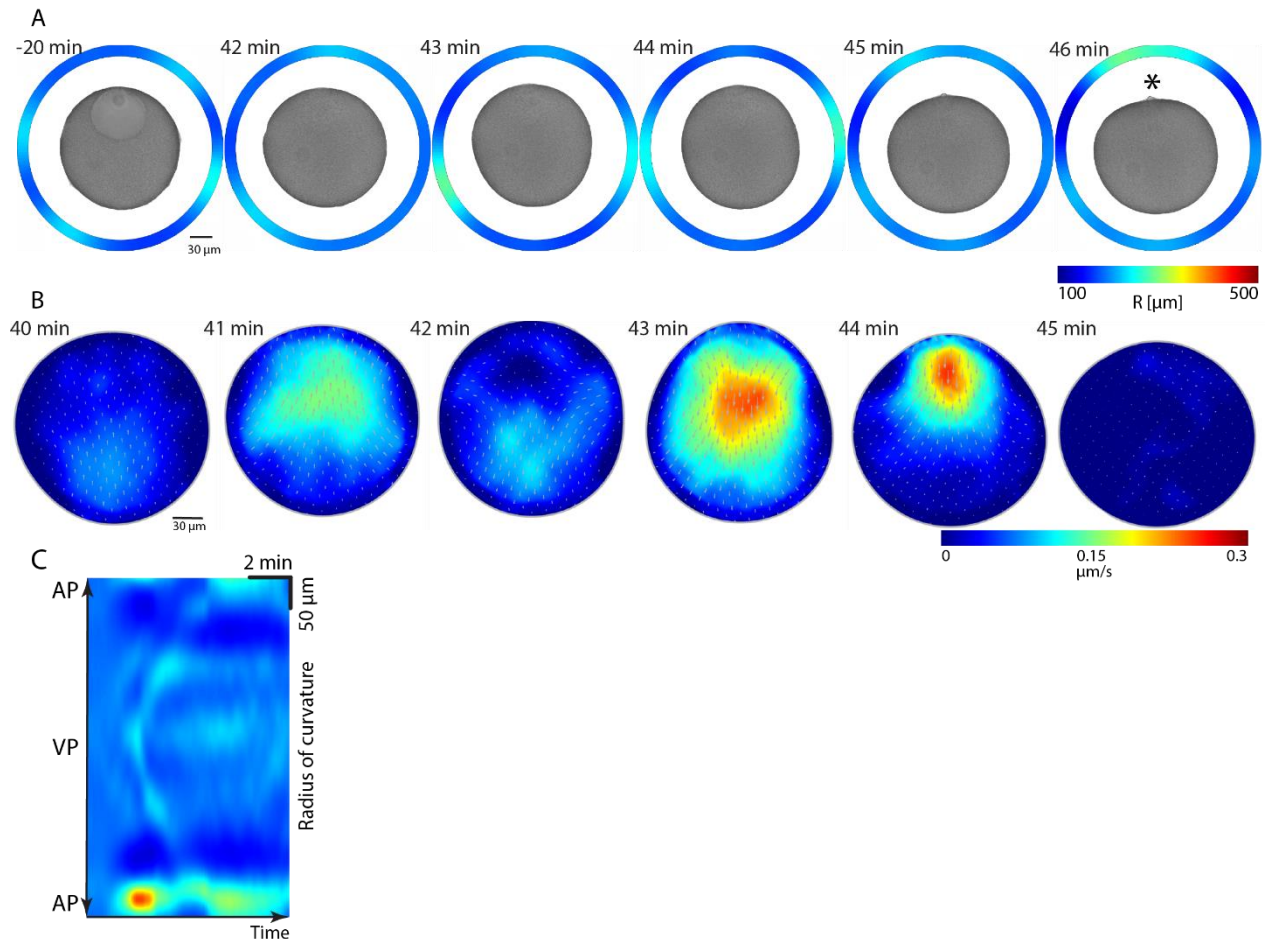


Figure 37: Surface contraction wave.

A) The radius of curvature plotted as a ring plot along the brightfield images of the oocyte. This shows the corresponding shape and the band of flattening moving from VP to AP. B) Cytoplasmic flow during the contraction wave measured by STICS, showing biphasic behaviour. C) Detailed view of the cortical flattening during the first SCW as kymograph along the cortex, measured as the radius of curvature. All times relative to NEBD. The asterisk marks the polar body.

This change in the cell shape leads to cytoplasmic flow along with the contraction wave. The flow was measured using spatiotemporal image correlation spectroscopy (STICS) and revealed to be biphasic (Figure 37B). In the first phase, when the contraction starts and progresses across the vegetal hemisphere of the cell, the flow is relatively slow and is directed towards the animal pole. When the contraction reaches the equator halfway between animal and vegetal pole the flow stops and subsequently reverses as the contraction continues towards the animal pole. It reaches its peak velocity pointing away from the animal pole immediately prior to the protrusion of the polar body (Figure 37B). This flow behaviour is consistent with the cytoplasm behaving as a passive fluid which is

pushed around the cell by the contraction of the cortex. It is important to note that the observed flow in the oocyte takes place in the bulk of the cytoplasm and there is no or very little flow in the region close to the cortex. The flow we observe in response to the contraction wave is, therefore, distinct from the cortical streaming phenomenon observed in *C. elegans* embryos prior to cytokinesis which is mainly observed in the subcortical regions (Munro et al. 2004).

The detailed analysis of the contraction using brightfield imaging with high time resolution allows me to link the shape changes and flow patterns to form a model of the physical process of the contraction wave (Figure 38). When we compare this model to the original model of contraction waves and cytoplasmic flow in starfish oocytes established by Hamaguchi and Hiramoto in 1971, we find that in the basic description of the shape change the models agree (Figure 38). At the same time, with the higher time resolution and sophisticated image analysis techniques, I can detect the more subtle early shape changes and can correctly assign the cell shape to the observed flow. This was not possible in the previous work and this explains why the correlation between shape change and flow pattern that I find is somewhat in opposition to the correlation established by Hamaguchi and Hiramoto.

In summary, a simple observation of the contraction wave along with detailed image analysis revealed the contraction wave to be a band of flattening of the cortex that moves across the cell from the vegetal to the animal pole. The contraction results in a flow of the cytoplasm whose direction changes in accordance with the passing of the wave.

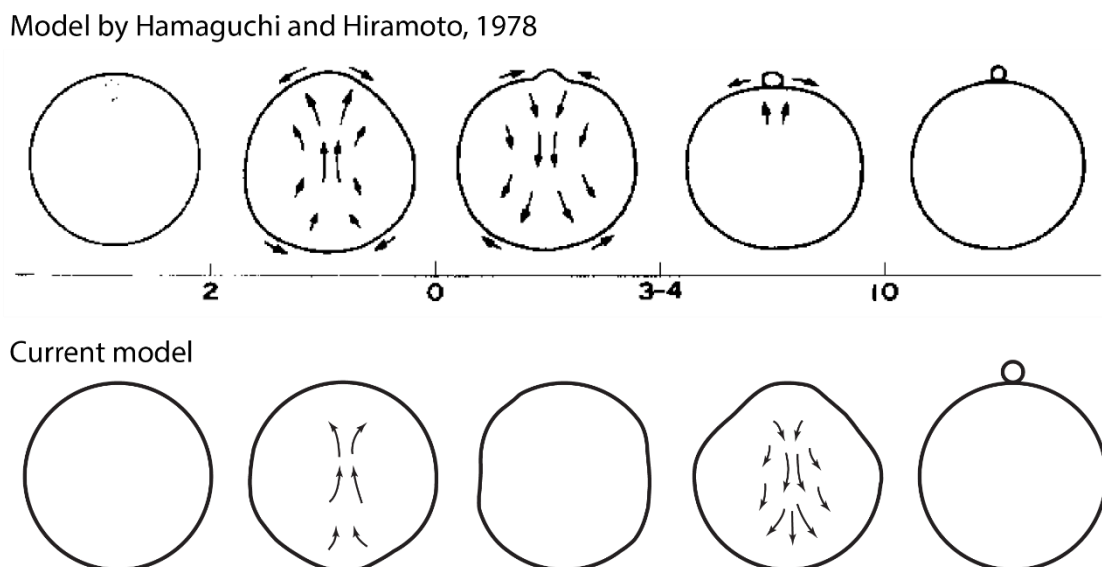


Figure 38: Model of the shape changes of the contraction wave and the cytoplasmic flow. Upper panel shows the original model from (Hamaguchi & Hiramoto 1978) while the lower panel shows the model based on my data with the improved assignment of shape and flow stages. Reprinted with permission from Elsevier.

4.2 MOLECULAR PATHWAY LEADING TO CONTRACTION

4.2.1 Role of myosin II in the contraction wave

4.2.1.1 *Myosin II is one of the most abundant molecules in the oocyte*

As the analysis above revealed the surface contraction wave to be a flattening of the cortex, this indicates a contractile event. It is therefore of great interest to identify the origin of the contractile force. As myosin II is the key motor protein in cells, it is an ideal candidate for driving the contraction wave.

Indeed, myosin II is one of the most abundant proteins in the starfish oocyte. It is found among the top 10 proteins in a whole cell proteomics analysis along with key oocyte components such as the yolk-related proteins Vitellogenin and fertilisation envelope protein Proteoliasin (Table 5).

Table 5: Top 10 proteins in the starfish oocyte as determined by Mass-Spec sorted by counts.

#	Identified Proteins	Molecular Weight	average counts
1	Sp-vitellogenin1	153 kDa	281.4167
2	Sp-vitellogenin1	219 kDa	124.1667
3	Sp-vitellogenin3	429 kDa	56.91667
4	Sp-proteoliasin	149 kDa	45.58333
5	Sp-myosin-2	438 kDa	32
6	Receptor-type tyrosine-protein phosphatase R	67 kDa	27
7	Sp-Macf1-2, microtubule-actin crosslinking factor 1-2	922 kDa	27.08333
8	Sp-vitellogenin3	138 kDa	25.75
9	Sp-EMI-EGF	202 kDa	24
10	Sp-heat shock protein 90 kDa	84 kDa	23

4.2.1.2 *Myosin II localises to the flattened cortex*

To investigate the involvement of myosin II in the contraction wave its localisation was to be determined. Commonly in the literature, the localisation of myosin II is investigated using a GFP fusion to either one of the myosin light chains (MRLC or MELC). I tested the GFP-tagged version of the starfish MRLC, but due to the large cytoplasmic pool, I could not observe any specific localisation of the protein during the contraction wave using this fluorescent protein (Figure 39 D). Therefore, I used a GFP-tagged version of the myosin heavy chain of *Patiria miniata*¹. Starfish oocytes expressing this protein allowed me to observe the localisation of myosin II, especially when the myosin heavy chain construct was co-expressed with MRLC.

¹ The starfish Myosin II heavy chain-EGFP construct was cloned by Kalman Somogyi and Sarah Thome in the Lenart lab.

In the immature oocyte myosin II is localised to the cortex (Figure 39 A), from where it is lost at NEBD in accordance with the observed softening of the oocyte at this time (Figure 36 B). During the contraction, myosin II returns to the part of the cortex which is flattened at the time, and moves along the cortex as a band until it reaches the animal pole (Figure 39 A). The myosin signal and the cortical flattening overlap completely (Figure 39 B). If I quantify the myosin fluorescence intensity in a band of cytoplasm underlying the cortex (but not including the cortex), it becomes clear that myosin II is recruited from the cytoplasm to the abutting cortex (Figure 39 C). Some of the myosin II molecular may also travel along the cortex with the contraction wave. It is important to note that here I observed the localisation of myosin II molecules to the cortex going along with the contraction wave, independent of their activation via phosphorylation.

In summary, myosin II is recruited from the cytoplasm to the cortex which is flattened during the contraction wave and forms a band moving across the cell.

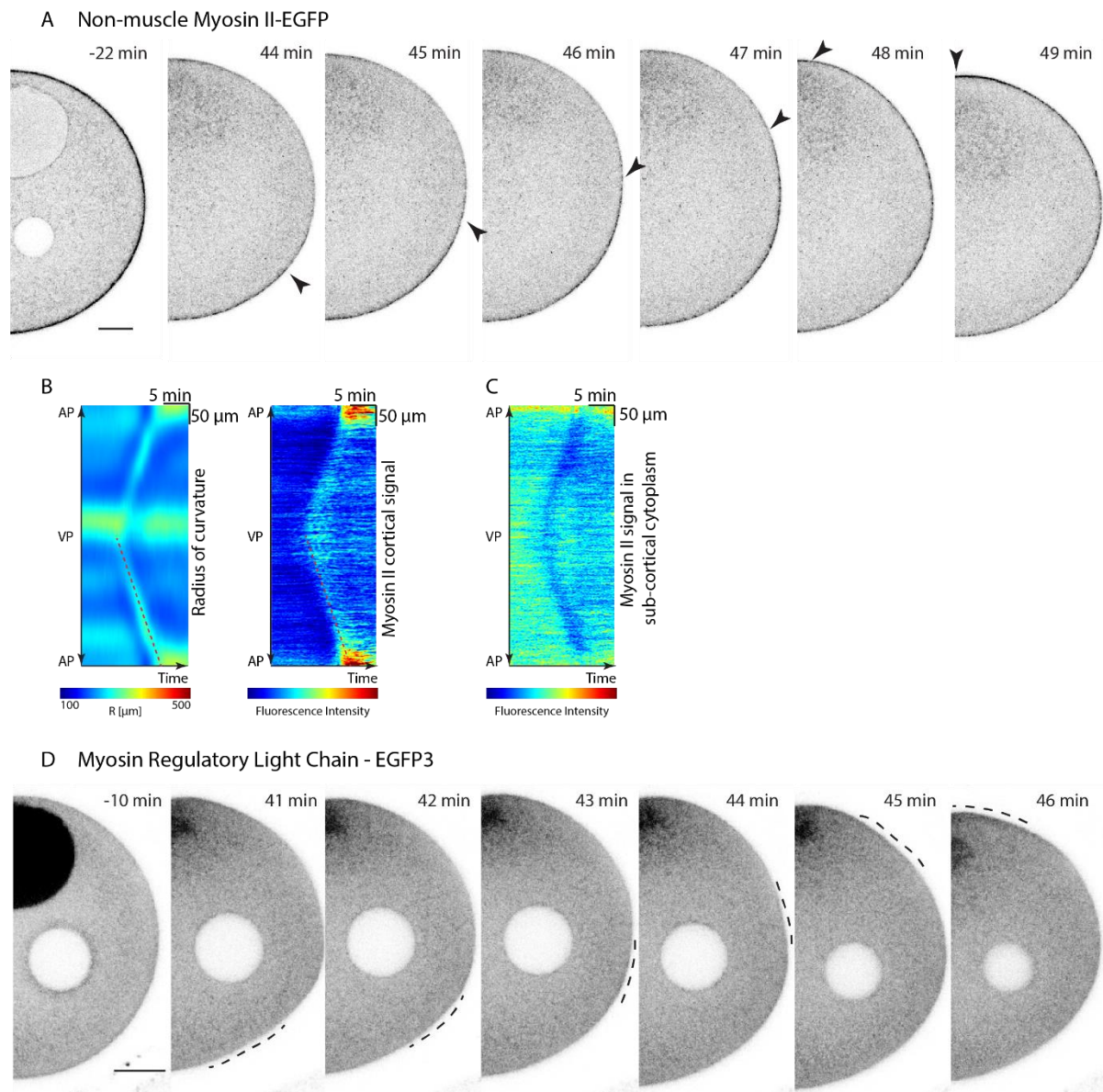


Figure 39: Myosin II in the contraction wave.

A) Localisation of myosin II heavy chain-EGFP construct in the immature oocyte (first image) and during the contraction wave, the arrows show the front of myosin II recruitment to the cortex. B) Quantification of the surface curvature (left panel) and the fluorescence intensity along the cortex (right panel) showing the overlap of the two (dashed line). C) Fluorescence intensity of myosin II heavy chain in the subcortical cytoplasm, showing depletion of the signal during the contraction wave. D) Localisation of the MRLC-EGFP3 construct in the immature oocyte (first image) and during the contraction wave. Dashed line indicates flattened cortex area. Scale bars 30 μm , all times relative to NEBD.

4.2.1.3 Changing myosin II activity affects strength of contraction wave

The above-observed colocalisation of myosin II molecules with the flattening of the cortex is a good indication that myosin II causes the flattening, but to prove a causal relation between the two I changed the levels of myosin II activity in the cell. Firstly, to reduce myosin II activity the oocytes were treated with the specific non-muscle myosin II inhibitor (-)-Blebbistatin. This inhibitor blocks the ATPase activity of the myosin head domain and thereby blocks the force generation of the molecule (Straight et al. 2003).

Inhibiting myosin II activity in the oocytes leads to a significant reduction of the contraction strength. This can be seen in both the stills and kymographs of curvature plots (Figure 40 A and C). Blebbistatin treatment on average reduced the contraction strength from a variance of the radius of curvature in the control of $417 \pm 170 \mu\text{m}^2$ to $70 \pm 35 \mu\text{m}^2$ ($p < 0.005$) (Figure 40G). To allow for the comparison of the contraction strength I used the variance of the radius of curvature along the whole cortex measured for all time points of the contraction wave (for details see 3.9.2 Curvature measurement, page 65).

At the same time Blebbistatin, while very specific in its inhibition, is in this system not a very efficient inhibitor and has several drawbacks. Firstly, it is converted to a cytotoxic form upon exposure to blue light, limiting the use of fluorescence microscopy, and at the high concentration necessary for successful inhibition it forms precipitates in the sea water in which the oocytes are maintained (Figure 40 F). The high necessary concentration for inhibition is likely due to the large pool of myosin II in the oocyte, as described above. In hopes of alleviating these problems, I have tested a recently developed derivative of Blebbistatin called para-Nitroblebbistatin (Kepiró et al. 2014)². I tested the efficiency of this drug compared to Blebbistatin in the context of cytokinesis in the embryo as this allowed for an easy large-scale comparison. In the embryo myosin II inhibition leads the failure of cytokinesis and lack of blastomere formation. It is clear that both para-Nitroblebbistatin and Blebbistatin strongly inhibit cytokinesis compared to control treatments, although the effect is stronger for Blebbistatin (Figure 40F). At the same time para-Nitroblebbistatin clearly forms much less severe aggregates. The lower inhibition of myosin II observed for para-Nitroblebbistatin in cytokinesis was also observed during the contraction wave, making it not a viable alternative to Blebbistatin in this context.

Overall, it is clear that Blebbistatin inhibits the contraction wave, therefore proving that myosin II is driving the flattening of the cortex via its motor action.

² I received an early sample of para-Nitroblebbistatin from András Málnási-Csizmadia, Department of Biochemistry, Eötvös Loránd University Budapest as a gift for which I am very grateful.

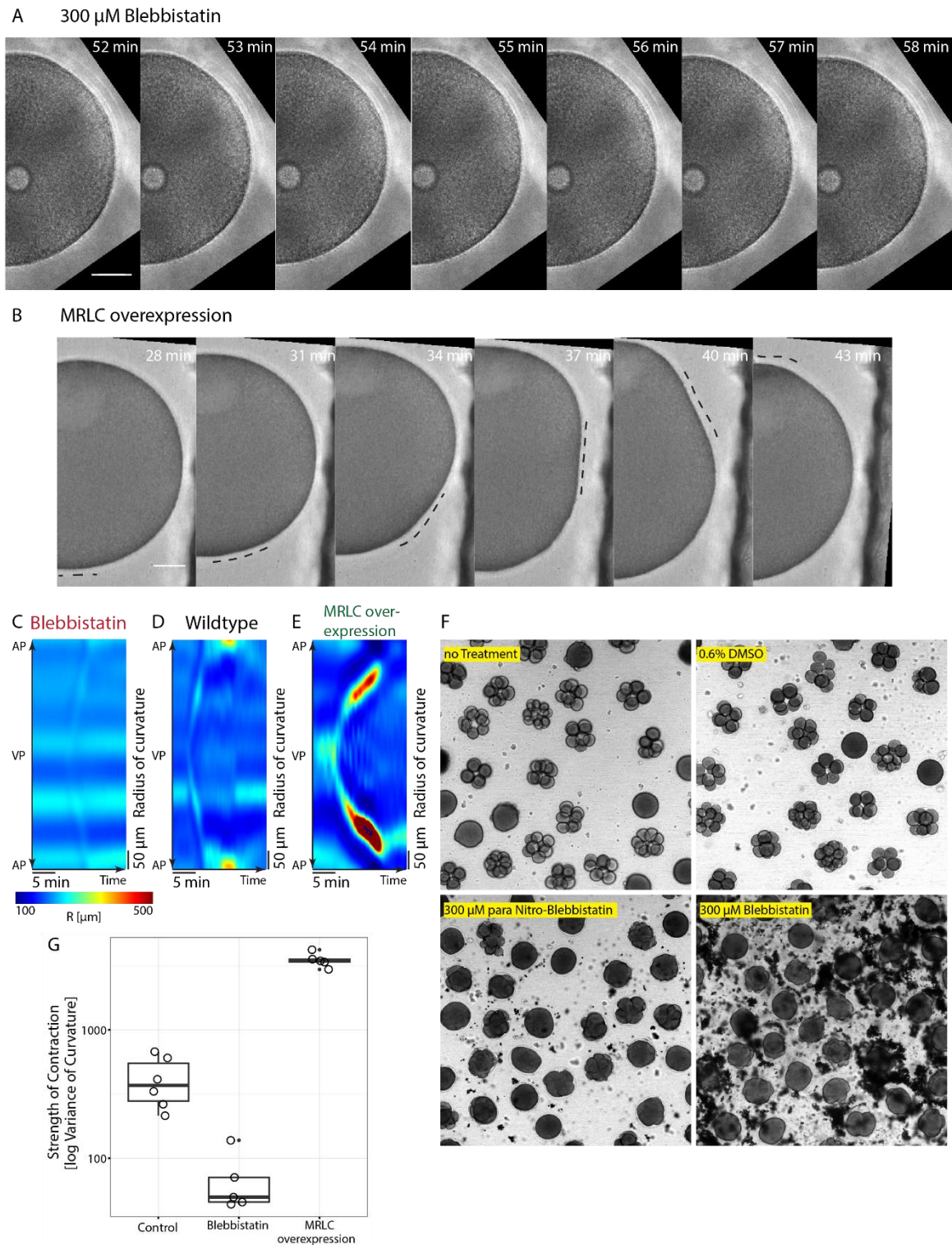


Figure 40: Changing myosin II activity.

A) Oocyte treated with 300 μM Blebbistatin showing no changes in cell shape at the time of contraction wave. B) Oocyte overexpressing MRLC showing a stronger contraction wave. Dashed line indicates flattened cortex area. C) Kymograph showing the surface curvature change in a Blebbistatin treated oocyte. D) Kymograph showing the surface curvature change in a non-treated oocyte. E) Kymograph showing the surface curvature change in an MRLC overexpressing oocyte. F) Efficiency of para-Nitroblebbistatin and Blebbistatin in inhibition of cytokinesis in embryos as a measure of myosin II inhibition efficiency. G) Quantification of the contraction strength measured as variance of the surface curvature during the contraction resulting from the various myosin activity manipulations. Scale bar 30 μm , all times relative to NEBD.

To further probe the specific role of myosin II in the contraction process, I overexpressed the myosin regulatory light chain (MRLC) in the oocytes (Figure 40B). This overexpression has the effect of strongly increasing the contraction strength from a variance in the control of $417 \pm 170 \mu\text{m}^2$ to $3505 \pm 404 \mu\text{m}^2$ ($p < 0.001$). The shape change of the oocyte becomes much more striking, as visible in the still images as well as the curvature kymographs (Figure 40B and E).

This observation suggests that the oocyte has an overabundance of myosin II heavy chain molecules that are not formed into complexes and the overexpression of MRLC allows the formation of more fully assembled functional complexes. It also suggests that in the untreated oocyte the strength of the contraction could be limited by the number of available myosin molecules.

All in all, this data shows for the first time that the surface contraction wave is a truly contractile process driven by myosin II.

4.2.2 Myosin II regulation

4.2.2.1 Myosin II activity is regulated via the phosphorylation site TS17.18

As myosin II drives the contraction, I next addressed the question of how myosin II is activated during the contraction wave. To answer this question, I first explored which phosphorylation sites in the myosin regulatory light chain (MRLC) needs to be phosphorylated for proper myosin II function in the contraction wave. There are two described phosphorylation sites - the key one at T17 and S18 (TS17.18) phosphorylated by MLCK, Rok and citron kinase as well as the less common site S1 and S2 (SS1.2), which has been proposed to be phosphorylated by Cdk1-cyclin B (Figure 41)(Satterwhite et al. 1992).



Figure 41: Phosphorylation sites of myosin regulatory light chain (MRLC).

I generated phosphomutants of these specific sites by replacing the wildtype amino acids with glutamic acid or with alanine for phosphomimetic and non-phosphorylatable mutants respectively (Figure 42 A). These mutants were overexpressed in the oocytes on the background of the endogenous MRLC, which cannot be removed as the oocyte stores proteins in large amounts. This treatment, therefore, results only in partial phenotypes, which are nevertheless detectable in the quantification of the contraction strength.

In all cases of overexpression, the contraction wave is stronger than in the untreated cell as indicated by the MRLC overexpression described above (Figure 42 B). The mutants at the TS17.18 site show on average a contraction that is stronger compared to the overexpression of the non-mutant version, which is visible in the stills as well as the kymographs (Figure 42 D and E compared to C). The phosphomimetic TS17.18EE mutant contraction is stronger than that of the non-phosphorylatable TS17.18AA, which is the expected pattern (Figure 42 I and J) ($4050 \pm 622 \mu\text{m}^2$ and $3024 \pm 555 \mu\text{m}^2$ vs $2090 \pm 998 \mu\text{m}^2$ for the non-mutant version respectively, $p < 0.001$).

The mutants at the SS1.2 site show no difference between the phosphomimetic and the non-phosphorylatable form, even though on average their contraction strength is slightly higher than the overexpression of the wildtype MRLC ($2537 \pm 940 \mu\text{m}^2$ and $2528 \pm 904 \mu\text{m}^2$ compared to $2090 \pm 998 \mu\text{m}^2$ respectively), but this difference is relatively small and not statistically significant (Figure 42 F and G).

From the data present, it seems likely that the TS17.18 site, which is the target of MLCK, Rok and citron kinase, is the site by which myosin activity during the contraction wave is controlled. The observation that the SS1.2 mutants show no significant difference between each other as well as towards the control suggests that this potential phosphorylation site is not important in the context of the contraction wave. These results conform to findings in other contractile processes, where TS17.18 is also the main regulatory site while the evidence for SS1.2 is relatively weak.

As the overexpression of a non-phosphorylatable form leads to an increase in contraction strength, it is clear that the non-phosphorylatable MRLC has some partial activity. This can be mediated by myosins with non-phosphorylatable MRLC assembling into mini-filaments with non-mutated myosins, as previously described in the literature (Watanabe et al. 2007). The same can also happen on the single-molecule level with non-phosphorylatable MRLC co-assembling into semi-functional myosin complexes with non-mutated MRLC present in the cell.

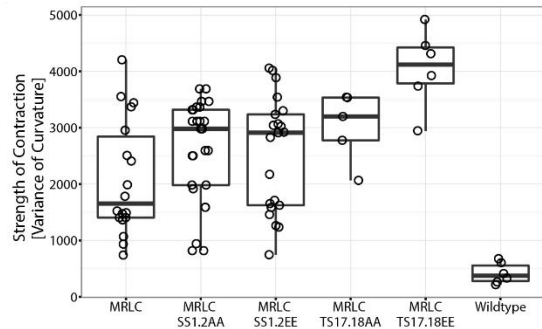
The role of differential phosphorylation of the sites TS17.18 was not explored here even though it would be worth further study as the single and double-phosphorylated forms of MRLC can clearly play differential roles in regulating contractility (Watanabe et al. 2007).

In summary, although the data is slightly obscured by the presence of the endogenous protein, it is clear that of the two potential myosin phosphorylation sites, the site which is key for controlling myosin activity during the contraction wave is the site at TS17.18 rather than the SS1.2 site.

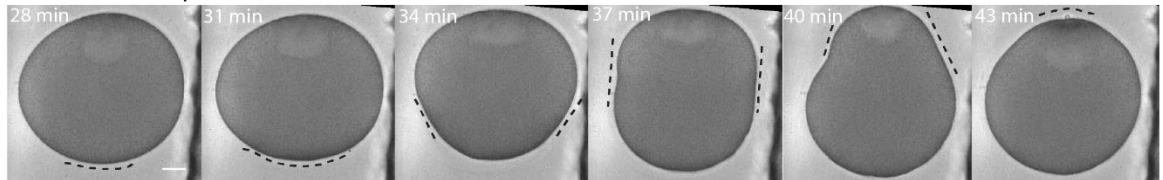
A

P. miniata MRLC ssrktkgkqpkkraqratsnfv
 MRLC TS17.18AA ssrktkgkqpkkraqr^aaaⁿfv
 MRLC TS17.18EE ssrktkgkqpkkraqr^aeeⁿfv
 MRLC SS1.2AA ^aar^kktkgkqpkkraqratsnfv
 MRLC SS1.2EE ^aer^kktkgkqpkkraqratsnfv

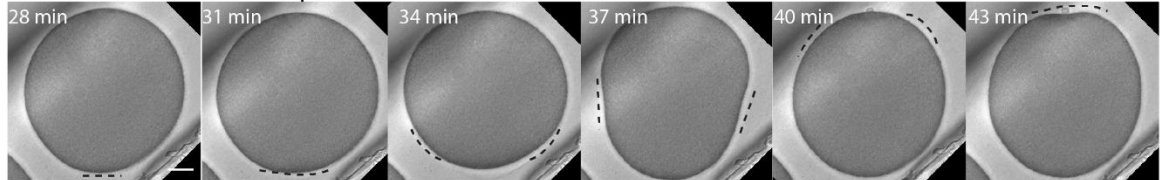
B



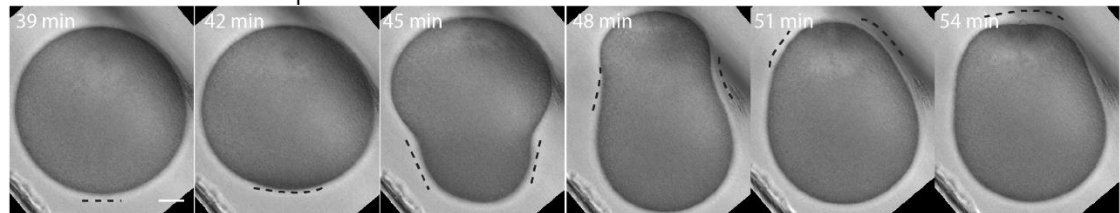
C MRLC overexpression



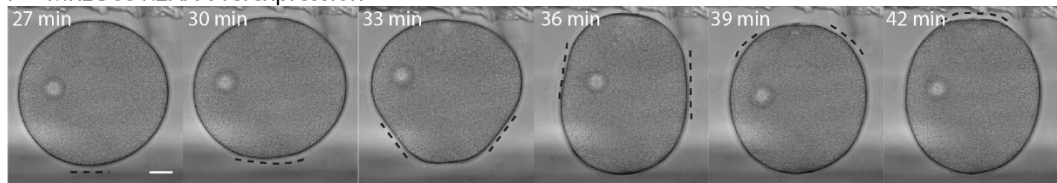
D MRLC TS17.18AA overexpression



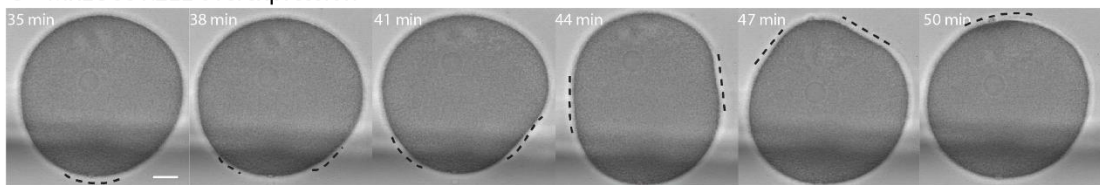
E MRLC TS17.18EE overexpression



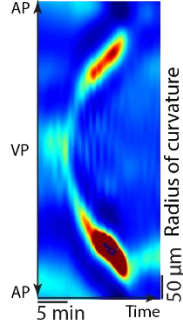
F MRLC SS1.2AA overexpression



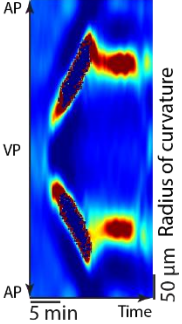
G MRLC SS1.2EE overexpression



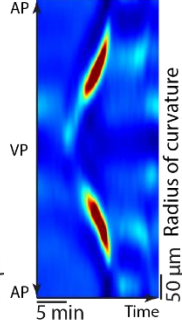
H TS17.18



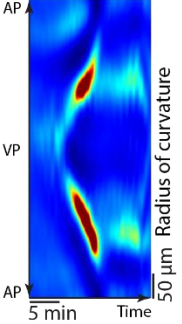
I TS17.18EE



J TS17.18AA



K SS1.2AA



L SS1.2EE

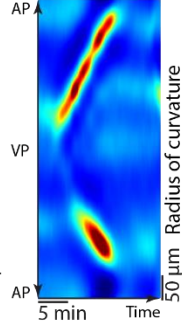


Figure 42: MRLC phosphomutants.

A) Beginning of the MRLC sequence in *Patiria miniata*, showing the two tested phosphorylation sites with the respective changed amino acids for phosphomimetic (EE) and non-phosphorylatable (AA). B) Quantification of the contraction strength resulting from the overexpression of the different MRLC mutants compared to overexpression of the non-mutant form and wildtype. C-G) Stills of oocyte overexpressing the various MRLC mutant forms as well as non-mutant control during the contraction wave. The dashed line indicates the flattened cortex H-L) Kymographs of the surface curvature of oocyte overexpressing the various MRLC mutant forms as well as non-mutant control during the contraction wave. Scale bar 30 μm , all times relative to NEBD.

4.2.2.2 Myosin II is phosphorylated by Rok

Given that above I find evidence suggesting that the most common phosphorylation site of MRLC TS17.18 is the site through which myosin activity in the contraction wave is controlled, the next question was which kinase is responsible for the phosphorylation at this site. The candidates are myosin light chain kinase (MLCK), RhoA-dependent kinase (Rok) and citron kinase, of which the first two are much better studied and chemical inhibitors are available against these. Therefore, I focussed on elucidating whether MLCK or Rok is responsible for phosphorylating myosin in the context of the contraction wave.

Firstly I tested two inhibitors against MLCK, ML-7 and MLCK inhibitory peptide 18 (Lukas et al. 1999). The application of both inhibitors on the oocytes did not lead to any reduction in the strength of the contraction (Figure 43 A, B and C). While MLCK is present in the sequenced transcriptome of the starfish, the mass spectroscopy dataset of both mature and immature oocytes do not show the presence of MLCK. This indicates that likely MLCK is not present in the oocyte. Overall, the lack of effect of the inhibitors and the absence from the mass-spec data indicate that MLCK does not function in the contraction wave process.

Rok can activate myosin II via two distinct mechanisms - either by directly phosphorylating MRLC or by inhibiting the myosin inhibitor myosin phosphatase. There is a specific small molecule inhibitor for Rok called Y27632 (Ishizaki et al. 2000). Application of this inhibitor to the oocytes or injection into the cytoplasm lead to the abolishment of the contraction (from a variance of curvature in the control of $292 \pm 141 \mu\text{m}^2$ to $30 \pm 30 \mu\text{m}^2$, $p < 0.001$) (Figure 43 D, E, F). This proves that in the context of the contraction wave myosin regulatory light chain is phosphorylated and thereby activated by the RhoA kinase (Rok). Whether this activation is achieved directly or through myosin phosphatase cannot be judged from this data.

The involvement of Rok in activating myosin is consistent with previous knowledge, as Rok is also the driving factor of the activation of myosin in cytokinesis which is a similarly contractile process that happens in very close temporal correlation with the contraction wave (Kosako et al. 2000).

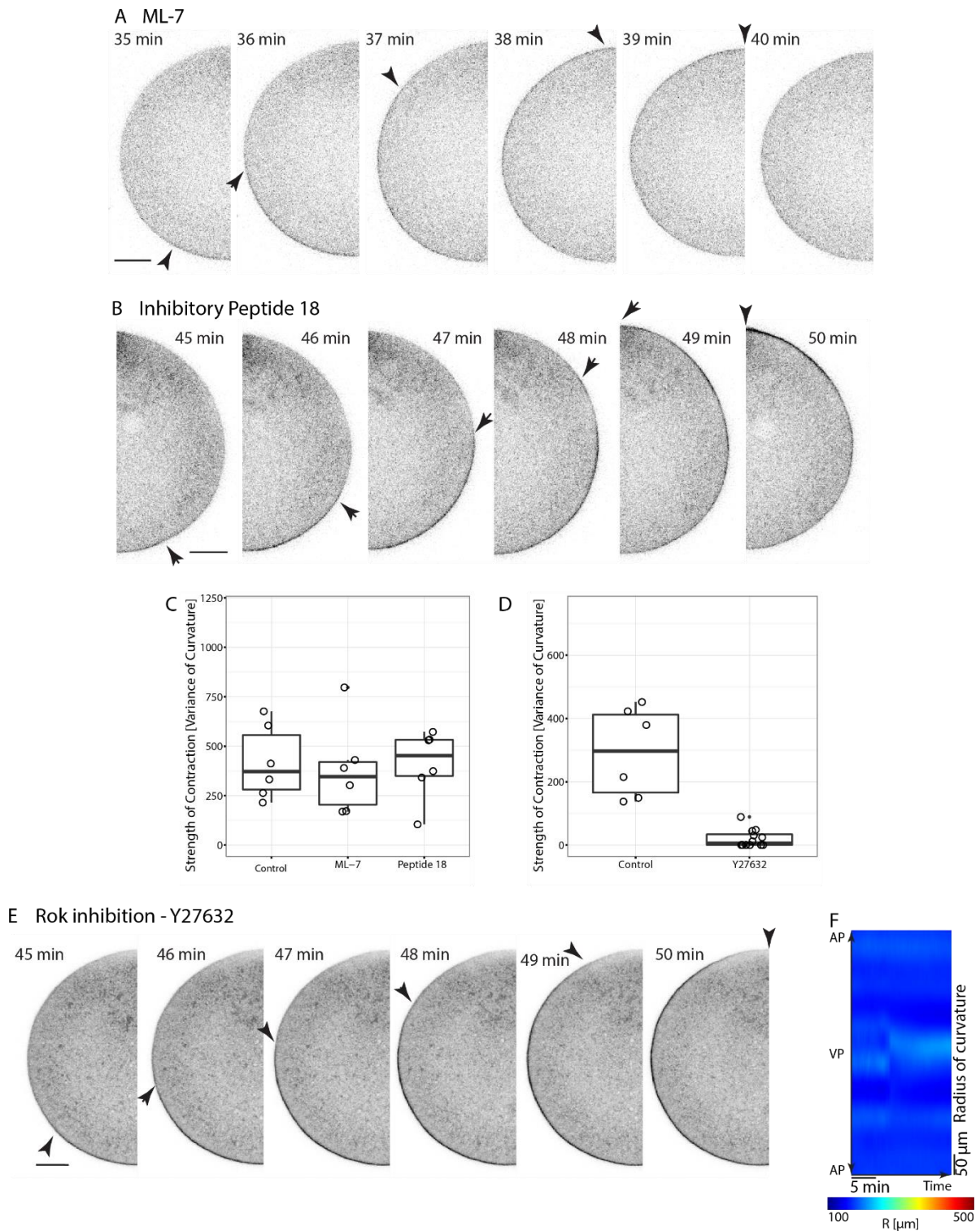


Figure 43: Kinases activating myosin II via phosphorylation.

A) Stills of oocyte treated with MLCK inhibitor ML-7 and B) Inhibitory peptide 18 during the contraction wave, arrows indicate progression of the RhoA signal. C) Quantification of the contraction strength in oocytes treated with MLCK inhibitors showing no change in the strength compared to control. D) Quantification of the contraction strength in oocyte treated with Rok inhibitor Y27632 compared to control, showing abolishment of contraction. E) Stills of oocyte treated with Rok inhibitor Y27632 during the contraction wave. F) Kymograph showing the absence of surface curvature change in oocyte treated with Y27632. Scale bar 30 μm , all time relative to NEBD.

4.2.3 RhoA controls the contraction wave

From the above-presented data, it is clear that Rok phosphorylates myosin II in the context of the contraction wave. This involvement of Rok suggests that RhoA could serve as the upstream regulator of the contraction wave, which was investigated next. While in higher vertebrates RhoA is present in cells together with the closely related RhoB and RhoC (Wheeler & Ridley 2004), in the starfish RhoA is the only homolog of these three isoforms present in the genome.

RhoA can exist in an active GTP-bound and an inactive GDP-bound form, which makes a mere study of the localisation of RhoA as a protein insufficient. To visualise the localisation of the active form of RhoA there are a number of probes, most of which are based on the GTPase-binding domain (GBD) of downstream effectors which specifically bind to the RhoA-GTP form. I herein used a probe consisting of the GBD of rhotekin (rGBD)³ to visualise the active RhoA form (Figure 44A).

The rGBD-GFP probe shows that active RhoA localises to the contractile cortex and moves as a band across the cell along with the contraction wave (Figure 44 B), similar to what is observed for myosin II. Active RhoA forms a sharp high-intensity band which goes along with the contraction wave but RhoA remains at the cortex at lower levels for some time after the wave has passed. It is then lost from the cortex very abruptly, simultaneously all over the cell (Figure 44 C).

To prove the functional involvement of RhoA in the contraction wave oocytes were injected with C3 transferase, an enzyme which ADP-ribosylates RhoA and keeps it terminally in its inactive form in the cytoplasm (Mohr et al. 1992; Vogelsang et al. 2007). Increasing the dose of the injected inhibitor progressively decreased the contraction strength (Figure 44D). Injection of high concentrations of this inhibitor fully blocks the recruitment of active RhoA to the cortex and blocks all downstream contractile activity (Figure 44 E and F, compared to control G and H) (from an average variance of curvature in the control of $695 \pm 150 \mu\text{m}^2$ to $10 \pm 11 \mu\text{m}^2$, $p < 0.001$).

Overall this data clearly shows that RhoA is the upstream control factor regulating the recruitment of myosin II to the oocyte cortex during the contraction wave.

³ This probe was originally developed by the Bement lab (Benink & Bement 2005) and we received the constructs as a kind gift from them.

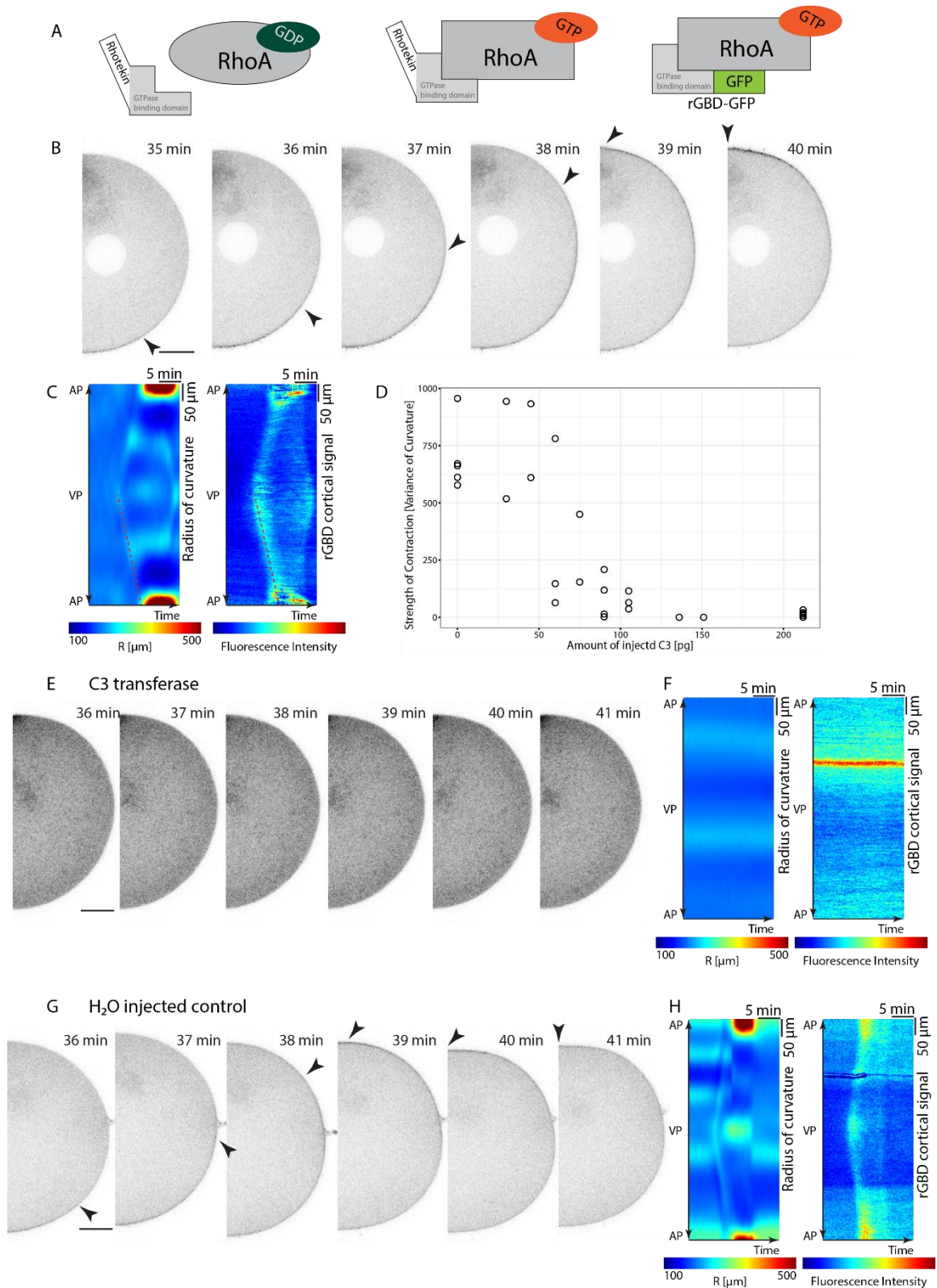


Figure 44: RhoA activity during the contraction wave.

A) Scheme illustrating the function of the rGBD-GFP probe used to detect RhoA activity. B) Stills of an oocyte expressing the probe for RhoA activity during the contraction wave showing signal travelling along the cortex with shape change, marked with arrow heads. C) Kymographs showing the surface curvature and cortical fluorescence intensity of RhoA during the contraction wave. D) Reducing strength of contraction with increasing amounts of injected RhoA inhibitor C3 transferase. E) Stills of an oocyte expressing probe for RhoA activity treated with RhoA inhibitor C3 transferase at the time when the control oocyte (G) undergoes contraction, showing a lack of shape change and RhoA activity. F) and H) Kymographs showing the

surface curvature and cortical fluorescence intensity of cells in E) and F) respectively. Arrows indicate progression of RhoA signal. Scale bar 30 μm , all times relative to NEBD, with time for injection estimated at 5 min.

4.2.4 Activation of RhoA

4.2.4.1 Contraction wave is independent of microtubules

To understand what activates RhoA in this context we can look at the regulation of RhoA activity during cytokinesis, as this is a process that shares the above illustrated molecular pathway and occurs in close temporal correlation to the contraction wave. Cytokinesis can, therefore, serve to provide candidates as starting points for the investigation of the upstream control of RhoA activation. In cytokinesis, RhoA activity is spatially patterned by microtubules, via the RhoA activating GEF Ect2.

To explore whether cytokinesis and the surface contraction wave share this activation pathway, I first tested the role of microtubules in the contraction wave. Treating the oocytes with Nocodazole very quickly and efficiently depolymerised the microtubules of the spindle (Figure 45D). This complete removal of microtubules did not affect the contraction wave in any way. It neither changes the orientation nor the strength of the contraction wave (Figure 45 A, B and C). The variance of the radius of curvature was $445 \pm 233 \mu\text{m}^2$ for the Nocodazole-treated cells compared to $463 \pm 206 \mu\text{m}^2$ for control.

This indicates that the contraction wave is independent of microtubules. This is a very interesting observation which shows that while the downstream RhoA-Rok-Myosin II pathway is the same in the contraction wave and in cytokinesis, their upstream regulation shows differences. From this observation, we can essentially frame the contraction wave as the cortical response to cytokinetic signals in a large cell independent and unconstrained by the microtubules.

The independence of the contraction wave from microtubules furthermore asks the question of how RhoA is then activated in this system.

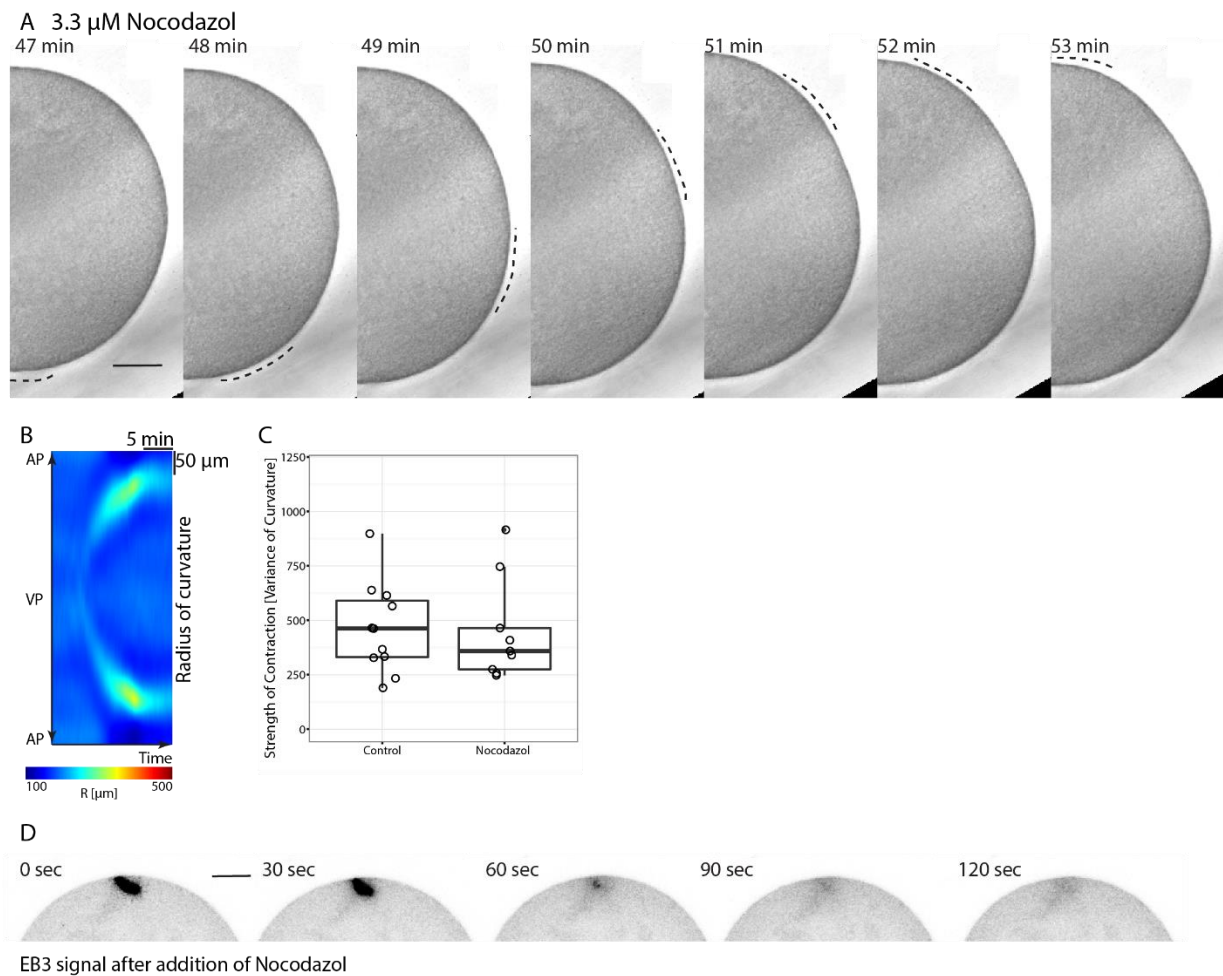


Figure 45: Function of microtubules during the contraction wave.

A) Stills of oocyte treated with microtubule depolymerising agent Nocodazole during the contraction wave. Time relative to NEBD. B) Kymograph of the surface curvature change of the cell in A). C) Quantification of the contraction strength in oocytes treated with Nocodazole relative to control treatment. D) Stills of an oocyte expressing microtubule (+)-end label EB3 showing the speed of microtubule depolymerisation after Nocodazole treatment at 0 sec. Scale bar 30 μm .

4.2.4.2 Ect2 as a possible RhoA activator

To transfer RhoA into its active GTP-bound state there are a number of activator proteins called GEFs, the most important and well-studied of which is Ect2. This protein is key in activating RhoA during cytokinesis and so was the first candidate for the activation of RhoA in the contraction wave that I tested.

Ect2 shows a strong nuclear localisation in the immature oocyte but there is no visible localisation to the contractile cortex (Figure 46 A and E)⁴. At the same time, Ect2 shows a clear localisation to the base of the polar body, prepatternning the contractile ring (Figure 46A). This localisation is expected from its function in cytokinesis and indicates that the construct localised functionally in this system.

⁴ I received the *Patiria miniata* Ect2 construct from the Bement lab.

This means that the lack of a signal during the contraction wave may be due either to too low signal levels or a lack of localisation to the contractile cortex.

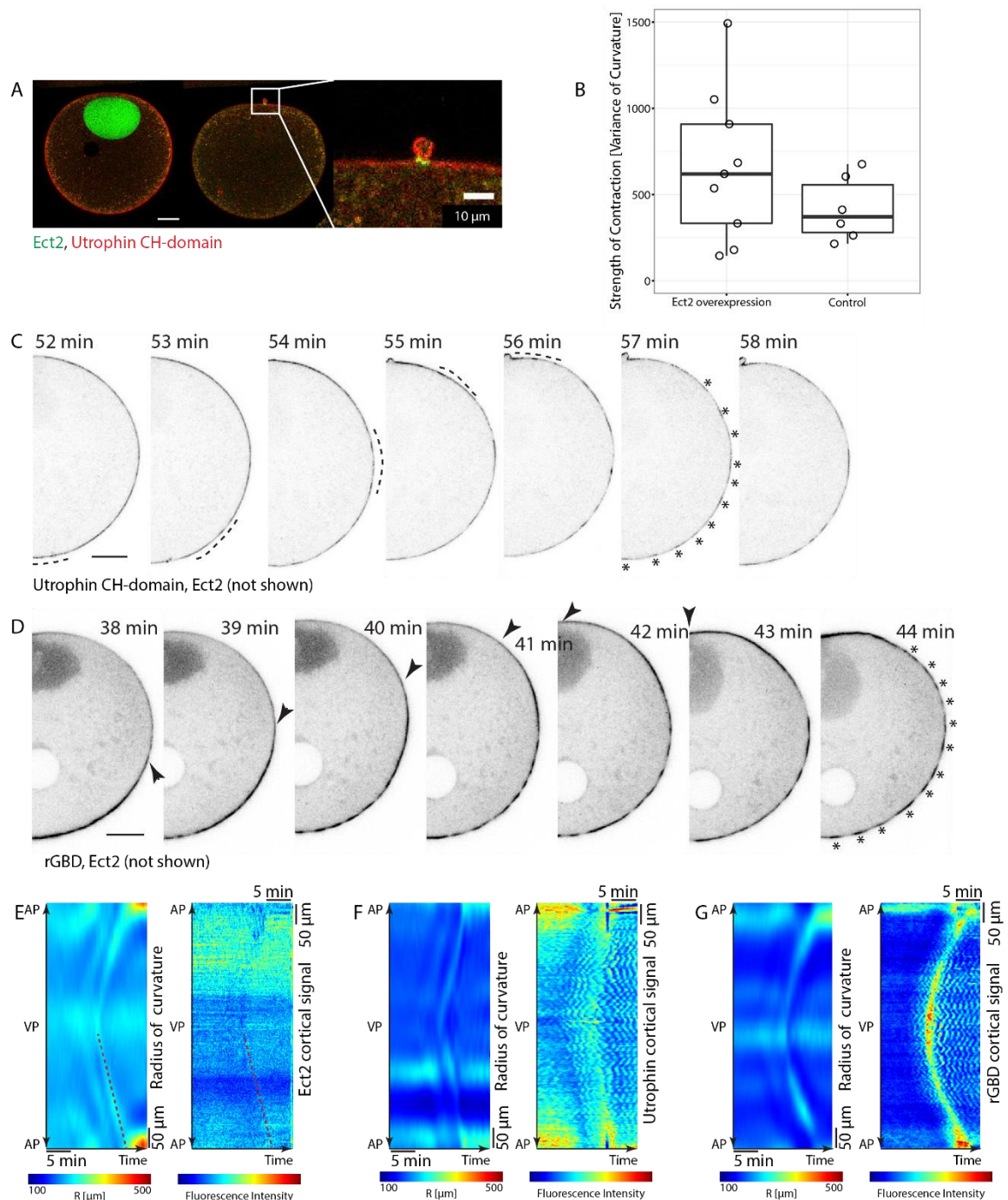


Figure 46: Ect2 in the contraction wave.

A) Oocyte expressing Ect2 (in green) and the marker for F-actin Utrophin CH-domain (in red) in the immature stage (left panel), as well as during polar body formation (middle panel) and zoom on the polar body (right panel), showing Ect2 in the contractile ring at the base of the polar body. B) Quantification of the contraction strength in oocytes expressing Ect2 compared to untreated cells. C) Stills of an oocyte expressing F-actin marker Utrophin as well as D) the probe for RhoA activity (rGBD), both on the background of Ect2 (channel not shown) during the contraction wave showing the rippling behaviour. The dashed line marks the flattened cortex while the arrows mark the front of the rGBD signal. Asterisks mark the ripples – note the even spacing. E-G) Kymographs of surface curvature and cortical fluorescence intensity of Ect2, F-actin marker Utrophin and the probe for RhoA activity (rGBD) respectively. Scale bar 30 μ m, all times relative the NEBD.

The expression of the GFP-Ect2 construct has no significant effect on the strength of the contraction (Figure 46 B). In some cases, stronger contraction waves were observed but no significant difference was found ($661 \pm 437 \mu\text{m}^2$ for Ect2 compared to $417 \pm 186 \mu\text{m}^2$ for control).

At the same time, Ect2 overexpression has an interesting effect both on the actin cortex and RhoA behaviour. With Ect2 overexpression both RhoA and actin exhibit a strong rippling behaviour, starting immediately before the contraction and continuing for some time after the contraction wave has passed until RhoA activity is switched off (Figure 46 C, D and F, G). These ripples have a near constant wavelength and frequency and were recently described in detail (Bement et al. 2015). They are a sign that the cortex is in a division-ready, active state. But there seems to be no functional link to the contraction wave apart from the fact that they are both cortical phenomenon occurring at the same time. This is consistent with the data from (Bement et al. 2015), who showed no connection to the contraction waves.

From the localisation to the contractile ring and the induction of cortical ripples it is clear that the Ect2 construct I am using is functional and can induce effects on the level of RhoA signalling when overexpressed. The fact that I do not observe a localisation or a significant response to Ect2 overexpression for the contraction wave can be due to the fact that either Ect2 is not involved in the process or that the strength of the contraction wave is limited at a point downstream of Ect2 and therefore an overactivation will not show a visible effect. The latter explanation is consistent with the MRLC overexpression data shown above, which indicate that myosin levels might limit the contraction strength. A further investigation of the involvement of Ect2 is limited by the fact that no specific chemical inhibitors for Ect2 are available.

In summary, I can neither exclude the involvement of Ect2 in the contraction wave nor do I find any evidence supporting the idea that Ect2 activates RhoA in the context of the contraction wave.

4.2.4.3 Alternative GEFs

As the investigation of Ect2 in the contraction wave remained inconclusive, I investigated alternative GEFs which might act instead of Ect2 as RhoA activators. The two candidates I choose based on the literature were GEF-H1 and MyoGEF. Both of these have been implicated as alternatives to Ect2 in activating RhoA during cytokinesis and are present in the starfish transcriptome. GEF-H1 is inactivated via Cdk1-cyclin B phosphorylation and is bound to microtubules in its inactive form, thereby linking cell-cycle, microtubules dynamics and RhoA activation, while a knockdown of GEF-H1 leads to cytokinesis defects (Birkenfeld et al. 2007; Krendel et al. 2002). MyoGEF, or myosin-interacting GEF, is a much less described GEF but is an exciting candidate in the context of the contraction wave as it

interacts with cortical myosin II and activates RhoA. The inhibition of MyoGEF in U2OS cells has been reported as causing cytokinesis defects (Wu et al. 2006).

Expressing the GFP-tagged version of either GEF-H1 or MyoGEF showed no localisation to the contractile cortex as well as no effect on the strength of the contraction wave (Figure 47 E) ($419 \pm 233 \mu\text{m}^2$ for MyoGEF, and $337 \pm 102 \mu\text{m}^2$ for GEF-H1 compared to $417 \pm 186 \mu\text{m}^2$ for non-treated cells). At the same time, expressing GEF-H1 had an interesting effect in the immature oocyte, causing the cells to become misshapen and bumpy, but this effect disappears with the cortex softening at NEBD (Figure 47 A). Also, the GEF-H1 expressing cells show division defects in the embryos (Figure 47 B), indicating that GEF-H1 plays a role in maintaining both immature oocyte shape and in mitotic divisions in the embryo. Interestingly polar body formation – the cell division in the oocyte – was not affected by the expression of GEF-H1. These clear effects of an overexpression of GEF-H1 in other contexts are at least indications that even though a specific localisation cannot be observed with the GFP-tagged protein, the construct is functional.

While GEF-H1 shows these interesting phenotypes, expressing MyoGEF in the oocytes had no effect on either contraction wave, immature cell shape or embryonic development which the embryos reaching the blastula stage without issues (Figure 47 C and D). From this, no conclusions can be drawn as to whether the MyoGEF construct is functional.

From this brief exploration of the alternative GEFs in the activation of RhoA, I find no strong evidence implicating either GEF-H1 or MyoGEF in the contraction wave. At the same time as I only overexpressed the GFP-tagged construct and there are no chemical inhibitors available, I was not able to firmly exclude their function either.

It is clear that a GEF must be involved in the activation of RhoA during the contraction wave. It is possible that a so far unidentified or uncharacterised GEF fulfils this function in the starfish oocyte. Perhaps more likely Ect2 as the highly conserved activator of RhoA might still be active in this system without me being able to detect its functionality with the current tools. Further investigations using mutant or truncated versions of Ect2 are required to settle the question of its involvement.

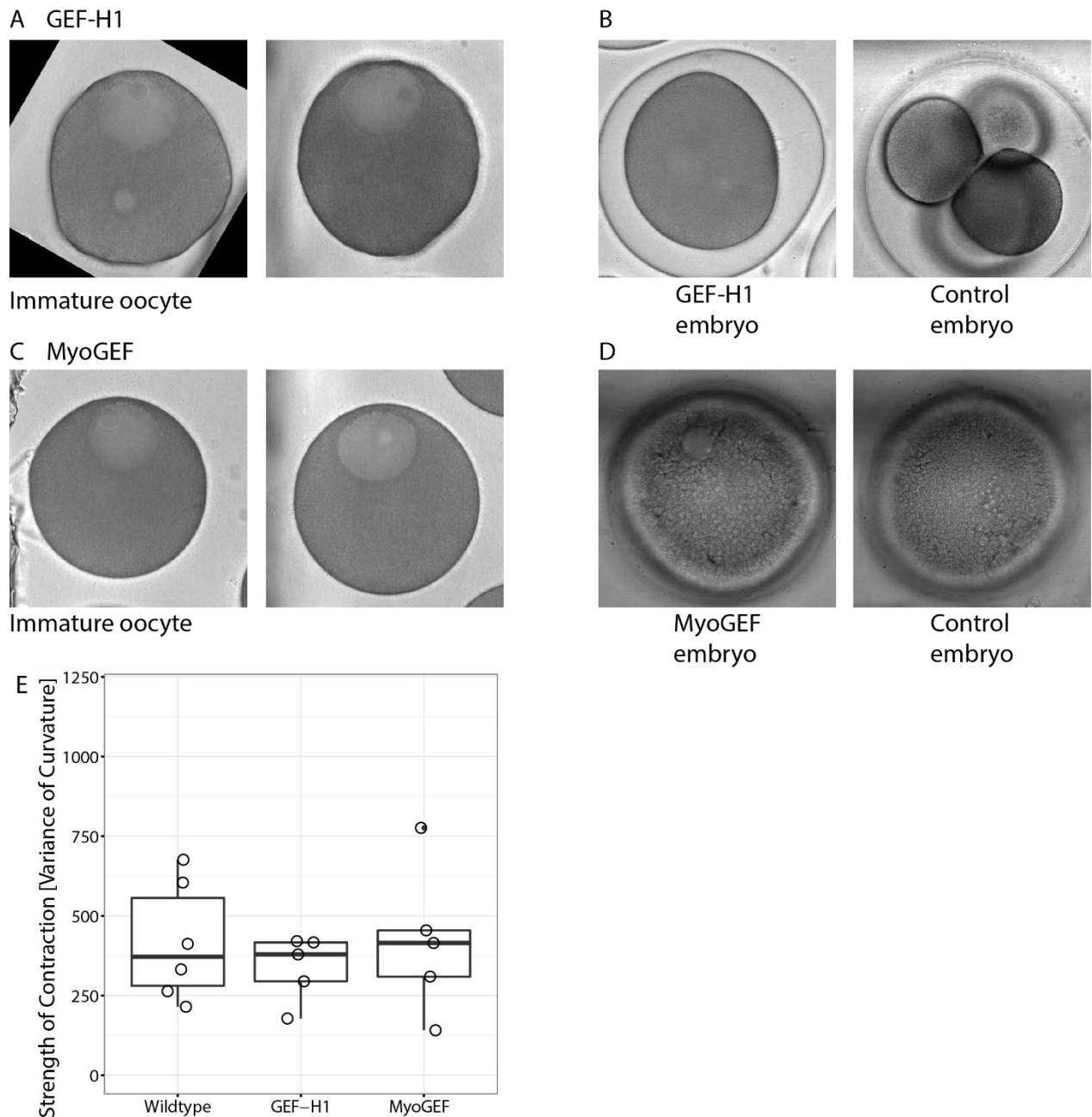


Figure 47: Alternative GEF candidates for RhoA activation.

A) Two examples of immature oocytes expressing GEF-H1 showing the 'bumpy' surface phenotype. B) Early embryo from an oocyte expressing GEF-H1 compared to control embryo showing division defects. C) Two examples of immature oocytes expressing MyoGEF showing no abnormalities. D) Early blastula stage of the embryo arising from MyoGEF injected oocyte and control embryo. E) Quantification of the contraction strength in oocytes expressing either GEF-H1 or MyoGEF compared to wildtype.

4.2.5 The actin cortex serves as a substrate for contraction

In the contraction wave myosin II generates the force of contractility but so far I have only focussed on the pathway leading to the activation of myosin and have disregarded the substrate on which myosin contracts. This shall be rectified in the following section which focusses on the role of the actin cortex in the contraction wave.

The cortex is a fascinating complex system of actin and a number of interacting proteins. To visualise the behaviour of the cortex, oocytes expressing a marker for filamentous actin, Utrophin-CH domain, were used. This marker strongly labels the cortex (Figure 48A) but during the contraction wave the changes in actin levels at the cortex are relatively subtle (Figure 48A). A closer examination using the kymograph of cortical fluorescence intensity allows us to see an increase in the actin signal during the contraction (Figure 48B). This increase is however relatively small compared to either myosin II or RhoA-GTP, as the cortex shows a strong signal all the way through metaphase before the contraction wave. Interestingly, the ripples in the actin signal I already observed in the Ect2 overexpression (Figure 46 D and F), are also visible when actin is observed on its own, although again they are more subtle (Figure 48B).

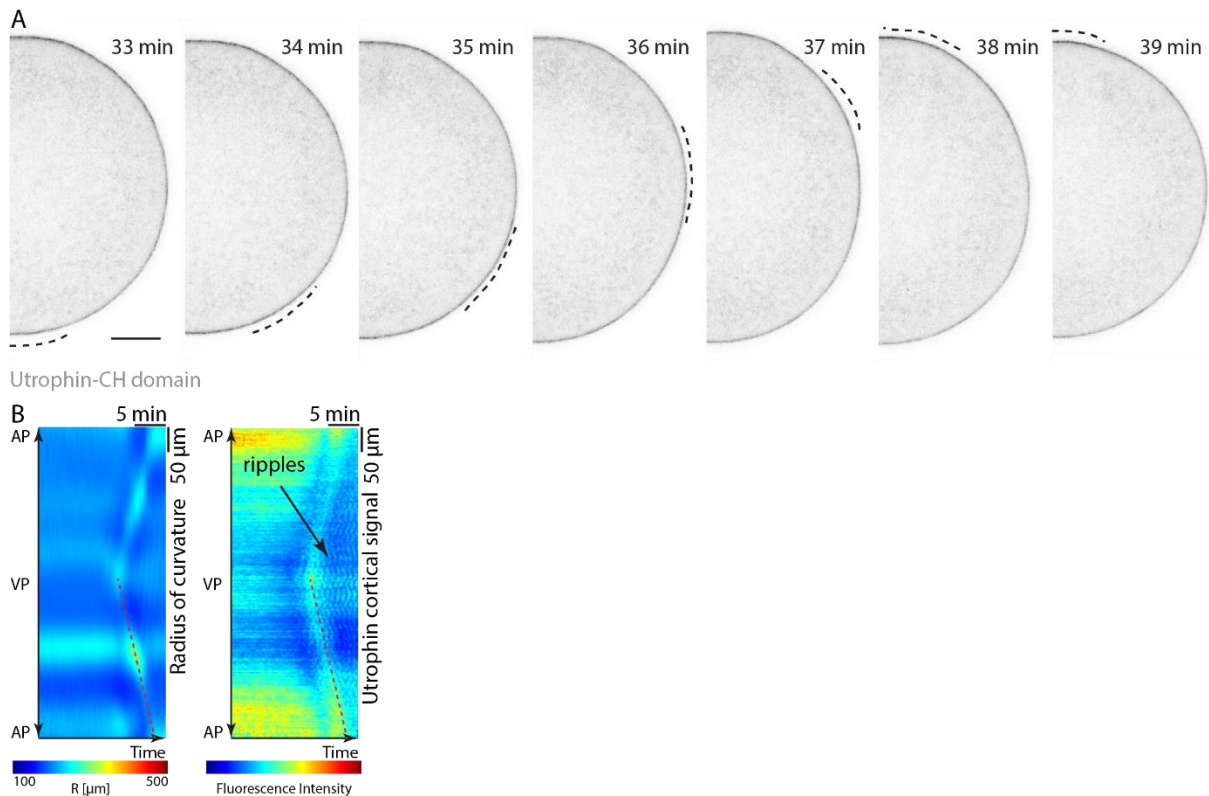


Figure 48: Actin localization during the contraction wave

A) Stills of an oocyte expressing F-actin marker Utrophin CH-domain during the contraction wave. The dashed lines indicate the flattened cortex. B) Kymograph of the surface curvature and cortical fluorescence intensity of the cell in A). Scale bar 30 μm, times relative to NEBD.

To investigate the feedback between the contractile behaviour, the signalling leading to myosin II activation and the actin cortex, I have chosen two methods to manipulate the actin cortex. The first is to inject the cells with Phalloidin, a fungal toxin which very efficiently stabilises actin filaments and thereby drives the equilibrium of actin assembly towards assembling all actin monomers into actin filaments (Wulf et al. 1979).

The Phalloidin injection has two effects – one is to stabilise and increase the size of the actin cortex while also generating a large number of filaments in the cytoplasm leading to a stiffening of the cytoplasm. There is no contraction wave taking place in cells injected with large doses of Phalloidin (Figure 49 A, B and F). The variance of the radius of surface curvature in Phalloidin injected oocytes was $13 \pm 40 \mu\text{m}^2$ compared to $417 \pm 186 \mu\text{m}^2$ in untreated cells ($p < 0.0005$). Whether this is due to myosin II not being able to contract the crosslinked and thickened cortex or whether the force is not sufficient to contract against the stiffened cytoplasm cannot be determined from these experiments. But at the same time, the RhoA signal still travels along the cortex, although the background signal at the cortex is higher in these oocytes (compare Figure 48B and Figure 49B).

The second and opposite manipulation is the depolymerisation of the actin cortex via the treatment with Cytochalasin D (Goddette & Frieden 1986). The effect of this drug treatment can be visualised in oocytes expressing Utrophin-GFP, which loose the actin signal from the cortex (Figure 49 E), although it is possible that small patches of actin remain at the cortex. The contraction wave does not move across the cell anymore if the cortex is removed (Figure 49 C) and no shape change takes place (Figure 49 C, D and F). The variance of the radius of cortex curvature in Cytochalasin D treated oocytes was $17 \pm 20 \mu\text{m}^2$ compared to $417 \pm 186 \mu\text{m}^2$ in untreated cells ($p < 0.0005$). This is due to the fact that myosin II requires actin as a substrate for its activity. On the other hand, the upstream regulatory RhoA signal still travels the whole distance from vegetal pole to animal pole (Figure 49 C and D).

It is clear when looking at the kymographs that RhoA levels at the cortex previous to the contraction wave are different in the cells were actin is manipulated either by Phalloidin or by Cytochalasin D compared to non-treated cells (Figure 49C and D, compared to Figure 44C). This is consistent with reports of a feedback system between RhoA and actin (Bement et al. 2015). At the same time, the distinct RhoA signal of the contraction wave is still visible in the kymographs. This suggests that while the reported actin-RhoA feedback system may be in effect, an additional regulatory system controls RhoA signalling leading to myosin II recruitment in the contraction wave, likely independent of actin.

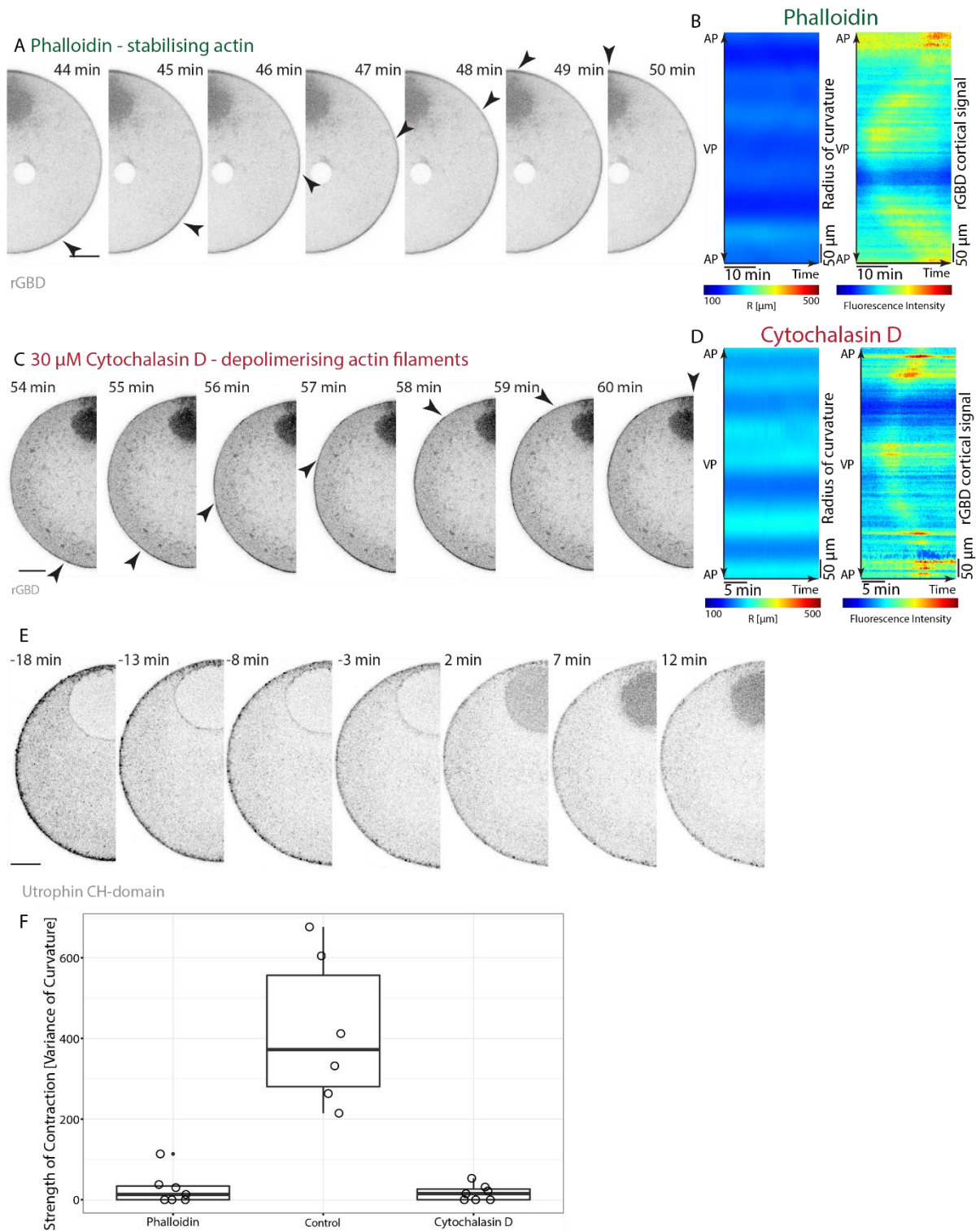


Figure 49: Actin manipulations during the contraction wave.

A) Stills of an oocyte expressing RhoA activity probe (rGBD) and injected with Phalloidin during the contraction wave. B) Kymograph of the surface curvature and cortical fluorescence intensity of the cells in A) treated with Phalloidin. C) Stills of an oocyte expressing RhoA activity probe (rGBD) treated with Cytochalasin D during the contraction wave. D) Kymograph of the surface curvature and cortical fluorescence intensity of the cells in C) treated with Cytochalasin D. E) Stills of an oocyte expressing F-actin marker Utrophin CH-domain after treatment with Cytochalasin D showing actin depolymerisation. F) Quantification of the contraction strength in oocyte injected with Phalloidin or treated with Cytochalasin D compared to untreated cells. Scale bar 30 μ m, all times relative to NEBD.

4.2.6 Role of calcium in the contraction wave

As calcium is a common regulator of myosin contractility I also wanted to explore whether calcium plays a role in the contraction wave process.

To start investigating this, I injected oocytes with the reporter of calcium concentration CalciumGreen™, whose fluorescence scales with the amount of calcium in the cell (Rajdev & Reynolds 1993). When I quantified the levels of CalciumGreen™ fluorescence across the whole cell over the course of the cell cycle, I observe a steady rise during metaphase and a small but consistent spike during the contraction wave (Figure 50 A and C). There is also a lesser peak in calcium levels at NEBD. At the same time, the rise of calcium observed during the contraction wave (and the whole of meiosis) is negligible compared to the spike in calcium levels which go along with fertilisation (Figure 50 B and C).

To test whether the observed change in calcium levels during the contraction wave are functionally relevant, I observed oocytes undergoing maturation in calcium-free seawater with added EGTA. The contraction wave changes by the removal of Calcium from the cell, leading to a reduction in the contraction strength (Figure 50 F). Even though the contraction is lost, the upstream signalling of RhoA still progresses around the cell in a normal pattern (Figure 50 D and E).

It is important to note though, that as the starfish oocytes natural environment is very calcium-rich, the perturbations of the calcium levels in the oocyte lead to obvious defects in many cells. The common defects I observe are a collapse of the animal pole (Figure 50 G) and a “granulation” of the cytoplasm (Figure 50 H). This granulation may signify a change in the viscoelastic properties of the cytoplasm which could explain the reduced contraction strength if the cytoplasm becomes stiffer. At the same time, the actin cortex could be changed by a reduction in calcium through a gelation effect, which may affect myosin’s ability to contract the cortex. Apart from a possible side-effect of the treatment, it is also possible that myosin is additionally regulated in the context of the contraction wave through the calmodulin-dependent light chain kinase or via a modulation of the actin cortex.

Overall it is clear that calcium is an important component of the oocytes environment and removal impacts the contraction wave, although the mechanism by which this happens remains unclear.

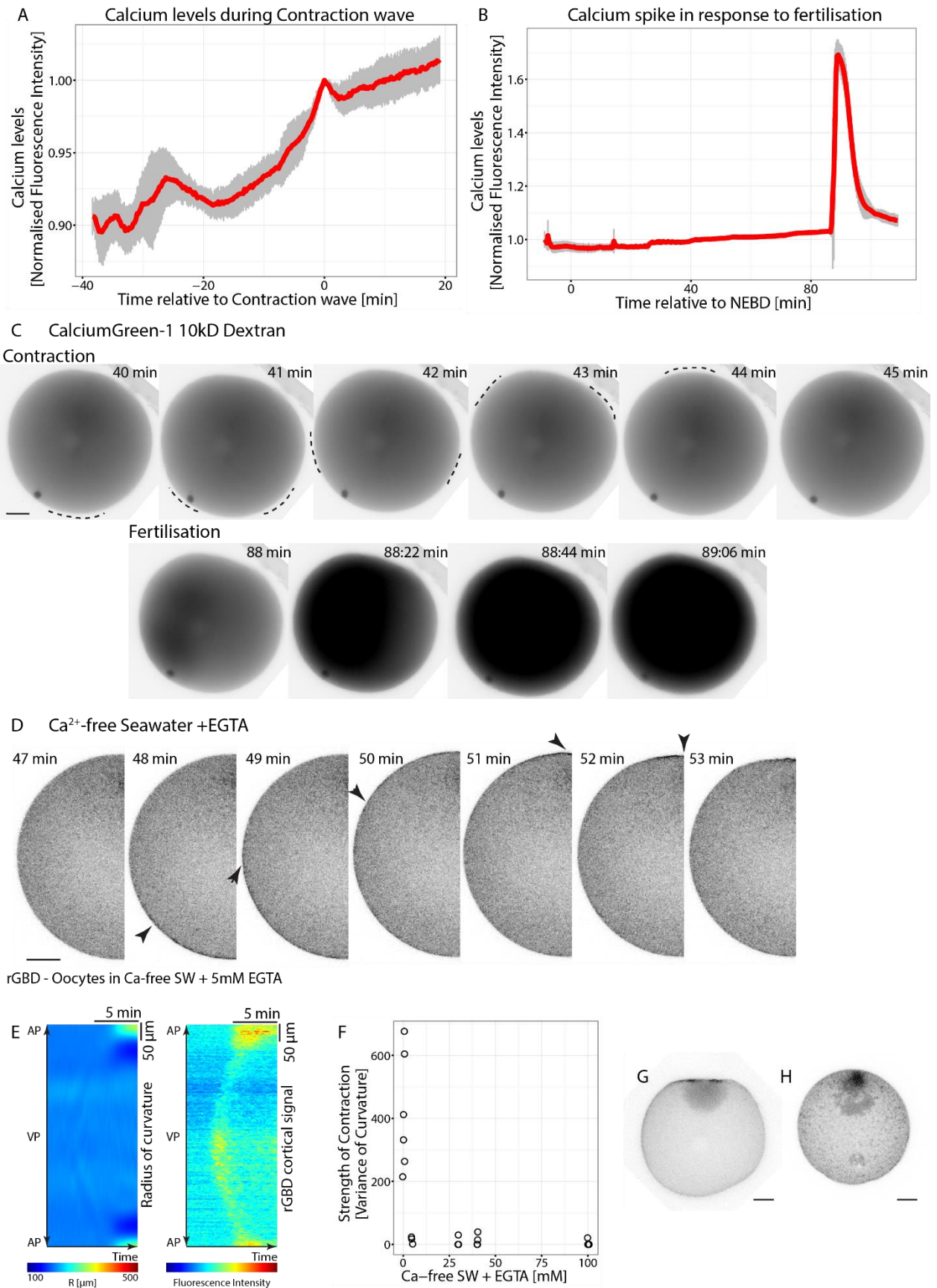


Figure 50: Role of calcium in the contraction wave.

A) Calcium levels during the contraction measured via CalciumGreen showing a spike at contraction wave. B) Calcium levels in the oocyte in response to fertilisation measured via CalciumGreen. C) Still of oocyte injected with CalciumGreen during contraction wave (upper panel) and during fertilisation (lower panel). D) Oocyte expressing RhoA activity probe (rGBD)

maintained in Calcium-free SW with 5 mM EGTA during the contraction wave. E) Kymograph of surface curvature and cortical fluorescence intensity of cell D) showing reduced contraction strength. F) Contraction strength with varying doses of EGTA added to the Calcium-free SW. G) 'Animal pole collapse' phenotype. H) 'Cytoplasmic granulation' phenotype. Scale bar 30 μm , times relative to NEBD.

4.2.7 Summary of the molecular pathway controlling contraction

So far I have established the direct molecular control pathway of the contraction wave (Figure 51).

In this pathway, RhoA is the most upstream control factor. It is activated by a GEF factor whose identity I have not been able to determine. RhoA activity then activates RhoA kinase, which in turn activates and drives myosin II localization to the cortex. The cortex serves as a substrate for myosin contractility and the localisation of myosin II leads to cortex flattening. The progression of this flattening across the cell gives rise to the contraction wave.

This pathway is a highly conserved one that is active in many cellular contexts. One of the key processes that is also driven by this pathway is the formation of the contractile ring in cytokinesis (Miller 2011). In this context the GEF that activates RhoA is Ect2 and this signal is localised by the microtubules of the spindle. This is to be seen in contrast to the contraction wave, where microtubules are not involved, indicating that Ect2 is either localised by an alternative mechanism or another GEF activates RhoA.

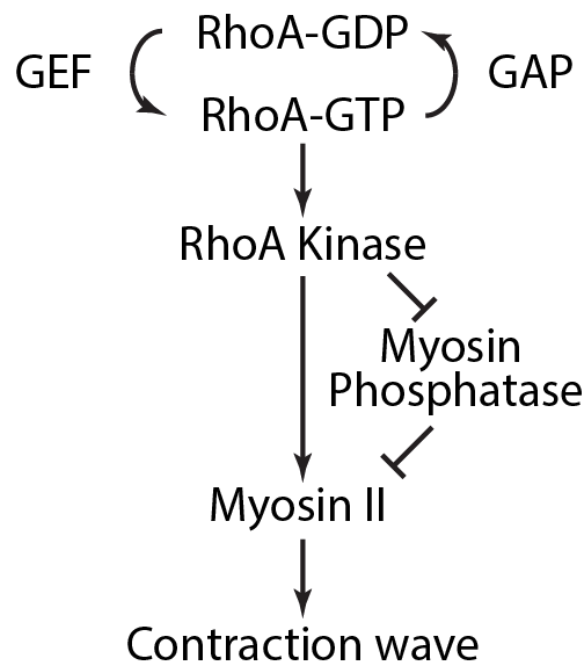


Figure 51: Molecular pathway regulating myosin II activity in the contraction wave.

But this molecular pathway is intrinsically static and can only explain the recruitment and activation of myosin II at each individual cortical position. How the wave behaviour arises and how the signal is spread across the cell will be explored in the next section.

4.3 HOW TO FORM A WAVE

4.3.1 Initiation of the contraction wave

4.3.1.1 *The contraction wave starts opposite of the nucleus*

To determine the mechanism by which a wave is formed, the first aspect to be explored is the setting of its starting point. There are two plausible hypothesis to explain the observation that the contraction wave always starts at the vegetal pole of the oocyte. Firstly, there could be a predetermined factor localised at the vegetal pole which in response to a certain signal sets off the contraction wave. On the other hand, the oocyte could respond to the specific cell layout, i.e. to have the wave always start opposite of the nucleus. In the wildtype these two possibilities are indistinguishable.

To allow the differentiation between the two hypotheses, the oocytes can be centrifuged. This is a well-established technique which has been applied to the starfish oocytes (Miyazaki et al. 2000). Centrifugation allows the repositioning of the nucleus relative to the remainder of the cytoplasm and thereby the setting of a new animal-vegetal axis that is distinct from the old animal-vegetal axis (Figure 52 A). When the oocytes are matured after centrifugation, it can be observed which of the two animal-vegetal axes the wave follows.

From the observation of a number of cells I can conclude that the contraction wave always follows the new animal-vegetal axis, that is, the wave is always oriented towards the nucleus, independent of where the nucleus previously was. This becomes obvious upon observation of a sample oocyte (Figure 52 C), where the centrosomes (in green) mark the position of the nucleus previous to centrifugation (Figure 52 C white arrow) while the nucleus is positioned at the top of the oocyte after centrifugation. The contraction wave then moves towards the top. This can also be seen in the kymograph, where the flattening no longer starts at the old (pre-centrifugation) vegetal pole but rather at the new (post-centrifugation) vegetal pole (Figure 52 D).

The effect of the centrifugation can be quantified for a larger number of cells by measuring the angle α between the axis of contraction and the old and new animal-vegetal axis respectively (Figure 52 B). The angle between the contraction wave and the new animal-vegetal axis is always near 0, i.e. both go in parallel, while there is no pattern in the angle between the axis of contraction and the old animal-vegetal axis (Figure 52 B).

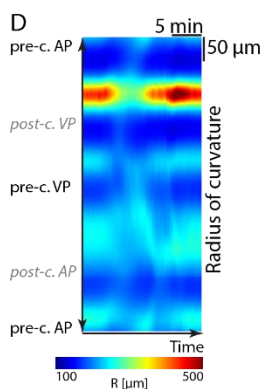
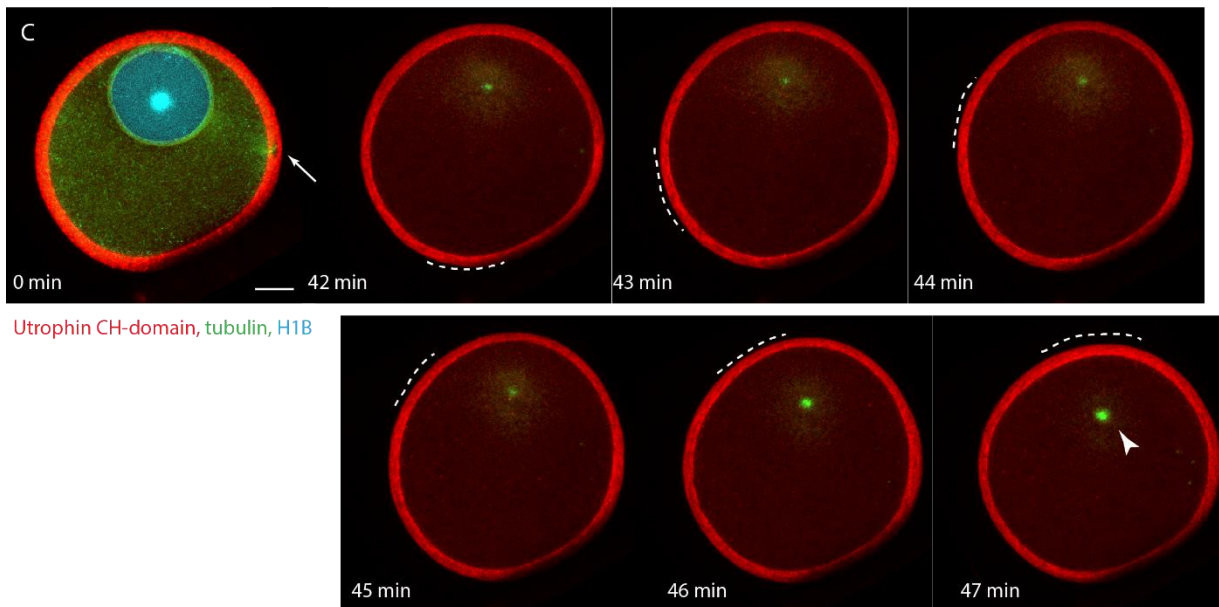
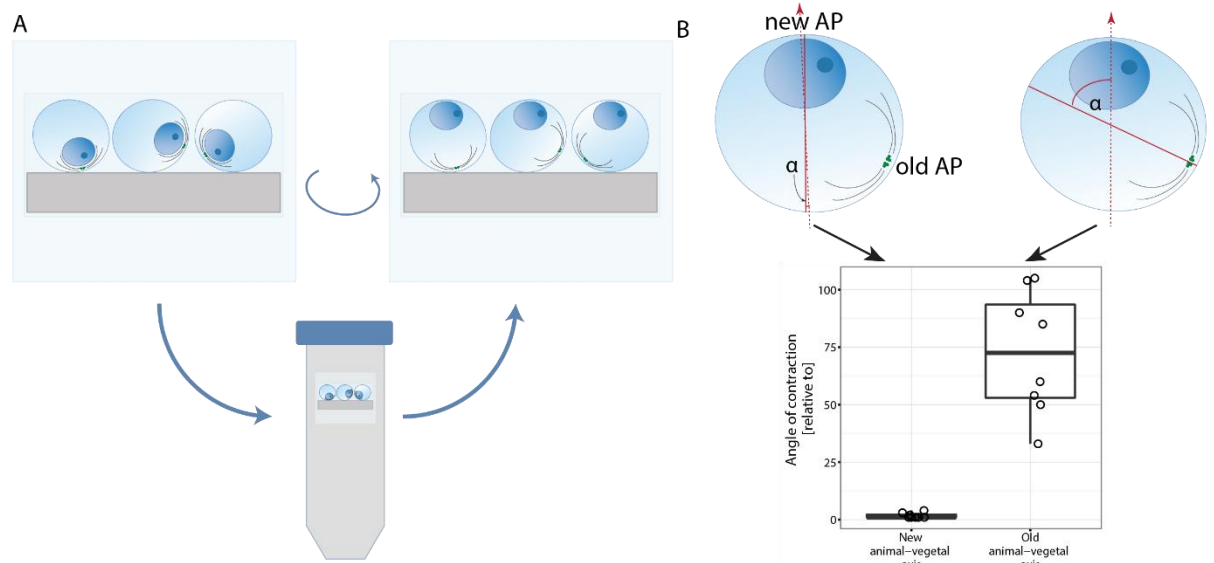


Figure 52: Changing AP-VP axis via centrifugation.

A) Scheme showing the set-up used for centrifugation, adapted from (Borrego Pinto 2015), which a random orientation of oocytes before centrifugation and all nuclei facing upwards after centrifugation. B) Quantification of the angle between the axis of contraction and the old and new animal-vegetal axis respectively. C) Oocyte expressing F-actin marker Utrophin CH-domain and injected with fluorescently labelled tubulin and H1B protein. The first image shows immature oocyte after centrifugation with the arrow indicating the centrosomes marking the original animal pole (AP) and later images showing the contraction wave moving towards the new nuclear position. The dashed line marks the flattened cortex during the

contraction wave. D) Kymograph of the surface curvature of the cell in C), with marks indicating both the pre-centrifugation (pre-c.) and post-centrifugation (post-c.) poles. Scale bar 30 μm , all time relative to NEBD.

These results indicate that the axis of the oocyte is not predetermined early in the development of the oocyte but is responsive to change. At the same time, the change induced by centrifugation is a very drastic perturbation, which will not occur in nature as there the nucleus is held in position by the microtubules at the animal pole against gravitational forces (Miyazaki et al. 2000). I can conclude from this data that the factor controlling the starting point of the contraction wave is the position of the nucleus and is therefore likely by a nuclear factor.

4.3.1.2 A gradient of cell cycle activity is present in the oocyte

In the search for a potential nuclear factor which controls the orientation of the contraction wave, a good candidate is the central metaphase regulator Cdk1-cyclin B. This is due to the fact that it is imported into the nucleus immediately before metaphase entry (Terasaki et al. 2003). Furthermore, Cdk1-cyclin B levels change drastically at the exit of metaphase, and given the tight temporal correlation between the contraction wave and metaphase exit, this suggests that Cdk1-cyclin B could play a role in controlling the contraction wave.

As a first step to investigate whether Cdk1/Cyclin B plays a role in controlling the contraction wave, I generated a GFP-tagged form of the *Patiria miniata* Cyclin B. Cyclin B shows very interesting and temporally varied localisations throughout the cell cycle (Figure 53 A).

In the immature oocyte cyclin B forms aggregates in the cytoplasm (Figure 53 A arrows), which had previously been reported (Terasaki et al. 2003), while the nucleus is devoid of cyclin B. As maturation starts, within the first 5 min after hormone addition the aggregates disappear, and 10 min later cyclin B begins to be imported into the nucleus. The import leads to a strong concentration of cyclin B in the nucleus immediately preceding NEBD, which then leads to a spread of concentrated cyclin B at the whole animal pole. Due to the localisation of the nucleus at the cortex, the import establishes a gradient of cyclin B across the whole of the oocyte. This means that the highest levels of cyclin B are located at the animal pole while the levels at the vegetal pole are lower (Figure 53 B).

Over the time course of metaphase the levels of cyclin B drop progressively, as cyclin B is degraded by targeting of the protein to the proteasome by the APC/C (Oita et al. 2004). The degradation is equal all over the cell, meaning that the gradient is maintained throughout metaphase. This becomes clear when the cyclin B levels are quantified along the animal-vegetal axis (Figure 53 B). During the contraction wave, cyclin B levels are already very low, but higher levels at the animal pole still remain, and levels continue to fall as the wave progresses (Figure 53 A).

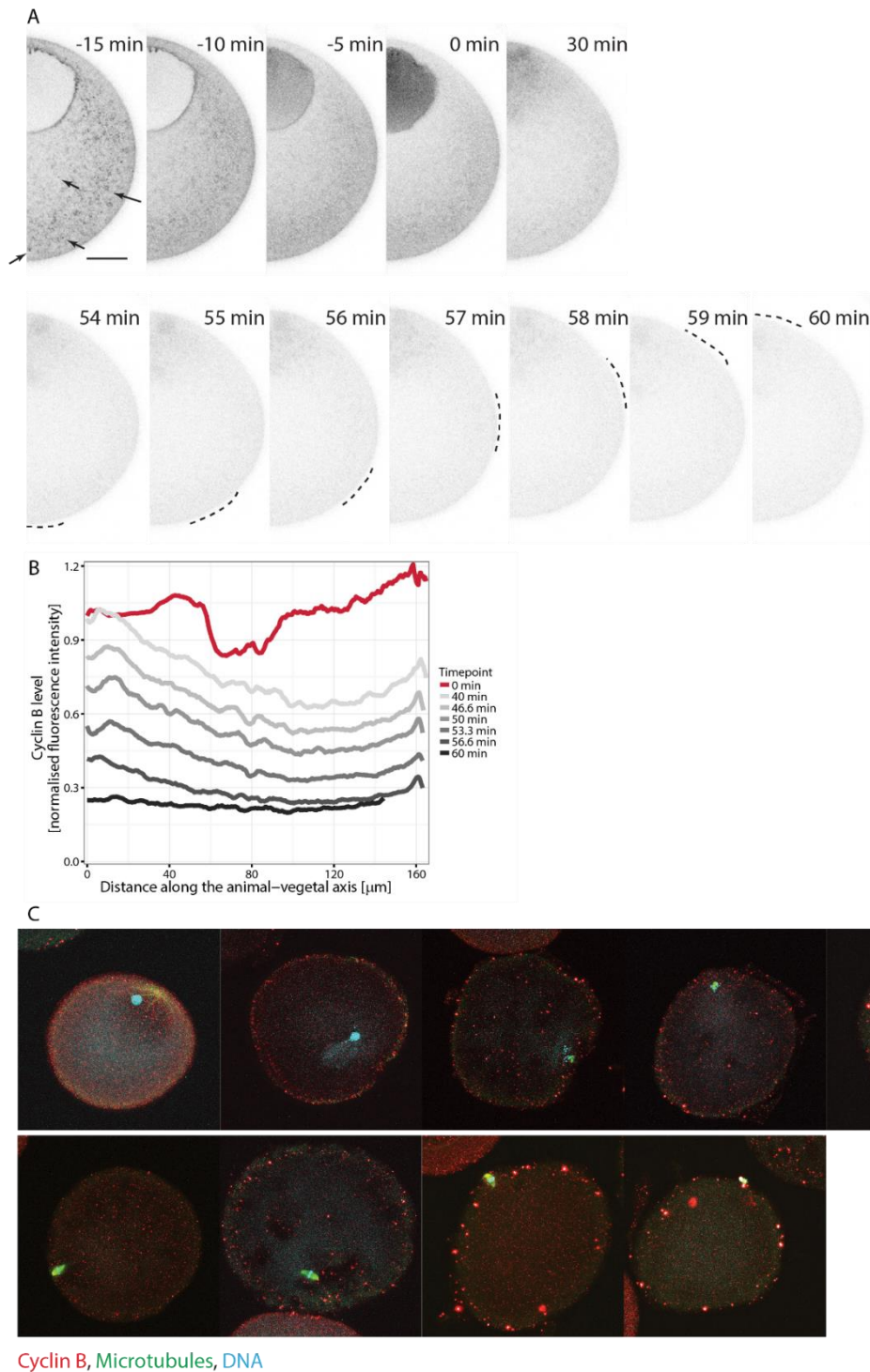


Figure 53: Cyclin B.

A) Oocyte expressing cyclin B-EGFP at various time points before NEBD (upper panel) and contraction wave (lower panel). Arrows mark cytoplasmic cyclin B aggregates. The dashed line indicates the flattened cortex. B) Quantification of fluorescence intensity of cyclin B normalised to background injected Dextran 10kD along the animal-vegetal axis at various time points. C) Virtual time series of cold MeOH-fixed oocytes, stained using cyclin B antibody (red), anti-tubulin (green) and DNA marker Draq5 (blue). Scale bar 30 μm , all times relative to NEBD.

These results indicate that Cdk1-cyclin B could serve as a guide for the contraction wave as it forms a gradient based on the nuclear position, giving the cell a molecular marker for its animal-vegetal axis.

To observe the gradient via an alternative technique, I tested various antibodies against Cdk1 activity and cyclin B localisation. Antibodies against starfish cyclin B were generated by the Kishimoto-Tachibana and Chiba labs and I received aliquots from both⁵. Testing multiple fixation and staining protocols for both the anti-cyclin B and the anti-Cdk1 Y15 antibodies led to very low and unspecific stainings (not shown). For the cyclin B antibody from the Chiba lab, I could observe changes in the intensity of staining over the time course, but the signal was too low to allow the visualisation of the gradient (Figure 53 C). The time course of the fixed oocytes was generated on the basis of spindle and chromosome morphology which were additionally stained.

There are multiple possible reasons for why the immunostaining of cyclin B did not allow easy visualisation of the cyclin B gradient. Firstly the Cdk1 activity antibody is not specific against the starfish protein and likely did not recognise it sufficiently. Secondly, while the starfish cyclin B antibody clearly recognised the protein, it is difficult to observe a specific staining as cyclin B is spread throughout the cytoplasm and not localised to a specific structure. This makes it difficult to normalise the signal against the background staining. Furthermore, small cytoplasmic proteins are much easier lost during the fixation and permeabilisation step, which can contribute to the low signal. I can also not be sure of the quality of the antibody I received, and a preliminary testing of the antibody on western blot showed very low signal levels. To solve this problem, either a new antibody against the starfish cyclin B protein would have to be produced or a further optimisation of the fixation/staining protocols would be necessary. As I have other lines of evidence to prove the idea of a gradient of Cdk1-cyclin B activity across the cell, I did not pursue these options.

4.3.1.3 The Cdk1 gradient controls the direction of the contraction wave

Based on the observations above indicating a gradient of cyclin B across the cell which would go along with a gradient of Cdk1 activity, I hypothesise that this gradient inhibits the activation of myosin II downstream of RhoA in metaphase. As the Cdk1-cyclin B activity is progressively reduced over the course of metaphase the threshold at which the inhibition is no longer sufficient will be hit first at the lowest point of the gradient, i.e. at the vegetal pole.

To test this hypothesis, I locally treated the oocytes at the animal pole with Cdk1 inhibitors at a time before the contraction wave would normally occur. There are a number of these inhibitors commercially available with varying inhibition efficiency. I used both the less efficient Roscovitine (Meijer et al. 1997), as well as the more efficient Flavopiridol (Kaur et al. 1992) and RO-3306 (Vassilev et al. 2006). I hypothesise that the local treatment with the Cdk1 inhibitor at the animal pole results

⁵ I am very grateful for the generous gifts of these antibodies from Prof. Chiba at Ochanomizu University, Japan and Profs. Kishimoto and Tachibana at the Tokyo Institute of Technology.

in the flipping of the gradient. This is due to the fact that the lowest point of Cdk1 activity is induced at the animal pole due to the treatment while some level of Cdk1 activity remains at the vegetal pole as the treatment was performed during metaphase. This flipping of the gradient results in a reversal of the direction of the contraction wave (Figure 54). In the treated oocytes I can observe both a reversal of the physical shape change as the contraction wave moves in the opposite direction (Figure 54 B, D and F) as well as in the underlying signal at the level of RhoA (Figure 54 A, C and E).

The same result can be reached with all three inhibitors (compare Figure 54 A, C and E). After treatment, the contraction wave starts at whatever point was treated with the inhibitor and progresses to the opposite end of the cell. I also applied the inhibitors in various geometries inducing contraction wave starts laterally in the cells as well as a full reversal in which the contraction wave runs from the animal pole to the vegetal pole (Figure 54 C compared to A and E).

The ability to start the wave at the point of local Cdk1 inhibitor treatment supports the idea that the lowest point of the Cdk1 gradient normally marks the starting point of the contraction wave. As the same result is reached with a number of different inhibitors, it is unlikely that the observed effect is due to side-effects of the individual inhibitors.

The local inhibitor treatment furthermore induces the wave at different times compared to when it normally occurs in the maturation process (compare timing in treatment Figure 54 A and control Figure 54 G). Treatment of cells with Cdk1 inhibitors is known to force metaphase exit in cells (Vassilev et al. 2006), and the fact that the contraction wave can be induced prematurely strongly indicates that the contraction wave itself is an effect of metaphase exit, connected to the Cdk1 activity levels. This becomes further clear when oocytes expressing cyclin B are treated with the inhibitor. In this case, the contraction wave starts while the cyclin B levels are still much higher than they would be in the wildtype case where the contraction wave is allowed to start naturally (Figure 54 C). This is due to the fact that the mechanism by which Cdk1 inhibitors act is based on blocking the kinase activity of Cdk1 while cyclin B is in the normal case degraded by targeting to the proteasome. Therefore, Cdk1 inhibitors can override the normal cell cycle regulation and force the starting of the contraction wave.

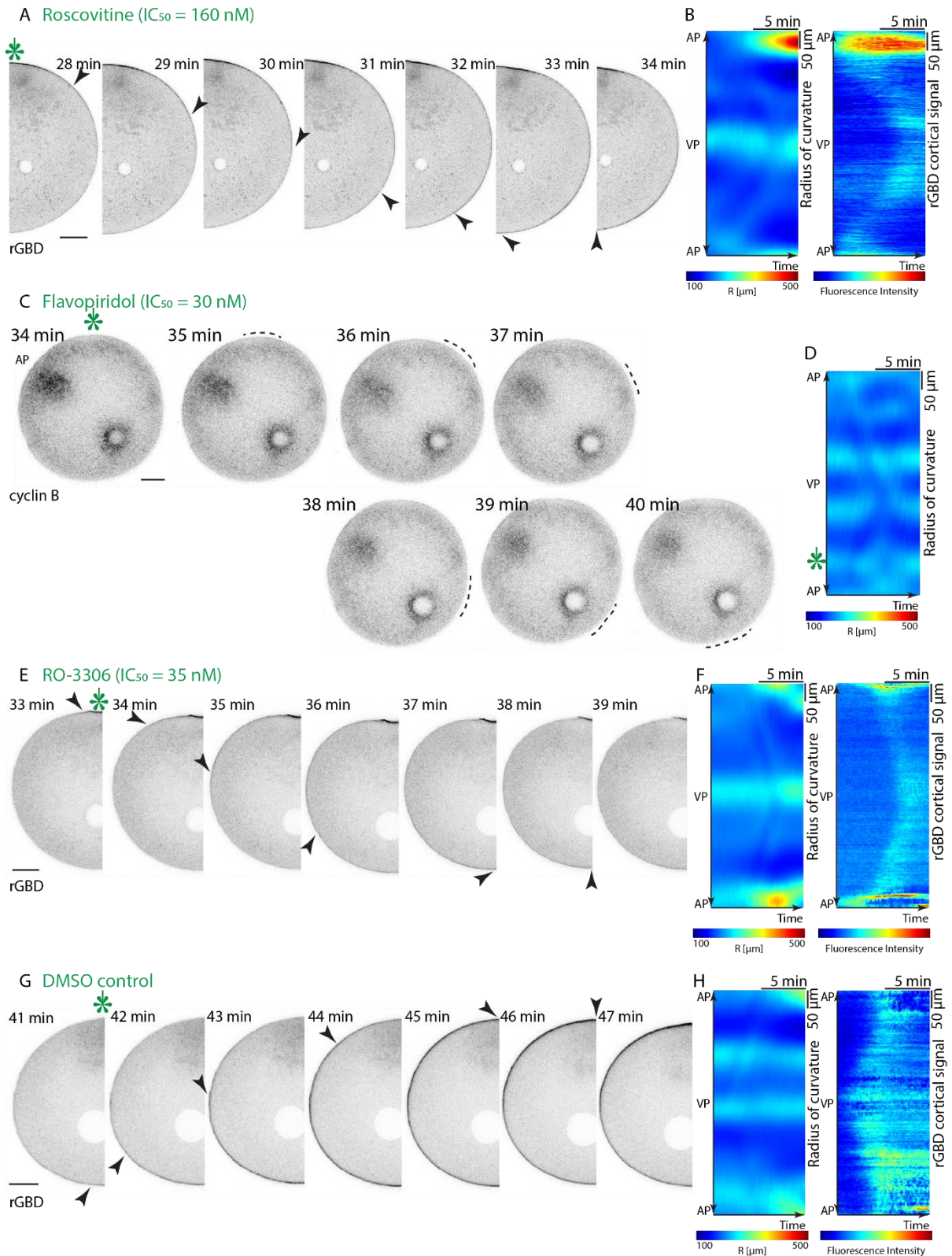


Figure 54: Local Cdk1 inhibitor treatment.

A&B) Stills and kymographs of an oocyte expressing the RhoA activity probe (rGBD) treated locally at the animal pole (*) with Cdk1 inhibitor Roscovitine, showing the reversal of contraction wave and RhoA signal. C&D) Stills and kymograph of an oocyte expressing cyclin B-EGFP treated with Flavopiridol laterally (*) during induced contraction. E&F) Kymographs and stills of an oocyte expressing the RhoA activity probe (rGBD) treated locally (*) at the animal pole with Cdk1 inhibitor RO-3306, showing the reversal of contraction wave and RhoA signal. G&H) Stills and kymographs of an oocyte expressing the RhoA activity probe (rGBD) treated locally (*) with DMSO as control, showing no change in the pattern of contraction. Scale bar 30 μ m, all times relative to NEBD.

From this I can conclude that the contraction wave starts at whatever point in the cell has the lowest level of Cdk1 activity, which is normally at the vegetal pole. This indicates that during metaphase Cdk1 activity suppresses RhoA, while once it drops below a certain threshold during the transition to anaphase the contraction wave can start.

4.3.1.4 The Cdk1 gradient controls the starting point of the contraction wave

To further test the hypothesis of an inhibitory gradient of Cdk1-cyclin B, I injected active Cdk1-cyclin B protein into the oocyte. The active protein complex can be purified from starfish oocytes as established by (Okumura 1996)⁶. As the purified protein is unlabelled, it was co-injected with a fluorescently labelled 500 kDa Dextran to mark the site of injection. Oocytes expressing the marker for active RhoA were injected as close to the vegetal pole as possible without injuring the cell, to visualise the progression of both the contraction wave itself as well as the upstream signalling in response to the manipulation of the Cdk1 activity gradient (Figure 55 A).

Oocyte injected with active Cdk1 protein showed abnormal contraction behaviour, with the contraction wave starting laterally in the cell, somewhere between vegetal and animal pole (Figure 55 B and D). The wave then progresses around the oocyte from the starting point. The behaviour varies slightly even with relatively similar injection sites as in the two examples shown here (Figure 55 C and E), likely due to slight differences in injection position and volumes.

At the same time injecting additional Cdk1/Cyclin B slightly delays the start of the contraction wave (timing of Figure 55 B and D), which is understandable as the degradation machinery of the APC/C has to degrade more substrate to reach the same threshold which increases the duration of metaphase.

This behaviour of the contraction wave confirms that the low point of the gradient is the starting point of the contraction wave.

⁶ I received purified Cdk1/Cyclin B protein as a kind gift from Dr Okumura, Tokyo Institute of Technology.

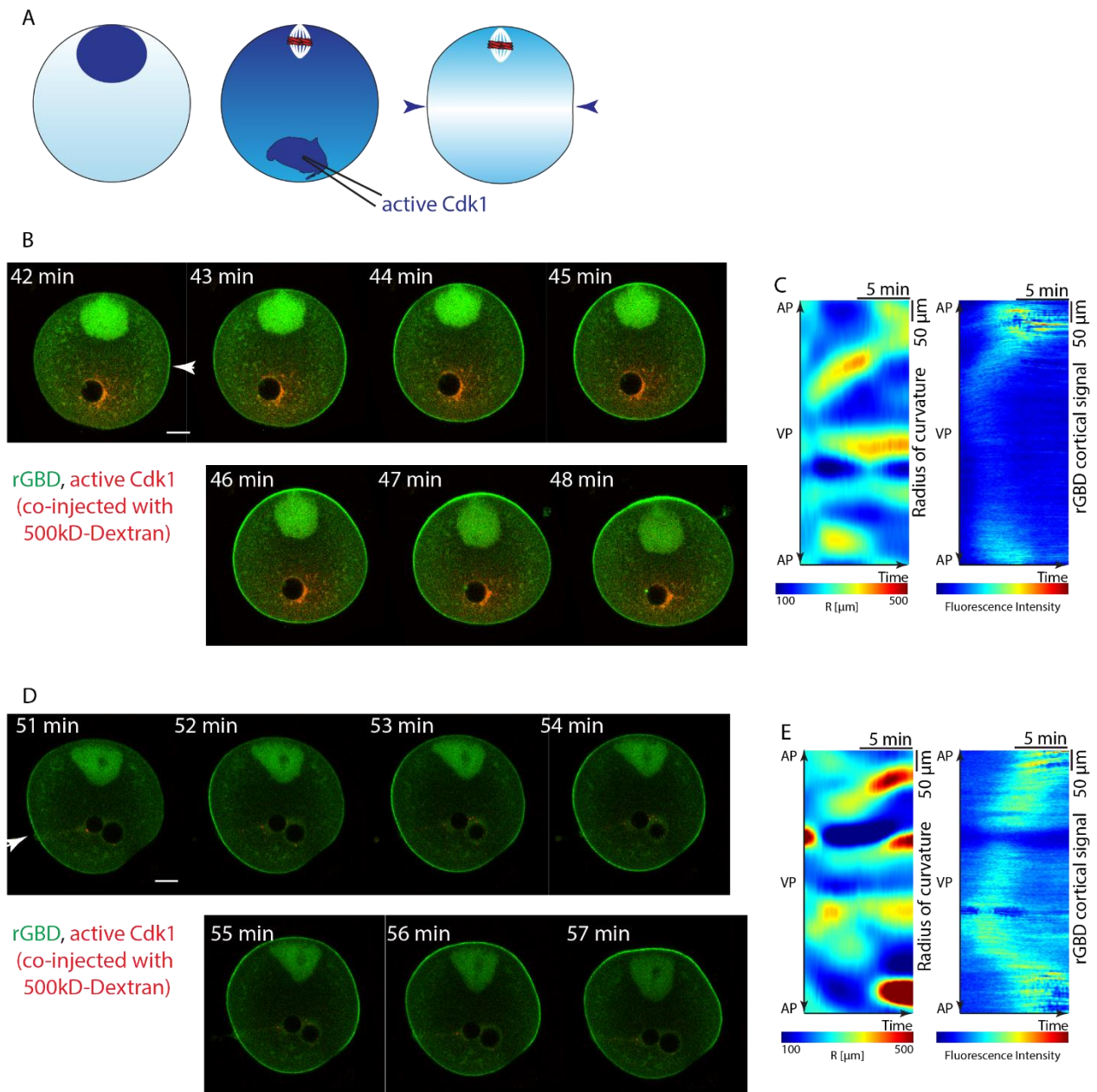


Figure 55: Injection of *Cdk1*-cyclin B protein complex. A) Scheme of the oocyte with the hypothetical *Cdk1* gradient (in blue) showing the injection position. B and D) Stills of two sample oocytes expressing the RhoA activity marker (rGBD in green), injected with *Cdk1* protein and labelled Dextran (in red) during the contraction wave. Arrow marks the start site of the contraction wave. C and E) Kymographs of surface curvature and cortical fluorescence intensity of the cells in B) and D). Scale bar 30 μm , all times relative to NEBD.

4.3.2 Propagation of the wave

4.3.2.1 The *Cdk1* gradient controls the progression of the contraction wave

From the above experiments, it is clear that the point of lowest *Cdk1* activity regulates the starting point of the contraction wave. There are two potential pathways by which the wave can then spread from this starting point. The proposed gradient suggest an intuitive explanation where contractility is induced at each site along the cortex in response the *Cdk1* activity locally dropping below the threshold and inducing the activation of myosin II. Alternatively, it can be imagined that once the

contraction wave has started at the point of lowest Cdk1 activity it progresses across the cell via an independent contractile module.

To test how the progression of the contraction wave across the cell is controlled I changed the shape of the oocyte by placing them in small microfabricated wells. This allowed me to change the length of the animal-vegetal axis and thereby affect the gradient and observe the resulting contraction wave.

The first variants of the shape change which are interesting in answering this question are the ones in which the cells are compressed either along the AP-VP axis or perpendicular to it. In the examples shown in Figure 56, the animal pole is marked by the microtubules marker EB3 (in red), showing the different aspect ratios achieved by the shape change. In Figure 56A, the AP-VP axis is elongated by a factor of 1.4 compared to the control cell in Figure 56B in which the normal round shape is maintained while in the cell in Figure 56C the AP-VP distance is compressed to roughly half.

Firstly from the round cell which is compressed but not changed in its shape, it is clear that the cells behave normally in these experimental conditions, with active RhoA being recruited normally to the cortex (rGBD in green) and a normal polar body forming. The duration of the contraction wave is also normal with 8 min.

Of course, both other cells have a similar ellipse shape with a roughly comparable half-circumference (i.e. distance from AP to VP along the cortex on one side) with 266 μm and 255 μm respectively while the distance across the cytoplasm is drastically different with 213 μm versus 84 μm . Crucially the time that the contraction takes to cross the cell scales with the distance across the cytoplasm, taking much longer in the cell with the elongated AP-VP axis (Figure 56A vs C, Table 6).

Table 6: Results of the shape change experiments

	Elongated AP-VP axis (A)	Normal AP-VP axis (B)	Shortened AP-VP axis (C)
Cytoplasmic distance AP-VP	216 μm	152 μm	85 μm
Cortical distance AP-VP (half-circumference)	266 μm	236 μm	255 μm
Duration of contraction wave	24 min	8 min	6 min
Speed of wave along the cortex	11 $\mu\text{m}/\text{min}$	29 $\mu\text{m}/\text{min}$	42 $\mu\text{m}/\text{min}$

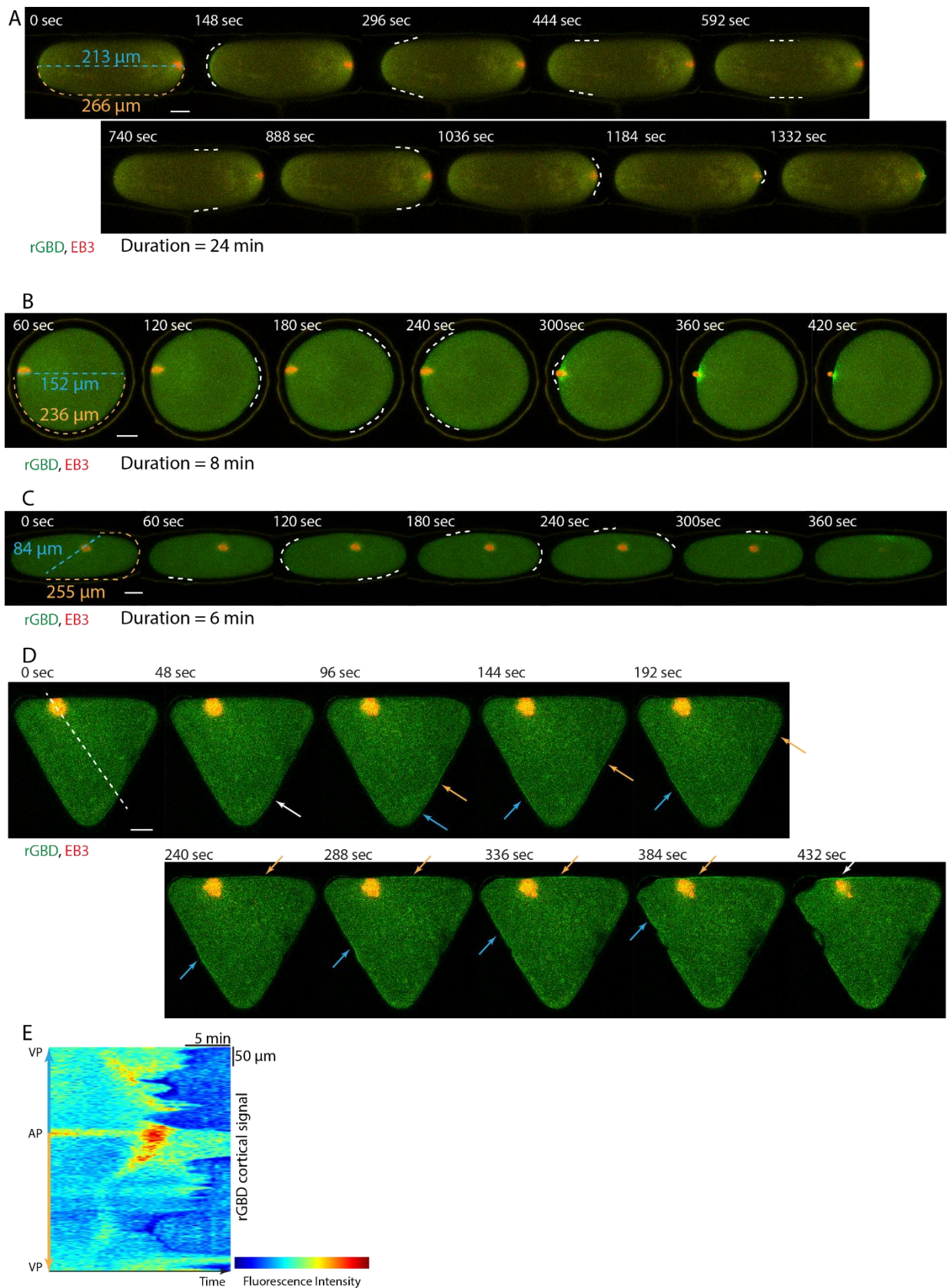


Figure 56: Effect of shape change on the contraction wave.

A) Stills of an oocyte with an elongated AP-VP axis. B) Stills of oocyte whose shape is not changed. C) Stills of an oocyte with a shortened AP-VP axis. D) Stills of an oocyte in a triangle shape with the two paths of the contraction wave marked by orange and blue arrows and white dashed line marking the AP-VP axis. E) Kymograph of the cortical fluorescence intensity of the cell in D), showing the blue and orange half and the varying speeds at which the wave progresses. All cells are expressing microtubule marker EB3 (red) and RhoA activity probe (rGBD in green), with the direct AP-VP distance as well as the half-

circumference marked on the respective first frames and the white dashed line indicating the contracting cortex. Scale bar 30 μm , time starts at the beginning of contraction wave as NEBD was induced outside of the shapes.

This indicates that the speed of the contraction wave depends on the cytoplasmic distance, arguing that the wave progression is controlled in the cytoplasm, likely by the Cdk1 gradient.

The gradient hypothesis is further strengthened when we look at different shapes that the cells can be turned into, such as the triangle in Figure 56D. In this case, we have two unequal sides of the cell in relation to the animal-vegetal axis and we can observe the contraction wave moving across them disparately. In the normal oocyte, the wave progresses equally on both halves of the cell and at a constant speed. In this case though, the two sides (marked in blue and orange) exhibit very different behaviours.

Of most interest is the half of the cell which contains two sides of the triangle which are positioned at very different angles to the AP-VP axis (orange side). If we assume the Cdk1 gradient driving the contraction wave goes along the AP-VP axis, the different angles at which the sides of the triangle are oriented towards the gradient should result in a different speed at which the wave moves along these sides. This is exactly what I observe in the kymograph of RhoA activity moving along the cortex (Figure 56E) where the orange half of the triangle clearly exhibits three separate phases of wave progression along the cortex. In the first phase the cortex is close to perpendicular to the AP-VP axis and the wave progresses relatively fast across it as the threshold value will be reached in very similar time frames for each position of this cortex. Then in the second phase the wave passes the corner and moves very fast, which may be in part due to geometric effects at the high cortex curvature. In the third phase the cortex is positioned at a roughly 45° angle to the AP-VP axis and the wave moves slower than in the previous phases, indicating that the thresholds are hit at higher time intervals between neighbouring points of the cortex as these are exposed to more of the gradient than points on the other side of the triangle.

4.3.2.2 Feedback between contraction strength and wave speed

While the gradient guides the progression of the contraction wave, it is not the sole controller. I find evidence for additional regulation of the wave speed when I manipulated myosin activity, which changes not only the contraction strength but also affects the speed of the contraction. When plotting the respective strength and speed values for these treatments it becomes apparent that there is an exponential correlation between these two variables (Figure 57 A). This correlation is only true for the direct manipulations of myosin – that is Blebbistatin treatment and MRLC overexpression. At the same time inhibition of the regulatory pathway above myosin, i.e. inhibition of Rok, does not affect the speed of the signalling wave while the contraction is inhibited (Figure 58A and B). This means that only

when changing myosin II activity itself a stronger wave progresses slower while a weaker wave progresses faster. This indicates a feedback from myosin II activity to the upstream control pathway.

As this is a quite surprising observation I choose to explore this further using oocytes overexpressing MRLC with a slower wave. To determine at which point of the regulatory pathway this feedback enters, I probed the various steps in the cells overexpressing MRLC.

It is clear that the curvature change that is the manifestation of the contraction wave is caused by myosin II localisations and we can, therefore, assume that the recruitment of myosin itself progresses slower around the cell when MRLC is overexpressed.

When looking at the RhoA signal in the case of MRLC overexpression, it is clear that this signal also travels slower and there is no separation between the active RhoA signal and the flattening of the cell cortex (Figure 57 C and D). Therefore, the feedback from MRLC overexpression which leads to the slowing down affects the speed at which RhoA is recruited along the cortex. When I measured the rate at which cyclin B is degraded in the oocytes in which MRLC is overexpressed, I could find no difference to the wildtype degradation rates in untreated cells (Figure 57 B). This conforms to expectations, as a feedback from myosin II levels to the cell cycle machinery would be very surprising and lacking any precedent.

That the feedback arises from myosin activity in this context is further underscored by the fact that the speed change is also observed in oocytes treated with Blebbistatin. Blebbistatin blocks the myosin power stroke while it does not affect the binding of myosin II to the cortex. The fact that the speed is affected by Blebbistatin, therefore, means that the actual myosin activity is what feeds back to the speed of wave progression not merely its localisation. Manipulations of the actin levels in the oocyte also change the speed at which the RhoA signal progresses across the cell (Figure 58), especially in Phalloidin injected cells which exhibited a slowing down of the wave. Although this slowing is non-significant compared to wildtype and it is less pronounced than for the slowing down achieved by manipulation of myosin II.

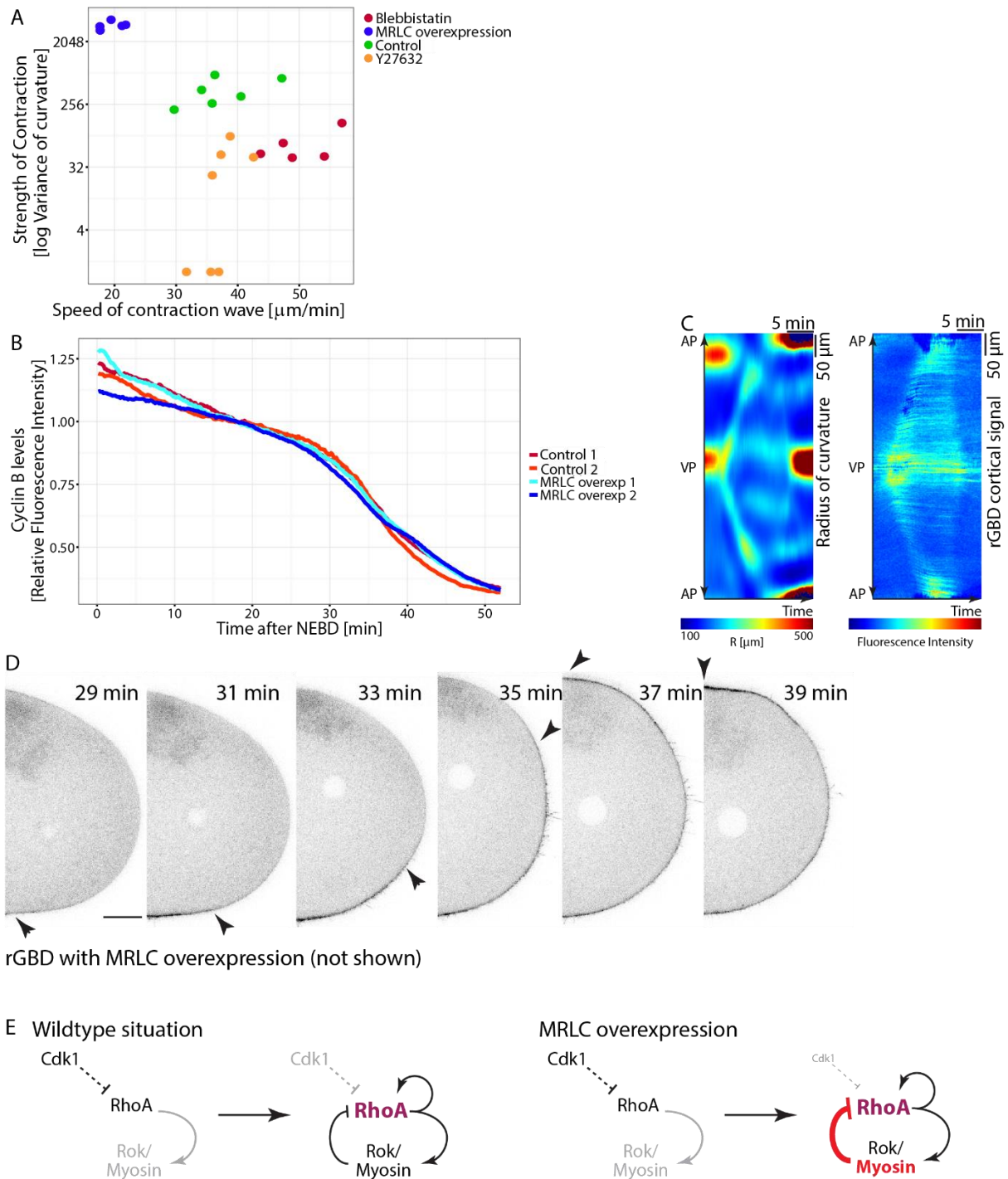


Figure 57: Correlation of wave speed and contraction strength.

A) The strength of contraction plotted against the speed of the contraction wave for various manipulations of myosin activity. B) Cyclin B degradation in the whole oocyte compared between non-treated cells and cells overexpression MRLC. C) Kymograph of the surface curvature and the cortical fluorescence intensity of the cell in D). D) Stills of an oocyte expressing RhoA activity probe (rGBD) and overexpressing MRLC (channel not shown) during the contraction wave. E) Scheme showing potential regulatory network in metaphase (left side) and in anaphase (right side) compared to that in the case of myosin overexpression. Scale bar 30 μm , all times relative to NEBD.

I, therefore, conclude that the feedback from myosin activity targets the activation of RhoA. This can be explained as follows (Figure 57E):

RhoA exists in two states – an active and an inactive one – and it is held in the inactive form by Cdk1 activity while once RhoA is activated there is both a positive autocatalytic feedback to RhoA itself, as has been reported in the literature (Bement et al. 2015) as well as a negative feedback from the downstream pathway. When I overexpress MRLC the negative feedback to RhoA is strengthened, therefore leading to an overall greater inhibition of RhoA. To achieve the same amount of RhoA activation under these conditions, Cdk1 inhibition needs to be lifted more compared to the non-treated case. These different levels of Cdk1 required for the RhoA activation in the case of MRLC overexpression compared to untreated cells shifts the threshold at which the Cdk1 gradient starts the contraction at each point along the cortex and therefore slows down the progression of the wave.

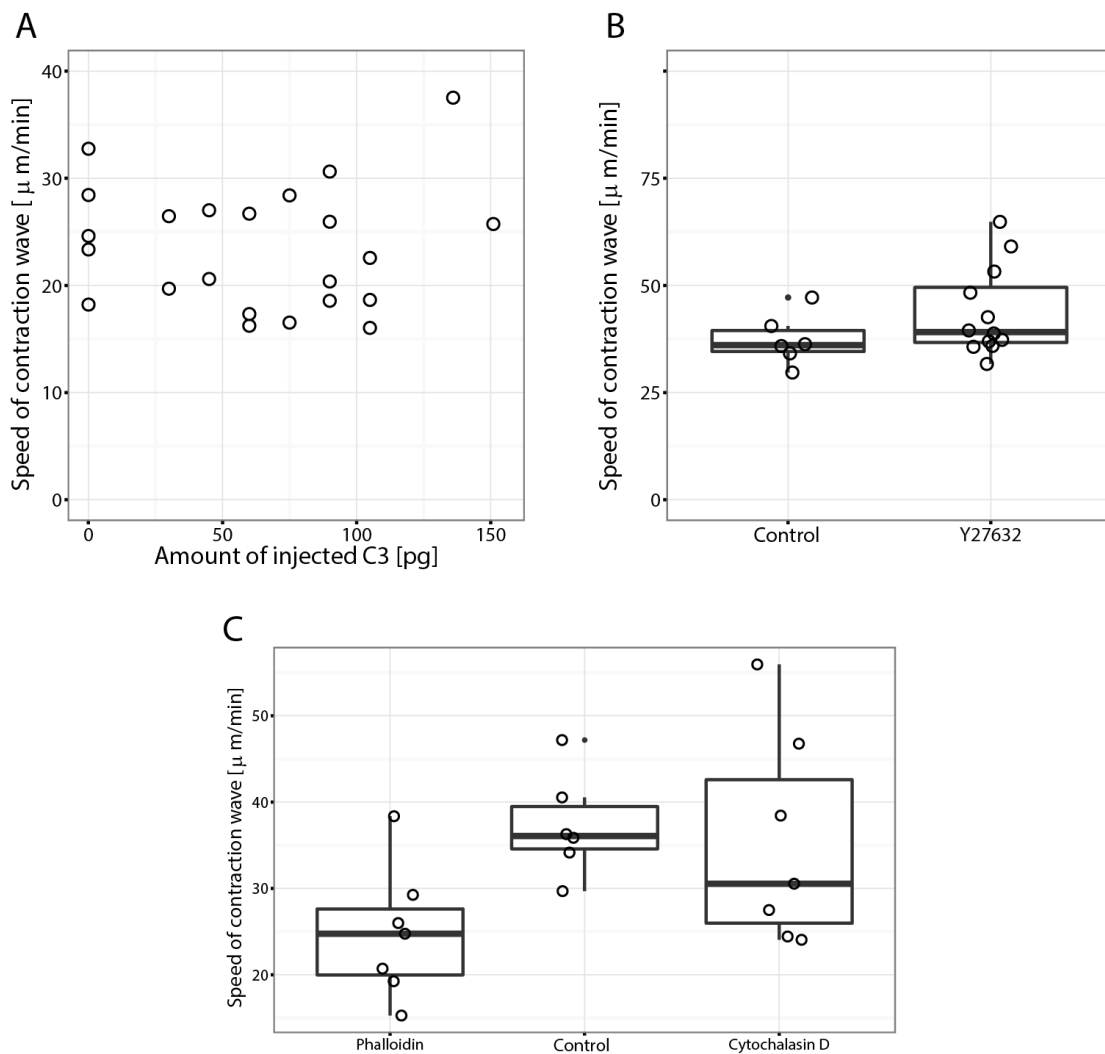


Figure 58: Speed of contraction wave with manipulations of RhoA, Rok and actin. A) The speed of the contraction wave with increasing doses of injected RhoA inhibitor C3 transferase. B) The speed of contraction wave in cells treated with the Rok inhibitor Y27632 compared to control. C) The speed of contraction wave compared to control for actin manipulations, i.e. injection with Phalloidin and treatment with Cytochalasin D.

4.3.2.3 Feedback to regulate band width

The above serves to explain the starting of the wave as well as the progression of the wave across the cell, but it does not touch on the process by which the contraction is limited to a band. This band

nature of the contraction wave is seen on all levels, from the flattening to the myosin II and active RhoA signals.

However, when I perturb the RhoA effector Rok, which results in a block of the contraction but does not affect the recruitment of RhoA to the cortex (Figure 43E), the band is no longer formed. This means that blocking the pathway downstream of RhoA impacts the off-switch behaviour of RhoA after the contraction wave has passed. When the Rok inhibitor is applied to the cells active RhoA is no longer recruited only in a band but stays at constant high levels at the cortex during the whole time of contraction until it is switched off completely (Figure 59 A and B). With increasing concentrations of the Rok inhibitor, as can be achieved via injection, the pattern of the off-switching behaviour changes even further, with RhoA no longer disappearing from the cortex all over the cell simultaneously but rather in a drawn-out process (Figure 59C) until at higher concentrations there is no off-switching to be observed (Figure 59D). These observations of an aberrant off-switch behaviour of RhoA following Rok manipulation suggest a feedback regulating RhoA activity from further downstream in the signalling pathway.

As what is regulated here is clearly a GAP factor which deactivates RhoA, this feedback is consistent with the feedback affecting the wave speed described above. From the Rok inhibition data, it is not clear at which step downstream of RhoA the feedback arises, i.e. whether it originates from Rok itself or from myosin.

It is, however, clear that while the progression of the contraction wave is controlled by the Cdk1 gradient, feedback within the pathway from myosin II activity regulates the progression in concert with Cdk1 while feedback from Rok regulates the deactivation of RhoA and thereby controls the width of the band of activity (Figure 60).

A Rok inhibition - Y27632

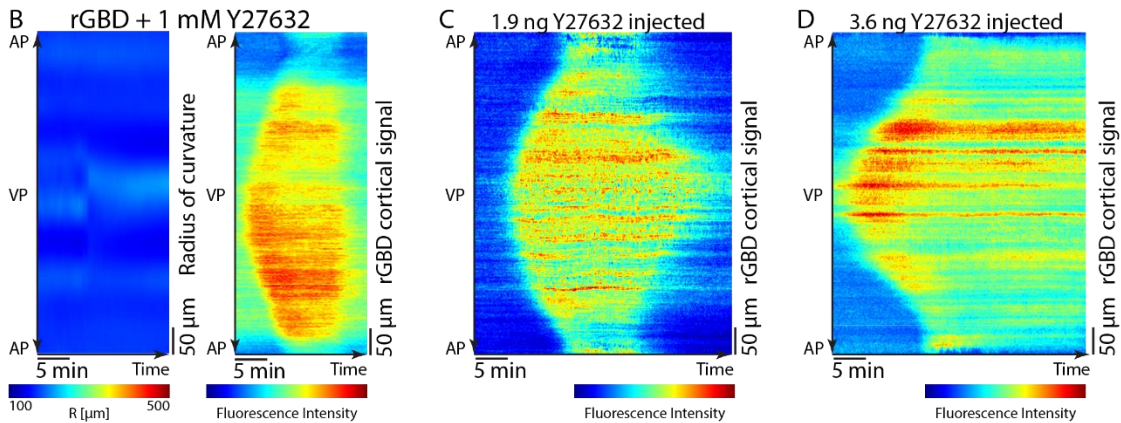
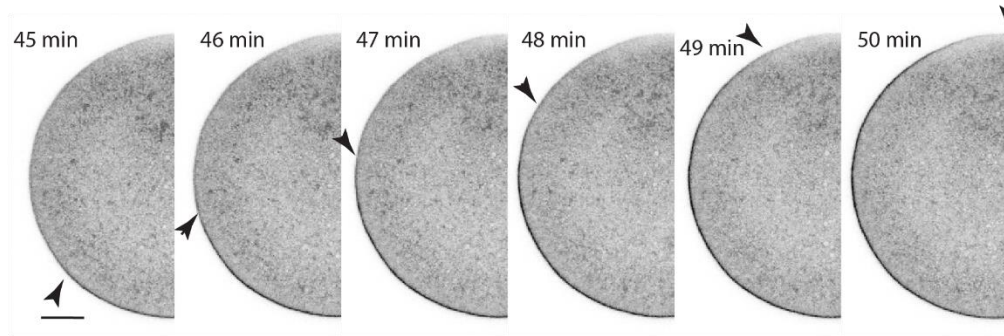


Figure 59: Regulation of RhoA inactivation.

A) Stills of an oocyte expressing RhoA activity marker (rGBD) treated with Rok inhibitor Y27632 during the contraction wave. The arrows show the progression of the RhoA signal front. B) Kymographs of surface curvature and cortical fluorescence intensity of the cell in A). C and D) Kymograph of cortical fluorescence intensity of the RhoA activity probe (rGBD) in oocytes injected with increasing amounts of Rok inhibitor Y27632. Scale bar 30 μm , all times relative to NEBD.

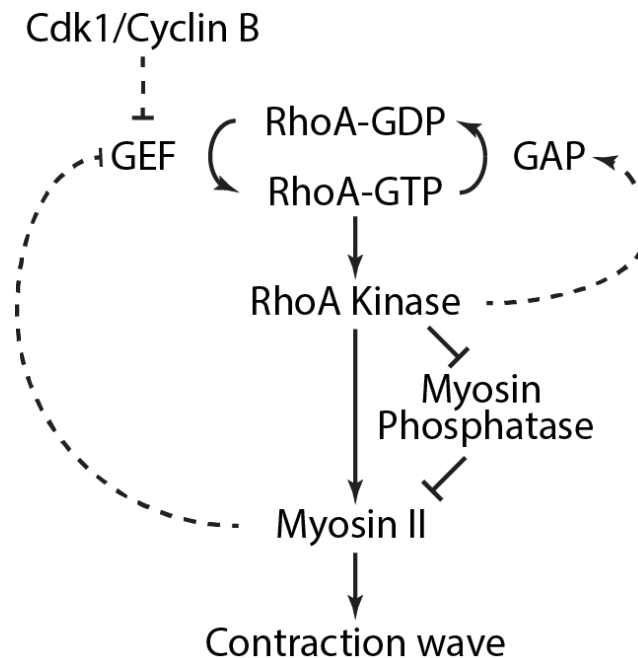


Figure 60: Complete molecular pathway regulation the contraction wave.

In this system the core signalling pathway RhoA-Rok-Myosin II is regulated by Cdk1 and feedback from Myosin II and Rok, controlling the progression of the wave and the inactivation of RhoA respectively.

4.4 POTENTIAL FUNCTION OF THE CONTRACTION WAVE

4.4.1 Polar Body Formation as a function of contraction wave

It was originally proposed by Hamaguchi and Hiramoto in 1978 during the first description of the contraction wave in the starfish oocyte that there is a causative relationship between the contraction wave and polar body formation (Hamaguchi & Hiramoto 1978). This idea has a large intuitive appeal as the two processes are closely correlated and it is easy to imagine that the contraction wave generates the forces required to push out the polar body from the oocyte. But the idea of the polar body as a global pressure release was historically contradicted by the work of Rappaport who argued that the polar body extrusion was a local phenomenon, independent of the contraction wave and pressure (Rappaport & Rappaport 1985). The divergence between these two ideas has remained unresolved to this day.

Given the variety of methods I have here established to manipulate the contraction wave, I can test these two proposed mechanisms. When I observe the formation of the polar body in oocytes where the contraction wave is manipulated, I find that the polar body still protrudes out of the cell normally (compare Figure 61 A and C to B). This is true for both the inhibited contraction with Blebbistatin (Figure 61A) as well as an increased contraction by the overexpression of MRLC (Figure 61 C). It has to be noted though that I can here only look at the protrusion of the polar body and not at the full polar body formation as the latter requires cytokinesis, which is inhibited by all inhibitors of the contraction wave. Therefore in the case of Blebbistatin (and all other inhibitors of the regulatory pathway), cytokinesis cannot be completed and the polar body is reabsorbed into the oocyte a few minutes after protrusion.

However the protrusion process of the polar body is identical in the Blebbistatin treated oocyte compared to control when measuring the height of the protrusion (Figure 61 D), while obviously the width of the protrusion changes in the control case when the contractile ring starts ingressing, which does not happen in the case of the Blebbistatin treated oocyte. This similarity in the protrusion speed and height, as well as the identical area, indicates that the contraction wave and any potential resultant pressure is not required for the protrusion of the polar body (Figure 61E).

The pressure hypothesis is further inconsistent with my measurements of the cytoplasmic flow and arises in the Hamaguchi and Hiramoto model from a wrong assignment of the specific shape change to the resulting flow (see Figure 38). When I observe the cytoplasmic flow at the moment when polar body protrusion starts it has peak values pointing away from the animal pole and comes to a still at later time points of the protrusion formation. This is inconsistent with the flow pushing out the polar body.

Furthermore when I reverse the contraction wave via the local application of a Cdk1 inhibitor at a late stage close to when the contraction wave would occur normally, the oocyte forms a normal polar body even when the direction of the contraction wave is reversed and any potential pressure should be directed away from the site of polar body formation (Figure 61F).

Summarising all this evidence it is clear that polar body formation does not depend on the contraction wave but is a local process that is independent of the remainder of the oocyte.

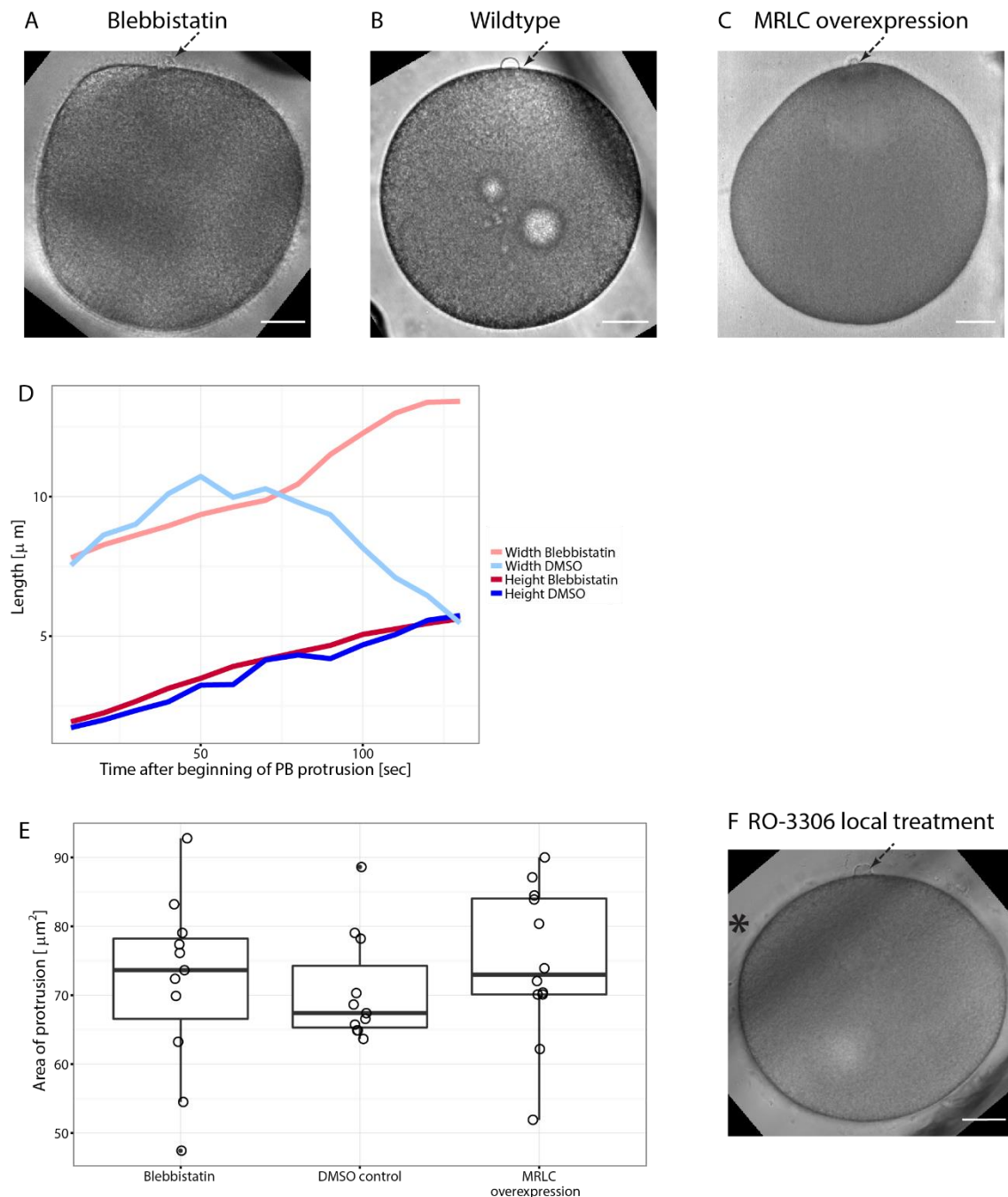


Figure 61: Polar body formation.

A) Oocyte treated with Blebbistatin showing protruding polar body (arrow). B) Wildtype oocyte with protruding polar body (arrow). C) Oocyte overexpressing MRLC with protruding polar body (arrow). D) Width and height of polar body protrusion over time in DMSO treated control cells and Blebbistatin treated oocyte. E) Area of the polar body in optical sections for various treatments. F) Oocyte locally treated with a Cdk1 inhibitor (*) and subsequent contraction wave starting at the marked position, showing normally protruding polar body (arrow). Scale bar 30 μm .

5 DISCUSSION

5.1 CONTRACTION WAVES AS A CORTICAL PHENOMENON DURING CYTOKINESIS

The cellular cortex is key for many cellular functions, including cell division and migration, and therefore regulation of cortical contractility is an important aspect controlling cellular behaviour. The cortex integrates a wide variety of signals, especially during cell division, as this is a process involving a large degree of cortical remodelling and is driven by the cortex.

One effect of the cortical remodelling during cytokinesis observed in very large dividing cells are surface contraction waves (SCWs). These waves of contraction occur immediately prior to cell division, indicating a link to cell cycle regulation (Hara 1971). Therefore, surface contraction waves offer an exciting system to study the cell cycle regulation of cortical contractility. But while contraction waves are a striking phenomenon, they are not very well characterised in the literature. Few papers go above a description of the phenomenon (Hamaguchi & Hiramoto 1978), and those that do focus specifically on the cell cycle process with little regard to the regulation of the contractile process (Rankin & Kirschner 1997; Chang & Ferrell 2013; Hara et al. 1980). No molecular details of the contraction process were known, necessitating a lot of groundwork to establish the pathway regulating cortical contractility in the contraction waves, before questions of the overarching regulation by the cell cycle could be answered.

Specifically, I studied the contraction wave which occurs in the starfish oocyte during meiosis as the cell transitions from metaphase to anaphase. In summary, I find that this contraction wave arises from a band of flattening that moves across the oocyte, caused by the accumulation of myosin II in a band along the cortex. The accumulation of myosin II is regulated by the RhoA-Rok-Myosin II pathway and the movement of the contraction across the cell depends on a gradient of Cdk1 activity. Cdk1-cyclin B is the central cell cycle controlling complex and forms a gradient across the oocyte, the lowest point of which sets the start point of the contraction wave while the progression of the wavefront is regulated by the gradient itself. At the same time, feedback within the RhoA-Rok-Myosin II signalling cascade interacts with the gradient in controlling the speed of the wave progression and the width of the band of activity.

In the following I will discuss further implications of these findings in the context of other research and illustrate some of the open questions that remain.

5.2 THE SPATIAL DIMENSION OF THE CELL CYCLE

The key finding presented herein is that the cell cycle gradient regulates the progression of the contraction wave.

Classically the cell cycle is seen as a one-dimensional process through which the cell moves. This is a reasonable view, as most dividing cells are small enough that mixing of components is near enough instantaneous allowing us to disregard the spatial dimension. Furthermore, most divisions are symmetric with the division signal originating in the middle of the cell, leading to identical behaviour in both sides of the cell. But there are examples of cells that do not fit these stereotypes of dividing cells and these specialised systems allow us to study an additional dimension of the cell cycle.

The starfish oocyte in meiosis is such a system due to two critical attributes. The first is its size. With a diameter of 180 μm the oocyte is large enough that diffusion cannot equilibrate things in a reasonable time frame compared to the time the cell cycle takes. Secondly, the meiotic division is a highly asymmetric division and this asymmetry is prepatterned by the nucleus which is positioned off-centre. These two characteristics are key adaptations to the oocyte function, with the size being required for nutrient storage while the polarisation of the nuclear position is necessary to allow for easy asymmetric cell division.

My work shows that the cell cycle gradient controls the contraction wave and this gradient arises from these two adaptations. The surface contraction wave is, therefore, an easily visible physical manifestation of the spatial dimension of the cell cycle. Essentially in the starfish oocyte the individual phases of the cell cycle do not happen simultaneously across the whole cell but rather start first at one end of the cell and move progressively across it (Figure 62).

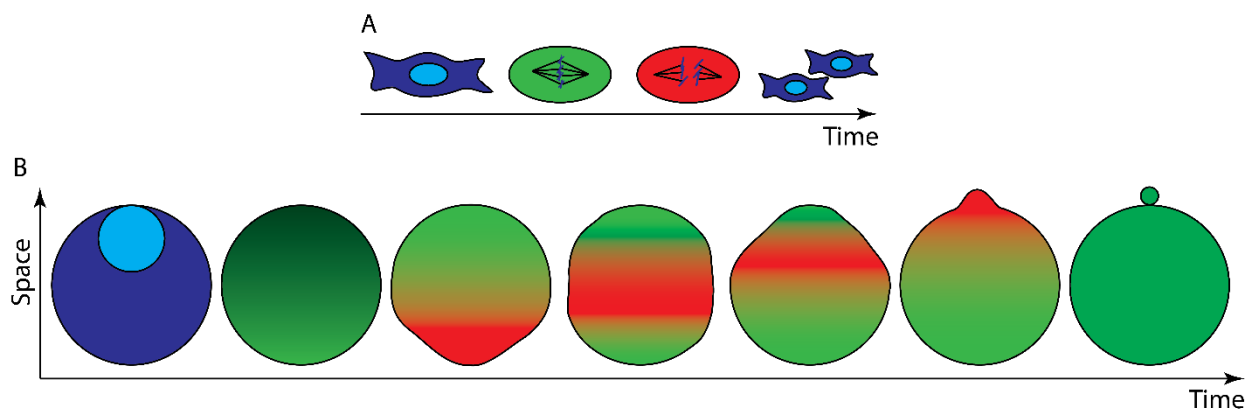


Figure 62: Cell cycle in space and time in starfish oocyte compared to a somatic cell in mitosis
A) In a somatic cell, the cell cycle transitions happen in the whole cell simultaneously. B) The cell cycle gradient in the starfish oocyte is spread in space and time. Interphase in blue, metaphase in green, anaphase in red. Size of the cells not to scale.

5.3 THE CELL CYCLE DEPENDENCE OF THE CONTRACTION WAVES IN STARFISH AND *XENOPUS*

The previously best-described example of contraction waves are the ones in the *Xenopus* embryo. In this system, it was recently shown that the spatial dimension of the cell cycle drives the SCWs. Work by Chang and Ferrell showed that in the very large *Xenopus* egg the cell cycle signal is spread by a mechanism other than diffusion (Chang & Ferrell 2013). They showed that the signal leading the entry of the cell into metaphase - the rise in Cdk1 levels - travels across the cell as a trigger wave and that

this underlies the SCWa. It is interesting to speculate what the parallels are between the contraction wave in the starfish oocyte and in the *Xenopus* embryo and if they share the same trigger wave mechanism controlling them.

If we compare the SCWs in these two systems, two key differences emerge (Figure 63). The first is that while both systems exhibit two contraction waves, one at metaphase entry and one at metaphase exit, the temporal spacing between the two waves is very different. In the *Xenopus*, the contraction waves occur within around 10 minutes from each other, while in the starfish oocyte around 40 minutes pass between them. Secondly, the directionality between the two waves is reversed. In the *Xenopus* system, both waves move in the same direction while in the starfish they travel in opposite directions.

These difference indicate a likely functional difference and make the transfer of knowledge from one system to the other difficult, especially as in *Xenopus* mainly the wave at metaphase entry has been studied while I focussed on the wave at metaphase exit.

My data show that in addition to forming a gradient, the degradation of cyclin B happens equally all across the cell maintaining the gradient with dropping levels. This suggests that it is likely not a trigger wave which controls the progression of the contraction wave but rather the gradient in the starfish system. Furthermore, it is likely that the regulatory network at metaphase exit is not able to give rise to the bistability needed to achieve a trigger wave. This is due to the fact that the metaphase exit network contains only a single feedback loop, while the metaphase entry network contains both a positive and a negative feedback loop (Figure 15). Whether the wave of relaxation at metaphase entry in this system is controlled by a trigger wave, or whether a gradient also acts there, remains to be explored in the future.

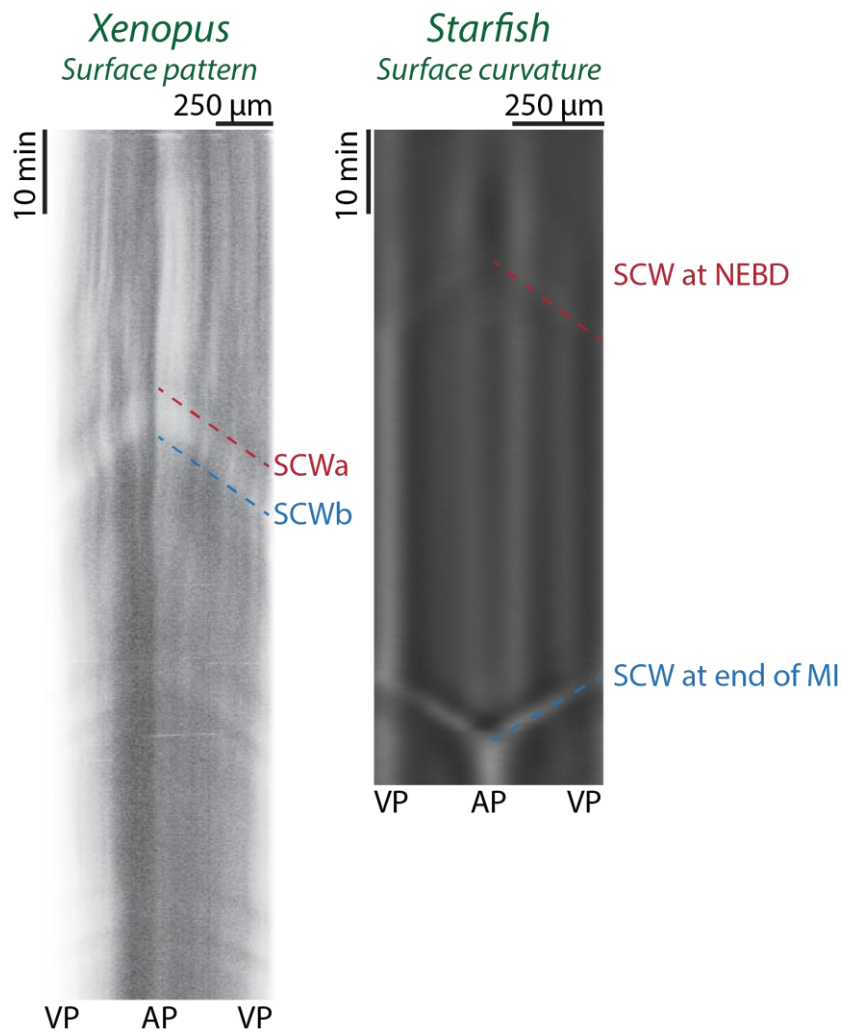


Figure 63: Comparison of contraction waves in *Xenopus* and starfish.

SCWs in *Xenopus* artificially activated egg as seen by the change in surface pigmentation. There are three pairs of SCWs in this kymograph, each going along with one cell cycle. In comparison in the starfish oocyte, the SCWs in meiosis are visualised by the surface curvature measurements. This comparison shows the difference in timing and direction between the two SCWs in *Xenopus* and starfish. *Xenopus* data reprinted by permission from Macmillan Publishers Ltd: *Nature* (Chang & Ferrell 2013), copyright 2013.

In summary, my data suggest the mechanism by which the cell cycle induces the contraction wave in the starfish is different from the one in *Xenopus*. But while the specific mechanism may differ, viewing the commonalities from both the starfish and the *Xenopus* system opens up a new view of the cell cycle, where its spatial dimension is a factor controlling cortical behaviour. This spatial dimension can only be studied in large cells or semi-*in vitro* systems like the *Xenopus* egg extract, making a case for the use of these models in addition to classical cell culture systems. This is especially important as the spatial dimension of the cell cycle opens up the view for new interactions between the cell cycle and its downstream targets, which can be investigated in the contraction waves, but may also occur elsewhere.

5.4 LINKING CDK1 ACTIVITY TO CONTRACTILITY

5.4.1 The contraction wave is independent of microtubules

The contraction wave offers an exciting system in which to study pure cortical responses to cell cycle signalling. In regular cell divisions, the cortical response is largely regulated by the microtubule spindle, which takes up a large part of the cellular volume. In a meiotic oocyte, however, the spindle is very small in comparison to the cell itself. This means that the vast majority of the cortex is exposed to the changing cell cycle signals directly without the intermediate regulation by the microtubules and the contraction wave can be interpreted as a direct consequence of this.

Consistent with this framing, complete removal of the microtubules did not change the contraction wave in any way. This finding of microtubule independence of the contraction wave is very interesting in terms of the parallels to cytokinesis. The two processes share the same downstream regulatory pathway of RhoA-Rok-Myosin II, which induces the contraction wave and cytokinetic ring formation respectively. But while this pathway is identical in the two processes, in cytokinesis it is regulated spatially by the microtubules and temporally in response to the cell cycle. But my data clearly shows that in the contraction wave the RhoA-Rok-Myosin II pathway is regulated in both time and space by the cell cycle alone. This makes the contraction wave a response of the cortex to the metaphase to anaphase transition without constraint by the microtubules, as is the case in somatic cells.

This is an interesting observation in light of evidence that is emerging for a general role of microtubules in regulating cortical contractility. In different cellular contexts, it appears that microtubules may consistently act to suppress local cortical contractility. The examples come mainly from cells during the adhesion process which have their microtubules removed (Pletjushkina et al. 2001; Paluch et al. 2005), leading to cortical oscillations while contractility is suppressed by the stabilisation of microtubules (Danowski 1989). There is furthermore clinical data in cardiomyocytes supporting this idea (Ishibashi & Tsutsui 1996).

This little-studied aspect of the regulation of cortical contractility certainly deserves further investigation as the molecular details by which microtubules could suppress cortical contractility are unknown. It is fascinating to speculate about the importance of this regulation in maintaining stable cellular shape and cortical cohesion by preventing hypercontractility and bleb formation. The contraction wave, as a contractile process unrestrained by microtubules, may serve as a system to understand what happens in the cortex in the absence of microtubule regulation.

5.4.2 GEFs regulating the contraction wave

While I was able to directly show both the role of the cell cycle regulation as well as the downstream pathway regulating contractility, the molecular connection between these two aspects proved hard to find. It is clear that the downregulation of Cdk1 activity at the end of metaphase leads to the activation of RhoA, which subsequently activates myosin II, and that these two factors must be linked via a GEF.

The GEFs in action in cytokinesis – Ect2 and GEF-H1 – are very well characterised in both their molecular function as well as in their response to the cell cycle, but both rely critically in their regulation on microtubules. As my data indicates a lack of microtubule-based regulation, it is perhaps not surprising that I cannot find evidence for the involvement of either Ect2 or GEF-H1 in the contraction wave. It has to be noted though that the tools I have for exploring the involvement of various GEFs are much more limited than the tools used in other aspects of this research. This is to a large degree due to the fact that there are no commercially available small molecule inhibitors of Ect2 as well as no efficient dominant negative mutants described in the literature. As the starfish oocyte is not amenable to genetic manipulation, this commonly used method for the study of various GEFs was not open to me. Due to these limitations, I cannot completely rule out the involvement of the classical cytokinetic GEFs in linking the cell cycle to the contraction wave. But given that I find effects based on the overexpression of either of these GEFs on other cellular contexts, it is quite possible that simply neither of them are involved in regulating the contraction wave.

In this case, there must be a different GEF at work in the context of the contraction wave linking cell cycle progression to RhoA activation. There is certainly no paucity of candidates, as the DbpA family of GEFs, the largest of the GEF families, to which both Ect2 and GEF-H1 belong, alone has 69 members in humans, active in many different cellular contexts (Rossman et al. 2005). Many of these proteins have not been characterised in any detail, illustrating how little we know about GTPases above the core few proteins and making it likely that the GEF controlling the contraction wave may be found in future. It is possible that the thus identified GEF will also play a role in the regulation of cortical contractility during the cell cycle outside of the specific case of the contraction wave.

5.5 MOLECULAR PATHWAY CONTROLLING THE CONTRACTION WAVE

5.5.1 The highly conserved RhoA-Rok-Myosin II signalling axis

While the GEF linking the cell cycle to cortical contractility remains a question for the future, I was able to identify the molecular pathway directly controlling the contraction wave. This is the first time the molecular basis of the contraction wave has been identified in any species.

The pathway itself is a highly conserved one, where RhoA activates its effector Rok, which in turn activates myosin II. This pathway is not only the one that drives cytokinesis (Miller 2011), but it is also important in cell migration and adhesion (Vicente-Manzanares et al. 2009), maintaining the cellular contacts of stem cells (Harb et al. 2008) and formation of the immune synapse (Rougerie & Delon 2012), to name just a few examples. It is therefore very well characterised, both in terms of the individual proteins as well as their interaction (Amano et al. 1996; Jordan & Canman 2012).

The novelty my data adds is to consistently prove the activity of the whole RhoA-Rok-Myosin II pathway in the contraction wave, for which the molecular players had previously been unknown. With this, I add another example of a contractile process regulated by the RhoA-Rok-Myosin II signalling axis, which shares interesting parallels to cytokinesis in terms of its cell cycle dependence but with a divergent upstream spatial regulation as discussed above.

5.5.2 Feedback in the RhoA-Rok-Myosin II pathway

Due to its dynamic nature, the contraction wave offers a system where I could uncover additional characteristics of the RhoA-Rok-Myosin II pathway. Specifically, as the contraction wave always forms a sharp band where the signal pathway is active which moves across the cell and I have a number of specific inhibitors of the individual components, I can study regulatory feedback in this system. The feedback within the RhoA-Rok-Myosin II pathway is not well studied, particularly in cytokinesis. Some data on mechanical feedback exists in cell migration and polarisation (Bhadriraju et al. 2007; Petrie & Yamada 2012), but how general these feedback mechanisms are, remains an open question. My evidence supports the idea of extensive feedback within the pathway.

The evidence I have for feedback within the pathway comes from two datasets. Firstly, I observe changes in the speed with which the wave progresses across the cell when I manipulate myosin II itself but not when the upstream pathway components are inhibited (Figure 57). Secondly, when Rok is inhibited, I observe abnormal off-switching behaviour for RhoA, which then no longer forms a band but rather remains active at the whole cortex after the wave has passed (Figure 59). These two feedbacks are independent, with the RhoA off-switching being normal in the case of the changed wave speed while the speed is normal when the abnormal off-switching behaviour is induced by Rok inhibition. But both feedbacks clearly impact the activity state of RhoA, although most likely via different pathways (Figure 64). The data suggests that myosin II negatively regulates the activation of RhoA in concert with Cdk1, likely targeting the GEF.

The feedback regulating the off-switching behaviour of RhoA clearly targets a GAP which is responsible for the transition from active RhoA-GTP to inactive RhoA-GDP. I have not identified the specific GAP

in question as there are a large number of GAPs, most of which are poorly characterised (Bernards 2003).

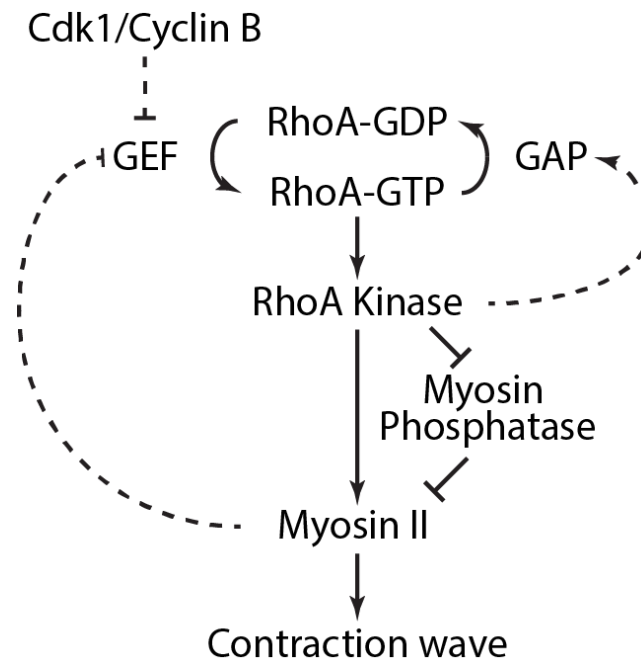


Figure 64: Complete molecular pathway regulating the contraction wave.

Overall it is clear that in the contraction wave the RhoA-Rok-Myosin II pathway exhibits two feedback loops (Figure 64). The first one controlling the speed of the wave progression originates from myosin II activity and therein interacts with the Cdk1 regulation in some manner, potentially by feeding back into the same GEF which is regulated by Cdk1 inhibition. The second feedback loop arises from Rok and activates a GAP, which is responsible for defining the width of the band of RhoA activity. There may very well be additional feedback systems at least partially in this pathway, such as the feedback between actin polymerisation and RhoA activation (Bement et al. 2015).

5.6 THE OOCYTE CORTEX AND ITS DYNAMICS

While I focussed my investigation of the contraction wave on understanding the regulation of myosin II activity, the cortex, which serves as the substrate for the contraction, is worth some considerations.

Cortex dynamics are a very important aspect of the regulation of cortical behaviour. It is assumed that the actin cortex, in general, has a turn-over time of around 1 min, although there are distinct subpopulations of actin with faster turnover (Salbreux et al. 2012). Other proteins in the cortex, such as myosin II and the actin crosslinker actinin have been shown to turn over significantly quicker (Fritzsche et al. 2013). All these measurements come from somatic cells in cell culture, and although

these values are widely used and generally accepted, if we can apply them to the starfish oocyte cortex remains an open question.

In general, we know very little about the organisation of the cortex in these cells and rely on assumptions from other systems. One fact which has been described in old papers, and which I re-established for the specific oocytes I was working with, is that their surface tension is very high. For HeLa cells in interphase the tension is measured at around 0.2 mN/m, rising to 1.6 mN/m in metaphase (Fischer-Friedrich et al. 2014). The starfish oocyte, on the other hand, has in its immature state, which is prophase arrest, a surface tension of 10 mN/m, dropping to around 1 mN/m at metaphase entry. These values for the resting/non-division phase cortices are surprisingly different and the mechanism by which the oocyte generate such higher pressure has so far not been investigated.

It is clear that the oocytes have very large amounts of myosin II, most of which is located in the cortex of the immature oocyte. This very likely strongly contributes to this high tension. How this higher tension affects cortex turnover rates and if the myosin is perhaps more stably bound in the cortex of the immature starfish oocyte remains an open question. A convenient method to explore these questions would be FRAP to measure the lifetime of different proteins in the cortex or laser ablations as recently proposed by (Saha et al. 2016).

It is also interesting to speculate why the starfish oocytes go to the effort of generating such very stiff cortices. One would instinctively assume that this is due to the external fertilisation and *ex utero* development that the oocytes of the starfish undergo in the open sea and the resulting requirement for physical toughness. But normally the oocytes are only released into the water in the middle of metaphase when they have softened considerably. The resulting tension of around 1 mN/m seems sufficient to allow survival even in the harsh conditions of the open ocean. So why do the oocytes have such a high tension in the prophase-arrested state when they are in the ovary and reasonably protected? It is possible that the high tension allows for the tight packing of the oocytes observed in the ovaries without damaging cellular integrity. Ultimately this remains an open question that will be interesting to explore in the future, especially if comparative measurements can be made on other marine and non-marine animals undergoing external fertilisation, to determine if the tension is an adaptation specific to starfish, the marine environment, external fertilisation, or oocyte generally.

5.7 SIMILARITY TO OTHER CONTRACTION WAVES

5.7.1 Other contraction waves in the starfish oocyte

While all experiments herein were performed with a focus on the main contraction wave associated with meiosis I, there are two other waves happening during the course of oocyte maturation. The first

wave is the one that occurs at NEBD and moves from the animal pole to the vegetal pole. And although this wave looks very similar to the contraction wave, it is in fact not a contractile wave at all. It is rather a wave of relaxation when the surface tension drops at the entry into metaphase, which is marked by NEBD. Along with this wave, I observe the loss of myosin from the cortex, causally explaining the underlying softening (Figure 65). This relaxation wave at NEBD is therefore very likely identical to the SCWa in the *Xenopus* eggs, which is also a wave of relaxation at metaphase entry and precedes the actually contractile SCWb (Sawai 1982; Rankin & Kirschner 1997).

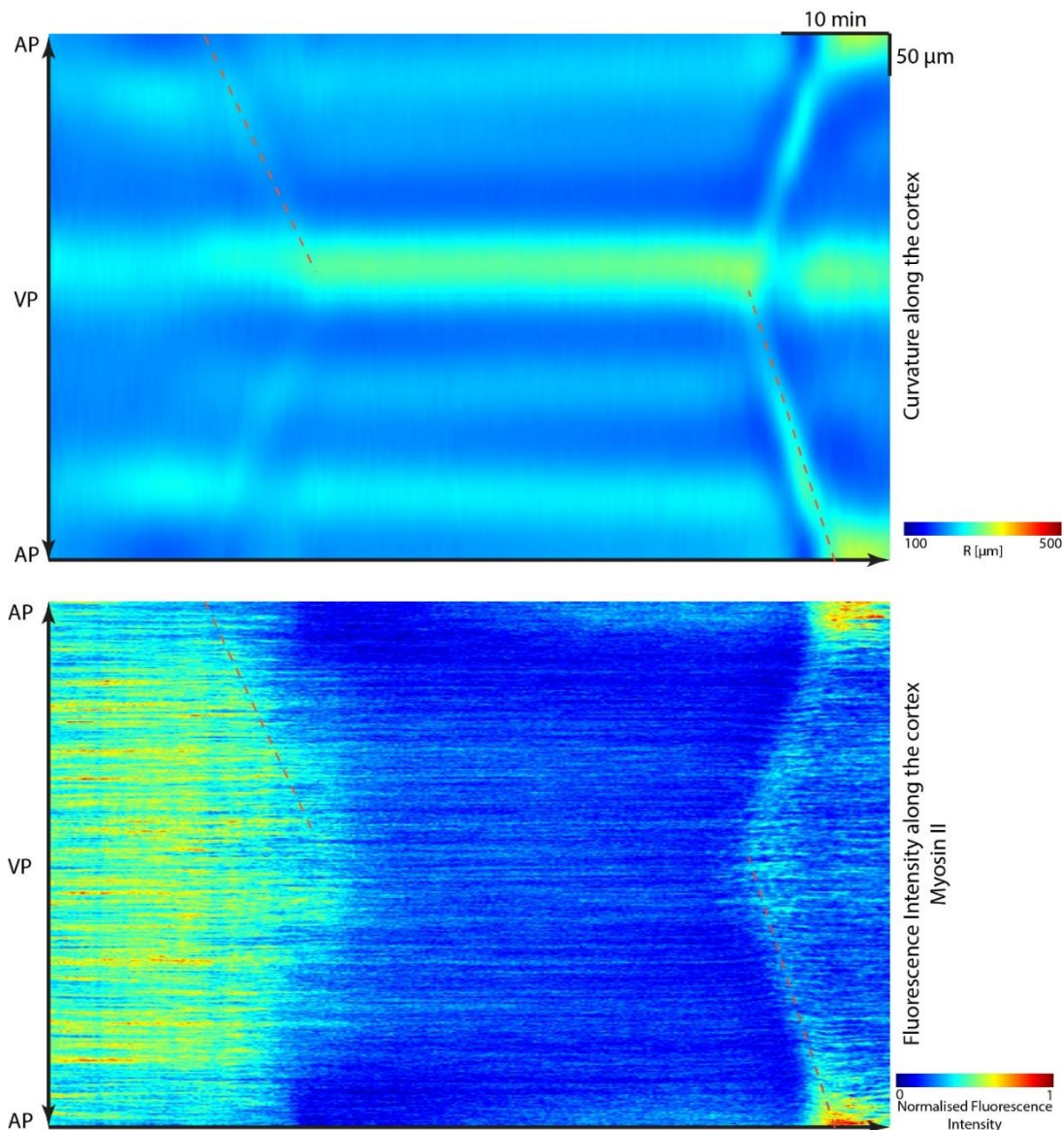


Figure 65: SCW at NEBD in the starfish oocyte. Kymograph of curvature (upper panel) and cortical myosin II intensity (lower) for complete meiosis I. This shows the relaxation wave at NEBD which goes along with the loss of myosin II from the cortex and later the contraction wave going along with myosin II recruitment to the cortex.

How similar the mechanisms between the relaxation wave at NEBD and the contraction wave at anaphase are, remains to be answered in the future. The basic involvement of myosin II is clearly a

common factor and both waves are responses to changes in the activity levels of Cdk1, with relaxation occurring in response to a rise in Cdk1 activity while contraction occurs in response to a drop. These similarities suggest quite a high level of mechanistic conservation but to really compare the two wave consistently a detailed analysis of the relaxation wave is required.

The second contraction wave that occurs during maturation in the starfish oocyte is associated with meiosis II. It occurs at exactly the same cell cycle stage as the first and main contraction wave, namely at the metaphase to anaphase transition alongside polar body formation. It is to be expected that these two processes are in every way molecularly equivalent. The only difference between them is the difference of their magnitude, with the second contraction wave being much more subtle than the first, inducing much less curvature change (Figure 36).

This difference in the magnitude of the second contraction wave can be explained by the cell cycle gradient controlling the contraction wave. In the run-up to meiosis II, cyclin B is re-synthesised to lower levels than during meiosis I and the whole cell cycle is much quicker (Okano-Uchida et al. 1998). It takes only around 30 min, compared to the 60 min of meiosis I. Therefore we can speculate that the resulting gradient will have lower peak levels and be potentially shallower, leading to a less pronounced contraction wave. But a detailed quantification of the gradient during meiosis II would be necessary to definitely answer this question, which is not possible using the fluorescently tagged constructs used herein as they are not resynthesized fast and specifically enough.

5.7.2 SCWs in other systems

With the work presented herein, the starfish oocyte becomes the systems with the best understood SCW, as we now have a more detailed molecular understanding than even the classical *Xenopus* model system. On the other hand, this means that apart from these two systems we have precious little data on SCWs, which makes a cross-species comparison very difficult. Although some level of evidence for surface contraction waves is present in a wide variety of species, most of the descriptions are very old and lack details and especially molecular data.

It appears quite clear that a good case can be made for the comparable nature of the SCWs in starfish and in the *Xenopus* egg, especially with regards to the dependence of the contraction wave on cell cycle regulation and the progression of the cell cycle across a large cell as discussed above. It furthermore seems likely that the molecular details of the contractile pathway are comparable, as the RhoA-Rok-Myosin II pathway is so conserved across species and can be hypothesised to drive SCWs in many systems. Whether the upstream regulation is quite the same remains an open question until more molecular details are available in the other system.

In addition to the lack of available data on SCWs in other species, an evolutionary comparison is made difficult by the diversity of oocyte behaviour. These behaviours including arrests and fertilisation at different cell cycle stages, in response to which the contraction waves in many of these systems occur (Prodon et al. 2008; Shimizu 1984). But it is perhaps possible that for all cases, where the SCWs are true contractions, the basic molecular pathway will be similar and therefore this study can serve as a starting point for the exploration of upstream regulatory elements in the contraction waves in other systems.

5.8 THE CONTRACTION WAVE AS A FUNCTION VS THE FUNCTION OF THE CONTRACTION WAVE

5.8.1 The contraction wave is a result of oocyte adaptation

As the contraction wave is such a striking phenomenon the early papers describing SCWs are full of speculations regarding their function. These functions have not been explored experimentally in any of the common systems.

The findings I present herein indicate that the search for a function of the contraction wave might, in fact, be a wild goose chase. The contraction wave is driven by a cell cycle gradient established due to the off-centre position of the nucleus. Following this logic, the contraction wave is merely a result or side-effect of the adaptations of the oocyte to its function. And while this may seem counterintuitive due to the striking nature of the process, it is important to consider that as long as there are no negative side effects or the evolutionary cost is not too high, there might be no reason for the cells to develop a mechanism to suppress this side-effect. This presupposes that it would even be possible to suppress the contractile phenomenon during the contraction wave without negatively impacting the contraction of the cytokinetic ring which occurs using the same molecular pathway at the same time.

The contraction wave can be fully explained as a result of oocyte adaptation, but of course, this does not rule out the possibility that the contraction wave has additional, potentially later acquired, functions.

5.8.2 Polar body protrusion is independent of the contraction wave

In the starfish system, the main proposed function is the generation of pressure to drive the protrusion of the polar body. This was originally proposed by Hamaguchi and Hiramoto when they first described the contraction wave in this system (Hamaguchi & Hiramoto 1978). This idea has been opposed by data from Rappaport who argued that polar body formation is independent of any global pressure built-up and is a locally induced phenomenon (Rappaport & Rappaport 1985).

The link to polar body formation is intuitively appealing due to its close temporal and spatial correlation. But the data I have gathered while investigating the contraction wave convincingly argues that polar body formation is independent of the contraction wave. Neither inhibiting nor strengthening the contraction wave made a difference to the size of the polar body protrusion. At the same time, it has to be noted that the full polar body formation cannot be observed when the contraction wave is inhibited as the molecules of the contraction wave and the contractile ring are identical, so the inhibitors block both. I, therefore, focussed on the formation of the protrusion of the polar body.

To underscore the independence of the polar body formation and contraction wave we also have to take a closer look at the pattern of cytoplasmic flow immediately prior to polar body formation. At the time point of polar body formation, the contraction wave is in the upper half close to the animal pole and the cytoplasmic flow is pointing away from the animal pole. This strongly argues against the idea that there even is pressure pointing in the right direction to drive polar body protrusion. It is also in opposition to the flow pattern assigned in the original study, explaining their opposing conclusion (Figure 66).

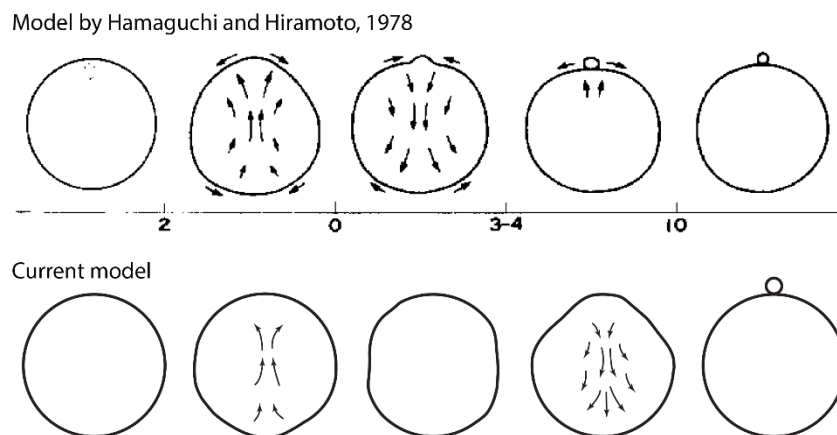


Figure 66: Curvature change and cytoplasmic flow in the oocyte. Upper panel shows the shapes and flow as originally proposed by Hamaguchi and Hiramoto, compared to my findings (lower panel). The early description showed some of the key shape changes, but the early ones were missed and the assignment of flow pattern to shape change has been updated by my detailed analysis. Upper panel reprinted from (Hamaguchi & Hiramoto 1978) with permission from Elsevier.

Due to the fact that inhibitor treatments that block the contraction wave also block the cytokinetic ring, with this data, I cannot rule out that the contraction wave plays a role in bringing the contractile machinery to the site of cytokinesis. This would be similar to the cortical flow which brings myosin II to the contractile furrow in dividing cells (Wang et al. 1994; Mandato et al. 2000). But we can rule out this potential function of the contraction wave in the experiments where I change the direction of the contraction wave. In this case, a full polar body forms even if the wave runs at an angle to it or against

it. Additionally in the cases of the reversed contraction wave I can detect strong recruitment of the upstream signalling factor RhoA at the animal pole even when the wave has passed across it. This signifies that the spindle is able to recruit the signals required for polar body formation independently of the contraction wave.

In conclusion, I can rule out the involvement of the contraction wave in the formation of the polar body. But polar body formation remains none the less an interesting question and the mechanism that regulates polar body formation are open for investigation. On the molecular side, there is good data from *Xenopus* oocytes indicating that polar body formation is driven by the small GTPase Cdc42 inducing Arp2/3 driven actin polymerisation (Zhang et al. 2008). In the starfish oocyte I also observe a strong accumulation of actin in the polar body, supporting this model on the base level (Figure 67). It could easily be further explored using Arp2/3 and Cdc42 inhibitors and reporters.

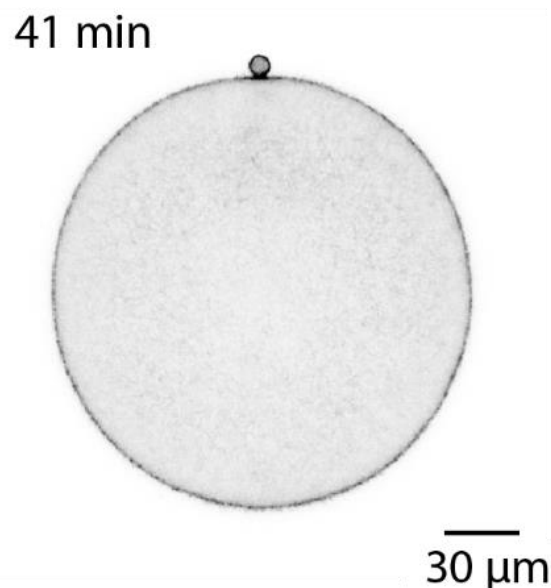


Figure 67: First polar body. Oocyte expressing the actin marker Utrophin CH-domain EGFP with the newly formed polar body, showing the accumulation of actin at the polar body cortex. Time relative to NEBD.

On the more upstream level, it is fascinating to speculate which factors drive the formation of the polar body. It is clear that the spindle alone is sufficient to cause polar body formation, as a translocation of the spindle along the cortex causes the polar body to form at the new site (Rappaport & Rappaport 1985). It would be interesting to know if the individual components of the spindle alone are sufficient to drive polar body formation, especially in light of data from mouse oocyte where DNA-coated beads along can induce the cortical differentiations that predetermine the polar body cortex (Figure 68) (Deng et al. 2007). It would be interesting to see if the same is true in starfish and if the pathway that links chromatin signals to Cdc42 activation can be illuminated.

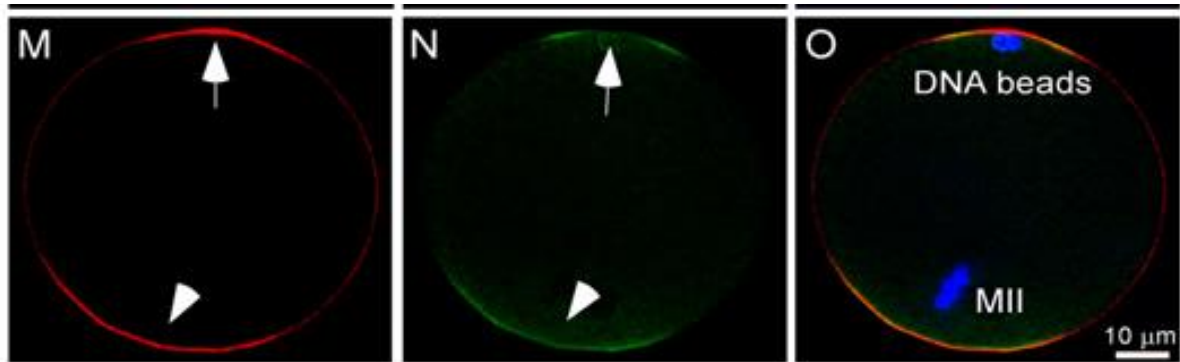


Figure 68: Cortical differentiation in response to chromatin signal. Both DNA beads (arrow) and MII spindle (arrowhead) cause cortical differentiation by accumulating actin (M) and myosin II (N) at the cortex in mouse oocytes in meiosis II. Reprinted from (Deng et al. 2007) with permission from Elsevier.

5.8.3 Potential function of the contraction wave in development

As the development of the oocyte sets the stage for embryonic development, many have suggested that the contraction waves may be required for localising some developmental determinants. The suggestions range from the localisation of broad cER-mRNA domains in ascidians (Figure 69) (Prodon et al. 2005) to the localisation of specific mRNAs in jellyfish (Houliston et al. 1993; Amiel & Houliston 2009). In general, these factors are thought to be involved with setting the embryonic animal-vegetal axis and determining micromere and resulting germ cell formation.

It is, however, unclear if there is a direct link between these localisations and the contraction wave or whether processes controlled by the same molecules are behind the localisation of these factors. Given that it is difficult to infer whether the contraction waves are evolutionarily similar between distally related species a speculation regarding a conserved function is even more difficult, especially in light of the paucity of evidence.

Mitochondria: DNA

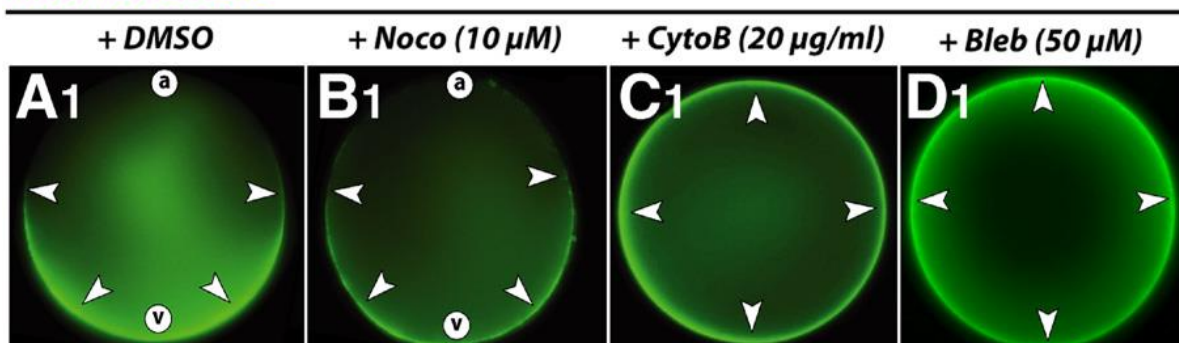


Figure 69: Polarisation of developmental determinants. Localisation of Mitochondria in an embryo of the ascidian *Halocynthia roretzi* after treatment with various cytoskeletal inhibitors. C and D) Removal of both actin and myosin II shows a lack of normal AP-VP polarisation of mitochondria distribution, compared to control and microtubule removal (A and B). Reprinted from (Prodon et al. 2008) with permission from Elsevier.

Sadly, none of the methods I have developed here to inhibit the contraction wave allow the formation of a fully mature oocyte. This is either due to polar body cytokinesis being inhibited (by the inhibitors

of the RhoA-Rok-Myosin II pathway) or the cell cycle being blocked (by Cdk1 inhibitors) for subsequent divisions. Therefore, I cannot generate fully mature and fertilisable oocyte which have never experienced a contraction wave, with which I could test the hypothesis of a developmental role of the contraction wave.

This will be an important challenge for the future, as a developmental role of the contraction wave is an exciting possibility with potentially wide-reaching developmental consequences.

It is well imaginable that the surface contraction waves developed originally only in response to the oocyte adaptations, but that they were later co-opted for the localisation of developmental determinants. The contraction waves are ideal candidates for this as they run along the animal-vegetal axis and thereby may help to communicate the cellular layout in these large cells. The cytoplasmic streaming taking place during the contraction wave would certainly give a plausible mechanism for how specific localisation could be achieved, especially in combination with specific binding sites, for example at the vegetal pole.

The identification of polarity markers, whose positioning happens during oocyte maturation and which can be visualised during maturation, will be an important first step in testing this intriguing hypothesis.

6 CONCLUSION

Surface contraction waves are a prominent example of spatially and temporally tightly regulated cortical contractility. They are commonly observed in large dividing cells, such as oocytes and early embryos, in a wide variety of species (Hara 1971; Hamaguchi & Hiramoto 1978). Previous studies have indicated that the contraction waves are linked to cell cycle transitions (Rankin & Kirschner 1997; Chang & Ferrell 2013), but the molecular basis of the contraction, its regulation by the cell cycle and the mechanisms that pattern this process in space and time had not previously been explored.

I studied surface contraction waves using starfish oocytes. They are a well-suited model system, exhibiting prominent contraction waves during meiosis, which can be imaged at high spatial and temporal resolution and are accessible to a variety of chemical and physical manipulations.

I first carefully and quantitatively characterised the cell shape changes associated with the contraction wave. This revealed that they arise from a band of flattening of the cortex which forms first at the vegetal pole and then moves across the cell towards the animal pole. Co-localized with the flattened cortex, I observed an accumulation of non-muscle myosin II molecules, and consistently, inhibition of myosin II weakens the contraction wave, while upregulation of myosin II strengthens it. As revealed by specific small molecule inhibitors, recruitment of myosin II to the cortex during the contraction wave is controlled by the RhoA kinase (Rok) which in turn is controlled by the localisation of active RhoA to the cortex. I further showed that RhoA activation was independent of microtubules, but depended on cdk1-cyclinB activity. Taken together, these data allow me to conclude that the pathway of RhoA-Rok-Myosin II drives the contraction wave. This offers the first molecular mechanism of surface contraction waves in any species. Indeed, the core signalling module composed of RhoA-Rok-Myosin II is a highly conserved pathway that controls cortical contractility in diverse physiological contexts including cytokinesis (Miller & Bement 2009) and embryo morphogenesis (Vasquez et al. 2014). The question that follows from this observation is how this pathway gives rise to the spatially and temporally complex pattern of contraction waves.

Indeed, a striking feature of the contraction wave is that it moves across the cell from one pole to the other. By investigating this dynamic behaviour in correlation with cell cycle regulators, I could show that the key cell cycle kinase, cdk1-cyclin B forms a gradient across the animal-vegetal axis of the oocyte and that this gradient defines the orientation of the contraction wave. The gradient is established early in meiosis due to the accumulation of cdk1-cyclinB in the nucleus, which is located at the animal pole. As the cell cycle proceeds, the cyclin B subunit of cdk1-cyclinB is progressively degraded, inactivating the kinase subunit, cdk1. Importantly, I could show that degradation of cyclin B is spatially homogenous and therefore the animal-vegetal gradient of cdk1-cyclinB is maintained throughout meiosis. As a consequence, the bottom threshold of cdk1 activity will be reached first

opposite of the nucleus that is at the vegetal pole. In a series of experiments using local application of inhibitors of cdk1 as well as locally introducing additional cdk1-cyclinB protein, I could demonstrate that the contraction wave initiates at the location where cdk1 activity first hits the bottom threshold. Furthermore, by changing the shape of the oocytes using microfabricated chambers, I could show that the gradient of cdk1-cyclin B across the oocyte regulates the progression of the wave.

From these data, I conclude that the activity gradient of cdk1-cyclin B provides the initial spatial cue setting the starting point and direction of the contraction wave. Additionally, I could show that feedbacks internal to the downstream signalling network further shape the contraction wave determining its speed and the width of the band of activity. In particular, I could show that myosin II activity feeds back to control the speed of the wave, and that a negative feedback from Rok controls RhoA deactivation and thereby defines the width of the wave.

In summary, based on the above experiments, I can propose the first comprehensive model for the molecular mechanism controlling surface contraction waves in space and time. My work reveals that while in small somatic cells the cell cycle machinery merely functions in temporal control and the microtubule spindle provides the spatial cues, in the large oocytes the cell cycle kinases form a spatial gradient that patterns contractile processes during cytokinesis. The spatial gradient arises from two specific features of the oocyte: the large size of the cell and the asymmetric nuclear position. In this sense, the contraction wave can be seen as a result of a cellular adaptation to the specific architecture of oocytes.

While cdk1-cyclin B activity is clearly the master regulator, my work also revealed important feedback mechanisms internal to the conserved RhoA-Rok-Myosin II signalling module wherein Rok and myosin II activity feeds back into the regulation of the contraction wave. These feedbacks have previously not been characterised, and I could detect and quantify them here for the first time due to the large size of the cell as well as the dynamic behaviour of the signalling cascade. As the pathway is highly conserved, this feedback is likely to be present and may have important functions in other systems.

Overall, my work identified the molecular regulatory pathway controlling the surface contraction waves in the starfish oocytes revealing how a spatial gradient of cell cycle factors in combination with feedbacks internal to the highly conserved RhoA-Rok-Myosin II pathway can pattern this spatially and temporally highly complex cellular behaviour.

7 BIBLIOGRAPHY

- Albertson, D., 1984. Formation of the first cleavage spindle in nematode embryos. *Developmental biology*.
- Amano, M. et al., 1996. Phosphorylation and activation of myosin by Rho-associated kinase (Rho-kinase). *Journal of Biological Chemistry*.
- Amiel, A. & Houlston, E., 2009. Three distinct RNA localization mechanisms contribute to oocyte polarity establishment in the cnidarian *Clytia hemisphaerica*. *Developmental biology*, 327(1), pp.191–203.
- Beach, J.R. & Egelhoff, T.T., 2009. Myosin II recruitment during cytokinesis independent of centralspindlin-mediated phosphorylation. *The Journal of biological chemistry*, 284(40), pp.27377–83.
- Bell, L.G.E., 1962. Some Mechanisms involved in Cell Division. *Nature*, 193, pp.190–191.
- Bement, W.M. et al., 2015. Activator–inhibitor coupling between Rho signalling and actin assembly makes the cell cortex an excitable medium. *Nature cell biology*, 17(11).
- Bement, W.M., Benink, H.A. & von Dassow, G., 2005. A microtubule-dependent zone of active RhoA during cleavage plane specification. *Journal of Cell Biology*, 170(1), pp.91–101.
- Bement, W.M. & von Dassow, G., 2014. Single cell pattern formation and transient cytoskeletal arrays. *Current Opinion in Cell Biology*, 26, pp.51–59.
- Bement, W.M., Miller, A.L. & von Dassow, G., 2006. Rho GTPase activity zones and transient contractile arrays. *BioEssays*, 28(10), pp.983–93.
- Benink, H.A. & Bement, W.M., 2005. Concentric zones of active RhoA and Cdc42 around single cell wounds. *The Journal of cell biology*, 168(3), pp.429–39.
- Bernards, A., 2003. GAPs galore! A survey of putative Ras superfamily GTPase activating proteins in man and *Drosophila*. *Biochimica et Biophysica Acta (BBA) - Reviews on Cancer*, 1603(2), pp.47–82.
- Betschinger, J. & Knoblich, J.J. a, 2004. Dare to be different: asymmetric cell division in *Drosophila*, *C. elegans* and vertebrates. *Current biology : CB*, 14(16), pp.R674–85.
- Bhadriraju, K. et al., 2007. Activation of ROCK by RhoA is regulated by cell adhesion, shape, and cytoskeletal tension. *Experimental cell research*, 313(16), pp.3616–23.

- Bieber, F., Nance, W. & Morton, C., 1981. Genetic studies of an acardiac monster: evidence of polar body twinning in man. *Science*.
- Birkenfeld, J. et al., 2007. GEF-H1 Modulates Localized RhoA Activation during Cytokinesis under the Control of Mitotic Kinases. *Developmental Cell*, 12(5), pp.699–712.
- Bishop, A.L. & Hall, A., 2000. Rho GTPases and their effector proteins. *Biochemical Journal*, 348(2), pp.241–255.
- Blanchoin, L. et al., 2014. Actin dynamics, architecture, and mechanics in cell motility. *Physiological reviews*, 94(1), pp.235–63.
- Borrego Pinto, J., 2015. *The mechanism of centriole inactivation in starfish oocytes*.
- Bovellan, M. et al., 2014. Cellular control of cortical actin nucleation. *Current biology : CB*, 24(14), pp.1628–35.
- Bray, D. & White, J., 1988. Cortical flow in animal cells. *Science*.
- Bringmann, H. & Hyman, A. a, 2005. A cytokinesis furrow is positioned by two consecutive signals. *Nature*, 436(7051), pp.731–4.
- Burkel, B.M., von Dassow, G. & Bement, W.M., 2007. Versatile fluorescent probes for actin filaments based on the actin-binding domain of utrophin. *Cell motility and the cytoskeleton*, 64(11), pp.822–32.
- Cameron, R.A. et al., 2009. SpBase: the sea urchin genome database and web site. *Nucleic acids research*, 37(Database issue), pp.D750–4.
- Canman, J.C., Hoffman, D.B. & Salmon, E.D., 2000. The role of pre- and post-anaphase microtubules in the cytokinesis phase of the cell cycle. *Current Biology*, 10, pp.611–614.
- Carvalho, A., Desai, A. & Oegema, K., 2009. Structural memory in the contractile ring makes the duration of cytokinesis independent of cell size. *Cell*, 137(5), pp.926–37.
- Chaigne, A. et al., 2013. A soft cortex is essential for asymmetric spindle positioning in mouse oocytes. *Nature cell biology*, 15(7), pp.1–7.
- Chan, T.F. & Vese, L.A., 2001. Active contours without edges. *IEEE transactions on image processing : a publication of the IEEE Signal Processing Society*, 10(2), pp.266–77.
- Chang, J.B. & Ferrell, J.E., 2013. Mitotic trigger waves and the spatial coordination of the *Xenopus* cell cycle. *Nature*, 500(7464), pp.603–607.

- Charras, G. & Paluch, E., 2008. Blebs lead the way: how to migrate without lamellipodia. *Nature reviews. Molecular cell biology*, 9(9), pp.730–6.
- Charras, G.T. et al., 2006. Reassembly of contractile actin cortex in cell blebs. *The Journal of Cell Biology*, 175(3), pp.477–490.
- Christensen, K. & Merriam, R.W., 1982. Insensitivity to cytochalasin B of surface contractions keyed to cleavage in the *Xenopus* egg. *Journal of embryology and experimental morphology*, 72, pp.143–151.
- Clark, A.G., Dierkes, K. & Paluch, E.K., 2013. Monitoring actin cortex thickness in live cells. *Biophysical journal*, 105(3), pp.570–80.
- Clute, P. & Pines, J., 1999. Temporal and spatial control of cyclin B1 destruction in metaphase. *Nature cell biology*, 1(2), pp.82–7.
- Conklin, E.G., 1902. Karyokinesis and cytokinesis in the maturation, fertilization and cleavage of *Crepidula* and other Gasteropoda. *J. Acad. Nat. Sci. (Philadelphia) Series 2*, 12(Part 1), pp.1–121.
- Cooper, G.M., 2000. *The Cell: A Molecular Approach. The Events of M Phase.*
- Cortes, D.B. et al., 2015. The asymmetry of female meiosis reduces the frequency of inheritance of unpaired chromosomes. *eLife*, 4, pp.1–21.
- Cramer, L.P., 2010. Forming the cell rear first: breaking cell symmetry to trigger directed cell migration. *Nature cell biology*, 12(7), pp.628–32.
- D’Avino, P. & Savoian, M., 2006. RacGAP50C is sufficient to signal cleavage furrow formation during cytokinesis. *Journal of Cell Science*.
- Danowski, B., 1989. Fibroblast contractility and actin organization are stimulated by microtubule inhibitors. *J. Cell Sci.*, 93(2), pp.255–266.
- von Dassow, G., 2009. Concurrent cues for cytokinetic furrow induction in animal cells. *Trends in cell biology*, 19(4), pp.165–73.
- Deng, M. et al., 2007. The Ran GTPase mediates chromatin signaling to control cortical polarity during polar body extrusion in mouse oocytes. *Developmental cell*, 12(2), pp.301–8.
- Dorn, J.F. et al., 2010. Actomyosin tube formation in polar body cytokinesis requires Anillin in *C. elegans*. *Current biology : CB*, 20(22), pp.2046–51.

- Dumollard, R. et al., 2011. Mos limits the number of meiotic divisions in urochordate eggs. *Development*, 138(5), pp.885–895.
- Eggert, U.S., Mitchison, T.J. & Field, C.M., 2006. Animal Cytokinesis : From Parts List to Mechanisms. *Annual Review of Biochemistry*, 75, pp.543–66.
- Fabritius, A., Flynn, J. & McNally, F., 2012. Initial diameter of the polar body contractile ring is minimized by the centralspindlin complex. *Developmental biology*, 359(1), pp.137–148.
- Falzone, T. et al., 2012. Assembly kinetics determine the architecture of α -actinin crosslinked F-actin networks. *Nature communications*.
- Fehon, R.G., McClatchey, A.I. & Bretscher, A., 2010. Organizing the cell cortex: the role of ERM proteins. *Nature reviews. Molecular cell biology*, 11(4), pp.276–87.
- Fischer-Friedrich, E. et al., 2014. Quantification of surface tension and internal pressure generated by single mitotic cells. *Scientific reports*, 4, p.6213.
- Foe, V.E. & von Dassow, G., 2008. Stable and dynamic microtubules coordinately shape the myosin activation zone during cytokinetic furrow formation. *The Journal of cell biology*, 183(3), pp.457–70.
- Fritzsche, M., Lewalle, A. & Duke, T., 2013. Analysis of turnover dynamics of the submembranous actin cortex. *Molecular biology of the cell*.
- Fung, T.K. & Poon, R.Y.C., 2005. A roller coaster ride with the mitotic cyclins. *Seminars in Cell and Developmental Biology*, 16(3), pp.335–342.
- Furuno, N. et al., 1994. Suppression of DNA replication via Mos function during meiotic divisions in *Xenopus* oocytes. *The EMBO journal*, 13(10), pp.2399–410.
- Gavet, O. & Pines, J., 2010. Activation of cyclin B1-Cdk1 synchronizes events in the nucleus and the cytoplasm at mitosis. *The Journal of cell biology*, 189(2), pp.247–59.
- Glotzer, M., 2004. Cleavage furrow positioning. *Journal of Cell Biology*, 164(3), pp.347–351.
- Goddette, D.W. & Frieden, C., 1986. Actin polymerization. The mechanism of action of cytochalasin D. *Journal of Biological Chemistry*, 261(34), pp.15974–15980.
- Green, R. a, Paluch, E. & Oegema, K., 2012. Cytokinesis in animal cells. *Annual review of cell and developmental biology*, 28, pp.29–58.
- Gudejko, H.F.M., Alford, L.M. & Burgess, D.R., 2012. Polar expansion during cytokinesis. *Cytoskeleton*

- (Hoboken, N.J.), 1009(November), pp.1000–1009.
- Haeusler, L., Blumenstein, L. & Stege, P., 2003. Comparative functional analysis of the Rac GTPases. *FEBS letters*.
- Hagting, A. et al., 2002. Human securin proteolysis is controlled by the spindle checkpoint and reveals when the APC/C switches from activation by Cdc20 to Cdh1. *The Journal of cell biology*, 157(7), pp.1125–37.
- Hagting, A. et al., 1999. Translocation of cyclin B1 to the nucleus at prophase requires a phosphorylation-dependent nuclear import signal. *Current biology : CB*, 9(13), pp.680–9.
- Hall, A., 1998. Rho GTPases and the actin cytoskeleton. *Science*.
- Hamaguchi, M.S. & Hiramoto, Y., 1978. Protoplasmic movement during polar-body formation in starfish oocytes. *Experimental cell research*, 112(1), pp.55–62.
- Hara, K., 1971. Cinematographic observation of “surface contraction waves” (SCW) during the early cleavage of axolotl eggs. *Wilhelm Roux Arch. EntwMech. Org.*, 167, pp.183–186.
- Hara, K. & Tydeman, P., 1979. Cinematographic Observation of an “ Activation Wave ” (AW) on the Locally Inseminated Egg of *Xenopus laevis*. *Roux’s Archives of Developmental Biology*, 186, pp.91–94.
- Hara, K., Tydeman, P. & Kirschner, M., 1980. A cytoplasmic clock with the same period as the division cycle in *Xenopus* eggs. *Proceedings of the National Academy of Sciences of the United States of America*, 77(1), pp.462–6.
- Harada, K., Oita, E. & Chiba, K., 2003. Metaphase I arrest of starfish oocytes induced via the MAP kinase pathway is released by an increase of intracellular pH. *Development*, 130(19), pp.4581–6.
- Harb, N., Archer, T.K. & Sato, N., 2008. The Rho-Rock-Myosin signaling axis determines cell-cell integrity of self-renewing pluripotent stem cells. *PloS one*, 3(8), p.e3001.
- Harvey, E.N. & Fankhauser, G., 1933. The tension at the surface of the eggs of the salamander, *Triturus (Diemyctylus) viridescens*. *Journal of Cellular and Comparative Physiology*, 3, pp.463–475.
- Hebert, B., Costantino, S. & Wiseman, P.W., 2005. Spatiotemporal image correlation spectroscopy (STICS) theory, verification, and application to protein velocity mapping in living CHO cells. *Biophysical journal*, 88(5), pp.3601–14.

- Higgs, H.N., 2005. Formin proteins: a domain-based approach. *Trends in biochemical sciences*, 30(6), pp.342–53.
- Hiramoto, Y., 1976. Mechanical properties of starfish oocytes. *Development growth differentiation*, 18(3), pp.205–209.
- Hiramoto, Y., 1962. Injection of spermatozoa into the egg. *Experimental cell research*, 27, pp.416–426.
- Hirata, N., Takahashi, M. & Yazawa, M., 2009. Diphosphorylation of regulatory light chain of myosin IIA is responsible for proper cell spreading. *Biochemical and biophysical research communications*, 381(4), pp.682–7.
- Houliston, E. et al., 1993. Axis establishment and microtubule-mediated waves prior to first cleavage in *Beroe ovata*. *Development*, 87, pp.75–87.
- Iden, S. & Collard, J.G., 2008. Crosstalk between small GTPases and polarity proteins in cell polarization. *Nature reviews. Molecular cell biology*, 9(11), pp.846–59.
- Ikebe, M., Hartshorne, D.J. & Elzinga, M., 1986. Identification, phosphorylation, and dephosphorylation of a second site for myosin light chain kinase on the 20,000-dalton light chain of smooth muscle myosin. *J. Biol. Chem.*, 261(1), pp.36–39.
- Ikeda, M., Nemoto, S.I. & Yoneda, M., 1976. Periodic changes in the content of protein-bound sulfhydryl groups and tension at the surface of starfish oocytes in correlation with the meiotic division cycle. *Development, Growth and Differentiation*, 18(3), pp.221–225.
- Ishibashi, Y. & Tsutsui, H., 1996. Role of microtubules in myocyte contractile dysfunction during cardiac hypertrophy in the rat. *American journal of physiology*.
- Ishihara, K. et al., 2014. Organization of early frog embryos by chemical waves emanating from centrosomes. *Philosophical Transactions of the Royal Society B: Biological Sciences*, 369.
- Ishizaki, T. et al., 2000. Pharmacological properties of Y-27632, a specific inhibitor of rho-associated kinases. *Molecular pharmacology*, 57(5), pp.976–983.
- Jaffe, A.B. & Hall, A., 2005. Rho GTPases: biochemistry and biology. *Annual review of cell and developmental biology*, 21, pp.247–69.
- Jantsch-Plunger, V. & Gönczy, P., 2000. CYK-4 a Rho family GTPase activating protein (GAP) required for central spindle formation and cytokinesis. *The Journal of cell biology*.

- Jordan, S.N. & Canman, J.C., 2012. Rho GTPases in animal cell cytokinesis: an occupation by the one percent. *Cytoskeleton (Hoboken, N.J.)*, 69(11), pp.919–30.
- Kaltschmidt, J.A. et al., 2000. Rotation and asymmetry of the mitotic spindle direct asymmetric cell division in the developing central nervous system. *Nature cell biology*, 2(1), pp.7–12.
- Kanatani, H. et al., 1969. Isolation and Identification of Meiosis inducing Substance in Starfish *Asterias amurensis*. *Nature*, 221.
- Katula, K.S. et al., 1997. Cyclin-dependent kinase activation and S-phase induction of the cyclin B1 gene are linked through the CCAAT elements. *Cell growth & differentiation: the molecular biology journal of the American Association for Cancer Research*, 8(7), pp.811–20.
- Kaur, G. et al., 1992. Growth Inhibition With Reversible Cell Cycle Arrest of Carcinoma Cells by Flavone L86-8275. *JNCI Journal of the National Cancer Institute*, 84(22), pp.1736–1740.
- Kepiró, M. et al., 2014. para -Nitroblebbistatin , the Non-Cytotoxic and Photostable Myosin II Inhibitor. *Angewandte Chemie - International Edition*, 53, pp.8211–8215.
- Kimura, K. et al., 1993. Regulation of Myosin Phosphatase by Rho and Rho-Associated Kinase (Rho-Kinase). *Science*, 273, pp.245–248.
- Kishimoto, T., 2011. A primer on meiotic resumption in starfish oocytes: the proposed signaling pathway triggered by maturation-inducing hormone. *Molecular reproduction and development*, 78(10-11), pp.704–7.
- Kishimoto, T., 1998. Cell cycle arrest and release in starfish oocytes and eggs. *Seminars in cell & developmental biology*, 9(5), pp.549–57.
- Kojima, M.K., 1962. Cyclic changes of the cortex and the cytoplasm of the fertilized and the activated sea urchin egg IV. Formation of sperm asters and cytoplasmic protrusions in re-fertilized eggs and eggs fertilized after activation. *EMBO reports*, 7(1), pp.81–94.
- Kosako, H. et al., 2000. Rho-kinase/ROCK is involved in cytokinesis through the phosphorylation of myosin light chain and not ezrin/radixin/moesin proteins at the cleavage furrow. *Oncogene*, 19(52), pp.6059–6064.
- Krendel, M. & Mooseker, M.S., 2005. Myosins: Tails (and Heads) of Functional Diversity. *Physiology*, 20, pp.239–251.
- Krendel, M., Zenke, F.T. & Bokoch, G.M., 2002. Nucleotide exchange factor GEF-H1 mediates cross-talk between microtubules and the actin cytoskeleton. *Nature cell biology*, 4(4), pp.294–301.

- Kubota, B.T., 1967. A regional change in the rigidity of the cortex of the egg of *Rana nigromaculata* following extrusion of the second polar body. *Development*, 17, pp.331–340.
- Kunda, P. et al., 2008. Moesin controls cortical rigidity, cell rounding, and spindle morphogenesis during mitosis. *Current biology : CB*, 18(2), pp.91–101.
- Lankton, S. & Tannenbaum, A., 2008. Localizing Region-Based Active Contours. *IEEE Transactions on Image Processing*, 17(11), pp.2029–2039.
- Larson, S.M. et al., 2010. Cortical Mechanics and Meiosis II Completion in Mammalian Oocytes Are Mediated by Myosin-II and Ezrin-Radixin-Moesin (ERM) Proteins. *Molecular biology of the cell*, 21, pp.3182–3192.
- Leblanc, J. et al., 2011. The small GTPase Cdc42 promotes membrane protrusion during polar body emission via ARP2-nucleated actin polymerization. *Molecular human reproduction*, 17(5), pp.305–16.
- Lekomtsev, S. et al., 2012. Centralspindlin links the mitotic spindle to the plasma membrane during cytokinesis. *Nature*, 492(7428), pp.276–9.
- Lenart, P. et al., 2005. A contractile nuclear actin network drives chromosome congression in oocytes. *Nature*, 436(August), p.812.
- Letunic, I. & Bork, P., 2007. Interactive Tree Of Life (iTOL): an online tool for phylogenetic tree display and annotation. *Bioinformatics*.
- Letunic, I., Doerks, T. & Bork, P., 2012. SMART 7: recent updates to the protein domain annotation resource. *Nucleic acids research*.
- Leung, T. et al., 1996. The p160 RhoA-binding kinase ROK alpha is a member of a kinase family and is involved in the reorganization of the cytoskeleton. *Molecular and Cellular Biology*, 16(10), pp.5313–5327.
- Levayer, R. & Lecuit, T., 2012. Biomechanical regulation of contractility: spatial control and dynamics. *Trends in cell biology*, 22(2), pp.61–81.
- Lindqvist, A., Rodríguez-Bravo, V. & Medema, R.H., 2009. The decision to enter mitosis: feedback and redundancy in the mitotic entry network. *The Journal of cell biology*, 185(2), pp.193–202.
- Liu, X.J., 2012. Polar body emission. *Cytoskeleton (Hoboken, N.J.)*, 69(10), pp.670–85.
- Lukas, T.J. et al., 1999. Identification of novel classes of protein kinase inhibitors using combinatorial

- peptide chemistry based on functional genomics knowledge. *Journal of medicinal chemistry*, 42(5), pp.910–9.
- Lyass, L., 1988. Microtubule-dependent effect of phorbol ester on the contractility of cytoskeleton of cultured fibroblasts. *Proceedings of the National Academy of Sciences of the United States of America*
- Ma, C. et al., 2006. Cdc42 activation couples spindle positioning to first polar body formation in oocyte maturation. *Current biology : CB*, 16(2), pp.214–20.
- Mabuchi, I. & Okuno, M., 1977. The effect of myosin antibody on the division of starfish blastomeres. *The Journal of cell biology*.
- Macaulay, C., Meier, E. & Forbes, D.J., 1995. Differential Mitotic Phosphorylation of Proteins of the Nuclear Pore Complex. *Journal of Biological Chemistry*, 270(1), pp.254–262.
- Maddox, A.S., Azoury, J. & Dumont, J., 2012. Polar body cytokinesis. *Cytoskeleton (Hoboken, N.J.)*, 000, pp.1–14.
- Maître, J.-L. et al., 2012. Adhesion Functions in Cell Sorting by of Adhering Cells. , *Science*, 253, pp.253–257.
- Maître, J.-L. et al., 2015. Pulsatile cell-autonomous contractility drives compaction in the mouse embryo. *Nature Cell Biology*, 17(7), pp.849–855.
- Mandato, C.A., Benink, H.A. & Bement, W.M., 2000. Microtubule-Actomyosin Interactions in Cortical Flow and Cytokinesis. *Cell Motility and the Cytoskeleton*, 92 (November 1999), pp.87–92.
- Martineau, S., Andreassen, P. & Margolis, R., 1995. Delay of HeLa cell cleavage into interphase using dihydrocytochalasin B: retention of a postmitotic spindle and telophase disc correlates with synchronous cleavage. *The Journal of cell biology*.
- Masui, Y. & Markert, C.L., 1971. Cytoplasmic control of nuclear behavior during meiotic maturation of frog oocytes. *Biology of the Cell*, 90(6-7), pp.461–466.
- Matsumura, F., 2005. Regulation of myosin II during cytokinesis in higher eukaryotes. *Trends in cell biology*, 15(7), pp.371–7.
- Matsumura, F. & Hartshorne, D.J., 2008. Myosin phosphatase target subunit: Many roles in cell function. *Biochemical and biophysical research communications*, 369(1), pp.149–56.
- Matsuura, R. & Chiba, K., 2004. Unequal cell division regulated by the contents of germinal vesicles.

- Developmental biology*, 273(1), pp.76–86.
- McCarthy Campbell, E.K., Werts, A.D. & Goldstein, B., 2009. A cell cycle timer for asymmetric spindle positioning. *PLoS biology*, 7(4), p.e1000088.
- Meijer, L. et al., 1997. Biochemical and cellular effects of roscovitine, a potent and selective inhibitor of the cyclin-dependent kinases cdc2, cdk2 and cdk5. *European journal of biochemistry / FEBS*, 243(1-2), pp.527–536.
- Mikawa, M., Su, L. & Parsons, S., 2008. Opposing roles of p190RhoGAP and Ect2 RhoGEF in regulating cytokinesis. *Cell Cycle*.
- Miller, A.L., 2011. The contractile ring. *Current Biology*, 21(24), pp.R976–R978.
- Miller, A.L. & Bement, W.M., 2009. Regulation of cytokinesis by Rho GTPase flux. *Nature cell biology*, 11(1), pp.71–7.
- Minc, N., Burgess, D. & Chang, F., 2011. Influence of cell geometry on division-plane positioning. *Cell*, 144(3), pp.414–26.
- Mishima, M., Kaitna, S. & Glotzer, M., 2002. Central spindle assembly and cytokinesis require a kinesin-like protein/RhoGAP complex with microtubule bundling activity. *Developmental cell*.
- Miyazaki, a, Kamitsubo, E. & Nemoto, S.I., 2000. Premeiotic aster as a device to anchor the germinal vesicle to the cell surface of the presumptive animal pole in starfish oocytes. *Developmental biology*, 218(2), pp.161–71.
- Mohr, C. et al., 1992. ADP-ribosylation by Clostridium botulinum C3 exoenzyme increases steady-state GTPase activities of recombinant rhoA and rhoB proteins. *FEBS Letters*, 297(1-2), pp.95–99.
- Morgan, D., 2007. The cell cycle: principles of control.
- Mullins, R.D., Heuser, J.A. & Pollard, T.D., 1998. The interaction of Arp2/3 complex with actin: Nucleation, high affinity pointed end capping, and formation of branching networks of filaments. *Proceedings of the National Academy of Sciences*, 95(11), pp.6181–6186.
- Munro, E., Nance, J. & Priess, J.R., 2004. Cortical Flows Powered by Asymmetrical Contraction Transport PAR Proteins to Establish and Maintain Anterior-Posterior Polarity in the Early C. elegans Embryo. *Developmental Cell*, 7, pp.413–424.
- Murrell, M. et al., 2015. Forcing cells into shape: the mechanics of actomyosin contractility. *Nature*

- Reviews Molecular Cell Biology*, 16(8), pp.486–498.
- Murthy, K. & Wadsworth, P., 2005. Myosin-II-dependent localization and dynamics of F-actin during cytokinesis. *Current biology : CB*, 15(8), pp.724–31.
- Nemoto, S., Yoneda, M. & Uemura, I., 1980. Marked decrease in the rigidity of starfish oocytes induced by 1-Methyladenine. *Development Growth and Differentiation*, 22(3), pp.315–325.
- Newman, S. a., 2009. E.E. Just’s “independent irritability” revisited: the activated egg as excitable soft matter. *Molecular reproduction and development*, 76(10), pp.966–74.
- Nishikawa, M. et al., 1984. Protein kinase C modulates in vitro phosphorylation of the smooth muscle heavy meromyosin by myosin light chain kinase. *J. Biol. Chem.*, 259(14), pp.8808–8814.
- Nishimura, Y. & Yonemura, S., 2006. Centralspindlin regulates ECT2 and RhoA accumulation at the equatorial cortex during cytokinesis. *Journal of cell science*.
- Nomura, A., Maruyama, Y.K. & Yoneda, M., 1991. Initiation of DNA replication cycle in fertilized eggs of the starfish, *Asterina pectinifera*. *Developmental biology*, 143(2), pp.289–96.
- Normark, B., 2004. The strange case of the armored scale insect and its bacteriome. *PLoS biology*.
- Ogihara, S., Carboni, J. & Condeelis, J., 1988. Electron microscopic localization of myosin II and ABP-120 in the cortical actin matrix of *Dictyostelium amoebae* using IgG-gold conjugates. *Developmental genetics*, 9(4-5), pp.505–20.
- Oita, E., Harada, K. & Chiba, K., 2004. Degradation of polyubiquitinated cyclin B is blocked by the MAPK pathway at the metaphase I arrest in starfish oocytes. *The Journal of biological chemistry*, 279(18), pp.18633–40.
- Okano-Uchida, T. et al., 1998. In vivo regulation of cyclin A/Cdc2 and cyclin B/Cdc2 through meiotic and early cleavage cycles in starfish. *Developmental biology*, 197(1), pp.39–53.
- Okumura, E. et al., 2002. Akt inhibits Myt1 in the signalling pathway that leads to meiotic G2/M-phase transition. *Nature cell biology*, 4(2), pp.111–6.
- Okumura, E., 1996. Initial triggering of M-phase in starfish oocytes: a possible novel component of maturation-promoting factor besides cdc2 kinase. *The Journal of Cell Biology*, 132(1), pp.125–135.
- Olofsson, B., 1999. Rho Guanine Dissociation Inhibitors. *Cellular Signalling*, 11(8), pp.545–554.
- Otomo, T., Otomo, C. & Tomchick, D., 2005. Structural basis of Rho GTPase-mediated activation of

- the formin mDia1. *Molecular cell*.
- Otsuki, J. et al., 2011. Symmetrical division of mouse oocytes during meiotic maturation can lead to the development of twin embryos that amalgamate to form a chimeric. *Human reproduction*.
- Ou, G. et al., 2010. Polarized myosin produces unequal-size daughters during asymmetric cell division. *Science (New York, N.Y.)*, 330(6004), pp.677–80.
- Paluch, E. et al., 2005. Cortical actomyosin breakage triggers shape oscillations in cells and cell fragments. *Biophysical journal*, 89(1), pp.724–733.
- Paluch, E. et al., 2006. Dynamic modes of the cortical actomyosin gel during cell locomotion and division. *Trends in cell biology*, 16(1), pp.5–10.
- Pavicic-Kaltenbrunner, V., 2007. Cooperative assembly of CYK-4/MgcRacGAP and ZEN-4/MKLP1 to form the centralspindlin complex. *Molecular biology of the cell*.
- Pérez-Mongiovi, D., Chang, P. & Houlston, E., 1998. A propagated wave of MPF activation accompanies surface contraction waves at first mitosis in *Xenopus*. *Journal of cell science*, 111 (Pt 3), pp.385–93.
- Peter, M. et al., 1991. Disassembly of in vitro formed lamin head-to-tail polymers by CDC2 kinase. *The EMBO journal*, 10(6), pp.1535–44.
- Petrie, R.J. & Yamada, K.M., 2012. At the leading edge of three-dimensional cell migration. *Journal of cell science*, 125(Pt 24), pp.5917–26.
- Piekny, A.J. & Mains, P.E., 2002. Rho-binding kinase (LET-502) and myosin phosphatase (MEL-11) regulate cytokinesis in the early *Caenorhabditis elegans* embryo. *Journal of Cell Science*, 115, pp.2271–2282.
- Pielak, R.M., Gaysinskaya, V. a & Cohen, W.D., 2004. Formation and function of the polar body contractile ring in *Spisula*. *Developmental biology*, 269(2), pp.421–32.
- Pines, J., 2006. Mitosis: a matter of getting rid of the right protein at the right time. *Trends in cell biology*, 16(1), pp.55–63.
- Pletjushkina, O.J. et al., 2001. Induction of cortical oscillations in spreading cells by depolymerization of microtubules. *Cell Motility and the Cytoskeleton*, 48(November 2000), pp.235–244.
- Prodon, F. et al., 2005. Polarity of the ascidian egg cortex and relocalization of cER and mRNAs in the early embryo. *Journal of cell science*, 118(Pt 11), pp.2393–404.

- Prodon, F., Sardet, C. & Nishida, H., 2008. Cortical and cytoplasmic flows driven by actin microfilaments polarize the cortical ER-mRNA domain along the a-v axis in ascidian oocytes. *Developmental biology*, 313(2), pp.682–99.
- Quaas, J. & Wylie, C., 2002. Surface contraction waves (SCWs) in the *Xenopus* egg are required for the localization of the germ plasm and are dependent upon maternal stores of the kinesin-like protein Xklp1. *Developmental biology*, 243(2), pp.272–80.
- R Core Team, 2016. R: A Language and Environment for Statistical Computing. *R Foundation for Statistical Computing*, p.www.R-project.org.
- Rajdev, S. & Reynolds, I.J., 1993. Calcium green-5N, a novel fluorescent probe for monitoring high intracellular free Ca²⁺ concentrations associated with glutamate excitotoxicity in cultured rat brain neurons. *Neuroscience Letters*, 162(1-2), pp.149–152.
- Ramanathan, S.P. et al., 2015. Cdk1-dependent mitotic enrichment of cortical myosin II promotes cell rounding against confinement. *Nature Cell Biology*, 17(2), pp.148–159.
- Rankin, S. & Kirschner, M.W., 1997. The surface contraction waves of *Xenopus* eggs reflect the metachronous cell-cycle state of the cytoplasm. *Current Biology*, 7, pp.451–454.
- Rappaport, R., 1961. Experiments concerning the cleavage stimulus in sand dollar eggs. *The Journal of experimental zoology*, 148, pp.81–89.
- Rappaport, R., 1964. Geometrical relations of the cleavage stimulus in constricted sand dollar eggs. *Journal of Experimental Zoology*, 155(2), pp.225–230.
- Rappaport, R., 1985. Repeated furrow formation from a single mitotic apparatus in cylindrical sand dollar eggs. *The Journal of experimental zoology*, 234(1), pp.167–71.
- Rappaport, R. & Rappaport, B.N., 1985. Experimental analysis of polar body formation in starfish eggs. *Journal of Experimental Zoology*, 235(1), pp.87–103.
- Ricketson, D., Johnston, C.A. & Prehoda, K.E., 2010. Multiple tail domain interactions stabilize nonmuscle myosin II bipolar filaments. *Proceedings of the National Academy of Sciences of the United States of America*, 107(49), pp.20964–9.
- Riedl, J. et al., 2008. Lifeact: a versatile marker to visualize F-actin. *Nature methods*, 5(7), pp.605–7.
- Rose, R., Weyand, M. & Lammers, M., 2005. Structural and mechanistic insights into the interaction between Rho and mammalian Dia. *Nature*.

- Ross, L., Pen, I. & Shuker, D., 2010. Genomic conflict in scale insects: the causes and consequences of bizarre genetic systems. *Biological Reviews*.
- Rossman, K.L., Der, C.J. & Sondek, J., 2005. GEF means go: turning on RHO GTPases with guanine nucleotide-exchange factors. *Nature Reviews Molecular Cell Biology*, 6(2), pp.167–180.
- Rougerie, P. & Delon, J., 2012. Rho GTPases: Masters of T lymphocyte migration and activation. *Immunology Letters*, 142(1-2), pp.1–13.
- Sage, D. et al., 2012. MIJ: Making interoperability between ImageJ and Matlab possible. *ImageJ User and Developer Conference*.
- Saha, A. et al., 2016. Determining Physical Properties of the Cell Cortex. *Biophysical Journal*, 110(6), pp.1421–1429.
- Salbreux, G., Charras, G. & Paluch, E., 2012. Actin cortex mechanics and cellular morphogenesis. *Trends in cell biology*, 22(10), pp.536–45.
- Sardet, C. et al., 1989. Fertilization and ooplasmic movements in the ascidian egg. *Development*, 105(2), pp.237–49.
- Satoh, N. & Deno, T., 1984. Periodic appearance and disappearance of microvilli associated with cleavage cycles in the egg of the ascidian, *Halocynthia roretzi*. *Developmental biology*, 102(2), pp.488–492.
- Satoh, S.K. et al., 2013. The Tension at the Top of the Animal Pole Decreases during Meiotic Cell Division. *PLoS one*, 8(11), p.e79389.
- Satterwhite, L.L. et al., 1992. Phosphorylation of myosin-II regulatory light chain by cyclin-p34cdc2: a mechanism for the timing of cytokinesis. *The Journal of cell biology*, 118(3), pp.595–605.
- Savoian, M.S. et al., 1999. Cleavage Furrows Formed between Centrosomes Lacking an Intervening Spindle and Chromosomes Contain Microtubule Bundles, INCENP, and CHO1 but Not CENP-E. *Molecular Biology of the Cell*, 10(2), pp.297–311.
- Sawai, T., 1982. Wavelike Propagation of Stretching and Shrinkage in the Surface of the Newt's Egg Before the First Cleavage. *Journal of Experimental Zoology*, 222, pp.59–68.
- Sawai, T. & Yoneda, M., 1974. Wave of stiffness propagating along the surface of the newt egg during cleavage. *The Journal of cell biology*, 60(1), pp.1–7.
- Schaller, V. et al., 2013. Crosslinking proteins modulate the self-organization of driven systems. *Soft*

- Matter*, 9(30), p.7229.
- Schindelin, J. et al., 2012. Fiji: an open-source platform for biological-image analysis. *Nature methods*, 9(7), pp.676–82.
- Schmerler, S. & Wessel, G.M., 2011. Polar bodies--more a lack of understanding than a lack of respect. *Molecular reproduction and development*, 78(1), pp.3–8.
- Schmidt, A. & Hall, A., 2002. Guanine nucleotide exchange factors for Rho GTPases: turning on the switch. *Genes & development*, 16(13), pp.1587–609.
- Schneider, C.A., Rasband, W.S. & Eliceiri, K.W., 2012. NIH Image to ImageJ: 25 years of image analysis. *Nature Methods*, 9(7), pp.671–675.
- Scholey, J.M., Taylor, K.A. & Kendrick-Jones, J., 1980. Regulation of non-muscle myosin assembly by calmodulin-dependent light chain kinase. *Nature*, 287(5779), pp.233–235.
- Schroeder, T.E., 1973. Actin in dividing cells: contractile ring filaments bind heavy meromyosin. *Proceedings of the National Academy of Sciences of the United States of America*, 70(6), pp.1688–92.
- Sedzinski, J. et al., 2011. Polar actomyosin contractility destabilizes the position of the cytokinetic furrow. *Nature*, 476(7361), pp.462–6.
- Sellers, J.R., Eisenberg, E. & Adelstein, R.S., 1982. The binding of smooth muscle heavy meromyosin to actin in the presence of ATP. Effect of phosphorylation. *J. Biol. Chem.*, 257(23), pp.13880–13883.
- Selman, G.G. & Waddington, C.H., 1955. The Mechanism of Cell Division in the Cleavage of the Newt's Egg. *The Journal of Experimental Biology*, 32, pp.700–733.
- Severson, A., Baillie, D. & Bowerman, B., 2002. A Formin Homology protein and a profilin are required for cytokinesis and Arp2/3-independent assembly of cortical microfilaments in *C. elegans*. *Current biology*.
- Shimizu, T., 1984. Dynamics of the actin microfilament system in the Tubifex egg during ooplasmic segregation. *Dev Biol*, 106(2), pp.414–426.
- Shimizu, T., 1983. Organization of actin filaments during polar body formation in eggs of Tubifex (Annelida, Oligochaeta). *European Journal of Cell Biology*, 30(1), pp.74–82.
- Shoji, Y., Hamaguchi, M.S. & Hiramoto, Y., 1978. Mechanical properties of the endoplasm in starfish

- oocytes. *Experimental cell research*, 117, p.79/87.
- Smith, L.D. & Ecker, R.E., 1971. The interaction of steroids with *Rana pipiens* Oocytes in the induction of maturation. *Developmental biology*, 25(2), pp.232–247.
- Somers, W. & Saint, R., 2003. A RhoGEF and Rho family GTPase-activating protein complex links the contractile ring to cortical microtubules at the onset of cytokinesis. *Developmental cell*.
- Somlyo, A.P. & Somlyo, A. V, 2003. Ca²⁺ sensitivity of smooth muscle and nonmuscle myosin II: modulated by G proteins, kinases, and myosin phosphatase. *Physiological reviews*, 83(4), pp.1325–58.
- Stepanova, T. et al., 2003. Visualization of microtubule growth in cultured neurons via the use of EB3-GFP (end-binding protein 3-green fluorescent protein). *The Journal of neuroscience : the official journal of the Society for Neuroscience*, 23(7), pp.2655–64.
- Stewart, M.P. et al., 2011. Hydrostatic pressure and the actomyosin cortex drive mitotic cell rounding. *Nature*, 469(7329), pp.226–30.
- Stossel, T.P. et al., 2001. Filamins as integrators of cell mechanics and signalling. *Nature reviews. Molecular cell biology*, 2(2), pp.138–45.
- Straight, A.F. et al., 2003. Dissecting temporal and spatial control of cytokinesis with a myosin II Inhibitor. *Science (New York, N.Y.)*, 299(5613), pp.1743–1747.
- Strand, M. & Grbic, M., 1996. The development and evolution of polyembryonic insects. *Current topics in developmental biology*.
- Strickland, L. et al., 2004. Light microscopy of echinoderm embryos. *Methods in cell biology*, 74, pp.371–409.
- Su, K.-C. et al., 2014. An astral simulacrum of the central spindle accounts for normal, spindle-less, and anucleate cytokinesis in echinoderm embryos. *Molecular biology of the cell*, 25(25), pp.4049–62.
- Su, L. et al., 2009. p190RhoGAP negatively regulates Rho activity at the cleavage furrow of mitotic cells. *Experimental cell research*.
- Swann, M. & Mitchison, J., 1958. The mechanism of cleavage in animal cells. *Biological Reviews*.
- Tachibana, K. et al., 2000. c-Mos forces the mitotic cell cycle to undergo meiosis II to produce haploid gametes. *Proceedings of the National Academy of Sciences of the United States of*

America, 97(26), pp.14301–6.

Takahashi, N. & Kanatani, H., 1981. Effect of 17 beta-Estradiol on Growth of Oocytes in Cultured Ovarian Fragments of the Starfish, *Asterina Pectinifera*. *Development, Growth & Differentiation*, 23(6), pp.565–569.

Takenawa, T. & Miki, H., 2001. WASP and WAVE family proteins: key molecules for rapid rearrangement of cortical actin filaments and cell movement. *J. Cell Sci.*, 114(10), pp.1801–1809.

Tan, I. et al., 2008. A tripartite complex containing MRCK modulates lamellar actomyosin retrograde flow. *Cell*, 135(1), pp.123–36.

Telford, M.J., Budd, G.E. & Philippe, H., 2015. Phylogenomic Insights into Animal Evolution. *Current Biology*, 25(19), pp.R876–R887.

Terasaki, M. et al., 2001. A new model for nuclear envelope breakdown. *Molecular biology of the cell*, 12(2), pp.503–510.

Terasaki, M. et al., 2003. Localization and Dynamics of Cdc2-Cyclin B during Meiotic Reinitiation in Starfish Oocytes. *Molecular biology of the cell*, 14(November), pp.4685–4694.

Terasaki, M., 2006. Quantification of fluorescence in thick specimens, with an application to cyclin B-GFP expression in starfish oocytes. *Biology of the cell / under the auspices of the European Cell Biology Organization*, 98(4), pp.245–52.

Touré, A., Dorseuil, O. & Morin, L., 1998. MgcRacGAP, a new human GTPase-activating protein for Rac and Cdc42 similar to *Drosophila rotundRacGAP* gene product, is expressed in male germ cells. *Journal of Biological Chemistry*.

Vasquez, C.G., Tworoger, M. & Martin, A.C., 2014. Dynamic myosin phosphorylation regulates contractile pulses and tissue integrity during epithelial morphogenesis. *Journal of Cell Biology*, 206(3), pp.435–450.

Vassilev, L.T. et al., 2006. Selective small-molecule inhibitor reveals critical mitotic functions of human CDK1. *Proceedings of the National Academy of Sciences of the United States of America*, 103(28), pp.10660–5.

Verlinsky, Y. & Rechitsky, S., 1999. Prepregnancy testing for single-gene disorders by polar body analysis. *Genetic Testing*.

Vicente-Manzanares, M. et al., 2009. Non-muscle myosin II takes centre stage in cell adhesion and

- migration. *Nature reviews. Molecular cell biology*, 10(11), pp.778–790.
- Vogelsgesang, M., Pautsch, A. & Aktories, K., 2007. C3 exoenzymes, novel insights into structure and action of Rho-ADP-ribosylating toxins. *Naunyn-Schmiedeberg's Archives of Pharmacology*, 374(5-6), pp.347–360.
- Wagner, E. & Glotzer, M., 2016. Local RhoA activation induces cytokinetic furrows independent of spindle position and cell cycle stage. *BioRxiv*.
- Wakayama, T. & Yanagimachi, R., 1998. Fertilisability and developmental ability of mouse oocytes with reduced amounts of cytoplasm. *Zygote*.
- Wang, Y.L., Silverman, J.D. & Cao, L.G., 1994. Single particle tracking of surface receptor movement during cell division. *The Journal of Cell Biology*, 127(4), pp.963–971.
- Watanabe, T., Hosoya, H. & Yonemura, S., 2007. Regulation of myosin II dynamics by phosphorylation and dephosphorylation of its light chain in epithelial cells. *Molecular biology of the cell*, 18(2), pp.605–16.
- Wheeler, A.P. & Ridley, A.J., 2004. Why three Rho proteins? RhoA, RhoB, RhoC, and cell motility. *Experimental cell research*, 301(1), pp.43–9.
- Wickham, H., 2009. *ggplot2: elegant graphics for data analysis* R. Gentleman, K. Hornik, & G. Parmigiani, eds., New York: Springer-Verlag.
- Wu, D., Asiedu, M. & Adelstein, R.S., 2006. A Novel Guanine Nucleotide Exchange Factor MyoGEF is Required for Cytokinesis. *Cell Cycle*, (June), pp.1234–1239.
- Wu, Z. et al., 2013. Phosphorylation of Crm1 by CDK1-cyclin-B promotes Ran-dependent mitotic spindle assembly. *Journal of cell science*, 126(Pt 15), pp.3417–28.
- Wulf, E. et al., 1979. Fluorescent phallotoxin, a tool for the visualization of cellular actin. *Proceedings of the National Academy of Sciences*, 76(9), pp.4498–4502.
- Yamashita, M., 1998. Molecular mechanisms of meiotic maturation and arrest in fish and amphibian oocytes. *Seminars in cell & developmental biology*, 9(5), pp.569–79.
- Yeong, F.M., 2013. Multi-step down-regulation of the secretory pathway in mitosis: a fresh perspective on protein trafficking. *BioEssays : news and reviews in molecular, cellular and developmental biology*, 35(5), pp.462–71.
- Yoneda, B.Y.M. & Dan, K., 1972. Tension At the Surface of the Dividing Sea-Urchin Egg. *Journal of*

Experimental Biology, 52, pp.575–587.

Yoneda, M. et al., 1982. Surface contraction waves in amphibian eggs. *Journal of cell science*, 54, pp.35–46.

Yoshikawa, S.-I., 1996. Centrifugal bisection of starfish oocytes. *Development Growth and Differentiation*, pp.175–183.

Yoshizaki, H. & Ohba, Y., 2004. Cell type-specific regulation of RhoA activity during cytokinesis. *Journal of Biological Chemistry*.

Yu, F., 2003. Distinct roles of G_i and G_{13F} subunits of the heterotrimeric G protein complex in the mediation of *Drosophila* neuroblast asymmetric divisions. *The Journal of Cell Biology*, 162(4), pp.623–633.

Yüce, O., Piekny, A. & Glotzer, M., 2005. An ECT2-centralspindlin complex regulates the localization and function of RhoA. *The Journal of cell biology*, 170(4), pp.571–82.

Zhang, X. et al., 2008. Polar body emission requires a RhoA contractile ring and Cdc42-mediated membrane protrusion. *Developmental cell*, 15(3), pp.386–400.

Zile, M.R. et al., 1999. Role of microtubules in the contractile dysfunction of hypertrophied myocardium. *Journal of the American College of Cardiology*, 33(1), pp.250–260.